Structures and Deformation in Glaciers and Ice Sheets

Jennings, Stephen J.A.; Hambrey, Michael J.

Published in:
Reviews of Geophysics

DOI:
10.1029/2021RG000743

Publication date:
2021

Citation for published version (APA):
Jennings, S. J. A., & Hambrey, M. J. (2021). Structures and Deformation in Glaciers and Ice Sheets. *Reviews of Geophysics*, *59*(3), [e2021RG000743]. https://doi.org/10.1029/2021RG000743

AGU ADVANCING EARTH AND SPACE SCIENCE

Reviews of Geophysics

REVIEW ARTICLE
10.1029/2021RG000743

Structures and Deformation in Glaciers and Ice Sheets

Stephen J. A. Jennings[1] and **Michael J. Hambrey**[2]

[1]Polar-Geo-Lab, Department of Geography, Faculty of Science, Masaryk University, Brno, Czech Republic, [2]Centre for Glaciology, Department of Geography and Earth Sciences, Aberystwyth University, Aberystwyth, UK

Key Points:

- Glaciers and ice sheets display a wide range of structures that inform us about past and present ice dynamics
- Glaciers reveal structures that are analogous to those in rocks that have deformed close to their melting point in the Earth's crust
- Glacier structures influence hydrology, glacial sedimentology and geomorphology, ice microbiology, and help the interpretation of landforms

Correspondence to:
S. J. A. Jennings,
242540@mail.muni.cz

Citation:
Jennings, S. J. A., & Hambrey, M. J. (2021). Structures and deformation in glaciers and ice sheets. *Reviews of Geophysics*, *59*, e2021RG000743. https://doi.org/10.1029/2021RG000743

Received 22 MAR 2021
Accepted 25 JUN 2021

Abstract The aims of this review are to: (a) describe and interpret structures in valley glaciers in relation to strain history; and (b) to explore how these structures inform our understanding of the kinematics of large ice masses, and a wide range of other aspects of glaciology. Structures in glaciers give insight as to how ice deforms at the macroscopic and larger scale. Structures also provide information concerning the deformation history of ice masses over centuries and millennia. From a geological perspective, glaciers can be considered to be models of rock deformation, but with rates of change that are measurable on a human time-scale. However, structural assemblages in glaciers are commonly complex, and unraveling them to determine the deformation history is challenging; it thus requires the approach of the structural geologist. A wide range of structures are present in valley glaciers: (a) primary structures include sedimentary stratification and various veins; (b) secondary structures that are the result of brittle and ductile deformation include crevasses, faults, crevasse traces, foliation, folds, and boudinage structures. Some of these structures, notably crevasses, relate well to measured strain-rates, but to explain ductile structures analysis of cumulative strain is required. Some structures occur in all glaciers irrespective of size, and they are therefore recognizable in ice streams and ice shelves. Structural approaches have wide (but as yet under-developed potential) application to other sub-disciplines of glaciology, notably glacier hydrology, debris entrainment and transfer, landform development, microbiological investigations, and in the interpretation of glacier-like features on Mars.

Plain Language Summary Glacier ice covers about 10% of Earth's land surface and has a profound influence on human activity. As ice continues to melt around the world in response to anthropogenic and natural global heating, the dynamics of glaciers and ice sheets are changing. As this review emphasizes, understanding glacier dynamics is achieved by investigating the brittle and ductile structures that characterize glaciers. The importance of this aspect of glaciology is increasingly being recognized, and draws on its close affinity with structural geology, although interaction between the disciplines to date has been limited. Brittle structures include crevasses, crevasse traces, and a wide variety of faults. Ductile structures include foliation (a layered structure that results from deformation), folds on many scales, and less universally known structures such as ogives and boudins. This review describes, illustrates, and explains the origin of these structures in terms of stress and strain. It also considers areas of controversy, unresolved issues, and offers pointers to future research. A more comprehensive understanding of glacier and ice sheet dynamics is needed to better predict their response to climate change, and ultimately their contribution to sea-level rise. Structural glaciology can play a large part in this process.

1. Introduction

The purpose of this review is to provide a comprehensive assessment of the state of knowledge concerning the manner in which macroscopic structures evolve within glaciers, and to evaluate their meaning in terms of understanding the flow of glaciers and ice sheets. Using concepts drawn from structural geology (e.g., Fossen, 2010; Hobbs et al., 1976; Ramsay, 1967; Ramsay & Huber, 1983), attention is drawn to the similarities between glacier ice and deformed rocks. The review emphasizes those structures that can be observed at the glacier surface and considers their three-dimensional (3-D) geometry. Structures in glaciers are commonly complex and challenging to interpret, especially where several phases of deformation over-print one another. Hence, to aid the reader in the field, many of the described structures and their cross-cutting relationships are illustrated in photographs, maps, and conceptual diagrams, with examples ranging from the Arctic, through mid-latitude mountain ranges, to the Antarctic.

This review does not, however, focus in detail on basal ice, except where deformation structures demonstrate interaction between the basal ice layer and bulk glacier ice, as several reviews already exist on this topic (Alley et al., 1997; Hubbard et al., 2009; Knight, 1997; Moore, 2014).

Structural glaciology has strong, but relatively unexplored, relationships with other glaciological sub-disciplines, including temporal changes of glacier mechanics, debris entrainment and transfer, glacier hydrology, glacial geomorphology, the distribution of microbiota, and Martian glaciology. Some of these key themes are highlighted in this review.

Our approach is to define the concepts of stress and strain relevant to glacier structures, present a classification and evaluation of ductile and brittle structures, and consider typical structural assemblages and structural sequences in valley glaciers. This approach draws on decades of field-based research by the authors, colleagues, and other glaciologists, and forms the basis for interpreting features observed in satellite imagery of ice sheets and ice shelves, which are far too large to investigate at ground level. Similarly, structural analysis of glacier-like forms on Mars provides an opportunity to gauge the former dynamics of these controversial features.

The development of concepts in structural glaciology has consistently lagged behind those in structural geology, and it remains an under-developed sub-discipline of glaciology. This is largely because few geologists have studied glaciers, which have generally been the preserve of physicists, chemists, geophysicists, and geographers. These scientists have not always appreciated the 3-D complexity of glaciers, nor have they recognized that structures are the cumulative effect of deformation over centuries and millennia.

On the other hand, structural geologists have rarely taken advantage of the fact that glacier ice can be regarded as a monomineralic metamorphic rock, which deforms at rates several orders of magnitude faster than in rocks in active mountain belts. As such, glaciers can be regarded as natural laboratories of rock deformation. Specifically, glacier ice deforms under temperature conditions close to its melting point. It begins as a subaerial sediment (snow) and over several decades, centuries, or millennia (depending on the climatic regime), becomes buried, undergoes diagenesis, regional high-grade metamorphism (including partial melting and recrystallization), flow, and fracture. As the ice passes into the ablation zone, deeper, older, more highly deformed ice is exposed (Hambrey & Milnes, 1977).

By highlighting key areas where structural glaciology needs to develop, and where it can inform other sub-disciplines, we hope that more practitioners will take up the challenge of investigating glaciers in this way, in order to better understand the dynamics of ice masses whatever their scale.

2. Historical Background

Interest in glacier structures dates back to the infancy of glaciology in the 19th century, when early researchers drew comparisons with the deformational characteristics of rocks (Hambrey & Lawson, 2000). This early work used glacier structures to underpin the fundamental principles of glacier flow and vice versa. Two men stand out as early pioneers of structural glaciology in the 19th century: James Forbes, a Scot who was Professor of Natural Philosophy at Edinburgh University and an Alpine mountaineer, and John Tyndall, a geologist and an accomplished mountaineer born in Ireland, who became one of the century's best-known physicists. Early ideas concerning the principles of glacier theory were synthesized by the Swiss natural historian, Louis Agassiz in the volume entitled *Etudes des Glaciers* (Agassiz, 1840). Like Agassiz, Forbes and Tyndall also undertook fieldwork in the Swiss and French Alps around the same time, and both focused on glacier structure, as well as evaluating the relative merits of plasticity, viscosity, and water expansion as drivers of glacier flow.

Forbes wrote extensively about structures in glaciers, his lyrical style combining scientific observation with his field experiences. In 1842, he produced one of the earliest structural maps of a valley glacier, the Mer de Glace in the French Alps (Forbes, 1859, 1900). The map depicts a series of medial moraines and a series of curving dirt bands originating in an icefall, structures which today we refer to as ogives or Forbes bands (Figure 1a). He was the first to describe the ubiquitous "veined structure" that we now know as foliation (Figure 1b). His first encounter with this phenomenon led him to state, with reference to fresh stream-cut surfaces that "their structure appeared with the beauty and sharpness of a delicately veined chalcedony"

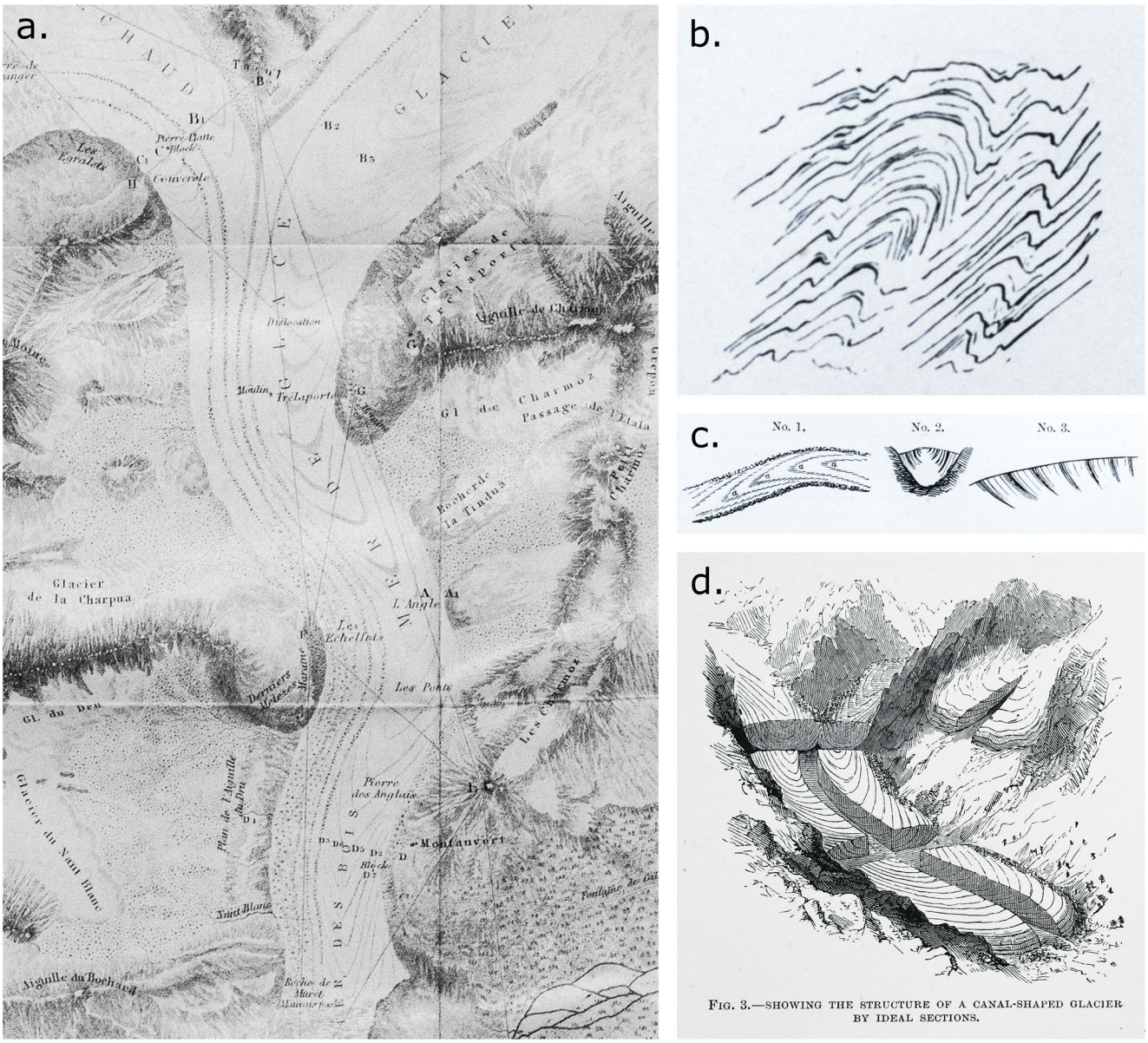

Figure 1. Examples of the pioneering structural glaciological work of James Forbes in the French Alps from "Travels Through the Alps" (Forbes, 1900, revised and annotated by W. A. B. Coolidge, including 1842 map, and Forbes, 1859). (a) Extract from Forbes' 1842 map of Mer de Glace, showing medial moraines and dirt bands (ogives). (b) Sketch of "twisted veins," now interpreted as folded foliation. (c) The 3-D geometry of dirt bands (ogives) in the Mer de Glace. (d) "The structure of a canal-shaped glacier by ideal sections," that is, a conceptual model of the evolution of dirt bands and associated arcuate foliation in a valley glacier.

(Forbes, 1859). He established that in glaciers with icefalls, such as the Mer de Glace, the veined structure was parallel to flow at the edges, but became transverse to flow in the middle, reflecting differential flow and internal deformation. He even recognized the 3-D geometry of the structure, as having a "spoon-shaped arrangement" (Figure 1c). He further noted that this structure was quite distinct from stratification in snow and névé (firn), and was commonly intersected by crevasses. He used his observations to derive a 3-D conceptual model of the evolution of transverse foliation within a valley glacier (Figure 1d).

Tyndall (1859, 1860, reprinted 2011), taking a more rigorous physical approach explained the origin of crevasses in terms of tension and compression, and the "veined structure" (foliation) as the product of differential flow. Furthermore, he was the first to use strain ellipses in an experiment involving mud to demonstrate the relationship between structure and strain, and recognized the analogy with slaty cleavage, and its

cross-cutting relationship with stratification in rocks. He was also fascinated by the origin of the curved dirt bands (ogives) and crevasses, as well as glacier flow theory more generally.

Taking a mathematical approach, Hopkins (1862), was highly critical of how loosely early glacier researchers used key physical terms, such as sliding, viscosity, plasticity, fracture, and regelation. He also argued that at the time there was little cross-investigation between theory and observation. By developing a rigorous mathematical framework, Hopkins was able to develop ideas about the origins of such structures as crevasses and "veining" (foliation).

Other late 19th century (Garwood & Gregory, 1898) and early 20th century (Wright & Priestley, 1922) researchers were also interested in the structures of glaciers, especially from the perspective of debris entrainment. These authors documented the principal attributes of glaciers and their margins in Svalbard and Antarctica, respectively.

The perceptive observations and interpretations of Forbes and Tyndall were not surpassed for another century. In fact, the first half of the 20th century saw only limited progress with regard to understanding glacier flow or dynamics, and few structural studies were undertaken. However, the development of a flow law for ice led to renewal of interest in glaciers during the early 1950s culminating in new robust theories for glacier flow (e.g., Glen, 1955; Nye, 1952, 1953, 1957). Subsequently, interest in structural glaciology was rejuvenated by the notable contributions of Schwarzacher and Untersteiner (1953) on Pasterzenkees, Austria; by Allen et al. (1960) on Blue Glacier, Washington State; by Meier (1960) on Saskatchewan Glacier, Alberta; and by Rutter (1965) on Gulkana Glacier, Alaska. For the first time, the 3-D orientations of all the major structures present on each glacier were documented, and the origins of different ice types (coarse bubbly, coarse clear, and fine) assessed using the ratio of isotopes O^{18} and O^{16} in comparison with Standard Mean Ocean Water (SMOW). Attempts at relating the observed structures to measured strain-rates, however, on the whole proved to be unsuccessful at that time. Then, in the 1970s and 1980s, structural geological concepts were applied to understanding structures in Canadian Arctic and Swiss glaciers, combining 3-D mapping, velocity and strain analyses, borehole deformation analysis, ice crystallography, and isotopic analysis. Pioneering work that investigated the relationship between foliation development and strain was undertaken on the Barnes Ice Cap on Baffin Island, Canada (Hooke & Hudleston, 1978; Hudleston, 1983; Hudleston & Hooke, 1980). Simultaneously, research on Norwegian, Canadian Arctic, and Swiss glaciers also followed a structural geological approach, and explored the relationship between structures and strain (Hambrey, 1975, 1976a, 1976b; Hambrey & Milnes, 1977; Hambrey & Müller, 1978; Hambrey et al., 1980; Milnes & Hambrey, 1976). This research determined that ductile structures such as folds and foliation were more likely to be related to cumulative strain, reflecting the initial formation and continuing evolution (strain history) of these structures.

More recent research, undertaken toward the end of the 20th century, focused on the formation and evolution of structures in surge-type glaciers, notably in Alaska and Svalbard (e.g., Hambrey & Dowdeswell, 1997; Lawson et al., 1994; Murray et al., 1997; Sharp, 1988a, 1988b). Furthermore, field-derived structural principles developed for small-scale valley glaciers were applied to ice streams and ice shelves in Antarctica using remotely sensed data (e.g., Ely & Clark, 2016; Glasser & Gudmundsson, 2012; Glasser & Scambos, 2008; Glasser et al., 2011, 2015; Hambrey & Dowdeswell, 1994; Reynolds, 1988; Reynolds & Hambrey, 1988) and the Russian High Arctic (Dowdeswell & Williams, 1997).

All the above research has been largely driven by field observations and measurements. In other fields of glaciology, numerical modeling approaches are well established and widely applied, but the prediction of structural evolution as glaciers respond to climatic change is still in its infancy. The earliest attempts to numerically model structures such as folds and foliation, were undertaken by Hooke and Hudleston (1978), Hudleston (1983), and Hudleston and Hooke (1980), using a finite element approach. Their work was largely based on the Barnes Ice Cap on Baffin Island. Among the earliest work on valley glaciers, that by Pohjola (1996) on Storglaciären, Sweden, stands out. Using a two-dimensional (2-D) flow model, using Nye's (1953) generalization of Glen's Flow Law for ice, he simulated particle paths, travel times, and deformation, in order to explain the geometry of crevasses and their relationship to arcuate structures. A further advance at the turn of the century was the development of high-resolution glacier-flow modeling to explain

a range of structures in Haut Glacier d'Arolla in the Swiss Alps (Goodsell, Hambrey, Glasser, Nienow, & Mair, 2005; Hubbard & Hubbard, 2000), and in Midtre Lovénbreen in Svalbard (Hambrey et al., 2005).

Some structures, such as alleged thrust-faulting, have received specific modeling attention to demonstrate that this process is unfeasible in most conditions (Moore et al., 2010). However, this approach does not address, how the geological and structural characteristics observed in the field point to the viability of this process.

A thermomechanical modeling approach to simulating the evolution of various structures (foliation, crevasses, crevasse traces, and medial moraines) was developed for Trapridge Glacier in Yukon Territory, Canada, based on field observations. This glacier had, over 20 years, undergone a "slow surge," ending in 2000 (Frappé-Sénéclauze & Clarke, 2007). Field observations were made, post-surge, in 2006, and the observed and 3-D measured structures were replicated using a numerical modeling approach (Hambrey & Clarke, 2019). This then formed the basis for creating generalized numerical models of structural evolution for a "Traplike" glacier (Clarke & Hambrey, 2019).

The above studies demonstrate that, although the application of numerical modeling approaches to understanding structural evolution is still at an early stage, the scope for wider application, especially to large ice masses is enormous. Whereas the key approach on valley glaciers is to use 3-D field mapping to inform the modeling, this cannot be done with larger ice masses, and here field observations have to be substituted for satellite data interpretation and airborne geophysical investigations.

Although structural glaciology is intrinsically interesting in its own right, especially in terms of understanding glacier dynamics, the subject is now being applied to the interpretation of debris entrainment, transfer, and deposition. This understanding is crucial for explaining the genesis of Quaternary glacial landforms. Boulton (1967, 1970), initiated this trend with his ground-breaking studies of debris entrainment and deposition at the margins of several glaciers in Svalbard. His investigations have been built upon through the study of glacier ablation areas and ice-marginal landforms at polythermal glaciers in the Canadian Arctic, Greenland, and Svalbard (e.g., Evans, 1989a, 1989b, 2003, 2009; Hambrey et al., 1999; Ó Cofaigh et al., 2003), temperate glaciers in the European Alps (Goodsell, Hambrey, Glasser, Nienow, & Mair, 2005; Jennings et al., 2014; Roberson, 2008) and Iceland (Phillips et al., 2014, 2017; Swift et al., 2018), and cold glaciers in the Antarctic Dry Valleys (Fitzsimons & Howarth, 2019; Hambrey & Fitzsimons, 2010).

Another area of glaciology, where structural analysis has a vital contribution to make is in glacier hydrology. However, apart from an insightful study by Stenborg (1968) on a Swedish Arctic glacier, and a comprehensive review of the hydrology of polythermal glaciers by Irvine-Fynn et al. (2011), little research has been undertaken. We know from general observations that water-routing in glaciers is commonly controlled by crevasses, crevasse traces, and foliation. Furthermore, drainage itself is known to induce hydrofracturing in the Greenland Ice Sheet (Das et al., 2008; Doyle et al., 2013) and in valley glaciers during surging, such as in Skeiðarárjökull in Iceland (Bennett et al., 2000; Roberts et al., 2000). Structures such as crevasses and crevasse traces have been implicated in facilitating sediment transfer by water in the same glacier (Bennett et al., 2000).

The growing emphasis on the microbiology of glacier surfaces (Hodson et al., 2008) stresses the importance of meltwater, the distribution of which is commonly controlled by structure. These little-known relationships are ripe for future investigation. There is also a developing extra-terrestrial interest in structural glaciology, with Hubbard et al. (2014) having described a range of structural features, including crevasses and various landforms, on glacier-like forms on Mars. Each of these topics is considered in greater detail in Section 9 after describing the structural attributes of glaciers.

3. Theories of Ice Deformation and Glacier Flow

3.1. Background

Our understanding of the structural evolution of glaciers and ice sheets requires a multi-disciplinary approach, embracing physics, geology, geophysics, and geomorphology. Glaciers flow under the influence of gravity, and this fact determines how ice masses respond to the balance between accumulation and ablation, which in turn is driven by changes in climate. As glaciers flow, they are subject to stresses and,

consequently, the ice is deformed or strained. An outline of the concepts of stress and strain, as they apply to understanding glacier structures, is given below, with the intention that this be accessible to the nonspecialist. More advanced approaches to glacier flow are available in specialized textbooks which cover the physics in considerable depth (e.g., Cuffey & Paterson, 2010; Hooke, 2019).

3.2. Stress and Strain

Stress is defined as the force applied per unit area. Stress results in strain, which is the change in shape and dimensions of a body. Stress acting on a surface can be separated into two basic components: (a) stress acting perpendicular to a surface (normal stress, σ); and (b) stress acting parallel to a surface (shear stress, τ). In each case, the stress acting on the surface comprises two equal and opposite tractions. Normal stresses have opposing tractions across a surface, either pulling in opposite directions (tensile stress) or acting toward one another (compressive stress). Shear stresses have parallel tractions along a plane; however, the tractions act in opposite directions. Stress at a specific point can be illustrated using a stress element where the normal and shear stresses acting on an infinitesimal cube can be described by three perpendicular planes (Figure 2a). Therefore, as pairs of opposing shear stresses must be in equilibrium to ensure no rotational acceleration of the stress element, six independent stress components (three normal, three shear) can describe the stress state at any given point (Cuffey & Paterson, 2010). To describe stresses acting in an ice mass, a rectangular Cartesian coordinate system is used, with the x-axis oriented longitudinally along the glacier (parallel to ice-flow), the y-axis oriented transverse (perpendicular to ice-flow), and the z-axis in the vertical (Figure 2b). The stress type is identified by either σ or τ for normal or shear stresses respectively, each followed by two subscript letters, the first of which (i) indicates the direction in which the stress is acting, and the second (j) denotes the direction perpendicular to the plane on which the stress acts (following Benn & Evans, 2010—note that different conventions may be used by other authors and disciplines). Therefore, a normal stress acting in the x-direction is denoted σ_{xx}, whereas a shear stress acting in the x-direction on a plane oriented perpendicular to the y-axis would be denoted by τ_{xy} (Figure 2).

Normal stresses within the body of an ice mass can act in multiple directions, primarily as a result of the ice spreading under its own weight. It is therefore useful to consider the mean normal stress, or "cryostatic" pressure (also referred to as "hydrostatic" or "lithostatic" pressure by some authors), and how any given normal stress differs from this value. This "deviatoric stress" can be resolved, for example, in the x-direction (σ'_{xx}) using:

$$\sigma'_{xx} = \sigma_{xx} - \frac{1}{3}\left(\sigma_{xx} + \sigma_{yy} + \sigma_{zz}\right) \quad (1)$$

It is worth noting that in certain circumstances, the deviatoric stress may be tensile, despite the component normal stresses being compressive (Figure 3) (Benn & Evans, 2010).

Even though it is often useful to treat normal and shear stresses as mutually exclusive, they are end-members of a continuum, and are therefore fundamentally linked to one-another. For example, a body of ice experiencing shear stress is simultaneously experiencing normal stresses, which are greatest at a 45° angle from the shear plane, and vice versa. Consequently, by rotating the rectangular Cartesian coordinate system, it is possible to describe stress at a given point using only three normal stresses (known as principal stress tensors). In reality, ice is subjected to a combination of normal and shear stresses which coalesce to form a new set of deviatoric and shear stresses. The combined set of stresses can therefore be resolved into three principal stress component parts (maximum, intermediate, and minimum values) oriented perpendicular to one-another, termed σ_1, σ_2, and σ_3 where $\sigma_1 > \sigma_2 > \sigma_3$. It is especially useful to deduce the principal stress tensors when considering the formation of glaciological structures, for example, to explain the initiation and development of crevasses (Figure 4) (Nye, 1952; see also Ambach, 1968; Hambrey & Müller, 1978; Harper et al., 1998; Holdsworth, 1969; Meier, 1960; Meier et al., 1974). However, it is often more relevant for understanding structures in glaciers to use strain analysis, which involves measuring strain-rates directly in the field, or modeling cumulative strain.

The principles and equations relevant to determining stress and strain in glaciers are explained thoroughly by Cuffey and Paterson (2010) and Hooke (2019), and in rocks by Fossen (2010).

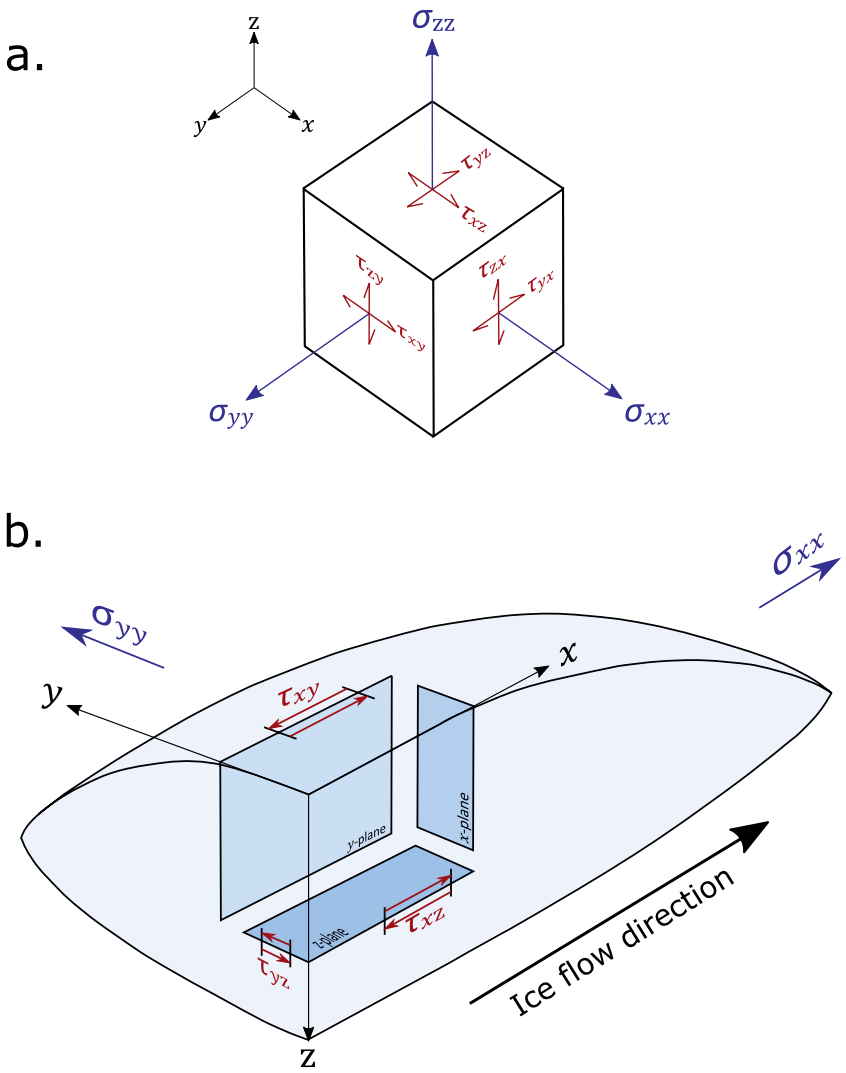

Figure 2. (a) An infinitesimal stress element illustrating the nine stress components acting on three perpendicular planes. Normal stresses (σ) are blue, and shear stresses (τ) are red, with the first subscript letter describing the direction of the stress, and the second describing the direction perpendicular to the plane on which the stress acts. To ensure no rotational acceleration, opposing shear stresses are equal ($\tau_{xy} = \tau_{yx}$, $\tau_{xz} = \tau_{zx}$, $\tau_{yz} = \tau_{zy}$), therefore, six independent stress components (three normal, three shear) can describe the stress state at any given point. (b) A conceptual diagram of a cross- and long- section through an idealized glacier, illustrating the main normal (σ) and shear (τ) stresses, in blue and red respectively, that are active within the tongue of a valley glacier. Note that arrow sizes are not to scale, and do not represent comparative stress magnitude.

3.3. Calculation of Strain

The amount of strain experienced by a "parcel" of ice is quantified by comparing the dimensions and shape before and after the application of stress. In its simplest form, this can be achieved by measuring the elongation (ε) of a line after deformation:

$$\varepsilon = \frac{\left(l_1 - l_0\right)}{l_0} \tag{2}$$

Where l_1 = length after straining, and l_0 = length before straining. Strain-rate ($\dot{\varepsilon}$), the amount of deformation occurring per unit time, is dependent on the rheology of the material and the amount of stress applied. For pure shear, the normal strain-rate in the x-direction can be resolved using:

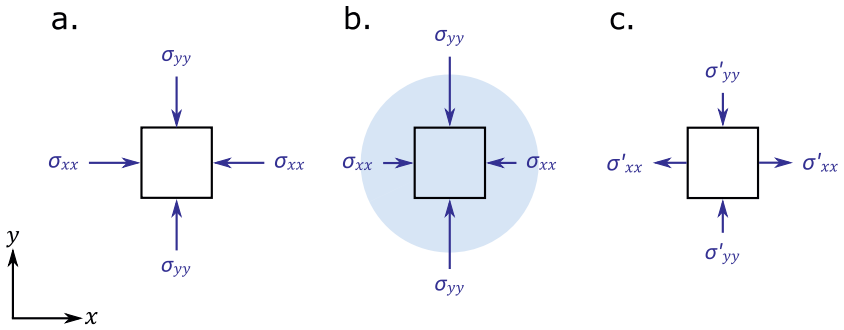

Figure 3. Normal stresses (σ) acting on a square element, with the first subscript letter denoting the direction that the stress is acting, and the second describing the direction perpendicular to the plane on which the stress acts. (a) Equal compressive normal stresses in the *x*- and *y*-directions. (b) Asymmetric compressive normal stresses acting in the *x*- and *y*-directions, with the blue circle representing the mean normal stress (cryostatic pressure). (c) The deviatoric stresses (σ') that result from the unequal normal stresses acting in (b). Note that even though the normal stresses acting in (b) are compressive, the resulting deviatoric stress in the *x*-direction is tensile (modified from Benn & Evans, 2010).

$$\dot{\varepsilon}_{xx} = \frac{\partial u}{\partial x} \tag{3}$$

Whereas, for simple shear:

$$\dot{\varepsilon}_{xy} = \frac{1}{2}\left(\frac{\partial v}{\partial x} + \frac{\partial u}{\partial y}\right) \tag{4}$$

where u and v are the velocities in the *x*- and *y*-direction, respectively. These equations define strain-rate as the difference in velocity between points separated by an infinitesimal distance. However, for laboratory and field measurements that are conducted over longer distances and time-frames, logarithmic strain is used:

$$\dot{\varepsilon} = \frac{1}{\Delta T}\ln\frac{l_1}{l_0} \tag{5}$$

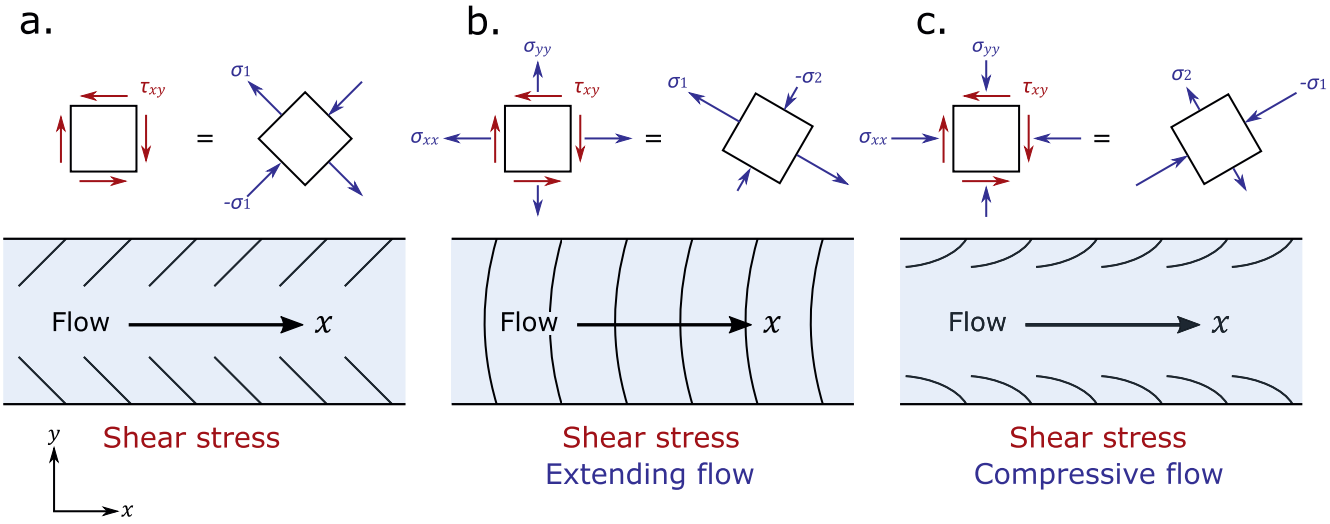

Figure 4. Plan view of basic crevasse patterns in a valley glacier. The square elements at the top of each diagram illustrate the normal (σ) and shear (τ) stresses, in blue and red respectively, acting at the glacier surface near to the upper margin (left), and the related principal stresses (right), with negative values indicating compressive principal stresses. Arrow sizes and orientations represent the direction and magnitude of principal stresses. (a) Chevron crevasses resulting from lateral shear stresses acting at the margin of the glacier. (b) Curved transverse crevasses resulting from lateral shear stress combined with longitudinal tensile stress (extensional flow regime). (c) Splaying crevasses resulting from lateral shear stress combined with longitudinal compressive stress (compressive flow regime) (modified from Nye, 1952).

where ΔT is the time interval between measurements, l_1 = length after straining, and l_0 = length before straining. These measures are particularly useful for analysis of deformation between stakes along the glacier centerline, such as when a glacier experiences a surge.

For an assessment of the strain regime, arrays of stakes are commonly used to determine the principal strain-rate tensors, for example, using an array of five stakes and applying a least squares analysis (Nye, 1959a), or, more rapidly but less precisely, using changes in length of the sides of triangular arrays of stakes using Mohr circle constructions (Milnes & Hambrey, 1976; following Ramsay, 1967). Examples of strain-rate tensor analysis include studies on Austerdalsbreen, Norway (Nye, 1959a); Saskatchewan Glacier, Alberta (Meier, 1960); Kaskawulsh Glacier, Yukon Territory (Anderton, 1973); Meserve Glacier, Antarctica (Holdsworth, 1969); Blue Glacier, Washington (Meier et al., 1974); Griesgletscher, Switzerland (Hambrey et al., 1980); Unteraargletscher, Switzerland (Gudmundsson et al., 1997); Bakaninbreen, Svalbard (Murray et al., 1998); and Worthington Glacier, Alaska (Harper et al., 1998; Pfeffer et al., 2000).

3.4. Modeling Structural Evolution in Relation to Cumulative Strain

To explain the kinematic context in which glacier structures evolve, particularly ductile structures, it is commonly more advantageous to consider how strains add up incrementally over time (Hambrey, 1977a; Hambrey & Lawson, 2000; Hooke & Hudleston, 1978; Hudleston & Hooke, 1980). As a parcel of ice moves through a glacier, the attributes of a structure reflect the adding up of the successive incremental strains. The sum of all the incremental strains is the total strain, more formally known as "cumulative strain" (as used in this review), or "finite strain" (Ramsay, 1967). To visualize strain, it is helpful to envisage how a passive 2-D circular marker evolves into a strain ellipse within a deforming material. In 3-D, a strain ellipsoid has two principal strain axes perpendicular to one another that indicate the direction of maximum (x-axis) and minimum (z-axis) strain, with a third intermediate axis (y-axis) normal to the xz-plane (i.e., $x > y > z$). Even though in reality deformation rarely occurs in only two dimensions, for the purpose of visualizing strain in glaciers, deformation is often considered as plane strain, where no particle movement occurs in the y-direction. Consequently, strain can be illustrated by an ellipse on a 2-D diagram where the y-axis is perpendicular to the page (Figure 5). However, care must be taken using this approach as it has been demonstrated that the 3-D flow field of valley glaciers, even with simple valley geometries, are spatially complex, and vary significantly from simple plane strain at length-scales less than the thickness of the ice (Harper et al., 2001).

The standard measure for cumulative/finite strain in a longitudinal direction is known as quadratic elongation, λ, which is the square of the amount of stretch:

$$\lambda = \left(\frac{l_1}{l_0}\right)^2 \tag{6}$$

where l_1 = length after straining, and l_0 = length before straining.

Cumulative strains were first calculated on a glacier (Griesgletscher, Switzerland) by defining the flow field from a network of stakes, and then applying a Mohr circle analysis (Hambrey & Milnes, 1977). Around the same time a study on Barnes Ice Cap, Baffin Island, used finite element modeling in a vertical longitudinal profile to determine strain history (Hooke & Hudleston, 1978). In both studies cumulative strain was represented by strain ellipses along flow lines through each ice mass (Figure 6).

More recently, the cumulative strain pattern was derived for the Haut Glacier d'Arolla, Switzerland, using a thermomechanical 3-D flow-modeling approach (Hubbard & Hubbard, 2000; Hubbard et al., 1998). The model is steady-state, and based on Blatter's (1995) finite-difference first-order solution of the ice-flow stress equations. This approach was used on the same glacier to evaluate the relationships with structures such as foliation, folds, and fractures by means of strain ellipses (Goodsell, Hambrey, Glasser, Nienow, & Mair, 2005). In this case, the flow modeling shows how circles (representing zero deformation) evolve into ellipses. The orientation and degree of elongation of the ellipses may therefore be compared with structures in order to discriminate simple shear, pure shear, or extensional regimes. In this way, the evolution of penetrative structure can be tracked from start to finish. This model was further developed for a study of

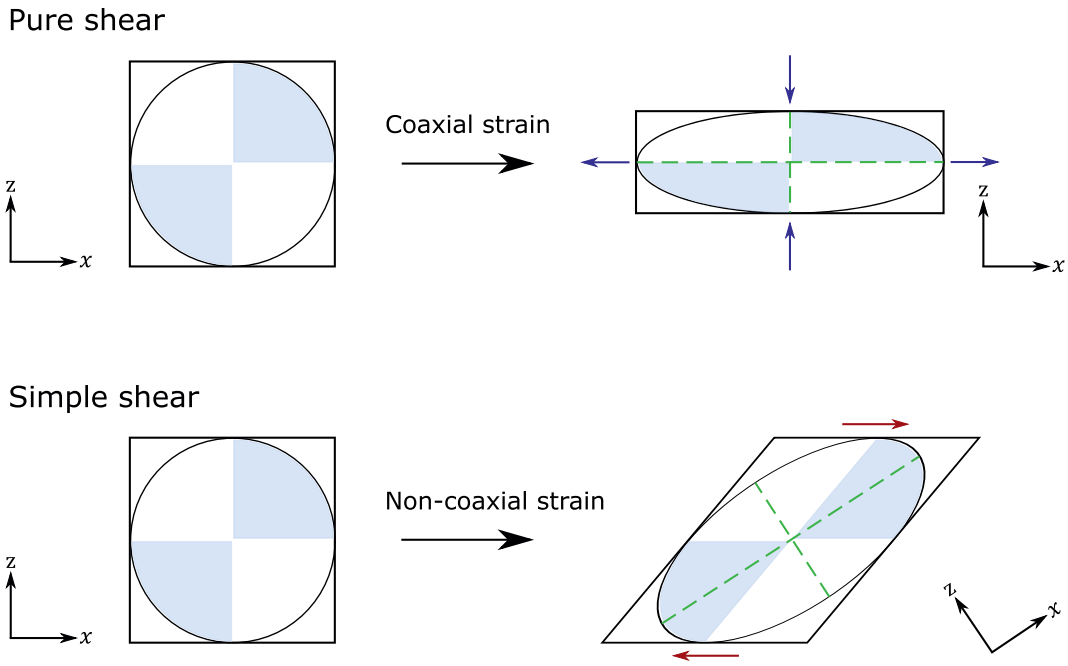

Figure 5. Graphical representation of the two main end-member types of strain: pure shear (coaxial strain) and simple shear (non-coaxial strain), as illustrated by the deformation of passive circle markers into ellipses. Passive blue quadrants illustrate the rotation/lack of rotation of axes within ellipses before and after deformation. Blue and red arrows represent normal and shear stresses, respectively, and the green dashed lines indicate the axes of maximum extension (*x*-axis) and maximum compression (*z*-axis).

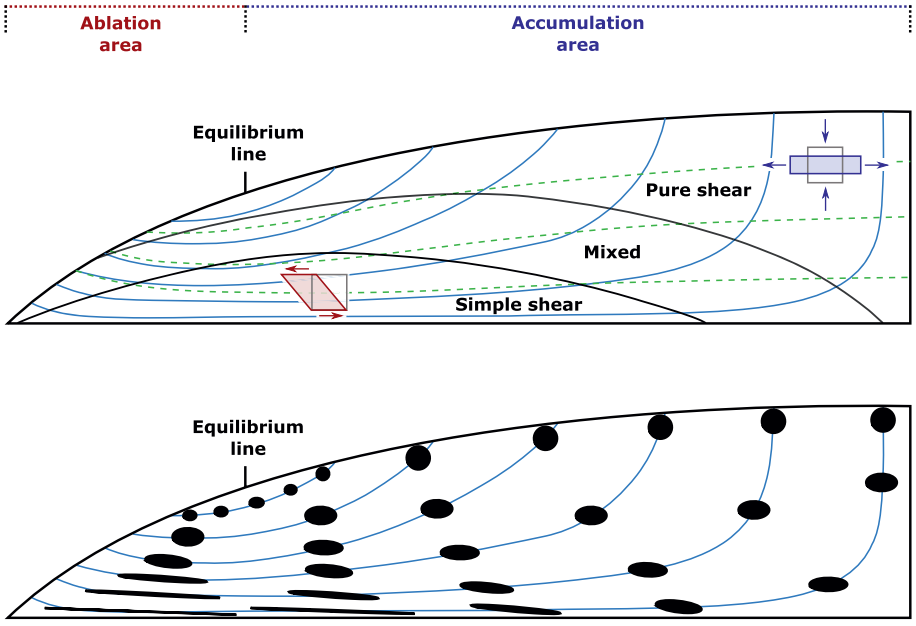

Figure 6. Schematic diagram illustrating the dominant zones of pure and simple shear in a longitudinal section through an idealized glacier or ice cap (top), with the corresponding evolution of strain ellipses along flow paths through the ice mass (bottom). Ice flow is from right to left, with solid blue lines representing flow paths and dashed green lines representing isochrones of uniform age. In an idealized valley glacier flowing from the glacier's headwall to the terminus, strain is considered to be plane strain. However, in an ice cap, an element of flattening results from the unconfined spreading of the ice in three-dimensions, therefore, particle movement also occurs perpendicular to the page (modified from Hooke & Hudleston, 1978).

structure-strain relationships on Midtre Lovénbreen in Svalbard, taking into account the thermal structure of this polythermal valley glacier (Figure 7) (Hambrey et al., 2005).

A recent study of Trapridge Glacier, a small surge-type glacier in the Yukon that has been monitored dynamically for 40 years, represents the first attempt to numerically model structural evolution in a surge-type glacier on a glacier-wide scale. Following the glacier's most recent slow surge cycle, which lasted from 1980 to 2000, several structural attributes were documented in 3-D. A thermomechanical ice dynamics model was used and this was constrained using field observations of different structures (Hambrey & Clarke, 2019).

Each of the above modeling studies of cumulative strain relate to a specific glacier. In a complementary study to the above field-based analysis of Trapridge Glacier, a vertically integrated thermomechanical ice dynamics model was developed to simulate structural evolution in a generalized "Traplike" glacier. Temporally evolving patterns of structures during a surge cycle were modeled, including a surficial moraine, stratification, foliation, the folding of glacier ice, and the density and orientation of traces of former crevasses (Clarke & Hambrey, 2019).

The challenge for structural glaciologists is to explain the links between processes and products. Hypotheses are based on field observation, and sometimes measurements of glacier velocity and strain-rates. Since glaciers are highly individualistic, care is needed when one applies hypotheses more widely. However, by using numerical ice dynamic models that are anchored in field observation to represent the evolution of structures, hypotheses can be effectively tested. This approach, used at Trapridge Glacier, is ready to be used in simulating other geometrical forms of glaciers and, indeed, ice sheets.

3.5. Glacier Flow

The basic principles of glacier flow by internal deformation were established following experiments on blocks of ice that led to the development of what has become known as "Glen's Flow Law," which relates strain-rate to shear stress (Glen, 1955). The quantified application of this law to glaciers was subsequently generalized for glaciers by Nye (1952, 1957), following the first studies of deformation in a glacier borehole at Jungfraujoch, Switzerland. Experimental and theoretical analyses relating applied stress to shear strain rate in polycrystalline ice assume a non-linear viscous flow law (for flow in steady-state creep) of the form:

$$\dot{\varepsilon}_{ij} = A\sigma'^{n-1}_{\mathrm{II}}\sigma'_{ij} \tag{7}$$

where $\dot{\varepsilon}_{ij}$ is an independent component of the strain-rate tensor, σ'_{ij} is the deviatoric stress tensor, σ'_{II} is the second tensor invariant, which is equal to $\frac{1}{2}\sigma'_{ij}\sigma'_{ij}$. The parameter A varies depending on the physical and chemical properties of the ice, but is strongly dependent on temperature. The typical value for the exponent n in glaciers is approximately three; however, values ranging from 1 to 4.2 have been suggested, and the factors influencing n in both field and laboratory experiments are still poorly understood (Cuffey & Paterson, 2010).

In response to applied stress and deformation, isotropic ice increasingly develops a crystallographic fabric resulting from dynamic recrystallization. As viscosity becomes anisotropic, Equation 7 no longer adequately describes the rheology, as the ice can either soften or harden depending on the stress configuration. To overcome this issue, a strain-rate enhancement factor is added to Equation 7, which therefore becomes:

$$\dot{\varepsilon}_{ij} = EA\sigma'^{n-1}_{\mathrm{II}}\sigma'_{ij} \tag{8}$$

where E is the factor by which strain rate diverges from the predicted values for isotropic polycrystalline ice. The exact value of the enhancement factor is dependent upon the characteristics of the crystallographic fabric; however, laboratory creep experiments have found strain-rate enhancement in simple shear to exceed that of uniaxial compression by more than double the amount (Treverrow et al., 2012).

In reality, ice masses are rarely composed of pure polycrystalline ice, but contain varying debris-ice mixtures. The impact that entrained debris has on ice flow has been reviewed by Moore (2014), combining observations from field-based, laboratory, and theoretical studies. However, the relationship between debris content and ice flow is not straightforward, with a wide range of first-order variables influencing the deformation mechanics of debris-ice mixtures. At low temperatures, debris-ice mixtures are usually more

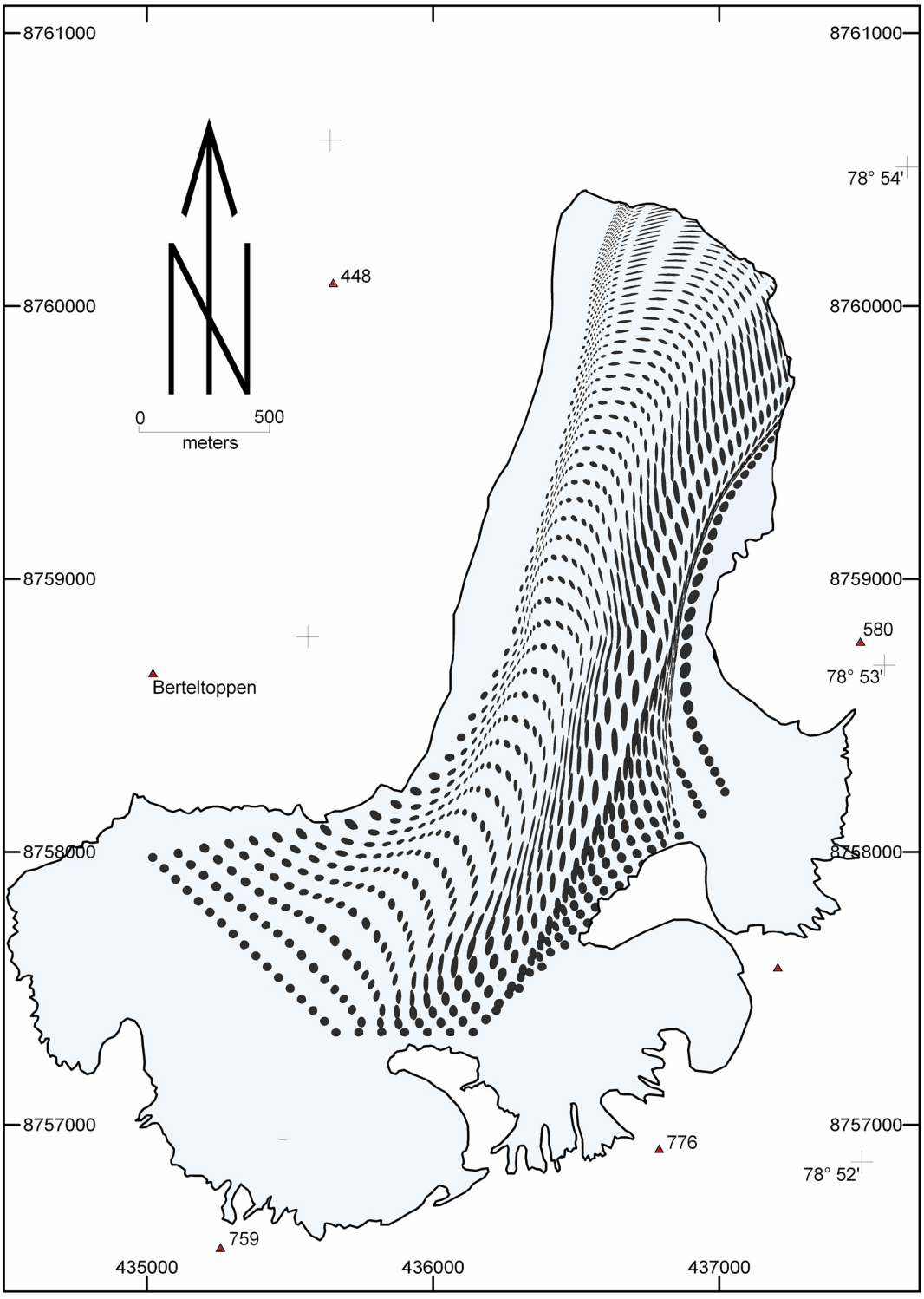

Figure 7. Generation of cumulative strain ellipses on Midtre Lovénbreen, Svalbard, through numerical modeling. Inputs to the model are velocity distribution, bed configuration, and thermal structure. Stretched-out flow-parallel ellipses indicate the zones of most intense shear (Hambrey et al., 2005).

resistant to deformation, as the debris impedes ice creep. However, nearer to the pressure-melting point, the development of liquid water films at ice-particle boundaries counteracts the initial strengthening effect, and in certain circumstances weakens the debris-ice mixture (Moore, 2014).

4. Approaches to Structural Glaciology

4.1. Principles

In geological terms, glacier ice can be considered to be a monomineralic metamorphic rock. In temperate glaciers ice deforms at temperatures close to the melting point, and in cold glaciers at temperatures that may be a few tens of degrees below the melting point. Glaciers can be used as a model of rock deformation because in a typical alpine glacier deformation rates are six orders of magnitude faster than in compressive mountain belts (Hambrey & Milnes, 1977), and are determined from field measurements of flow velocity and direction, and strain-rates. Velocity data can now be obtained using remote-sensing techniques, such as interferometry and feature-tracking, but few studies have been undertaken to date to calculate strain-rate fields or determine cumulative strains. The typical residence time for ice in a valley glacier is a few centuries, rising to millennia in major ice streams, and arguably millions of years in the Antarctic Ice Sheet. The deformation history of a "parcel" of ice follows a complex path. Starting as snow in the accumulation area, it undergoes burial and diagenesis into glacier ice. It is then subject to the equivalent of regional high-grade metamorphism, which involves partial melting and recrystallization, fracture, folding, and shearing (Hambrey & Lawson, 2000). More specifically, a valley glacier may be considered to be an analog of an extensional allochthon, where a rock mass moves under gravity, such as at passive continental margins (Herbst & Neubauer, 2000).

As is the case for rocks, strata systematically build up and subsequently become progressively deformed to produce a wide range of structures. As a result, structures that form in glaciers can be broadly classified as "primary" or "secondary." Primary structures form by the accumulation or accretion of new material, while secondary structures result from ice deformation. Secondary structures can be further generalized into two categories: the product of "plastic (ductile) deformation," or "brittle deformation." Ductile features form as primary structures are altered to varying degrees by ice creep, commonly resulting in folding, foliation, and boudinage. Brittle structures resulting from the brittle failure of ice form a wide range of fractures including open fractures (crevasses), closed fractures (crevasse traces), and faults (Colgan et al., 2016; Hambrey, 1994; Hambrey & Lawson, 2000).

Glacier structures are usually described in relation to the structural evolution of the whole glacier in an attempt to distinguish different phases of deformation and the sequential development of structures. Structural geological conventions are therefore adopted (cf. Hambrey & Milnes, 1977) to describe structures in order of formation, as indicated by cross-cutting relationships. Planar structures (surfaces) are usually labeled S_0, S_1, S_2... in ascending order of formation, using criteria outlined by Hambrey and Lawson (2000), Goodsell, Hambrey, and Glasser (2005), and Cuffey and Paterson (2010), with associated fold phases termed F_1, F_2... indicating major phases of deformation. As is the case for rocks, glacier ice undergoes polyphase deformation (i.e., it is subjected to several phases of deformation). However, polyphase deformation suggests that deformation phases are temporally separated. In glaciers, phases of deformation sometimes merge into one another to form continuous phases, whereas in some cases phases are totally separate. As the whole ice mass is deforming at the same time, separate deformation phases occur simultaneously (i.e., S_0 formation in the accumulation area may be occurring at the same time as S_3 formation lower down the glacier), thus temporal separation of deformation phases is impossible (Hambrey & Milnes, 1977; Hambrey & Lawson, 2000), a concept that is, tentatively being adopted in geological investigations (e.g., Gray & Mitra, 1993). Therefore, deformation phases in glaciers are not related to a temporal scale, but are related to the passage of a parcel of ice through the ice mass (Hambrey & Lawson, 2000). Lesser glaciological structures such as crystal quirks and unconformities are usually excluded from the sequential description of structure formation because they are regarded as unimportant with regard to the structural evolution of a whole ice mass (Goodsell, Hambrey, & Glasser, 2005).

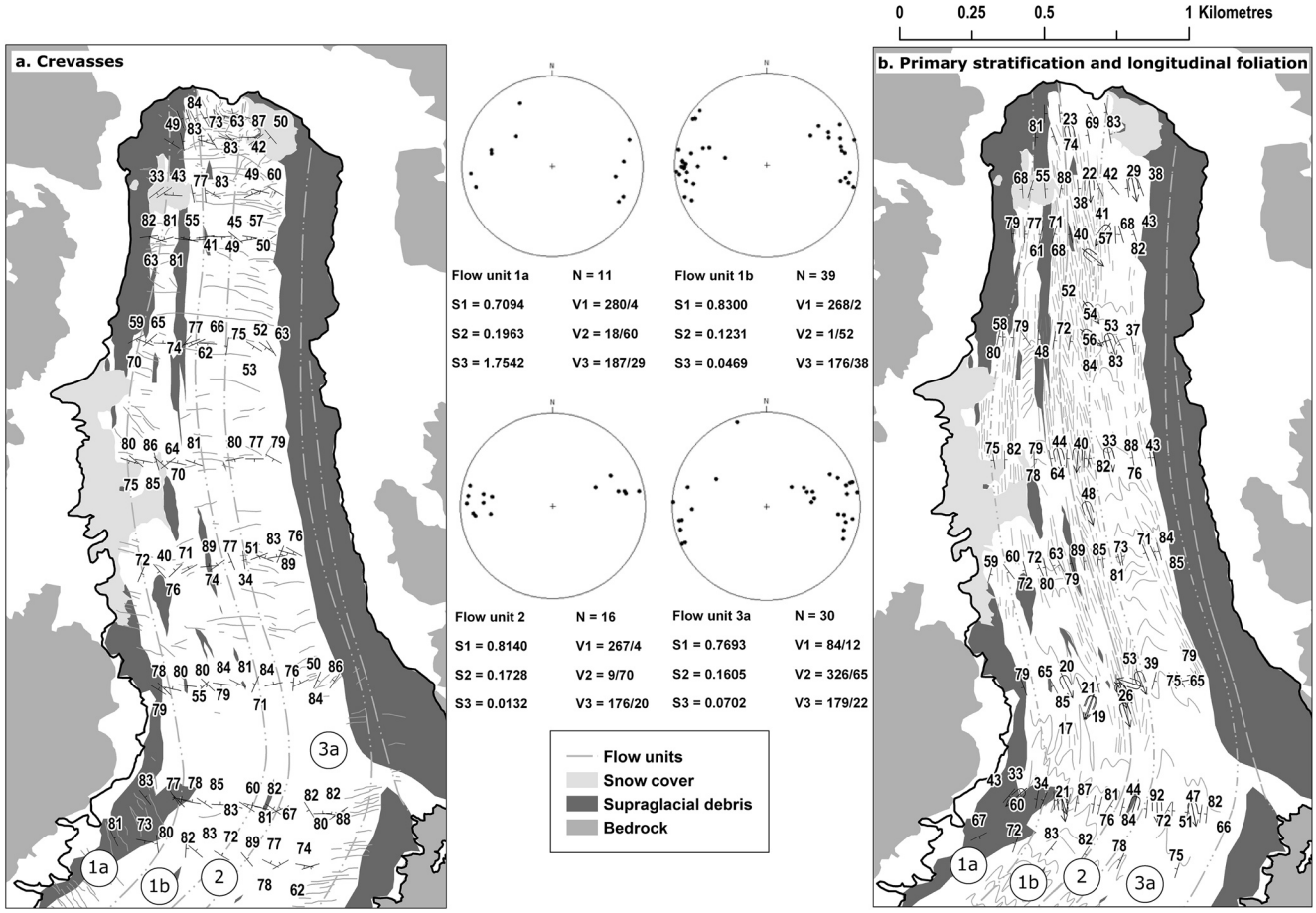

Figure 8. Example of a structural map with three-dimensional data: the tongue of Vadrec del Forno, SE Switzerland. (a) Flow unit boundaries, flow units, and crevasses. (b) Primary stratification and longitudinal foliation. In both maps dip and strike measurements are shown. The central column illustrates Schmidt equal-area stereographic projections (lower hemisphere) of longitudinal foliation in the individual flow units. Eigenvalues (S1, S2, and S3) and Eigenvectors (V1, V2, and V3) are also given (modified from Jennings et al., 2014).

4.2. Structural Glaciological Analytical Methods

The basis for analyzing structures in glaciers is field mapping. This involves the identification and spatial investigation of structures, determining their 3-D orientation, cross-cutting relationships, and progressive changes in geometry downglacier. Traditional analyses, from the 1960s to 1980s, relied on theodolite or plane-table mapping of key glacier features and the positions of stakes to record ice movement, supplemented by aerial photograph interpretation where available. Complementing these techniques was measuring the orientation of structures in the field using the simple but effective combination of an ice axe and a compass/clinometer (Figure 8). Data were then analyzed in 3-D using lower hemisphere stereographic projections, as widely used in structural geology (e.g., Allen et al., 1960; Hambrey, 1976b; Hambrey & Milnes, 1977; Hambrey & Müller, 1978; Meier, 1960; Ragan, 1969).

Using a similar approach to plotting 3-D data, measuring the orientation of stones (clasts) in basal ice has also contributed to better understanding of deformation mechanisms in glaciers, and also the deposition of different types of till, as demonstrated, for example, by Lawson (1979) on Matanuska Glacier, Alaska. Evolving from this technique is the relatively novel technique of determining the "anisotropy of magnetic susceptibility," which involves measuring the orientation of magnetic particles in small drill cores, and plotting the data on stereographic projections. The technique is useful for examining the deformation processes associated with glacier motion, including the development of lineations and folds (Fleming et al., 2013).

The importance of determining strain-rate tensors was recognized as important for understanding how some structures, such as foliation and crevasses, formed. Various methods using arrays of stakes have been used on scales of meters to hundreds of meters, by measuring the changes in length between stakes and calculating the principal strain-rate tensors (e.g., Hambrey & Müller, 1978; Knight, 1992; MacAyeal, 1985; Meier, 1960; Nye, 1959a).

Some of the early studies went hand-in-hand with geochemical analysis of the different ice types that make up the structures. Oxygen isotope analysis was based on the assumption that O^{18}/O^{16} ratios in fallen snow become more negative with altitude, and that the signal would transfer through a glacier at different depths and rates (Epstein & Sharp, 1959; Hambrey, 1974; Sharp et al., 1960). They could also be used to assess the role of meltwater refreezing into certain structures, such as basal ice or foliation (Hubbard & Sharp, 1993; Hubbard et al., 2004; Lawson & Kulla, 1978).

The above techniques have stood the test of time, and have remained the basis of many subsequent structural glaciological investigations. However, a much wider range of tools is now available. At ground level, mapping of glaciers is more efficiently achieved nowadays using differential GPS and laser-scanning techniques. Satellite remote sensing imagery has allowed the structure of large ice masses to be investigated, including ice shelves and ice streams (e.g., Ely & Clark, 2016; Ely et al., 2017; Fahnestock et al., 2000; Glasser & Gudmundsson, 2012; Glasser & Scambos, 2008; Glasser et al., 2015; Hambrey & Dowdeswell, 1994; Reynolds & Hambrey, 1988). Of indirect value to interpreting structures is the use of satellite data to quantify the dynamics of ice masses, including interferometry, feature-tracking, and speckle-tracking (e.g., Jiskoot et al., 2017; Luckman et al., 2002; Mansell et al., 2012; Medrzycka et al., 2019; Murray, Luckman, et al., 2003; Murray, Strozzi, et al., 2003; Pritchard et al., 2005; Quincey et al., 2009). Another remote-sensing technique which is in the early stages of implementation in glacier studies is Light Detection and Ranging (LiDAR), as reviewed for the cryosphere by Bhardwaj et al. (2016). To date, these techniques have been used to determine velocity, surface roughness, and surface shapes (Telling et al., 2017). However, these techniques have not yet been fully exploited to determine the strain-rates and cumulative strains that would be useful in structural interpretation.

Other techniques are now available for obtaining very-high resolution imagery of glacier surfaces and ice cliffs. They include unmanned aerial vehicles (UAVs) or drones, coupled with "structure-from-motion" (SfM) software using images from digital cameras to create ortho-rectified maps and digital elevation models (DEMs) (e.g., Jones et al., 2018; Rippin et al., 2015; Westoby et al., 2012). UAVs also provide an adaptable platform for a wide array of other sensor types (e.g., multispectral, hyperspectral, LiDAR, and photogrammetric stereos), that are increasingly being used for cryospheric research (cf. Gaffey & Bhardwaj, 2020; Li et al., 2020).

Ground-penetrating radar is now used widely to determine the subsurface structure of glaciers. On glaciers, radar instruments are dragged across the surface, either by hand (over bare ice) or by snow-scooter (over snow). Although generally used to investigate glacier hydrology, a few studies have focused on the formation of alleged thrust-faults and fold structures (Hambrey et al., 2005; Murray & Booth, 2010; Murray et al., 1997; Woodward et al., 2002, 2003) or debris content (K. Winter et al., 2019). In contrast, airborne radio-echo sounding can cover vast swathes of the Antarctic and Greenland ice sheets, revealing their internal structure, especially stratification and folding (e.g., Ross et al., 2020; Siegert & Kwok, 2000; Siegert et al., 2005). Increasingly, radiostratigraphic data are being correlated with intersecting deep ice cores to identify age-depth constraints for internal reflection horizons. As these englacial layers can often be considered as isochrones, these techniques enable the extrapolation of ice core data to much larger areas, providing valuable insights into past ice sheet dynamics and paleoaccumulation variability (e.g., Ashmore et al., 2020; Bodart et al., 2021; Cavitte et al., 2016; MacGregor et al., 2015, 2016; A. Winter et al., 2019).

It is also possible to investigate the internal structure of valley glaciers, ice sheets, and ice shelves, by using a hot-water drill to create a borehole, which is then imaged and logged using an optical televiewer (e.g., Ashmore et al., 2017; Hubbard & Malone, 2013; Hubbard et al., 2008, 2021; Roberson & Hubbard, 2010). The scanned image of the borehole is transformed to appear as a core; in this way structures such as primary stratification, crevasse traces, folds, and foliations can be measured.

In summary, with the technological advances of recent decades, including the manufacture of instruments that are affordable, the potential for structural analyses of glaciers and ice sheets is far greater than it was when the researchers of the 1960s and 1970s had relatively few tools available. That said, interpretations on a grand scale, still need to rely on familiarity with the intricacies of structures that can only be viewed at ground level. However, there has never been a more exciting time to engage with the field of structural glaciology.

5. Glacier Structures and Their Kinematic Significance

Glaciers can have multiple source areas which each provide a stream of ice, referred to as a "flow unit," that converge to form the glacier tongue. Glaciers in Svalbard are examples of those with multiple source areas, commonly associated with complex cirques. Adjacent flow units have different histories, with each being recognizable through the glacier to the snout. Flow-unit boundaries are defined either by medial moraines (Figure 9a) or zones of intense foliation (Figure 9b). This section provides a systematic description of all of the principal structures found in glacier ice, beginning with primary structures and then covering secondary structures (ductile and brittle). In the context of an evolving ice mass, the key structures are further interpreted in terms of their kinematic significance.

5.1. Primary Structures

The dominant primary structure found in glaciers is stratification, which generally comprises surface-parallel ice layers differentiated from one another by varying ice crystal size, bubble content, and dirt content. The stratified nature of the ice represents the annual layering of snowfall deposited parallel to the glacier surface, preserved during firnification (Figure 10a) (Hambrey, 1976b, 1994; Hambrey & Lawson, 2000; Lewis, 1960). Stratified ice, preserved in cores obtained through ice sheets and ice caps, provide a rich source of chemical data, from which high-resolution climatic records have been obtained. Boundaries between strata represent surfaces of uniform age or isochrones (Cuffey & Paterson, 2010, Ch. 15). In certain areas, notably the edges of ice caps or ice sheets that have undergone little-deformation, it is possible to obtain a stratigraphic record that is, equivalent to ice cores, albeit a less complete one (MacGregor et al., 2020). In some places, these isochrones are emphasized by ash layering in, or within range of, volcanically active regions. Examples of tephra within ice stratigraphy are in Greenland ice cores that originated from Iceland (Grönvold et al., 1995; Mortensen et al., 2005), in glaciers on active volcanoes in New Zealand (Figure 10b), in the Antarctic Peninsula region (Ximenis et al., 2000), and in correlating a single event 1,252 years ago across the East and West Antarctic Ice Sheets (Lee et al., 2019).

The different ice facies (i.e., types of ice) reflect seasonal variations in initial snowpack formation (Wadham & Nuttall, 2002). In a typical temperate glacier, relatively thick layers of coarse bubbly ice represent winter snow accumulation that has undergone partial melting and refreezing. High-density coarse clear ice is the result of meltwater refreezing as a layer at the base of the winter snowpack. Relatively thinner strata consisting of fine ice crystals represent summer snow accumulation. In polythermal glaciers, some or most of the accumulation is in the form of superimposed ice, which results from a saturated snowpack. The resulting ice is dense but retains air bubbles. In cold glaciers, where no melting occurs, a wind-hardened surface, or variations in bubble-concentrations controlled by temperature and accumulation rates (Spencer et al., 2006), may mark the boundary between strata. In all glacier types, summer layers often contain eolian-derived dust and organic material, which becomes trapped in surface snow (Cuffey & Paterson, 2010; Goodsell, Hambrey, & Glasser, 2005; Hambrey, 1994; Jennings et al., 2014; Oerlemans et al., 2009). Periods of excessive surface ablation may remove many previous layers producing an unconformity (Figure 10c), representing a hiatus in the systematic deposition of snow layers (Goodsell, Hambrey, & Glasser, 2005; Goodsell, Hambrey, Glasser, Nienow, & Mair, 2005; Hambrey, 1994). Conversely, unconformities can also arise from irregularities in topography, leading to local net accumulation in areas other than the upper reaches of the ice mass (Hudleston, 2015). Less important primary structures form as summer meltwater percolates down through the snowpack, refreezing as spatially limited ice lenses or glands (Hambrey, 1994; Hambrey & Lawson, 2000).

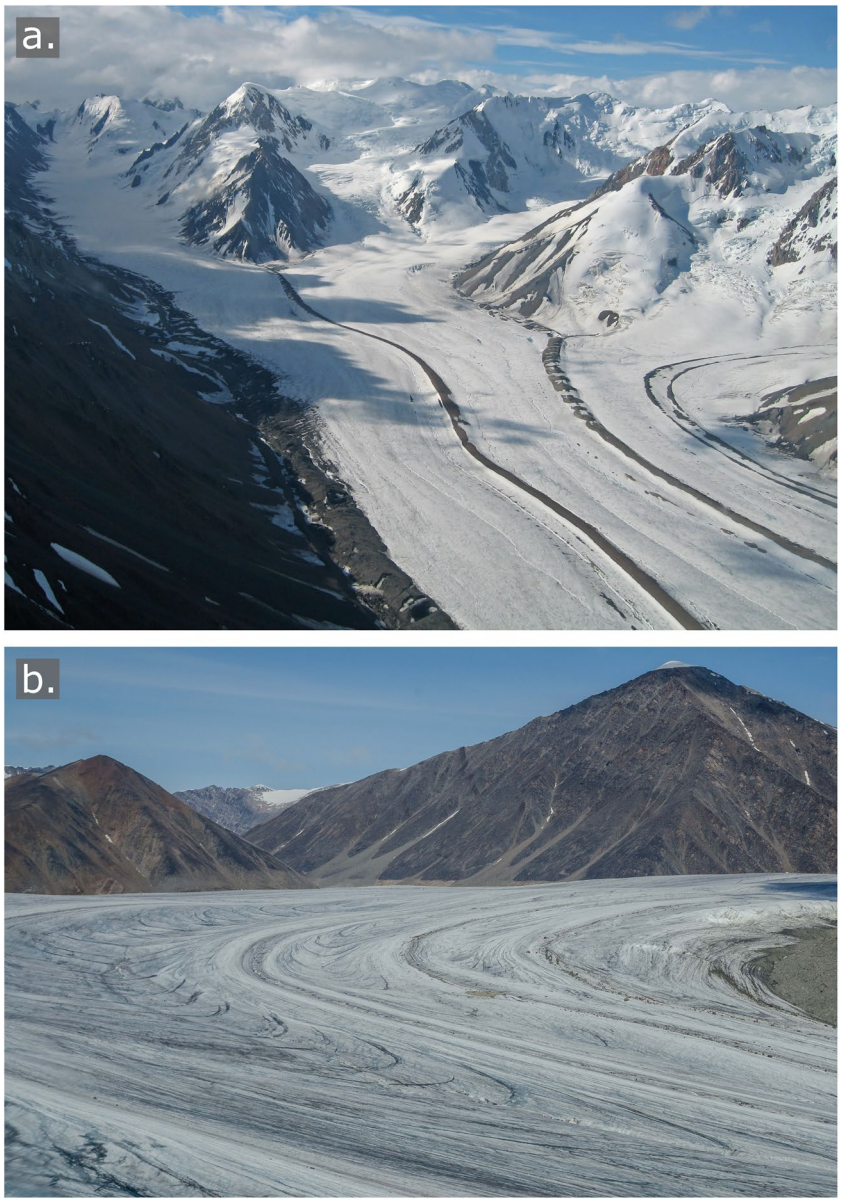

Figure 9. Flow units defined by: (a) Medial moraines, Kaskawulsh Glacier, South Arm, Yukon, Canada; (b) Zones of strong longitudinal foliation (the darker streaks) between sets of arcuate structures, Fountain Glacier, Bylot Island, Canada.

Spatially limited primary structures include snowbanks formed adjacent to ice cliffs, which may produce wedges or layers at the glacier base by the process of apron-entrainment (Figure 10d) (Evans, 1989b). Ice breccias form as ice walls collapse at glacier margins through dry calving, and may then be modified by being over-ridden during the apron-entrainment process (discussed further in Section 9.2) (Figure 10e). Ice breccias can form from the collapse of crevasse walls and séracs, and from incised or marginal meltwater channels. Breccias are also the principal component of rejuvenated glaciers, where ice avalanches down steep slopes provide a low-level accumulation zone, comprising broken ice from above. Trapped snow or refreezing of interstitial meltwater between ice debris particles commonly fuses the breccia together.

One structure that could be classified as both primary and secondary is regelation layering (Figure 10d). This structure forms as a result of glacier motion, whereby pressure melting at the ice-bed interface occurs upglacier of small bedrock hummocks, followed by refreezing downglacier of them. This process produces

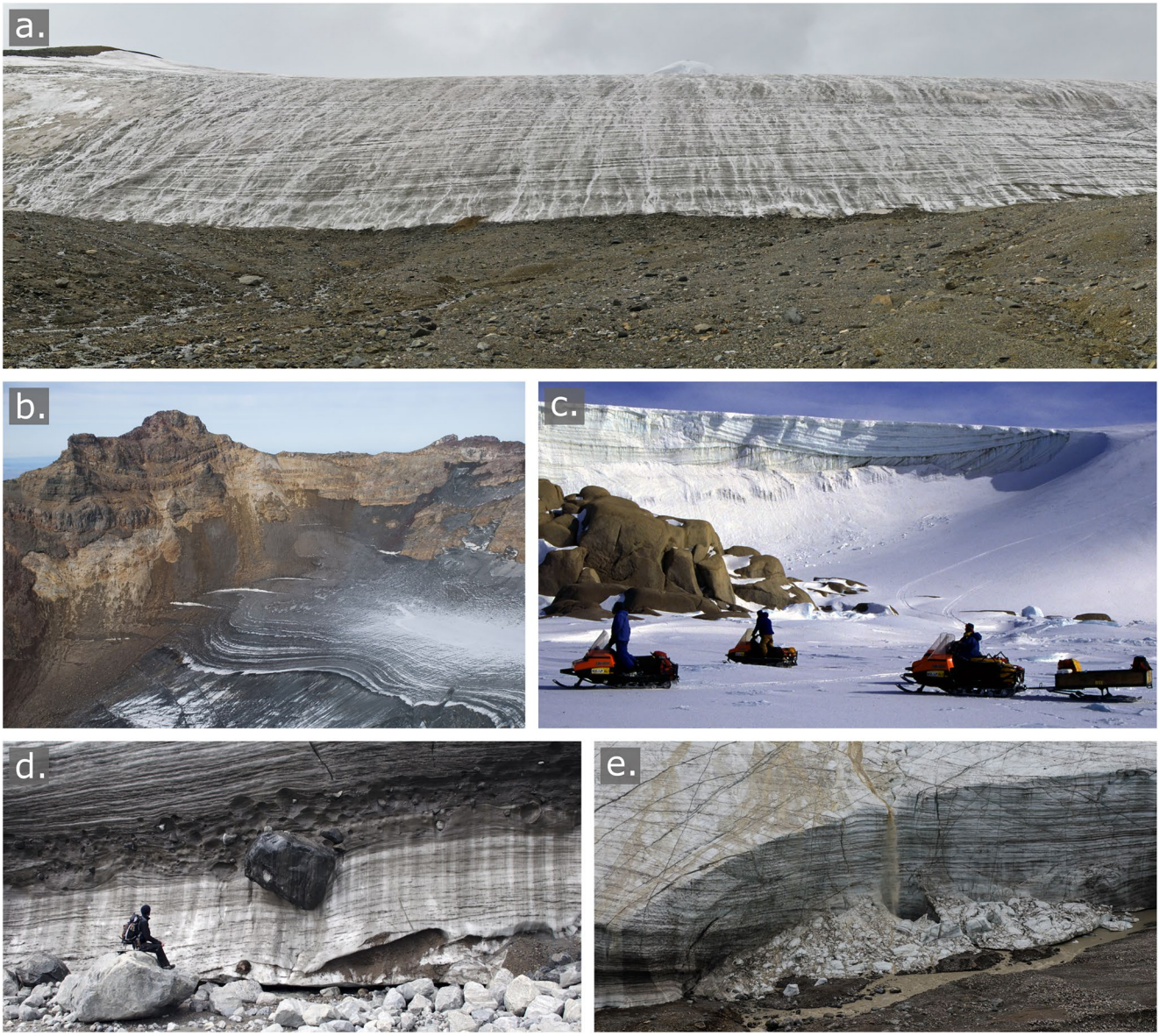

Figure 10. Principal types of primary structure. (a) Sedimentary stratification in the north arm of Trapridge Glacier, Yukon, with the summer snowline visible at top left. (b) Stratification, emphasized by ash layering, in a crater glacier on the active volcano of Ruapehu, New Zealand. (c) Unconformity in stratified ice exposed in an ice cliff above Granite Harbor, Victoria Land, Antarctica. (d) Snow bank (light-colored) accreted at the base of Fountain Glacier, Bylot Island, Canada, by apron-entrainment. The snow bank merges with the darker layered basal ice zone of the glacier, and together the ice and snow are sheared. (e) Dry calving at Fountain Glacier has resulted in the accumulation of ice blocks which form an ice breccia. Apron-entrainment would occur if the glacier was advancing, but in this 2014 photograph it is receding. The dominant structure in the glacier here is an assemblages of crevasse traces rotated to a near-horizontal attitude.

parallel-laminated ice layers (with individual layers usually 0.1–1 mm thick) that contain varying amounts of basal debris (a primary structure) (Hubbard & Sharp, 1989, 1995), but simple shear at the glacier bed results in this layering being deformed, and in such cases bed-parallel isoclinal folds are common (a secondary structure).

Primary structures are best preserved in cirque glaciers or small valley glaciers, good mapped examples being Veslgjuv-breen in southern Norway (Grove, 1960a); Charles Rabots Bre in northern Norway (Hambrey, 1976b); Johnsons Glacier on Livingston Island, Antarctica (Ximenis et al., 2000); and San José and Lachman glaciers on James Ross Island, Antarctica (Figure 11) (Carrivick et al., 2012). In larger valley glaciers, overprinting by foliation and crevasses destroys most vestiges of stratification.

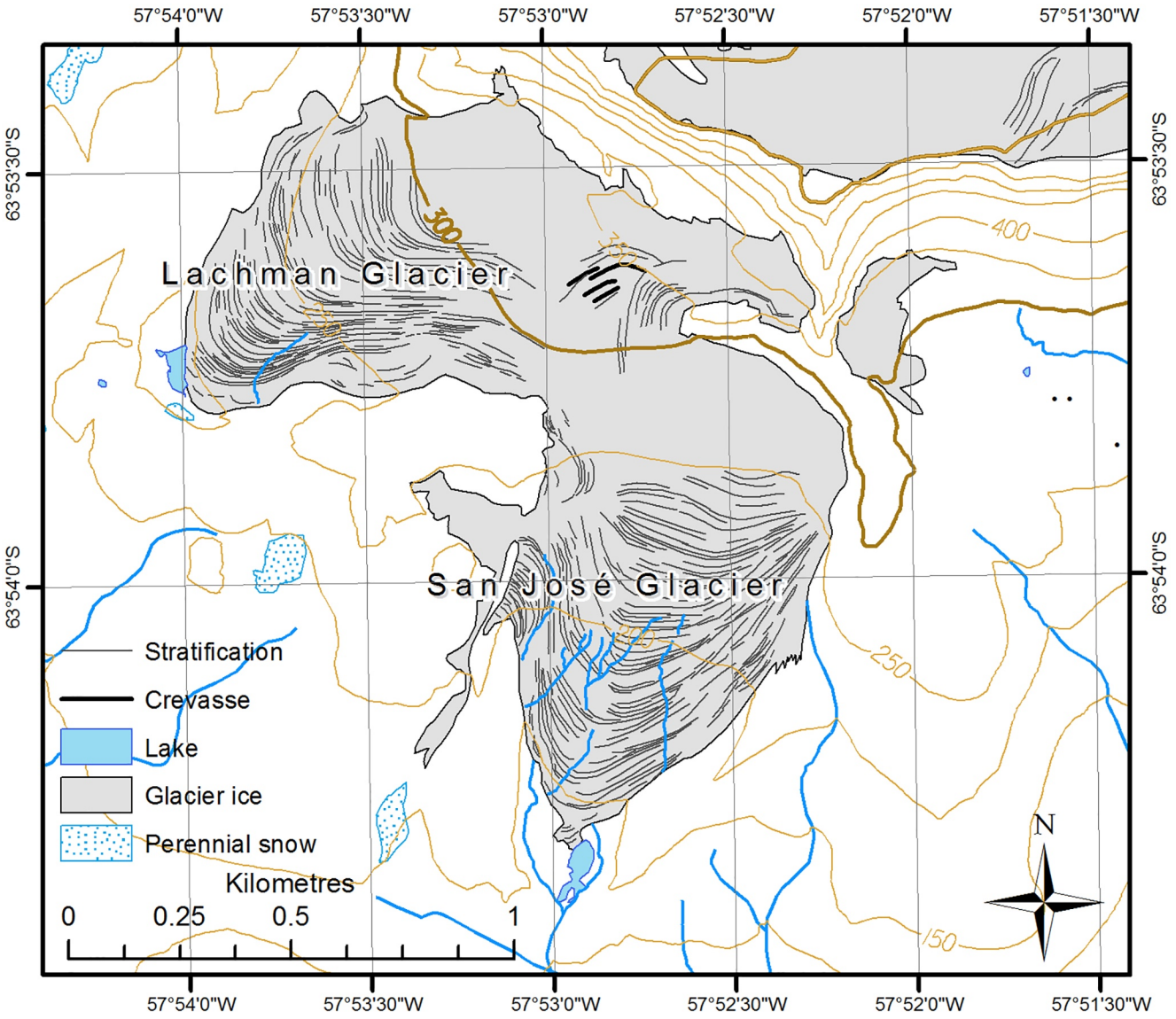

Figure 11. Map of stratification of two adjoining cirque glaciers, San José and Lachman glaciers, on James Ross Island, Antarctica. Surface-parallel accumulation layering becomes deformed by faster flow in the middle of each glacier (modified from Carrivick et al., 2012).

Stratification in glaciers within amphitheater-like cirques generally has a simple geometry, as studies on Vesl-Skautbreen have demonstrated (Grove, 1960b; McCall, 1960). The youngest snow and firn follows the contours of the glacier surface, dipping down glacier. Following the centerline of the glacier in the direction of flow, the stratified firn is transformed into ice through burial, and rotates to an up-glacier dip of 30°–45° at the firn line. Similarly, dip increases toward the margins of the glacier. Thereafter, the dip decreases as deeper ice is exposed by ablation, so that at the snout the structure is parallel to the bed. Spatially, the surface outcrop of stratification is deformed into convex down-facing arcs, giving rise to a basin-like structure in 3-D (Grove, 1960b). The flow process envisaged in this work was "rotational slip" (Clark & Lewis, 1951), which was subsequently elaborated to one combining a component of "extrusion flow," and showing analogies with rotational landslides (McCall, 1960).

Most cirques have a more complex morphology than that described above. The geometry of stratification reflects this, especially when ice flows out of a wide accumulation basin into a narrower tongue, as the studies of Charles Rabots Bre and Johnsons Glacier have shown. Valley glaciers may preserve folded

stratification throughout much of their length unless overprinted by foliation (Section 5.3.2) and crevasse traces (Section 5.2.2).

5.2. Brittle Structures

5.2.1. Crevasses

Crevasses are open tensional fractures that result from the brittle failure of glacier ice in response to stress, usually as a consequence of ice flowing over bed topography or through a variable channel geometry. They are a common structure, found in almost all ice masses (e.g., Benn & Evans, 2010; Colgan et al., 2016; Cuffey & Paterson, 2010; Hambrey & Lawson, 2000; Harper et al., 1998; Hodgkins & Dowdeswell, 1994; Holdsworth, 1969; Hudleston, 2015; Meier, 1960; Nath & Vaughan, 2003; van der Veen, 1998a), and can influence the surface mass balance of a glacier by enhancing supraglacial ablation and meltwater retention (Colgan et al., 2016). Crevasses range in length from a few meters to several kilometers, and reach depths of several tens of meters. Consequently, they are a major obstacle to glacier travel, and represent a major hazard when bridged by snow. Crevasses are important in understanding how glaciers flow and deform, how surface meltwater can reach the bed and influence basal sliding and discharge of ice into the ocean, and how calving and iceberg-forming processes take place. In a geological context, crevasse formation is analogous to brittle deformation at the surface of Earth's crust, for example, the faults in young oceanic crust on the Mid-Atlantic Ridge. This comparison contrasts with the deeper ductile structures, such and folds and foliation, which are more akin to deformation in metamorphic terrains (Herzfeld & Mayer, 1997). For a comprehensive review of crevasses, also see Colgan et al. (2016).

Fracture propagation occurs in three fundamental ways (fracture modes) depending on the configuration of the applied stress (Figure 12a) (Benn, Warren, & Mottram, 2007; van der Veen, 1998a, 1999):

1. *Mode I* ("*opening*"): Tensile stresses applied normal to the fracture plane pull the sides of the fracture apart. Crack propagation occurs perpendicular to the direction of maximum extension.
2. *Mode II* ("*sliding*"): The fracture walls remain in contact while shear stress is applied parallel to the fracture plane. Crack propagation occurs in the same direction as the applied shear stress.
3. *Mode III* ("*tearing*"): Shear stress is again applied parallel to the fracture plane; however, crack propagation occurs at right angles to the applied shear stress.

It is often assumed that surface crevasses form primarily in response to tensile stress (fracture Mode I), initially developing normal to the maximum extending strain-rate (van der Veen, 1998a). However, a combination of fracture modes can occur simultaneously, which is referred to as mixed-mode fracture (Colgan et al., 2016; van der Veen, 1999). A range of crevasse orientations can exist, depending on the morphology of the glacier trough and the stress regimes present. Nonetheless, surface fracturing is primarily associated with areas of fast and extending flow, such as in icefalls (Benn, Hulton, & Mottram, 2007; Benn, Warren, & Mottram, 2007; Hambrey & Lawson, 2000; Harper et al., 1998). Despite the widespread nature of the structure, crevasse formation is relatively poorly understood (Nath & Vaughan, 2003; van der Veen, 1998a), yet has been receiving increasing attention in recent years (Colgan et al., 2016).

The presence of a crevasse at the surface of glacier suggests that a fracture criterion must have been met or exceeded to induce fracturing (Campbell et al., 2013; Vaughan, 1993). A variety of studies have attempted to identify the criterion required to initiate crevasse formation, yet this has proved to be an intractable problem, primarily because the tensile strength of ice can be highly variable depending on different ice properties (Campbell et al., 2013). Some studies have suggested that fracturing occurs once a critical strain-rate value has been exceeded (e.g., Meier, 1958; Meier et al., 1974; Vornberger & Whillans, 1990). However, field observations on White Glacier, Axel Heiberg Island, indicated that this was not necessarily the case, and that there was no simple relationship between principal tensile strain-rate and crevasse initiation (Hambrey & Müller, 1978). Other authors have proposed that a critical tensile stress must be met to induce crevassing (e.g., Kehle, 1964). Vaughan (1993) further developed this idea, producing stress-failure envelopes for 17 polar and alpine glaciers. These data suggest that the tensile stress required for the fracture of glacier ice is variable, but generally lies in the range from 90 to 320 kPa (Campbell et al., 2013; van der Veen, 1998a, 1998b; Vaughan, 1993), whereas Forster et al. (1999) found that tensile stresses in the range of 169–224 kPa are sufficient for crevasse formation in temperate ice. Vaughan (1993) also found no systematic

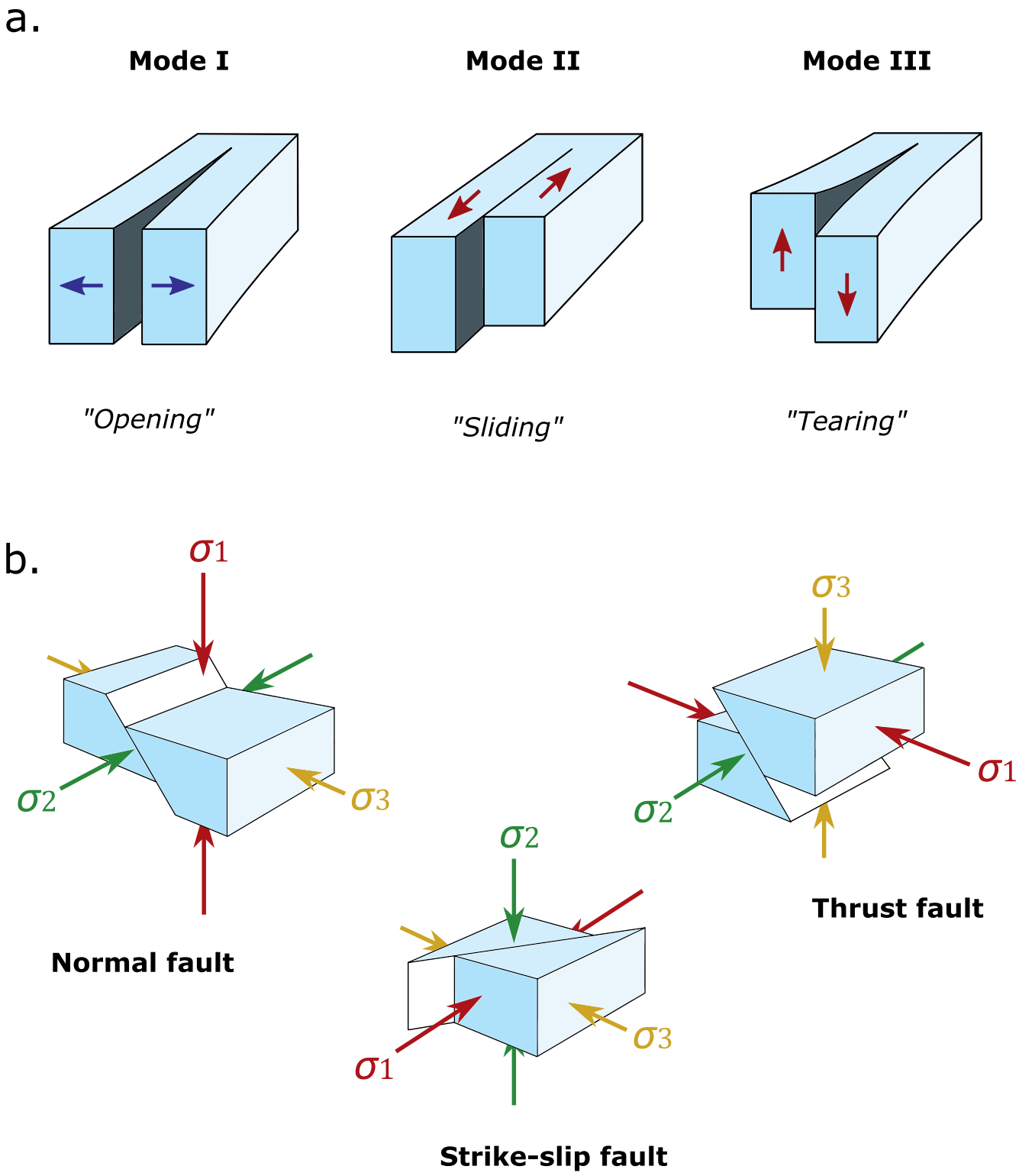

Figure 12. Schematic diagrams illustrating the different possible modes of fracture and types of fault in glacier ice. (a) The three different modes of fracturing that develop in response to tensile stresses (Mode I) and shear stresses (Modes II and III). Note that in all cases, fracture propagation is toward the page. (b) Graphical representation of the three main types of faulting in glacier ice with the orientation of the principal stress tensors at formation (σ_1—red—maximum, σ_2—green—intermediate, σ_3—yellow—minimum) (Figure 12a modified from Benn, Warren, & Mottram, 2007; and Figure 12b modified from Fossen, 2010).

relationship between tensile strength and temperature, in contrast to Meier's (1958) assumption that cold ice has a greater tensile strength than warm ice. Variations in tensile strength were explained by differences in ice rheology, such as ice crystal size, orientation, impurity content, or density (Campbell et al., 2013; van der Veen, 1998a; Vaughan, 1993). This conclusion was reiterated and amplified by Whillans et al. (1993) who suggested that surface crevasses in an Antarctic ice stream preferentially formed in veins of recrystallized ice with a softer rheology to the surrounding ice. Crevasse spacing may also be critical, with closely spaced crevasses requiring a larger tensile stress to form than well-spaced crevasses (van der Veen, 1999).

The depth to which crevasses propagate has also been an area of debate. Applied tensile stress often exceeds the tensile strength of the ice throughout the full thickness of the ice mass. However, open air-filled crevasses tend to be confined to a comparatively shallow surface layer. As the penetration depth of a crevasse increases, the deviatoric tensile stress that pulls the walls of the crevasse apart become increasingly offset by the compressive stress exerted by the overburden pressure of the overlying ice, also referred to as weight-induced lithostatic (cryostatic) stress (van der Veen, 1999). For closely spaced crevasses the maximum fracture depth can be defined as the point where the tensile stress equals the overburden compressive stress (Benn, Hulton, & Mottram, 2007; Benn, Warren, & Mottram, 2007; Nye, 1955, 1957; van der Veen, 1998a). On theoretical grounds, air-filled crevasses are thought to penetrate to a maximum depth of c. 30 m in temperate glaciers (Nye, 1957; Seligman, 1955), whereas a number of field observations indicate that fracturing can exceed this value by up to 50% (Hambrey, 1976b; Holdsworth, 1969; Meier, 1958; Mottram & Benn, 2009). Even though a maximum depth of c. 30 m is a good estimate for crevasse penetration depths in areas of closely spaced crevasses, Weertman (1973) argued that solitary crevasses could penetrate to a much greater depth. For an isolated fracture in a stressed material, stress concentrates at the crack tip, amplifying the applied stress at that point. As a consequence, crevasse depth may be significantly increased. Downward propagation of a crevasse tip can be modeled using a "linear elastic fracture mechanics" approach (van der Veen, 1999). This is based on the assumption that glacier ice contains small cracks and flaws that may develop into larger fractures if the stress concentrations are sufficiently large at the tip of the crack. The main drawbacks of this approach are: (a) that ice or firn is not strictly a linear elastic material and viscous flow and deformation may affect stress concentration at the tip; and (b) crevasse initiation requires starter cracks, such as microfractures in the ice crystal structure (van der Veen, 1999). Overall, however, in highly crevassed areas, the effect of stress concentration is comparatively small (van der Veen, 1998a). Therefore, in such areas, the theoretical penetration depth of Mode I fractures can be assumed to be where the tensile strain rate is exactly balanced with the overburden pressure, which is given by Nye's (1957) equation:

$$d = \frac{2}{\rho_i g}\left(\frac{\dot{\varepsilon}}{A}\right)^{1/n} \tag{9}$$

where d is depth, ρ_i is the density of ice, g is gravitational acceleration, $\dot{\varepsilon}$ is strain rate, and A and n are the flow law parameters.

The presence of water in a crevasse also has a large influence over the depth to which the fracture can penetrate, resulting from the density difference between ice and water (Alley et al., 2005; Benn, Warren, & Mottram, 2007; Boon & Sharp, 2003; Fountain, Jacobel, et al., 2005; Fountain, Schlichting, et al., 2005; Robin, 1974; van der Veen, 1998a, 2007; Weertman, 1973). In a water-filled crevasse, the pressure exerted by the weight of the water column acts in the same direction as the deviatoric tensile stress, forcing the crevasse walls apart by a process known as "hydrofracturing." As the crevasse propagates deeper, the pressure exerted by the increasing water column (provided there is a sufficient supply of water) enables the fracture to penetrate further, eventually reaching the bed (Alley et al., 2005; Benn, Warren, & Mottram, 2007; Benn et al., 2009; van der Veen, 1998a, 2007). In this situation, an additional term can be added to Equation 9 to account for the effect that water has on crevasse penetration depth:

$$d = \frac{2}{\rho_i g}\left[\left(\frac{\dot{\varepsilon}}{A}\right)^{1/n} + \left(\rho_w g d_w\right)\right] \tag{10}$$

where ρ_w and d_w are the density and depth of the water in the crevasse, respectively. Crevasse propagation to the bed has important implications for meltwater drainage and basal velocities in temperate and polythermal glaciers and in the Greenland Ice Sheet, as discussed in Section 9.4.

Basal crevasses are fractures that propagate from the bed of a glacier or base of an ice shelf up into the ice mass. Originally suggested by Weertman (1980), van der Veen (1998b) demonstrated that basal crevasses could only exist under specific circumstances. To overcome the high overburden compressive stresses present at the base of an ice mass, large tensile stresses and very high basal water pressure are required. It is likely that these conditions are almost exclusively met when ice is rapidly extending and near to, or at, flotation (Benn, Warren, & Mottram, 2007; Bentley et al., 1987; van der Veen, 1998b; Weertman, 1980), being primarily associated with tidewater glaciers (Mickelson & Berkson, 1974) and ice shelves (see Section 8.4.3) (Luckman et al., 2012; McGrath, Steffen, Rajaram, et al., 2012; McGeath, Steffen, Scambos, et al., 2012). Since they are rarely observed, few data have been collected on basal crevasses. However, it has been suggested that they play a role in ice-calving processes (e.g., Benn, Hulton, & Mottram, 2007, Benn, Warren, & Mottram, 2007; van der Veen, 1998b; Venteris, 1997), are important for the development of ice-shelf rifts and ice-shelf break-up (McGrath, Steffen, Rajaram, et al., 2012; McGeath, Steffen, Scambos, et al., 2012), and may be more abundant in Antarctic ice shelves than previously thought (Luckman et al., 2012). The formation of basal crevasses in grounded ice masses and valley glaciers was considered to be unlikely except in exceptional circumstances (Bentley et al., 1987); however, recent studies suggest that the formation of basal crevasses may be more common in these types of ice masses than previously assumed (Harper et al., 2010). The presence of crevasse-squeeze ridges on glacier forefields suggests that there could be sufficiently high basal water pressures to develop basal crevasses during a surge phase (e.g., Evans & Rea, 1999, 2003; Evans et al., 2007; Kamb et al., 1985; Lawson, 1996; Rea & Evans, 2011; Sharp, 1985), a jökulhlaup (e.g., Kozarski & Szupryczynski, 1973), or in glaciers with an overdeepened basin (e.g., Ensminger et al., 2001).

Crevasses present in the tongue of marine- and lacustrine-terminating glaciers play an important role in the calving of icebergs. Iceberg calving is a significant component of glacier mass loss, especially from the Antarctic and Greenland ice sheets, which has direct implications for sea-level rise. Water depth and glacier thermal regime determines whether or not the glacier tongue is floating, and that determines the nature of the resulting icebergs. Typically, polythermal glaciers terminating in deep water produce tabular icebergs, such as in the deep fjords of Greenland (Figures 13a and 13b). In contrast, in shallow water, such as found in the fjords and coastal areas of Svalbard, where the terminal ice cliff rests on the sea bottom, calving produces irregularly shaped and smaller icebergs (Figures 13c and 13d). Temperate glacier tongues, such as those in Alaska and Patagonia, rarely float, and calving characteristics resemble those in Svalbard.

The calving process requires that pre-existing or newly developed fractures penetrate to sufficient depths to isolate blocks from the main glacier body, which subsequently drift away from the glacier terminus. Therefore, the location, magnitude, and frequency of calving events are directly influenced by fracture propagation, orientation, and distribution (Benn, Warren, & Mottram, 2007). However, as the penetration of surface Mode I fractures is limited to a comparatively shallow surface layer, the presence of meltwater can play an important role, enabling deeper fracture propagation through hydrofracturing (Benn & Åström, 2018; Benn, Warren, & Mottram, 2007; Benn et al., 2009; van der Veen, 1998a, 2007). Also, in situations where the ice is at, or near, flotation, water-filled basal crevasses can play a major role by penetrating through much of the ice thickness (Benn & Åström, 2018; van der Veen, 1998b). In both cases, fracture propagation through the majority of a glacier's thickness can potentially lead to iceberg calving.

In addition to macro-scale crevassing, micro-scale fracturing of glacier ice also has implications for calving. Ice failure at low deformation rates can occur as micro-fractures accumulate, effectively on a large-scale softening the rheology of the ice (Benn & Åström, 2018; Pralong & Funk, 2005; Weiss, 2004). The combined effect of macro- and micro-fracturing is collectively termed "damage," which influences the bulk properties of glacier ice, and increases the likelihood of bulk ice failure.

In situations where ice accumulates a lot of damage, such as at the margins of ice streams, intense fracturing effectively softens the rheology of the ice. Consequently, when entering an ice shelf, the highly fractured ice has a reduced capability to buttress inland ice, increasing ice-flow velocities, and ultimately amplifying the potential for bulk failure and iceberg calving (Benn & Åström, 2018; Sun et al., 2017).

The ultimate end-member of damaged glacier ice is "sikussaq" or "ice mélange" (Figure 13a), which develops as calved icebergs, bergy bits, and brash ice accumulate, either as a mass of free-floating ice debris, or fused together by sea ice (Amundson et al., 2010; Benn & Åström, 2018; Burton et al., 2018).

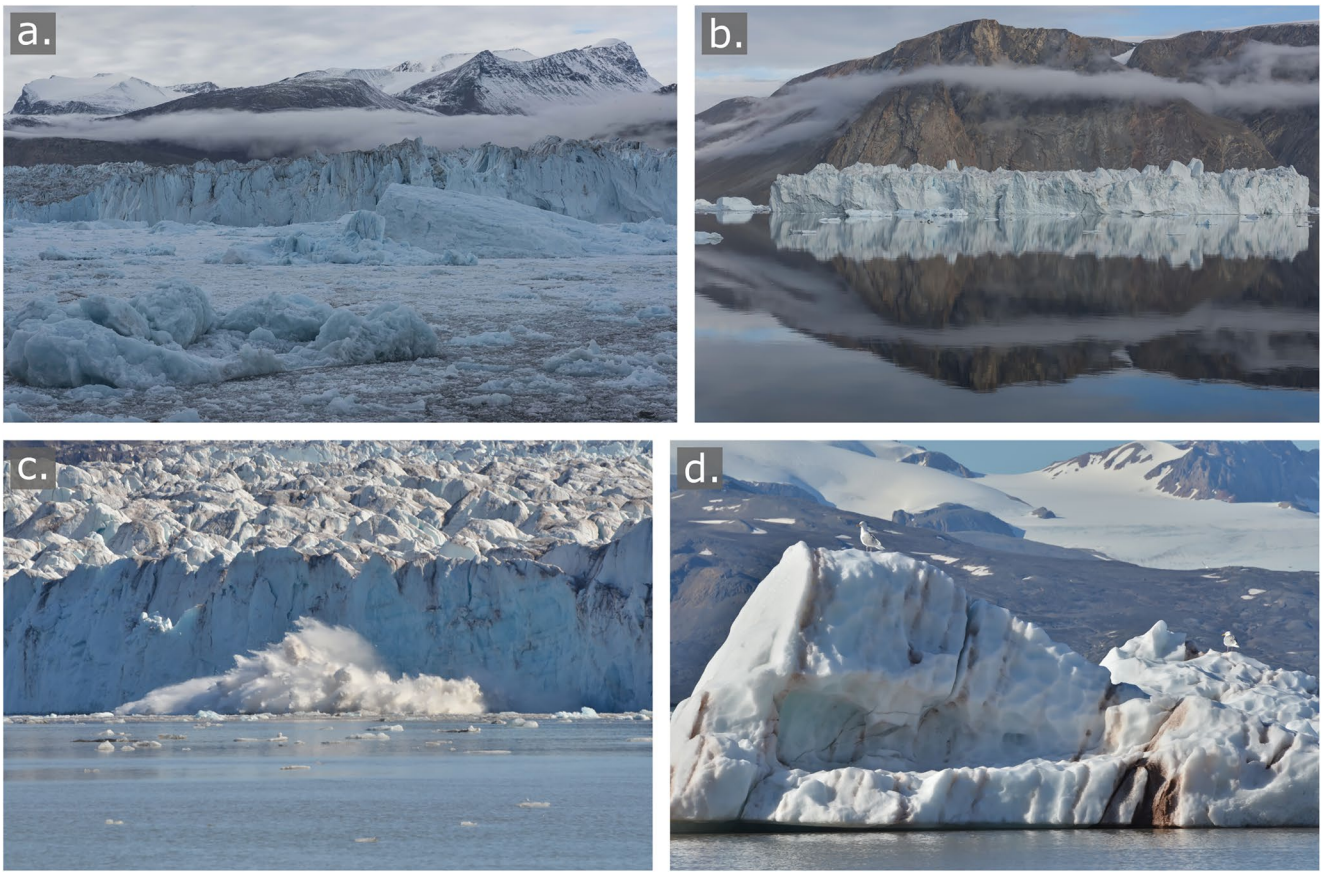

Figure 13. Crevasse formation linked to calving in marine-terminating valley glaciers. (a) A large tabular iceberg (with ice cliff) and smaller rotated icebergs recently calving from the floating glacier terminus of Daugaard-Jenson Gletscher, Nordvestfjord, East Greenland. The near-complete coverage of icebergs and fragments, and sea ice, is referred to as sikussaq or ice mélange. (b) A tabular iceberg, characterized by a heavily crevassed top, several hundred meters long, from Daugaard-Jensen Gletscher. (c) Calving event at the terminus of Kongsbreen, NW Spitsbergen, Svalbard, a glacier that is, resting on the sea bed; forward toppling of inter-crevasse blocks is evident in this photograph. (d) An irregular-shaped iceberg formed as a consequence of the process depicted in "c," Kongsfjorden.

Crevasse patterns vary greatly depending on the spatial distribution of fractures in the glacier and the stress configuration present during formation. Therefore, they can be useful indicators of past and present ice dynamics experienced within an ice mass (Harper et al., 1998; Herzfeld et al., 2004). The concept that crevasses formed in response to stress patterns was developed in the European Alps by Hopkins (1862), who argued that transverse crevasses in Alpine glaciers formed perpendicular to the direction of the "principal tensile force." Such crevasses are referred to as Mode I fractures (van der Veen, 1998a) and it is a common assumption that this principal tensile stress relationship holds for most crevasses (as discussed by Benn, Warren, & Mottram, 2007; Nye, 1952; van der Veen, 1998a). However, there are exceptions to this rule, such as where crevasses interact with the glacier margin or pass over bedrock bumps. Crevasses may change their orientations with respect to the principal tensile stress as they are advected by ice flow, especially in marginal areas where there is a zone of strong simple shear. Older crevasses may also be over-printed by new ones, commonly intersecting at a low angle (van der Veen, 1999, 2011).

By observing different crevasse patterns, it is possible to deduce approximately the orientation of principal surface strain-rates, and therefore the stress configuration required for their initial formation (e.g., Vornberger & Whillans, 1990). Even though a number of studies have found a good correlation between strain-rate trajectories and the orientation of crevasses (e.g., Harper et al., 1998; Meier et al., 1974), most field measurements have demonstrated that crevasses are not always perfectly aligned with the principal stress axes (Kehle, 1964; Whillans et al., 1993). This discrepancy has been attributed to crevasses undergoing rotation while being advected downglacier. However, van der Veen (1999) suggested that this was probably

a result of mixed-mode fracture, with Mode II fractures superimposed on Mode I fractures. Mixed-mode fracture is already generally accepted in other disciplines, for example, during the development of sea ice leads (e.g., Schulson, 2001), and in rocks (e.g., Aliha et al., 2012; Rück et al., 2017), and may be important for interpreting crevasse formation geometries. Nevertheless, crevasse patterns have proved useful for inferring surface strain and consequently stress configurations when detailed ice-flow data are not available. When considering crevasse formation at the surface of a glacier, the maximum principal stress direction is determined by the relationship between three stress components (σ_{xx}, σ_{yy}, σ_{xy}—see Section 3.2 for an in-depth explanation of stress and its notation) (Benn, Warren, & Mottram, 2007). However, despite the common assumption that fracturing is initiated at the glacier surface, it is likely that crevasses propagate upwards from depth (initially forming c. 15–30 m below the surface of the glacier) (Colgan et al., 2016; Nath & Vaughan, 2003; van der Veen, 1999; Vaughan, 1993).

Crevasse patterns change over time. During glacier recession, open crevasses generally decline in number as the ice becomes less dynamic. There are some exceptions, however, as Etzelmüller et al. (1993) have documented by comparing changes between 1970 and 1990 on Erikbreen, Svalbard. Although the glacier had a negative mass balance, crevasse patterns only changed significantly in the lower 1 km of the 6 km-long glacier. Many other glaciers that are currently undergoing thinning reveal widespread crevasse traces (see Section 5.2.2) that are indicative of former open fractures, for example, Midtre Lovénbreen (Hambrey et al., 2005), Tellbreen (Lovell, Fleming, Benn, Hubbard, Lukas, & Naegeli, 2015), and Austre Brøggerbreen (Jennings et al., 2016) in Svalbard.

The special case of crevasse formation in surge-type glaciers is interesting, because between surges, crevasses tend to disappear and ductile processes dominate. An aerial study of a surge of one of North America's largest glaciers, the Bagley Icefield—Bering Glacier system, explored the evolution of crevasses over the course of the 1993–1995 surge, in response to changing dynamics in different source areas and flow over an uneven bed (Herzfeld & Mayer, 1997; Mayer & Herzfeld, 2000). The pre-surge condition of Bering Glacier was a smooth ice surface, followed by a three-stage evolution of crevasses: (a) onset of the surge phase with a few new crevasse fields forming; (b) mature surge stage after the surge had reached the terminus; and (c) late-stage surge following the outburst of water that heralded the termination of the surge. Each of these stages reflected changes in the stress and velocity fields, as well as the availability of meltwater and its role in filling crevasses or influencing basal sliding (Herzfeld & Mayer, 1997).

The origin of common crevasse patterns and their associated stress configurations (notation explained in Section 3.2) are discussed in turn below:

Transverse crevasses develop in areas experiencing longitudinal extension (σ_{xx}). In the middle reaches of a glacier, the maximum principal stress tensor (σ_1) is aligned with ice-flow direction, and therefore linear crevasses develop normal to this direction of maximum extension (Benn, Warren, & Mottram, 2007; Cuffey & Paterson, 2010). Transverse crevasses typically develop near the centerline of glaciers or in icefalls where extending flow and pure shear dominates; however, they can extend toward the glacier margins, where they become increasingly rotated. Shear stresses at the glacier margins (τ_{xy}) rotate the maximum principal stress tensor (σ_1) at an acute angle to flow, resulting in crevasses that initially form slightly concave down-glacier (Benn & Evans, 2010; Nye, 1952) (Figure 14a).

Longitudinal crevasses form in areas dominated by local transverse extension (σ_{yy}). The maximum principal stress tensor (σ_1) is therefore oriented perpendicular to the main direction of ice-flow in the glacier tongue, developing linear fractures that are aligned longitudinally along the glacier. Longitudinal crevasses are primarily found in areas where the glacier tongue broadens, such as in a widening valley or after flowing past a constriction in the glacier trough (Figure 14b) (e.g., Meier, 1960).

Splaying crevasses develop in areas of longitudinally compressive flow. Toward the centerline of a glacier, the effect of lateral drag is negligible, therefore linear longitudinal crevasses develop as a result of transverse extension (σ_{yy}). However, toward the glacier margins a combination of longitudinal compression (σ_{xx}) and shear stresses (τ_{xy}) rotates the maximum principal stress tensor (σ_1) so that it is oriented obliquely to glacier flow, curving the initially longitudinal crevasses so that they meet the glacier sides at an angle of less than 45° (Figure 14b) (Nye, 1952).

Figure 14. Range of crevasse types. (a) The icefall zone of Vadret Pers, a tributary glacier to Vadret da Morteratsch, Switzerland. A prominent set of transverse crevasses, initially concave downglacier, extends across the glacier as the gradient steepens. Above this zone are chevron crevasses extending part-way upglacier at opposite margins, and in the main trunk of Morteratsch below. (b) Longitudinal and splaying crevasses at the snout of Austre Okstindbreen, Okstindan, Norway. (c) Chevron crevasses at the margin of Gornergletscher, near Zermatt, Switzerland (with the Matterhorn in background). (d) Telephoto view of en echelon crevasses in the upper part of Vadret Pers, Switzerland. (e) Aerial view of inter-crevasse blocks and séracs in the upper part of Fox Glacier, New Zealand.

Chevron crevasses are linear fractures oriented obliquely up-glacier that result from shear stresses acting at the glacier margins (τ_{xy}). Consequently, the direction of the maximum principal stress tensor (σ_1) is oriented down-glacier at 45° to the direction of flow. Chevron crevasses open perpendicular to the plane of maximum extension, thus develop obliquely up-glacier and intersecting the glacier margin at 45° (Figures 14a and 14c) (Nye, 1952). Although primarily associated with valley glacier margins, chevron crevasses also form at the boundary between fast-flowing and relatively immobile ice at the margins of ice streams.

En echelon crevasses develop in response to shear stresses and rotation, conditions usually found on the outside of a bend at the glacier margin, or near the edges of ice streams (e.g., Marmo & Wilson, 1998). Typically found in extensional regimes with lateral velocity gradients perpendicular to flow, en echelon crevasses initially form offset chains of comparatively short linear fractures normal to flow direction, analogous to tension gashes in deformed rocks (Figure 14d) (Hambrey & Lawson, 2000; Herbst & Neubauer, 2000). However, continuing ductile deformation can rotate the central section of the crevasses, altering the fracture into a sigmoidal shape. It is therefore possible to differentiate between different generations of en echelon fracture by observing the differing amounts of rotation (e.g., Patrick et al., 2003).

Radial crevasses result from the unconfined lateral spreading of ice, primarily associated with piedmont glaciers, yet commonly observed at the snout of valley glaciers that are no longer confined by valley sides or lateral moraines. Divergence of flow at the glacier terminus causes margin-parallel extension, enabling crevasses to develop at right angles to the glacier margin forming a radial pattern (Cuffey & Paterson, 2010).

Inter-crevasse blocks (Figure 14e) develop in highly crevassed areas where towers of ice (also known as séracs) remain between crevasses. Usually found in icefalls, irregular bed topography combined with extensional flow (σ_{xx}) is necessary for inter-crevasse block formation. Block collapse is common as séracs become unstable as a result of glacier movement and surface ablation. Accumulation of ice debris from block collapses often forms an ice breccia (Section 5.1). The re-orientation of stresses around open crevasses while fracturing is still active can lead to complex fracture patterns that are commonly seen in surging glaciers (e.g., Lawson et al., 2000) and in icefalls (Hudleston, 2015).

Once formed, crevasses can be passively transported downglacier into different stress regimes where crevasse shape, orientation, and dip are modified. It is common for crevasse patterns to completely change when entering new stress regimes. Fractures that remain open for extended periods of time often develop meltwater features (icicles) analogous to those that form in limestone karst, such as stalactites and glazing (Cook, 1956). However, crevasses often cease to remain as open fractures when advected downglacier, and close to form crevasse traces (Section 5.2.2). This transition is especially evident at the glacier margins where simple shear rotates and closes crevasses, often opening new crevasses that are oriented in a more favorable direction for the new stress regime. The formation of new open crevasses that cross-cut older healed fractures develop complex suites of crevasse traces with cross-cutting relationships, that can often be seen toward the terminus of valley glaciers. The ductile modification of sigmoidal en echelon crevasses and the subsequent opening of new cross-cutting fractures has also been described in the Sørsdal Glacier, East Antarctica, and compared with local principal strain rates (Patrick et al., 2003). Observations of deformed crevasses and crevasse traces, and how fractures evolve over time, can therefore prove useful for inferring ice-flow velocities (via feature-tracking techniques), dynamics, and changing stress regimes (Bindschadler & Scambos, 1991; Hambrey & Lawson, 2000; Herzfeld et al., 2004; Vornberger & Whillans, 1990; Whillans & Tseng, 1995; Whillans et al., 1993).

5.2.2. Crevasse Traces

Crevasse traces are linear or curvilinear planar scars that comprise layers of coarse clear ice that are related to tensional fracturing (Colgan et al., 2016; Hambrey, 1975, 1994; Hambrey & Lawson, 2000; Hambrey & Müller, 1978; Hudleston, 2015; Jennings et al., 2014, 2016). There are two main types: (a) tensional veins; and (b) healed water-filled crevasses.

Crevasse traces of the tensional vein type commonly occur within and below crevasse fields, extending from, and forming between, open crevasses. In valley glaciers they typically extend laterally for tens to hundreds of meters (e.g., Hambrey & Müller, 1978; Jennings et al., 2016), distances that are much longer than the majority of open crevasses. Consequently, it has been suggested that tensional veins not only form after open air-filled crevasses close, but also as the lateral and vertical extensions of currently open

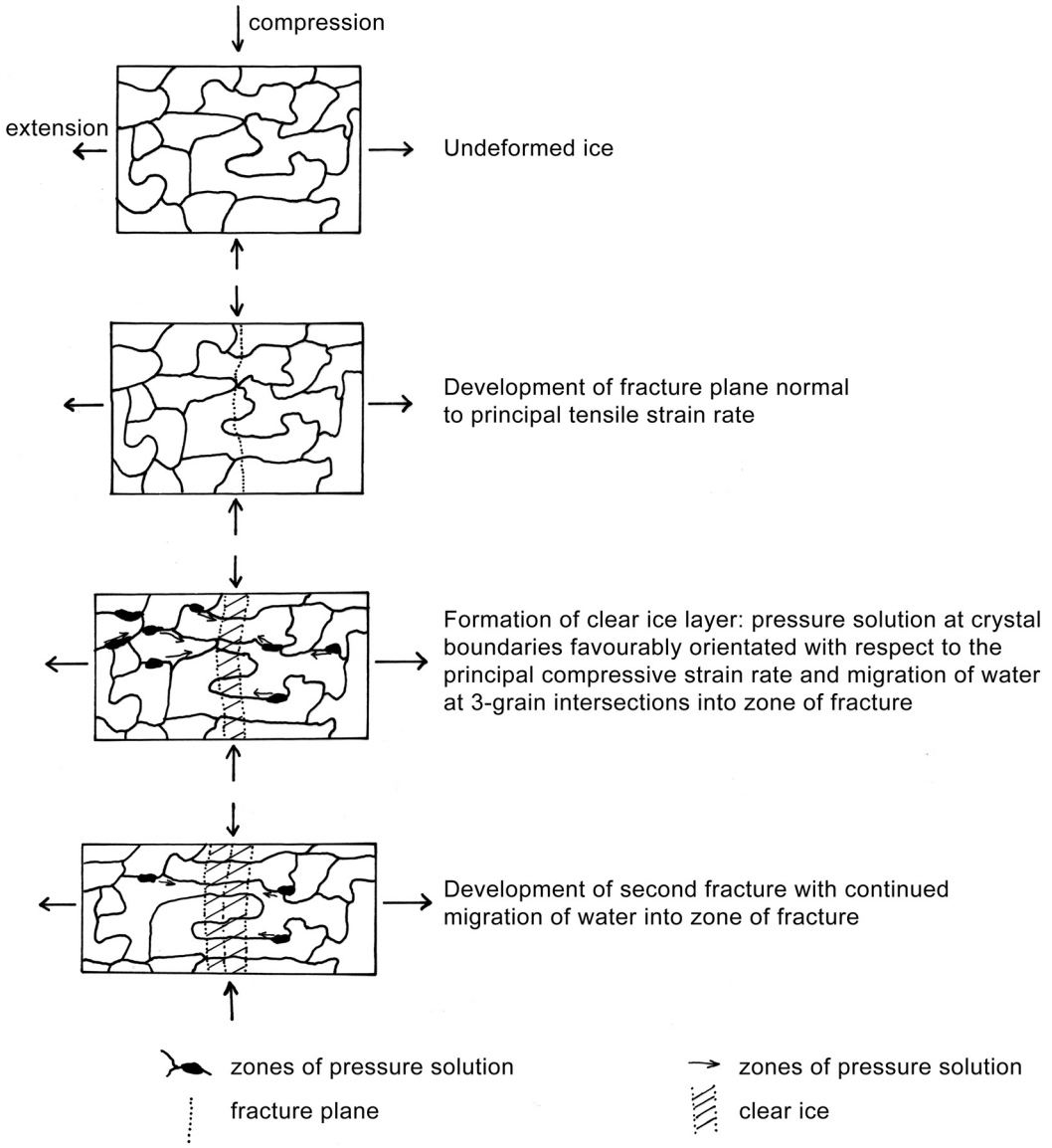

Figure 15. Schematic diagram to illustrate the formation of crevasse traces of the tensional vein type by recrystallization (after Hambrey et al., 1980; reproduced with permission of the International Glaciological Society).

crevasses (Goodsell, Hambrey, & Glasser, 2005; Hambrey & Milnes, 1977; Hambrey & Müller, 1978; Jennings et al., 2014, 2016). Tensional veins as features in their own right can be further divided into two subgroups: (a) fracture planes with no crystallographic growth; and (b) fracture planes with crystallographic growth. Tensional veins with no crystallographic growth develop as discrete fractures that experience no opening, and therefore represent a closed fracture trace. Typically, at the surface of a glacier, these tensional veins appear as thin dark traces, that occasionally experience enhanced surface ablation, rounding the fracture edges. Tensional veins with crystallographic growth also develop as discrete fracture planes; however, interlocking elongate crystals of coarse-clear comparatively bubble-free ice develop perpendicular to the fracture edge (Figure 15), occasionally with stringers of bubbles running through the center or along the margins of the fracture (Hambrey & Müller, 1978; Hambrey et al., 1980). These two categories of tensional vein effectively represent endmembers of a continuum. Even though they can develop as individual non-related features, a tensional vein that initially forms with no crystallographic growth may subsequently develop crystals when transported downglacier into a different stress regime. Crevasse traces normally form perpendicular to the maximum principal extending strain rate, but sometimes crystals develop at an angle

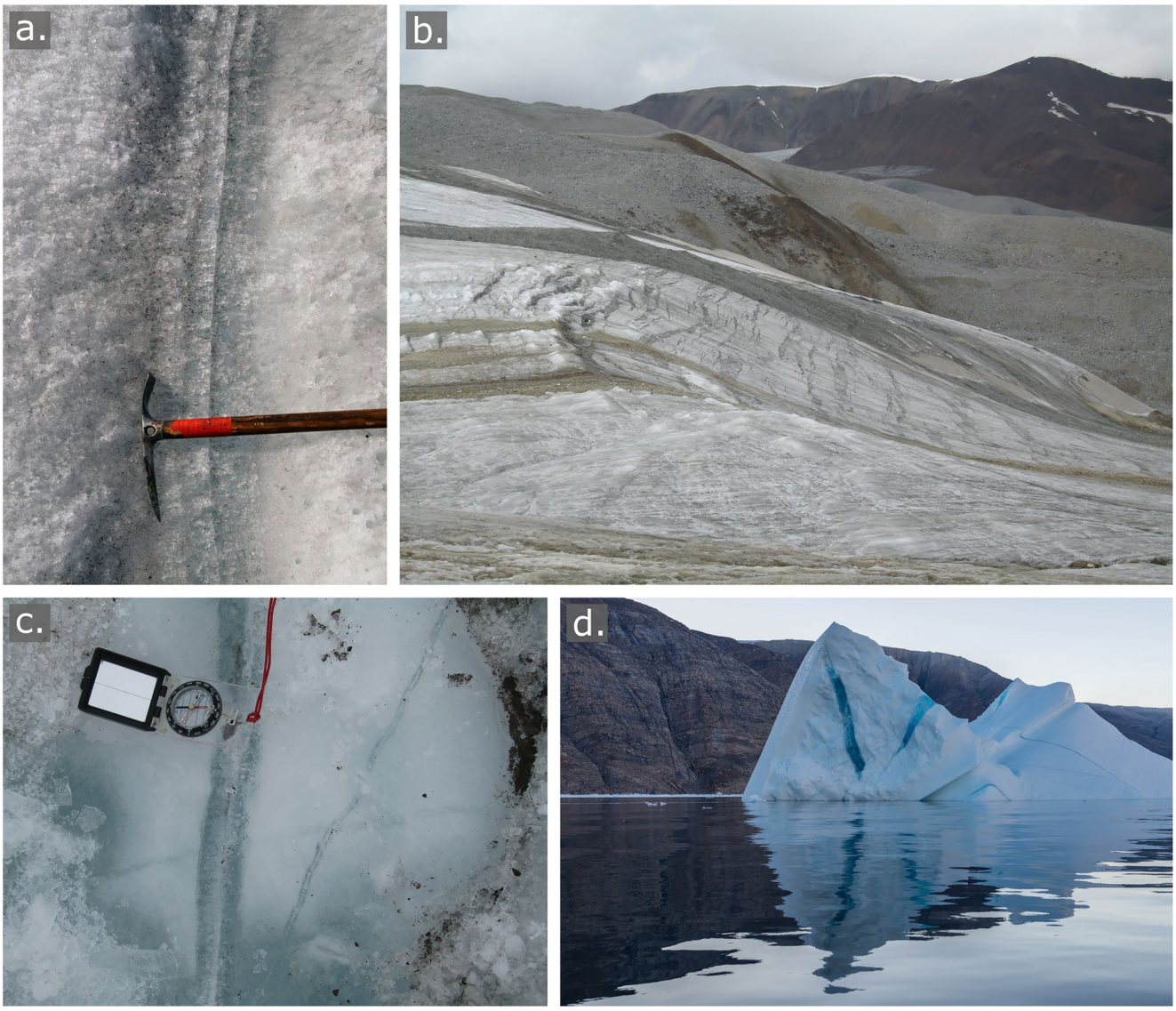

Figure 16. Crevasse trace types. (a) Crevasse trace of the tensional vein type in Fountain Glacier, Bylot Island, Canada, showing four veins of elongate crystals perpendicular to the fracture, representing two stages of extension. (b) Crevasse traces of the water-filled crevasse type in an unnamed branch of Trapridge Glacier, Yukon, Canada; their width is up to 3 or 4 m. (c) Plan view of crevasse traces in Trapridge Glacier, comprising coarse clear (blue) ice with distinctive central suture, defined by air bubbles; the weathered surface has been removed to reveal fresh glacier ice. (d) Large frozen water-filled crevasses in a tilted iceberg in Flyvefjord, East Greenland, seen in cross-section; this large, formerly tabular iceberg was derived from Daugaard-Jensen Gletscher.

to the fracture or become bent, implying formation in a slightly rotational strain regime, or by the process of mixed-mode fracture (van der Veen, 1999). Less commonly, a second fracture may form, or even a third, oriented parallel to the initial fracture, resulting in multiple coarse clear veins in juxtaposition (Figure 16a). The presence of so many crevasse traces in comparison to open fractures in many valley glaciers, combined with observations of crevasse traces located within, or close to, areas of open crevasses, suggests that tensional veins can occur as features in their own right, and do not necessarily experience any opening (Hambrey & Lawson, 2000; Jennings et al., 2014, 2016). Additionally, the ubiquitous nature of crevasse traces in many glaciers, even where ablation has removed open crevasses, indicates that fracture propagation may be relatively deep, sometimes reaching the bed (Goodsell, Hambrey, & Glasser, 2005; Hambrey & Müller, 1978; Jennings et al., 2014, 2016).

Even though Mode I "opening" fracturing is limited to a comparatively shallow surface layer, Mode II "sliding" and Mode III "tearing" fracturing do not require the physical separation of the facture walls as they

are associated with shear stresses acting parallel to the facture plane. As shear stresses are not compensated with depth, it is possible for Mode II or Mode III fractures superimposed on Mode I fractures to penetrate to much greater depths than Mode I fractures alone (van der Veen, 1999). Hambrey (1976b) suggested a similar mechanism, concluding that crevasse shear displacements may indicate that brittle failure could occur through the whole thickness of an ice mass. However, even though "strike-slip" displacements between crevasse walls have been directly observed (e.g., Kehle, 1964), the plausibility of crevasses initially forming as shear fractures has been questioned by Hudleston (2015). Rather, he suggested that the apparent strike-parallel displacement of crevasse walls in relation to one-another is the result of open crevasses experiencing rotation before closing. The lack of shear stresses acting along open fracture walls modifies the stress and strain-rate fields in the surrounding ice, resulting in the relative strike-slip displacement (Hudleston, 2015). However, this mechanism does not explain the apparently great depths to which crevasse traces penetrate. Borehole logging by optical televiewer of a crevassed zone of Store Glacier, a fast-flowing outlet glacier draining the Greenland Ice Sheet, revealed the presence of crevasse traces to a depth of 265 m (Hubbard et al., 2021). Furthermore, surface fracturing was inferred to extend to c. 400 m below the surface of the glacier, as indicated by excess ice temperatures. The great depths to which the fractures penetrate, along with offset fracture orientations in comparison with the direction of local principal extending strain, suggest that crevasse formation involved mixed-mode fracturing (Mode I and III). Multiple sutures in the fracture traces (Figure 17) indicates several reactivation phases, illustrating that once healed, fracture traces represent planes of weakness. Considering the depths to which the fractures penetrate, it is likely that many survive to the glacier terminus despite ablation and surface-lowering, and therefore may play an important role in iceberg calving (Hubbard et al., 2021).

In comparatively smaller valley glaciers, a high abundance of crevasse traces commonly reflects a time when the glacier was more dynamic, compared with the present-day when most glaciers are rapidly receding and down-wasting (Hambrey & Lawson, 2000; Jennings et al., 2016; Lovell, Fleming, Benn, Hubbard, Lukas, & Naegeli, 2015). Analogous structures occur in deformed rocks as a result of a crack-seal mechanism (Durney & Ramsey, 1973; Ramsay, 1980; Ramsay & Huber, 1983).

Healed water-filled crevasses form thick prominent vertical bluish coarse clear ice layers with comparatively few bubbles. They have a curvilinear geometry at the glacier surface, and may attain widths of up to a few meters (Figure 16b). In these features, ice crystals grow perpendicular to the edges of the crevasse as meltwater refreezes, forming large crystals that combine to form a suture when they meet in the middle, often defined by crystal boundaries and trains of bubbles (Figures 16c and 16d). Crystallographic evidence suggests that recrystallization after the freezing of meltwater in these fractures may occur (Colgan et al., 2016; Hambrey & Müller, 1978). Shear displacements of passive markers on either side of healed water-filled crevasse margins can regularly attain two meters, suggesting strike-slip faulting along the fracture plane (e.g., Hambrey, 1976b; van der Veen, 1999). Alternatively, the apparent strike-slip movement of markers results from a crevasse experiencing rotation before healing (Hudleston, 2015). In some cases, crevasse traces comprise thin white bubbly ice where snow has infilled the fracture, rather than water (Benn & Evans, 2010).

Within some glaciers, debris may accumulate in water-filled crevasses from supraglacial sources, or washed in by supraglacial streams, providing an important source for englacial debris entrainment. Debris-filled crevasse traces thus form where a crevasse fills with supraglacial debris and subsequently closes, a process that is, common on debris-mantled glaciers where the debris-filled crevasse can provide a route for englacial water flow (Benn et al., 2012; Gulley & Benn, 2007; Gulley, Benn, Screaton, & Martin, 2009).

Unlike tensional veins that can potentially propagate to great depths and are regularly observed near the snout of valley glaciers, healed water-filled crevasse traces may not always penetrate to such depths. In circumstances where there is an insufficient supply of meltwater to initiate and maintain hydrofracturing, healed water-filled crevasse traces may only reach depths similar to those of open air-filled crevasses. Consequently, these features may not survive for great distances downglacier because of ablation and surface-lowering (e.g., Jennings et al., 2016).

The geometry of crevasse traces mirrors the orientation of open crevasses initially, but they deform into an arcuate form (convex downglacier, reflecting the cross-glacier velocity gradient). Downglacier, crevasses become increasingly attenuated, while their upglacier dip declines as they move downglacier, reflecting

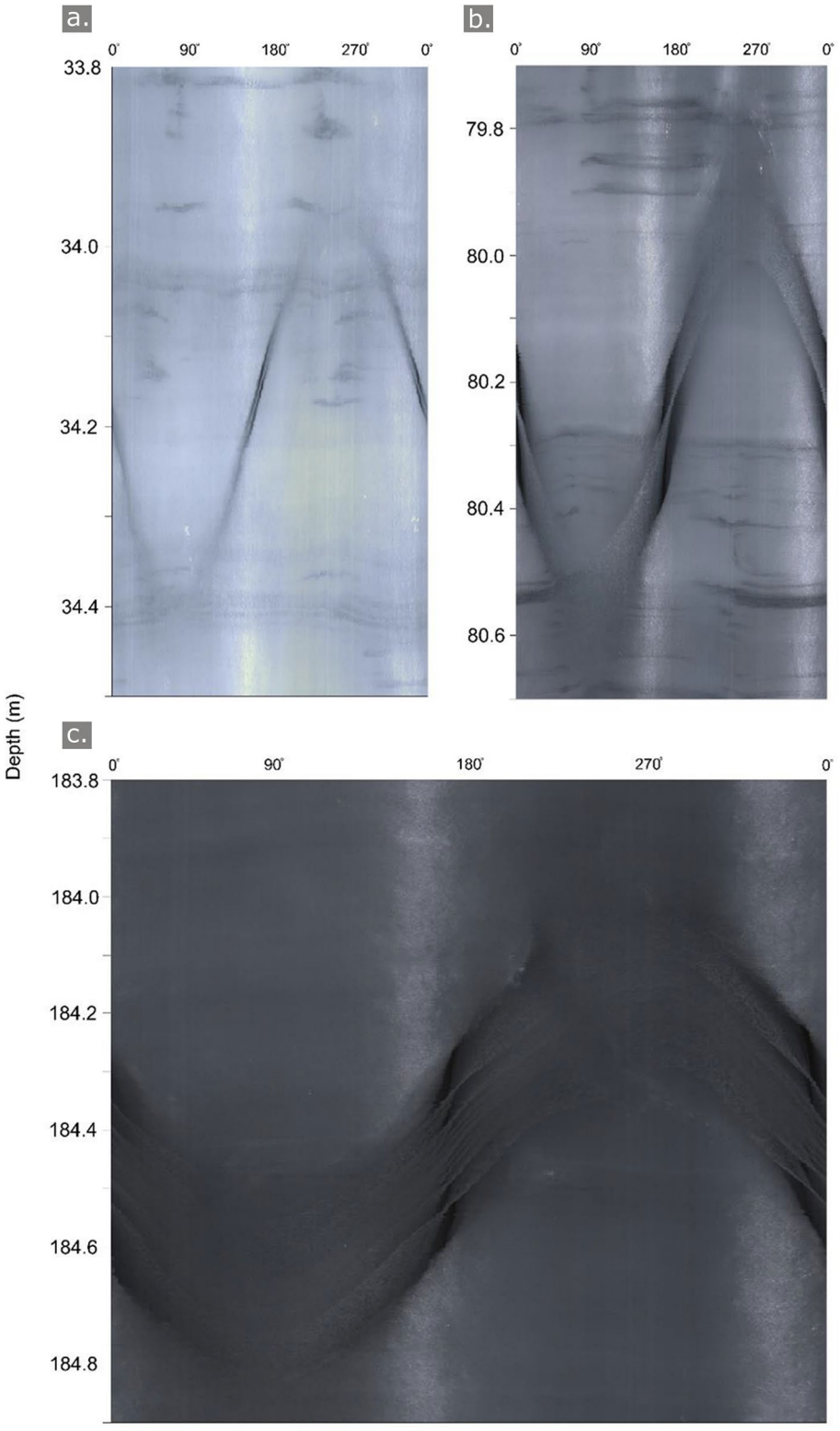
a.
b.
c.
0° 90° 180° 270° 0°
33.8
34.0
34.2
34.4
79.8
80.0
80.2
80.4
80.6
183.8
184.0
184.2
184.4
184.6
184.8
Depth (m)

Figure 17.

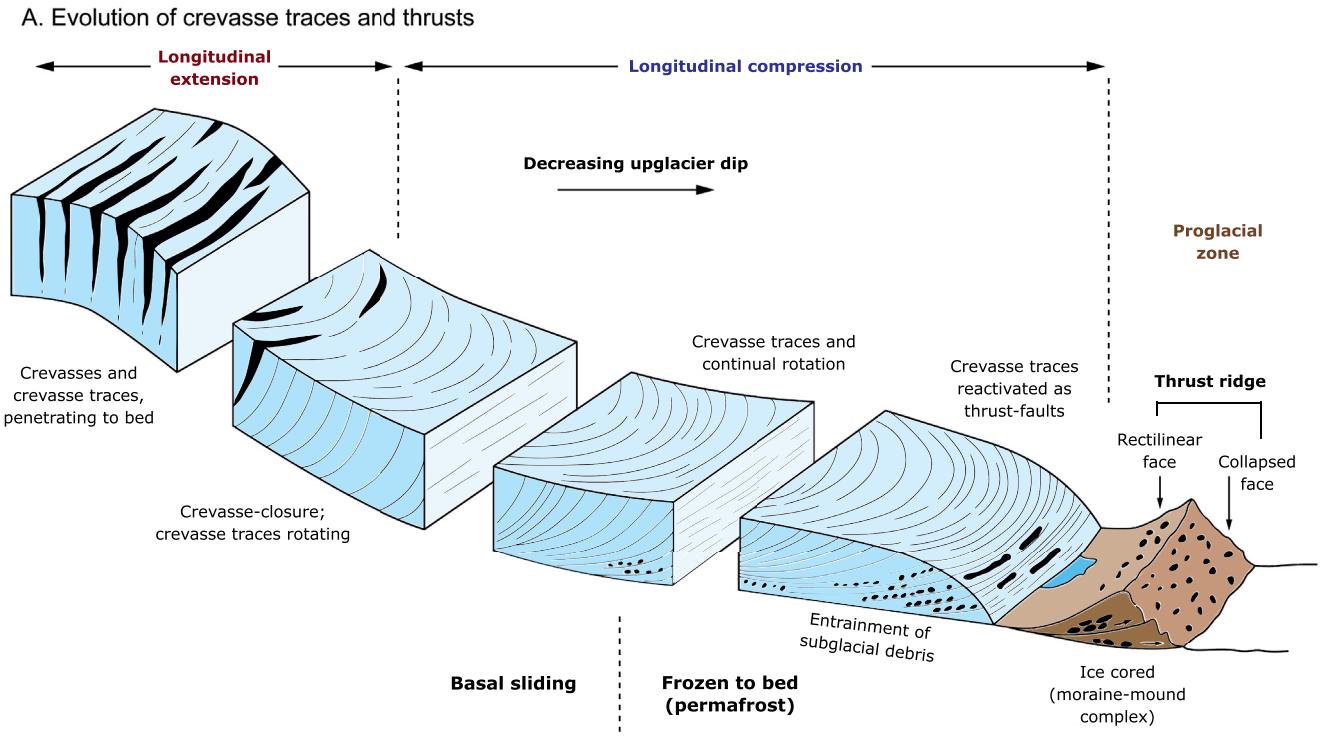

Figure 18. Schematic model to show the evolution and rotation of crevasse traces and thrusts in a valley glacier, based on observations on White Glacier, Axel Heiberg Island, Canada. Thrusts show incorporation of debris near the snout (modified from Hambrey & Müller, 1978).

the vertical velocity gradient. Arcuate crevasse traces represent planes of weakness and can be rotated until they are reoriented into a favorable position for future displacements to occur. They then may be reactivated as thrust-faults in the snout area of a glacier, as demonstrated on White Glacier, Axel Heiberg Island, Canadian Arctic (Figure 18) (Hambrey & Müller, 1978). Such faults are further discussed in Section 5.2.4.

Contrasting dynamics in adjacent flow units may result in fracture sets experiencing unique ductile evolutions within the same ice mass. For example, in Austre Brøggerbreen, Svalbard, crevasse traces in individual flow units experience differential evolutions downglacier (Jennings et al., 2016). In many glaciers, tensional veins survive as far as the terminus, despite substantial ablation and surface-lowering, indicating that the initial fractures probably propagated to the glacier bed.

5.2.3. Vertical Faults and Other Fractures

Several different types of fault have been observed in glaciers depending primarily the on different stress regimes present (Figure 12b) and the geometry of the glacier trough (Cuffey & Paterson, 2010; Hambrey & Lawson, 2000; Herbst & Neubauer, 2000).

Normal faults are predominantly found along or near the lateral margins of a glacier, resulting from horizontal extension perpendicular to the margin (Herbst et al., 2006), sometimes related to ice-marginal collapse

Figure 17. Selected three-dimensional optical televiewer imagery projected in two-dimensions (2-D), depicting high-angled crevasse traces cross-cutting primary stratification, from a borehole in a crevassed region of Store Glacier, an outlet glacier of the Greenland Ice Sheet. The planar crevasse traces appear as sinusoids when projected in 2-D, with primary stratification represented as horizontal layering. The selected imagery is located at: (a) 33.8–34.5 m depth; (b) 79.7–80.7 m depth; and (c) 183.8–184.9 m depth; however, planar traces were observed to penetrate to a depth of 265 m, suggesting, along with trace orientation, that fractures probably formed by mix-mode fracture (Mode I and III). Note that the decreasing luminosity with depth likely results from light-reflecting bubbles being progressively expelled with increasing pressure. Individual central sutures defined by laminae of bubbles visible in (a) and (b) represent freezing fronts where the fractures healed; however, the presence of nine such laminae in (c) suggests that healed fractures represent planes of weakness that can be reactivated multiple times (Hubbard et al., 2021).

or failure (Phillips et al., 2013). During initial formation, the intermediate (σ_2) and minimum (σ_3) principal stress tensors are oriented in the horizontal, parallel and perpendicular to the fault plane respectively, with the maximum principal stress tensor (σ_1) oriented vertically (Figure 12b). Ablation induces slumping or relaxation of ice that is, no longer constrained by the valley walls. Fault planes typically plunge steeply toward the glacier margin, displaying downward displacement in the direction of dip. Normal faults have also been observed: (a) at the glacier snout where the ice mass is no longer confined by its lateral moraines, and where ice collapses into a subglacial cavity (Figure 19a) (Herbst & Neubauer, 2000); and (b) in icefalls where the downstream walls of crevasses are displaced on the steep gradient (Cuffey & Paterson, 2010).

Concentric faults, so called because of their concentric geometry, are an increasingly common type of normal fault that arise from subglacial cavity-formation by meltwater as glacier tongues stagnate, leading to collapse of the ice surface. These faults are often found alongside, and in association with, tensional crevasses that also develop in this situation. A detailed aerial photograph-based study of the formation of concentric faults was undertaken on Pasterzenkees in the Austrian Alps between 1998 and 2012 (Kellerer-Pirklbauer & Kulmer, 2019), the tongue of which has been receding and down-wasting rapidly in recent decades. The glacier tongue is slowly becoming a large debris-covered ice body, the movement of which is steadily declining as the supply of ice from the accumulation area, via an icefall, is much diminished. Concentric fractures and crevasses are forming as ice collapses into cavities formed beneath the glacier. Fractures are mostly normal faults, but small strike-slip, en echelon, and thrust faults are also forming. The density of fractures doubled over the study period. Other examples have been documented in the European Alps where subglacial cavities have collapsed (e.g., Herbst et al., 2006; Jennings et al., 2014), which have also been referred to as "ring faults" (e.g., Azzoni et al., 2017) (Figure 19a).

Strike-slip faults develop where horizontal tension and compression are oriented perpendicular to one another in stress regimes where the maximum and minimum principal stresses (σ_1 and σ_3 respectively) reside in the horizontal plane, and the intermediate principal stress tensor (σ_2) is vertically oriented (fracture Mode III—Figure 12). Also referred to as "tear faults," strike-slip faulting is occasionally observed in glacier ice, and can be seen on a small scale when the faults cross-cut and offset crevasses and crevasse traces (Figure 19b). Strike-slip faults are usually linear vertical fractures; however, it is more common for structural weaknesses such as crevasse traces to be reoriented and reactivated as strike-slip faults. Transverse crevasse traces become increasingly convex downglacier over time, reorienting the limbs of the trace parallel to flow. Shear stresses acting along a crevasse trace reactivates it as a strike-slip fault, displacing the ice on either side of the fracture (Hambrey, 1976b; see also Cuffey & Paterson, 2010). However, the development of strike-slip faults as fractures in their own right has been questioned by Hudleston (2015) who suggested that the relative strike-slip displacement of passive markers was the result of velocity gradients in the surrounding ice, since open fracture walls are unable to sustain a shear stress before closing.

5.2.4. Thrust-Faults

Thrust-faulting is a major process in orogenic belts, where horizontal displacements of many tens of kilometers occur when two tectonic plates collide. The direction of thrust-faulting is always in the direction of the topographic surface slope, even if this means moving "up" the basal slope (Elliot, 1976). Horizontal gravitational or tectonic forces dominate in the development of a thrust-fault, the former being the most important. The toe of a thrust advances under compressive forces imposed by the main body of the gravitationally driven thrust sheet (Elliot, 1976). In these respects, glaciers represent a smaller-scale analog of the geological processes—if the thrust-faulting hypothesis is plausible.

In glaciers, it is hypothesized that thrust-faults occur in areas of longitudinal compression, usually at or near the snout in: (a) response to a rapid advance, where slow-moving or stagnant ice is obstructing flow; (b) where there is a topographic obstruction or a reverse slope; or (c) where there is a change in a downglacier direction from wet-based conditions to frozen-bed conditions. However, the importance of thrust-faulting in glacier ice is contested. From a visual structural geological perspective, the evidence for thrust-faulting is strong, but some authors have claimed that the process is not mechanically viable given the properties of glacier ice (Weertman, 1961), or is of limited scope (Moore et al., 2010).

The important role thrust-faulting plays in entraining debris is explained in Section 9.3.

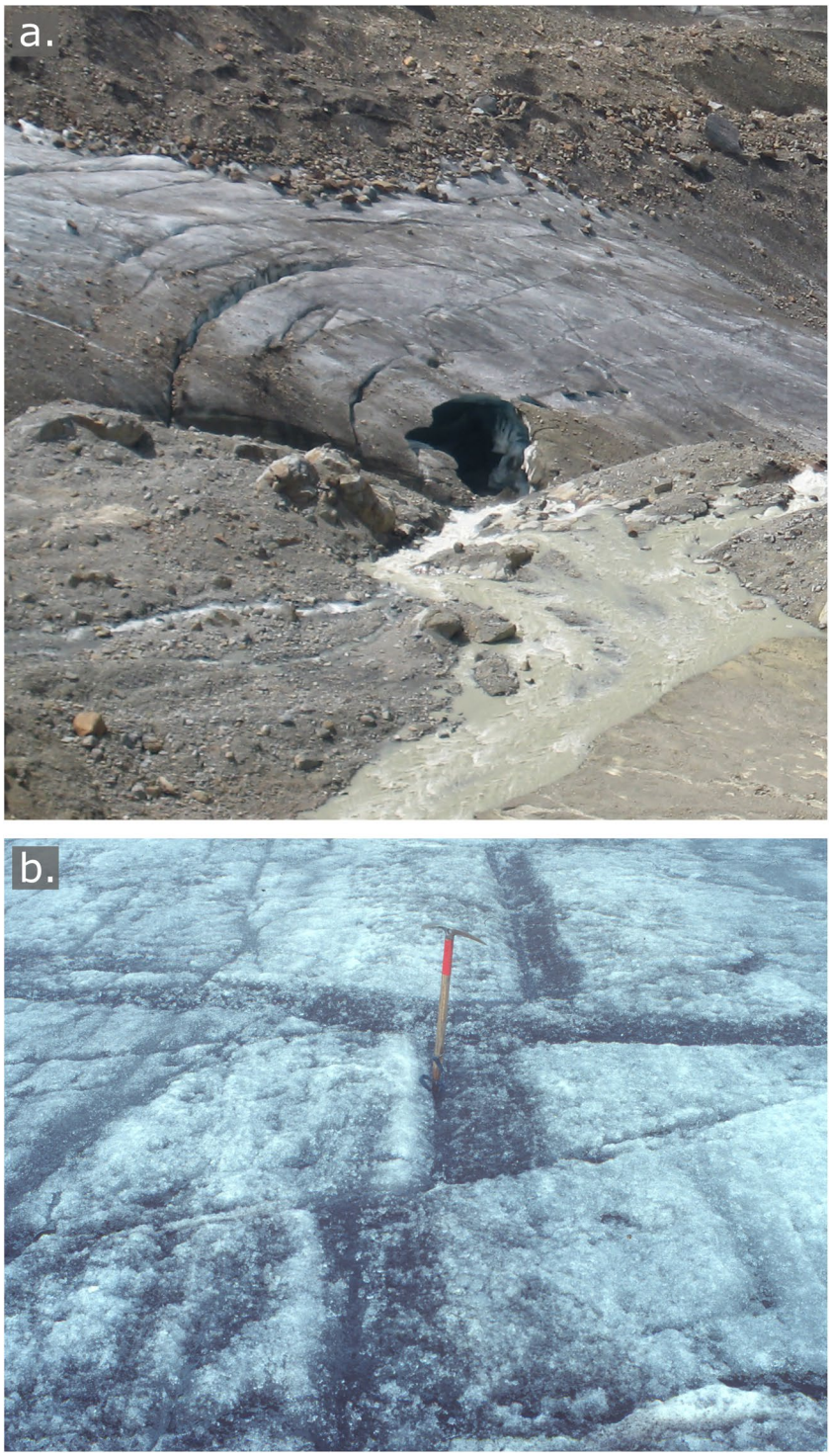

Figure 19. Fractures without opening in glacier ice. (a) Normal faulting, displaced downwards toward the ice margin, at the snout of Ghiaccciao dei Forni in the Italian Alps. In this context, the terms concentric or ring faults can also be applied. They are formed by brittle failure above a subglacial meltwater cavity. (b) Strike-slip faults cross-cutting longitudinal foliation in Hessbreen, Svalbard. Offsets are to the right (dextral strike-slip).

In explaining arcuate fractures, which are often associated with debris, at the surface near the snout of a glacier, our preferred hypothesis is that slow-moving or stagnant ice at the glacier terminus acts as an obstacle to faster-moving ice upglacier. Consequently, the faster-moving ice overrides the slower ice by way of a thrust-fault or a series of thrust-faults.

During thrust-faulting, the maximum (σ_1) and intermediate (σ_2) principal stress tensors are in the horizontal plane, oriented perpendicular and parallel to the fracture respectively, with the minimum (σ_3) tensor oriented vertically (Figure 12b). Movement is accommodated by a dip-slip relationship; however, it is worth noting that several studies have observed thrust-faults that cannot be solely explained by dip-slip movement, but also have a component of strike-slip, suggesting a transpressional stress regime (Fleming et al., 2013; Lovell, Fleming, Benn, Hubbard, Lukas, & Naegeli, 2015).

Thrust-faulting is inferred to be particularly common in land-based polythermal glaciers where the margins of the glacier, which are frozen to the bed, act as an obstacle for the interior zone of temperate sliding basal ice. These thrust-faults typically intersect the glacier surface at angles up to 40° and form an asymptotic relationship with the bed (Glasser et al., 1998, 2003; Hambrey & Dowdeswell, 1997; Hambrey & Müller, 1978; Hambrey et al., 1997, 1999, 2005; Larsen et al., 2010; Roberson & Hubbard, 2010; Souchez, 1967). On the other hand, some thrust-faults remain close to parallelism with the bed, rising only gently from it, such as in surge-type Trapridge Glacier in the Yukon (Figure 20a) (Clarke & Blake, 1991; Hambrey & Clarke, 2019). Thrust-faulting has also been recognized in polythermal tidewater glaciers where a surge front has passed through a glacier, reflecting a progressive change in the thermal boundary conditions from cold- to wet-based (Fleming et al., 2013; King et al., 2016; Lovell, Fleming, Benn, Hubbard, Lukas, & Naegeli, 2015; Murray et al., 1997, 2000).

On a large scale, thrust-faulting may occur in ice sheets, where remnant dead ice from the Last Glacial Maximum (LGM) is overridden by modern fast-flowing ice. An example of the latter is at Jakobshavn Isbræ (Sermeq Kujalleq), where a borehole study, using tiltmeters, identified stick-slip motion at the Holocene-LGM boundary at 682 m depth and 150 m above the bed (Lüthi et al., 2003).

Fractures interpreted as thrust-faults, commonly associated with debris, have also been described from the terminal zone of several temperate alpine and Icelandic valley glaciers, for example, where low-angle fractures have been initiated against a reverse bed slope or in a zone of longitudinal compression (Appleby et al., 2010; Goodsell, Hambrey, & Glasser, 2005; Herbst & Neubauer, 2000; Herbst et al., 2006; Phillips et al., 2014, 2017; Roberson, 2008; Swift et al., 2006, 2018). In detail, thrust-faults commonly form small steps or overhangs at the surface of the glacier, with the thrust-plane dipping upglacier (Figure 20b). Dip angles are generally shallow at the ice/bed interface, but steepen as they extend toward the glacier surface typically to 30°–40° (Figure 20c). Some glaciers, such as Pasterzenkees in Austria, have "over-steepened" thrust-faults, where angles at the surface of 70°–80° have been documented (Herbst & Neubauer, 2000). Mapping of these thrust planes indicates that they are arcuate at the glacier surface, suggesting a spoon-shaped plane. However, this geometry may be amplified by greater ice-flow velocities in the center of the glacier (Herbst & Neubauer, 2000; Herbst et al., 2006). Thrust-faults do not always reach the surface of the glacier, and may die out within the body of the glacier; such structures are referred to as "blind thrusts" (Hambrey & Lawson, 2000; Murray et al., 1997). The occurrence of blind thrusts that form at depth, which subsequently become exposed at the glacier surface as a result of ablation and surface-lowering, may explain the appearance of fractures that have no apparent supraglacial or englacial origin (i.e., formation in a crevasse field) (Colgan et al., 2016; van der Veen, 1999).

To observe thrust-faulting in motion is rare. One example was during a study of the temperate glacier, Variegated Glacier in Alaska, during its surge of 1985–1986. Intense deformation was associated with the passage of the velocity peak at the boundary between propagating surging ice and stagnant ice near the snout (Raymond et al., 1987; Sharp et al., 1988). As the velocity peak associated with the surge front passed downglacier, a phase of continuous and cumulative longitudinal compression was followed by continuous and cumulative longitudinal extension (Sharp et al., 1988). The former resulted in thrust-faults, and the latter crevasses. The passage of the surge front was also accompanied by microcracking, exfoliation, and buckling of surface ice; the formation of longitudinal cracking and longitudinal chasms; and an increase in glacier volume below the surge front (Raymond et al., 1987). By analogy with thrust-emplacement in

Figure 20.

geological tectonic regimes, the surging process is analogous to thrust-sheet emplacement by a combination of gravity-gliding over a weakened basal layer and "push from behind" (Lawson et al., 1994; Sharp et al., 1988).

Actual measurements of motion along thrust-faults are uncommon. Many such faults, in fact, are relict structures from the times when a glacier was more dynamically active. A good example of measured movement of active ice along a prominent detachment (or "basal sole thrust") adjacent to stagnant ice at the terminus is from the Icelandic glacier, Falljökull (Phillips et al., 2014). Velocities some distance above the detachment were measured to be over 50 m yr^{-1}, reducing to 17 m yr^{-1} at and just above the thrust, and only 4 m yr^{-1} in the stagnant snout.

In many glaciers, thrust-faults are hypothesized to develop along pre-existing planes of weakness, notably transverse crevasse traces (Goodsell, Hambrey, & Glasser, 2005; Hambrey & Müller, 1978) or pre-existing thrust-faults (e.g., Lawson et al., 1994). It has also been suggested that thrust-faulting is likely to occur where the lower limb of recumbent folds in basal ice become attenuated, eventually developing a narrow shear zone or discrete thrust-fault (Hambrey & Lawson, 2000). This topic is further discussed in Section 5.4.2.

Conversely, the conditions required for any type of thrust-fault to develop as a new structure has been questioned on theoretical grounds by Moore et al. (2010), who concluded that the criterion required for compressive fractures in ice is rarely met. Moore et al. (2010) contended that thrust-faulting in glacier ice is only plausible if high compressive stresses are experienced by a thin actively flowing ice mass with an abundance of pre-existing structural weaknesses or fractures, combined with high water pressures. They explored this problem using a 2-D finite element model for basal slip and nonslip, using data from surge-type Variegated Glacier, Alaska, and nonsurge-type glacier Storglaciären in Sweden. However, even during active surges, when the highest stresses in valley glaciers are generally experienced, field measurements of mid-surge strain rates tend not to favor thrust-faulting in glacier ice (Moore et al., 2010; see also Hudleston, 2015). Even under exceptional glaciological conditions, such as during a surge, the creation of a thrust-fault by compressive fracture in initially homogeneous ice is not possible. However, in reality, it is not normal for glacier ice to be homogeneous; rather it contains many fractures and other planar discontinuities, some of which reach the bed.

Fractures that are often interpreted as thrust-faults, commonly contain debris that has a basal origin. On melting out, these fractures leave accumulations of sediment at the glacier surface that range from fine-grained mud through to diamicton (Hambrey et al., 1999; Murray et al., 1997). Examples of glaciers where debris-laden fractures and bands have been interpreted as thrust-faults are found in Kongsvegen, Svalbard (Glasser et al., 1998), and in Storglaciären, Sweden (Glasser et al., 2003). However, these features have also been interpreted as basal crevasse-fill structures (Woodward et al., 2002), and entrained basal debris elevated by flow to a supraglacial position as a result of basal topography (Moore et al., 2011), respectively (also discussed in Section 9.3). Hudleston (2015) further suggested that the displacement of passive markers across fractures, that are cited as evidence of thrusting (Goodsell, Hambrey, & Glasser, 2005), are more likely to arise from the rotation of open tensile fractures. Open fracture walls cannot sustain a shear stress, therefore the embedding ice experiences a velocity gradient that rotates the open fracture before it closes. The varying stress field in the surrounding ice results in the relative displacement of passive markers, that resembles faulting once the fracture has closed (Hudleston, 2015). Despite the debate regarding the plausibility of thrust-faulting in glacier ice, it certainly seems to play an important role in debris-entrainment and the development of distinctive moraine complexes (Section 9.3).

Figure 20. Styles of thrust-faulting in valley glaciers. (a) The snout of polythermal surge-type Trapridge Glacier, Yukon, shortly after the termination of a "slow surge" (in 2006). A near bed-parallel debris-laden thrust-fault extends as far as the terminal cliff. Subsidiary thrust-faults rise up from this, some with debris, some without, several being "blind." (b) Close-up view of high-angle thrust-faults containing minor debris near the snout of Fox Glacier, New Zealand. These prominent fractures are cutting across a lower angle transverse foliation. (c) Closely spaced thrust-faults in Cascade Glacier, College Fiord, Alaska, illustrating how they rise up asymptotically from the glacier bed.

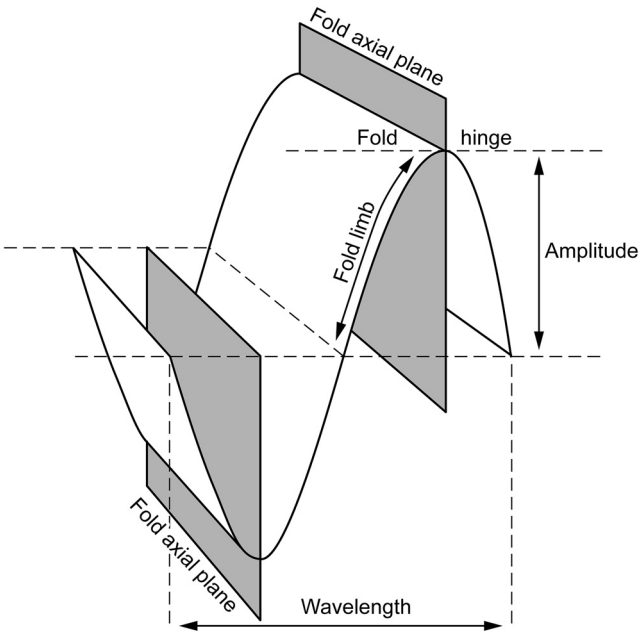

Figure 21. Principal attributes of, and terms defining, the components of a fold.

5.3. Ductile Structures

Although the terms "ductile" and "plastic" are used interchangeably in this review, and are also commonly interchangeably used in other glaciological studies, it is worth noting that, especially in geological literature, the two words have slightly different meanings. In geological texts plastic deformation refers to a permanent change of the shape and size of a body without fracture, whereas ductile deformation indicates deformation that preserves the continuity of passive layers and structures, yet is the product of different deformation mechanisms. This is a scale-dependent differentiation, as a structure that appears to have undergone plastic deformation when viewed at the mesoscopic-scale may have actually deformed by multiple small fractures when viewed at the microscopic-scale (Fossen, 2010). Here, the terms ductile and plastic both refer to materials that accumulate strain with no macroscopically visible fracturing. Even though this convention would be considered unsound in geology, because of the comparatively large crystal size and limited preservation of deformation phases in glacier ice, it is generally not possible to discriminate between the two terms in field-based glaciological investigations.

5.3.1. Folding

Structural geologists use standard terms for the different elements in folded rocks, which are equally applicable to glacier ice. Irrespective of scale, the main elements in a fold structure is shown in Figure 21. The information that can be gained from folds in rocks has been reviewed by Hudleston and Treagus (2010), especially with regard to fold theory, modeling, and analysis.

Folding of glacier ice occurs in most ice masses at a range of different scales as a consequence of changes in valley geometry and flow variations (Hambrey & Lawson, 2000). It is common for primary stratification and fractures to become folded by a combination of lateral compression and simple shear as ice flows from a broad accumulation area into a narrow tongue (Goodsell, Hambrey, & Glasser, 2005; Hambrey & Glasser, 2003; Hambrey et al., 1999, 2005; Lawson et al., 1994). The majority of folds observed at the surface of ice masses are "passive folds" that do not require any rheological differences between ice layers to develop. Folds can form in a range of different styles (Hambrey, 1977a), and have amplitudes ranging from centimeters to hundreds of meters. The most common types of passive fold observed on the surface of a glacier are "similar" folds that are characterized by thickened fold hinges and attenuated diverging limbs (Figures 22a and 22b), and "isoclinal" folds that also having thickened fold hinges but with parallel attenuated limbs (Figure 22c). In addition, other fold styles such as "parallel" (with fold hinge and limbs of a uniform thickness), "chevron" (zig-zag shaped), and "intrafolial" (isolated fold hinges severed from fold limbs) folds may be observed (Hambrey & Lawson, 2000). Fold axes at the surface of a glacier tend to plunge upglacier with angles that range from steep to shallow. Where folds are associated with longitudinal foliation, their axial planes are commonly parallel to flow direction, and form in a simple shear regime. Conversely, where transverse or arcuate foliation is developed, such as in a zone of longitudinal compression below an icefall, fold axial planes are normal to flow direction, and are the product of pure shear. Parasitic minor folds are common on larger scale fold structures, the geometry of both being the same (Figure 22d). Whereas large-scale folds may be barely traceable when walking on the surface of a glacier, they are usually readily apparent in aerial or satellite imagery (Figure 22e). Less frequently observed folds include "flanking folds" or "flanking structures" (Figure 23) (cf. Passchier, 2001). Flanking folds develop in relation to the formation of fractures in areas of foliation, and comprise a pair of "hook folds" separated by a fracture, which can prove useful as an indicator of the sense of shear (Mukherjee, 2014). The final geometry of flanking structures offsets passive foliation markers, which in certain circumstances can be offset in a direction opposite to that which is initially expected from the surrounding shear regime. In these instances, the common limb of the asymmetric hook folds appears to have been sheared out and replaced by a fracture or vein, with the offset being of the opposite sense to that expected from the sense of the fold asymmetry. These types

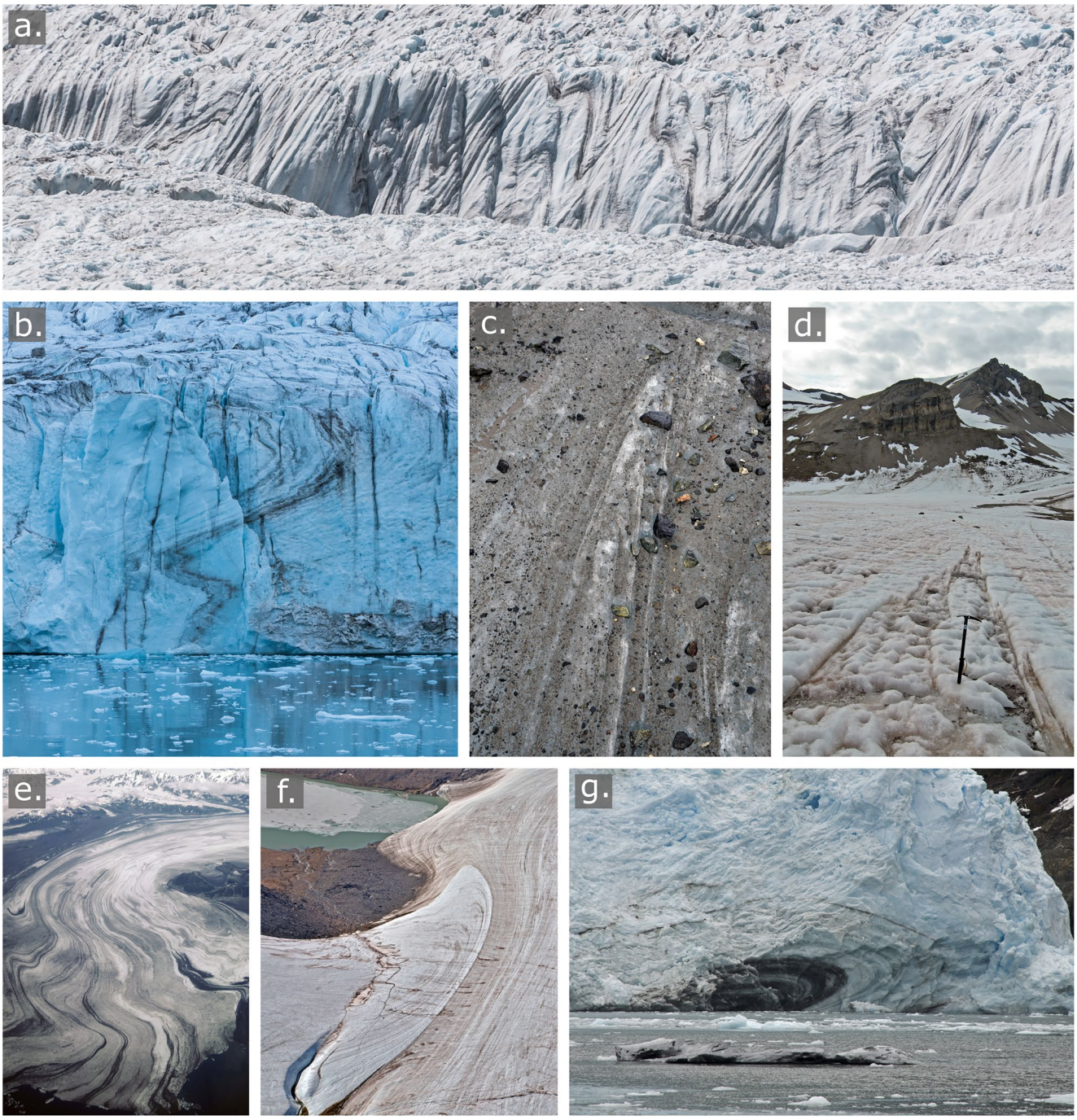

Figure 22. Fold styles in glacier ice. (a) A c. 500 m transverse section across Gornergletscher showing similar style folding of presumed primary stratification. (b) Similar folds in the c. 50 m-high terminal cliff of Sefstrøm Gletscher, Alpefjord, East Greenland, enhanced by a small amount of debris. (c) Isoclinal fold, with axis and limbs parallel to longitudinal foliation, Gulkana Glacier, Alaska. (d) Parasitic folds (decimeter scale) on a large fold (meter scale), with axial planes of the same orientation, Austre Brøggerbreen, Svalbard. (e) Large-scale folding in Bering Glacier, Alaska. The width of the debris-free part of the glacier at the neck is about 11 km. (f) Similar fold, representing a loop arising from a surge of the tributary glacier (lower left) into Aktineq Glacier, Bylot Island, Canada. (g) Recumbent fold, incorporating basal debris in the tidewater Meares Glacier, Alaska.

of flanking structure form as the stress field in the embedding ice is modified while a tensional fracture remains open, resulting in folding of the adjacent foliation once the fracture closes (Figure 23). Therefore, in these cases, folding is the consequence of fracture formation, and does not precede the brittle failure of the ice (Hudleston, 1989, 2015).

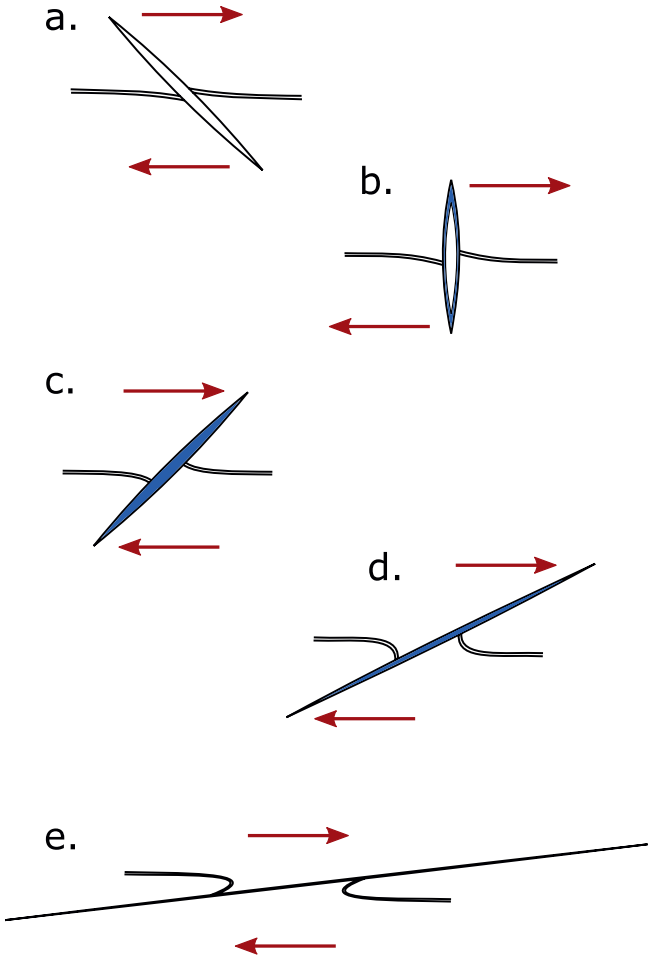

Figure 23. Two-dimensional model based on experiments with clay illustrating the development of flanking folds at the surface of a glacier. (a) Open fracture with passive cross-cutting layers located in a shear regime at the lateral margin of a glacier. The open fracture initially develops at a 45° angle to the margin. (b) Rotation of the fracture as it begins to in-fill by ice crystal development at the fracture edge, represented by blue coloring. (c) Continued rotation of the now water-healed fracture displaces the cross-cutting layers which are offset in a direction opposite to that initially expected from the surrounding shear regime. (d) Continued folding of the passive cross-cutting layers forms a pair of hook folds, as the water-healed fracture is attenuated. (e) Continued attenuation of the water-healed fracture in the shear regime results in a thin vein that offsets a pair of asymmetric hook folds (modified from Hudleston, 1989).

Piedmont glaciers are unique when compared with other ice masses because ice, which is initially strongly channelized, flows out into a broad topographically unconstrained lobe. Consequently, flow in the lobe is characterized by pronounced longitudinal compression. Longitudinal foliation and medial moraines become folded with axial planes aligned transverse to flow, and with folds attaining amplitudes of several kilometers (Figure 22e). However, the pattern of folding found in some piedmont glaciers may be complicated by surges (Hambrey & Lawson, 2000; Post, 1972; Sharp, 1958). This is true, for example, in some of North America's largest glaciers, the Bering and Malaspina glaciers in southeast Alaska (Figure 22e); however, despite these flow complications, the distinctive folds in Malaspina Glacier were successfully modeled experimentally by Ramberg (1964).

Looped medial moraines are distinctive tear-drop-shaped fold structures that result from surge-type behavior (Driscoll, 1980; Hambrey & Lawson, 2000; Lawson, 1996; Meier & Post, 1969; Post, 1972; Rutishauser, 1971). Surge-type glaciers experience short-lived periods of enhanced ice flow during their active phase, during which brittle deformation (crevassing) is dominant, separated by extended periods of comparative inactivity during their quiescent phase when ductile deformation predominates, as research on Variegated Glacier in Alaska has demonstrated (Lawson et al., 1994). Increased ice discharge from a surging tributary flow unit into neighboring less active ice commonly deforms the associated medial moraine or foliation into a bulbous shape (Figure 22f). Such looped medial moraine structures are useful for identifying surge-type glaciers that have not previously been observed to surge (Dowdeswell & Williams, 1997; Hambrey & Lawson, 2000; Post & LaChapelle, 1971). However, their absence does not necessarily indicate that surging has not occurred, as an unexpected surge of Comfortlessbreen in Svalbard has demonstrated (King et al., 2016).

All of these ductile structures are observable in plan view, but where glacier cliffs are formed from lateral stream-undercutting or calving (usually in polythermal or cold glaciers), somewhat different styles of folding are apparent in the lower layers of the glacier, where debris is a key component of the structure (Fleming et al., 2013). Simple shear is the dominant process in these lower parts, and protuberances in the bed can initiate recumbent folding (Figure 22g) (Hudleston, 1976, 1977). During steady-state flow, foliation at the base of an ice mass becomes parallel to particle flow paths. However, in non-steady flow regimes, changes in strain-rate may alter particle flow paths sufficiently to create gentle undulations in the foliation. Continued flow amplifies the undulations, eventually forming recumbent folds (Figure 24) (Hudleston, 1976, 1977). The geological counterpart of these folds have been well described from fold-and-thrust belts, such as the Caledonides of northwest Scotland (Alsop & Holdsworth, 2002, 2007), where they are referred to as "fold perturbations." They occur in high shear zones, and by detailed measurement of fold axes and axial planes in multiple locations, a good record of the scale and kinematics of heterogeneous flow can be recorded. Such an approach has not yet been applied to glaciers, but the flow perturbations described, for example, by Hudleston (1976) and Hambrey and Clarke (2019) would be examples where the geological approach could be instructive.

In situations where fold perturbations are actively forming in 3-D the resulting folds are "sheath folds" (Figure 25) (Fleming et al., 2013; Hudleston, 2015). Sheath folds were studied in Tunabreen, a surge-type glacier in Svalbard using the novel technique of measuring the "anisotropy of magnetic susceptibility" (AMS) to

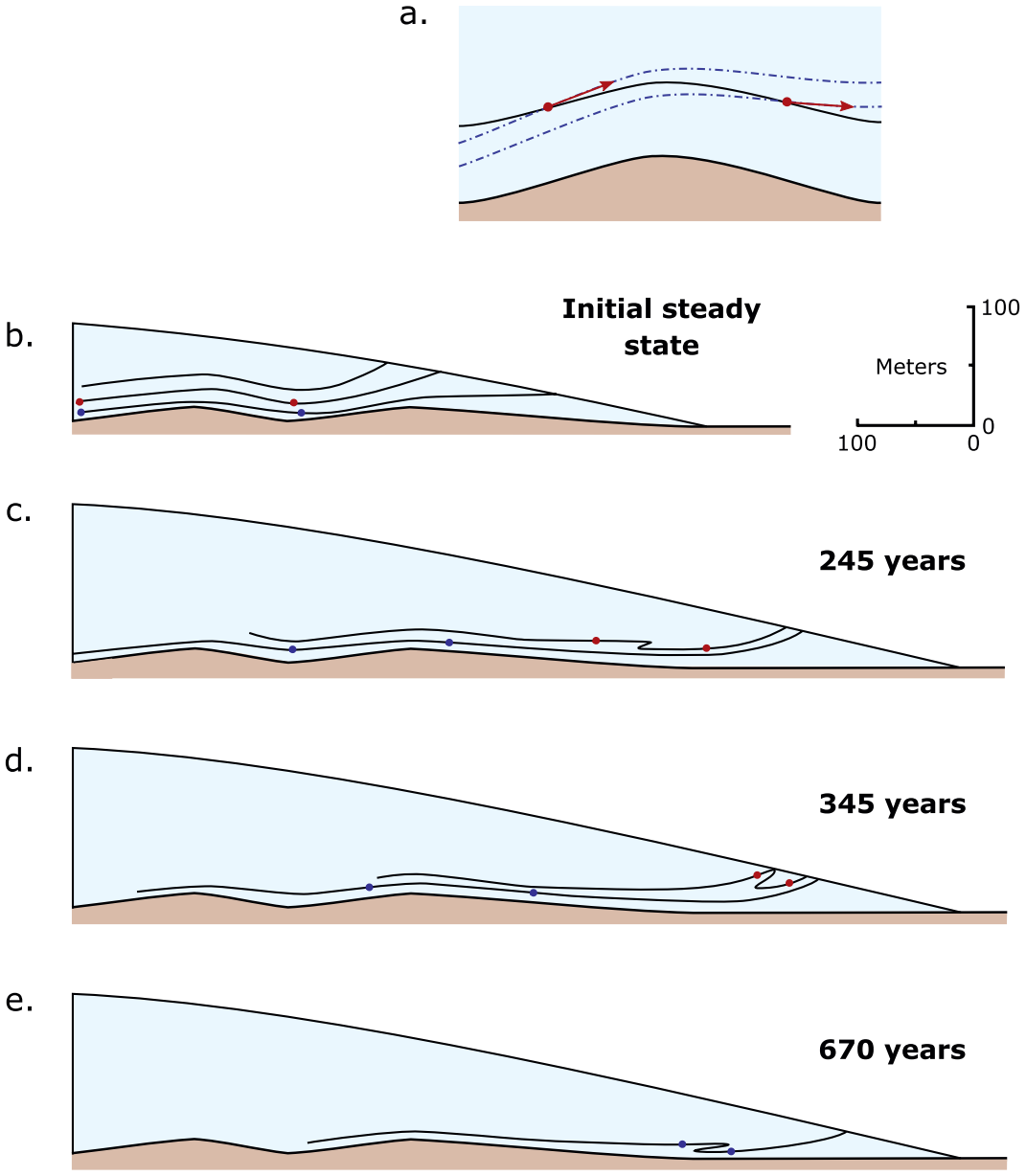

Figure 24. Basic model illustrating the possible formation of recumbent folds as a result of a changing flow regime. (a) Illustration demonstrating how the flow trajectories of two passive points (red) may be modified to follow two new flow paths (dashed blue lines) from an initial flow path (black line) as a result of a changing flow regime and irregular bed topography. (b) Initial steady state flow conditions with passive foliation developed approximately parallel to the bed of the glacier. Red and blue marker dots track the passive foliation through the remaining panels. (c) The ice mass experiences an advance of c. 200 m resulting in a new steady flow state, altering the flow trajectories of, and folding the foliation. (d) and (e) The ice mass remains in its new steady state, with continued flow folding the foliation into recumbent folds (modified from Hudleston, 1976 and Hooke, 2019).

determine the relationship between glacier flow, structure, and magnetic fabric; the latter was obtained from paramagnetic minerals (presumably phyllosilicate clays) embedded in basal ice (Fleming et al., 2013). AMS fabric showed a preferred alignment or lineation parallel to the axes of the sheath folds, a result that was confirmed by macrofabric stretching lineations defined by debris particles. As in structural geology, the lineations can be regarded as a proxy for representing the long axis of the strain ellipse (Fleming et al., 2013).

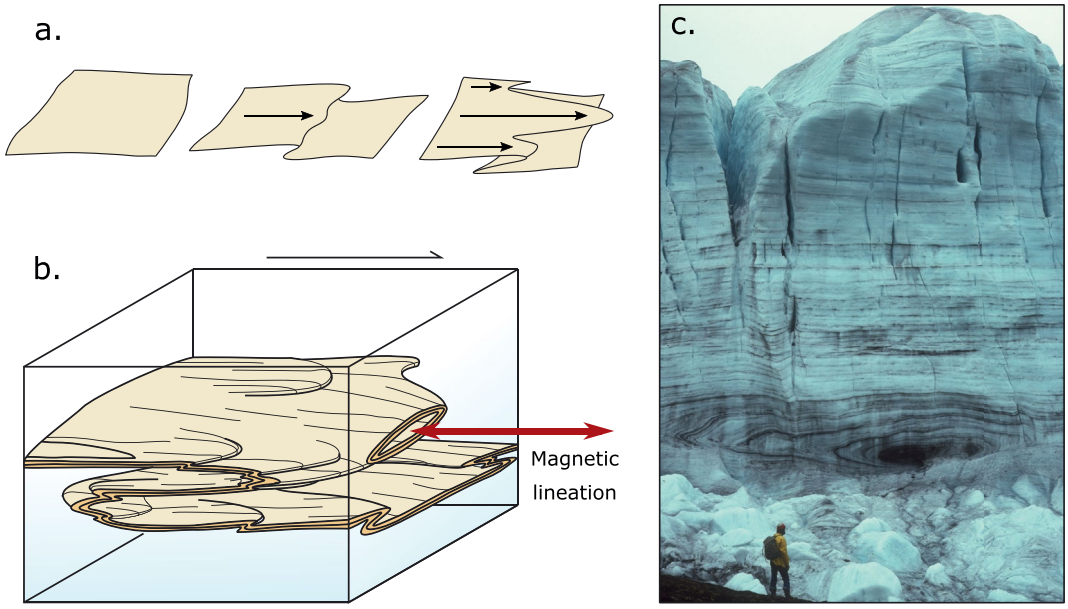

Figure 25. Sheath folding and its three-dimensional (3-D) morphology. (a) Conceptual diagram illustrating how sheath folds form. (b) Detailed illustration of a sheath fold based on observations from Tunabreen, Svalbard, depicting its 3-D geometry, magnetic lineation, and formation in a shear regime. Note that ice flow is from left to right, and the right face of the cube represents the calving front of the glacier. (c) Sheath fold with basal debris entrainment in the terminal face of Crusoe Glacier, Axel Heiberg Island, Canadian Arctic. The glacier was advancing toward the camera in this 1975 photograph ("a" and "b" are modified from Fleming et al., 2013).

Rheological differences are not necessary to produce sheath folds, with the foliation acting as a passive marker (Hudleston, 2015). The basal ice zone itself combines discrete shear planes, fractures, and folding (Section 5.4.1). In glaciers, sheath folds are not well studied, unlike the equivalent structures in deformed rocks. A detailed investigation in the Caledonides of northwest Scotland focused on sheath folding associated with thrust-faulting in the Moine Nappe (Alsop & Holdsworth, 1999). Sheath folds formed in regions of intense ductile shearing, with the rotation of fold hinges from orientations orthogonal to the shear direction progressively heading toward parallelism with the transport direction. Consequently, the folds have extremely curvilinear geometries, and they are viewed as characteristic of intense mid-crustal deformation. Such detailed studies have not yet been applied to sheath folds in glaciers, but they have the potential for generating a more thorough description of 3-D structural geometry in the basal zones of glaciers where intense ductile deformation is taking place.

The folds discussed above can all be classed as "passive" as they do not require rheological differences between ice layers to form. There are, however, examples of folds in ice masses that develop as a result of contrasting ice properties, with rheological differences between layers resulting in a buckling instability. High concentrations of entrained debris or tephra may alter the rheology of ice layers sufficiently to initiate buckling (Hudleston, 2015), with small-scale examples of this process having been described in Antarctic glaciers (e.g., Ximenis et al., 2000).

Mapping of folds at a glacier surface, combined with 3-D measurement and analysis of data in stereographic projections enables the internal fold geometry to be determined. If borehole optical televiewing (e.g., Roberson & Hubbard, 2010) or ground-penetrating radar equipment (e.g., Hambrey et al., 2005) is available, then assessment of fold structures and their kinematic significance may be enhanced, as demonstrated on Midtre Lovénbreen in Svalbard (Figure 26).

5.3.2. Foliation

Foliation is a pervasive planar structure found in most glaciers, and develops in two main configurations: (a) longitudinal (Figure 27a); and (b) arcuate (or transverse) (Figure 27b) (Allen et al., 1960; Hambrey, 1977a; Hambrey & Lawson, 2000; Meier, 1960). Foliation mainly comprises anastomosing discontinuous layers of

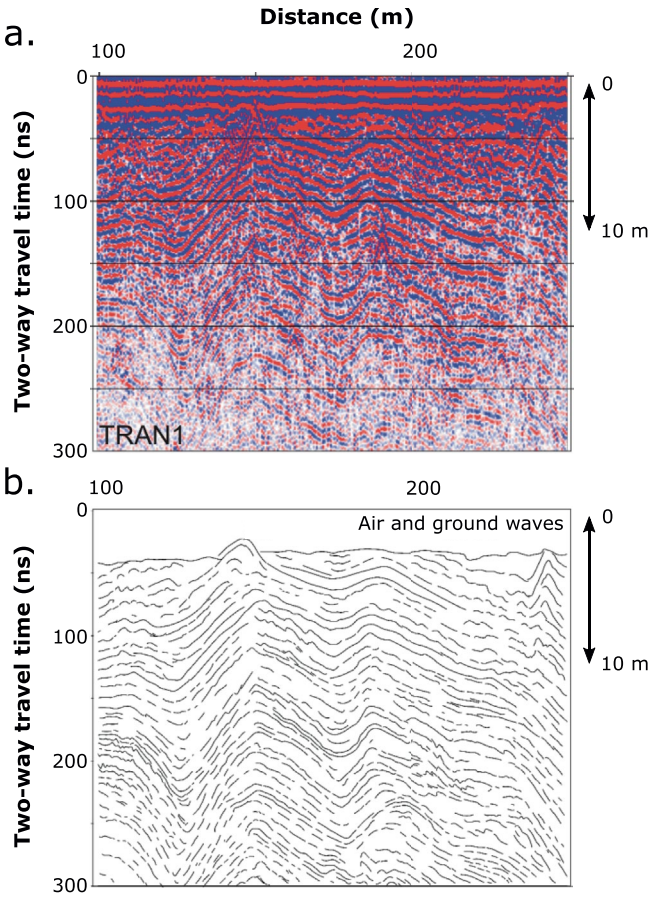

Figure 26. A ground-penetrating radar profile normal to ice flow in the middle reaches of Midtre Lovénbreen, Svalbard, illustrating the internal geometry of large scale and parasitic folds within primary stratification. (a) Radargram obtained by T. Murray using a Sensors and Software PulseEKKO 100 GPR, using 100 MHz antennae. (b) Interpretation of structure showing anticlines and synclines, as well as parasitic (small-scale) folds (adapted from Hambrey et al., 2005).

coarse clear, coarse bubbly, and fine-grained ice, with individual layers typically several meters long, but rarely exceeding several centimeters in thickness. Cryo-lithological logs measured across longitudinal foliation reveals the varying proportions of the different ice facies (Figure 28). In some High-Arctic glaciers, however, the individual layers within foliation may reach hundreds of meters in length, as on Bylot Island, Canada. Crystallographically, foliation is defined by variations in crystal size, shape, and bubble concentration, as well as occasionally by elongate air bubbles, elongate crystals, or discrete shear planes, or a combination of these (Figure 29) (Hambrey & Müller, 1978). Different modes of formation have been suggested for the various types of foliation.

Longitudinal foliation is commonly derived from stratification, as revealed by the similarity of ice facies and the transitional relationships between the two structures (Appleby et al., 2010; Goodsell, Hambrey, & Glasser, 2005; Hambrey, 1977a; Hambrey & Milnes, 1977; Hooke & Hudleston, 1978; Jennings et al., 2014; Lawson et al., 1994; Ragan, 1969; Roberson, 2008). As ice flows from broad accumulation basins and converges into a narrow tongue, ductile deformation of primary stratification in pure and simple shear regimes gradually folds the initially surface-parallel layers. Transposition occurs as continued folding and eventual attenuation of fold limbs reorients layers until they are parallel to flow and are longitudinally oriented (Figure 30a). Consequently, this type of foliation has an axial planar relationship with the folding. A comparable transition is observed in metamorphic rocks (Hambrey & Lawson, 2000; Hobbs et al., 1976). It is common for fold hinges to become severed from their limbs and isolated during this process, leaving remnant fold hinges or intrafolial folds (Hambrey, 1977a). Foliation formation is most pronounced where folding is tightest. This primarily occurs in areas dominated by simple shear, such as at the confluence of flow units and at the glacier margins (Hambrey, 1977a; Hambrey & Lawson, 2000). The foliation not only comprises the usual anastomosing coarse bubbly and coarse clear ice layers, but also fine-grained ice that is, believed to be the product of crystallographic modification of ice layers when experiencing simple shear (Hambrey & Milnes, 1977; Jennings et al., 2014). This process is similar to cataclasis in metamorphic rocks that produces mylonite. Cataclasis in ice arises when ice crystals develop subgrains when strained, which then evolve into discrete new millimeter-size crystals, commonly aligned along discrete shear planes (Figure 27c). The distinctive fine-grained ice is white and weathers into a sugary texture.

Longitudinal foliation also results from transposition of other planar structures such as crevasse traces. These crevasse traces may be transverse in orientation but rotate in a simple shear regime into a flow-parallel direction, particularly near the margins of a glacier. Attenuation of these layers results in anastomosing alternation of coarse bubbly and coarse clear ice (Hambrey & Milnes, 1977; Jennings et al., 2016).

Not all longitudinal foliation is inherited from pre-existing structures, and it has been documented as a completely new structure, commonly occurring in the middle of flow units rather than at the margins (Allen et al., 1960; Hambrey & Glasser, 2003; Hambrey et al., 1999, 2005; Jennings et al., 2014; Lawson, 1990; Lawson et al., 1994; Pfeffer, 1992). This type of foliation also has a clear axial planar relationship with folding, but unlike transposition foliation, shows a cross-cutting relationship with folded surfaces (Figures 27d and 30b). The foliation cross-cuts primary stratification in a geometrically similar fashion to the folding/slaty cleavage relationship observed in low-grade metamorphic rocks such as mudstones or phyllite. However, the exact crystallographic relationships and the genesis of this type of axial planar foliation remain unknown (Hambrey & Lawson, 2000; Hambrey et al., 2005; Jennings et al., 2014).

Figure 27. Types of foliation. (a) Typical longitudinal foliation of anastomosing layers of coarse clear, coarse bubbly, and fine ice facies, Austre Brøggerbreen, Svalbard. (b) Arcuate foliation formed by compression of crevasse traces below an icefall, Vadret da Morteratsch, Switzerland. (c) Longitudinal foliation with zones of heavily sheared (fine-grained) ice, with partial recrystallization into coarse-clear ice, enhanced by surficial mud, Austre Brøggerbreen, Svalbard. (d) Cleavage-like longitudinal foliation intersecting stratified ice that has been folded in the similar style, Austre Lovénbreen, Svalbard.

Individual flow units, and in many cases entire glaciers, tend to be dominated by one type of longitudinal foliation, that is, cleavage-like foliation (Hambrey et al., 2005) or transposition foliation (Roberson, 2008), and it has been suggested that each type is location-dependent (Jennings et al., 2014). Comparison of flow units that are dominated by different types of longitudinal foliation on Vadrec del Forno, a temperate Alpine valley glacier, illustrates that flow unit characteristics dictate what type of foliation preferentially forms. It is inferred that in flow units that undergo lateral narrowing over a short distance, there are higher rates of simple shear and substantial cumulative strain. Consequently, primary stratification is rapidly transposed into a transposition foliation relatively high up the glacier. In flow units with less pronounced lateral narrowing, cumulative strain values are inferred to be lower, therefore allowing primary stratification to be preserved further downglacier. When primary stratification is preserved relatively far downglacier, an axial planar foliation that cross-cuts the stratification develops (Jennings et al., 2014). If the analogy with slaty cleavage is correct, then this structure may form in a pure shear regime.

The different ice facies contained within foliation have variable albedos, hence they are subject to differential weathering. On a small scale, this may be reflected in the development of sub-meter-scale relief of ridges and furrows (Figure 27a), which becomes more pronounced if solar radiation is strong, but less so

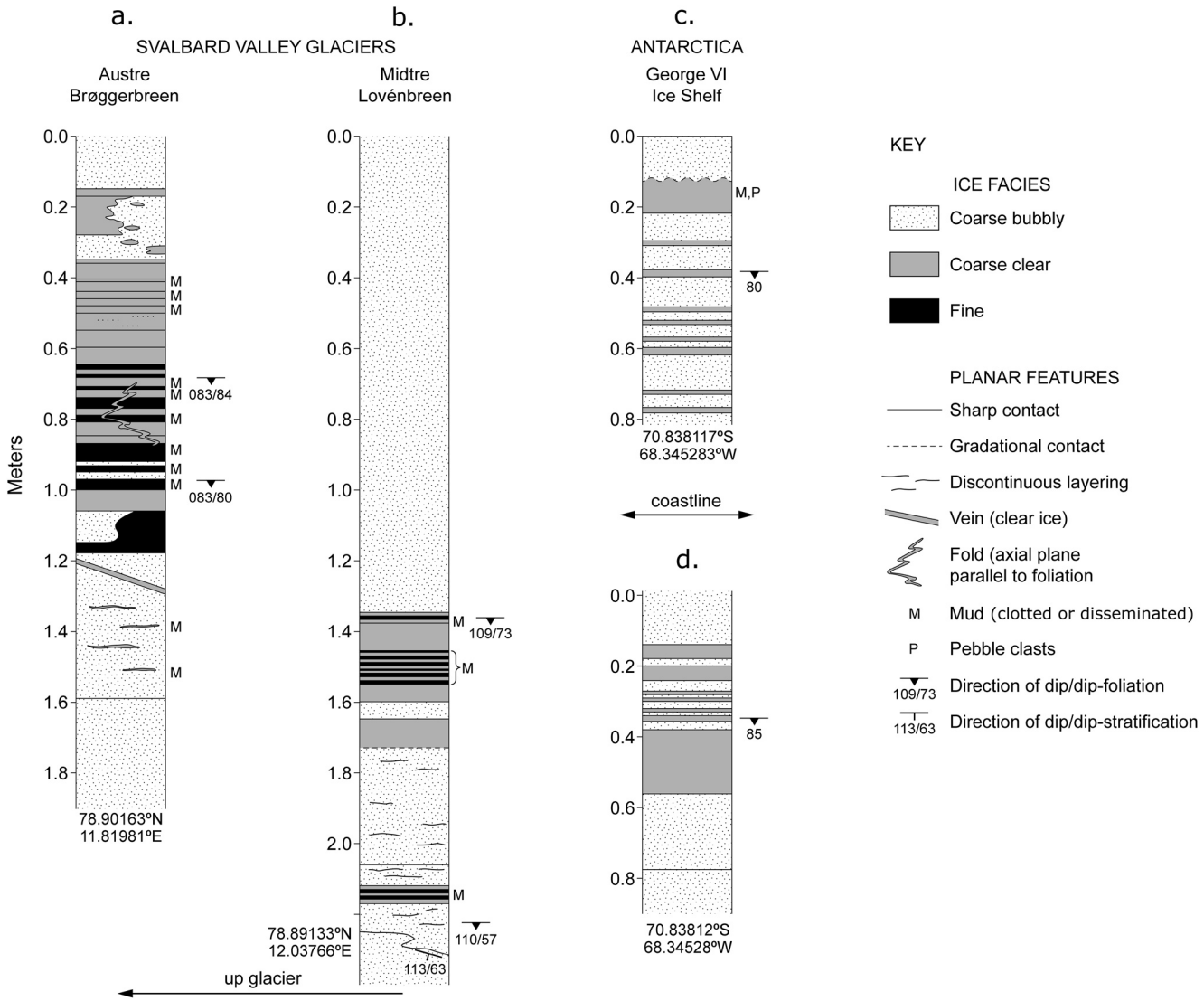

Figure 28. Measured logs through near-vertical foliation in two Svalbard valley glaciers (a, b) and an ice shelf in Antarctica (c, d), showing relative proportions of the different ice facies, the nature of facies boundaries, and other structures.

on rain-affected surfaces. On some glaciers foliation is responsible for relief on a scale of several meters, reflecting the different proportions of lighter and darker ice facies associations. At both scales, the influence on surface hydrology is strong (Section 9.4).

Several studies have attempted to reveal the relationship between longitudinal foliation and principal strain-rate tensors (Hambrey & Milnes, 1977; Hambrey & Müller, 1978; Meier, 1960; Ximenis et al., 2000), which in effect may be regarded as incremental strains (Milnes & Hambrey, 1976). Principal strain-rate tensors are determined by measuring changes in shape of arrays of five stakes inserted into the glacier surface using a least squares analysis (Nye, 1959a). Alternatively, changes of shape of triangular arrays may be used, an example being on Griesgletscher, Switzerland, where Hambrey and Milnes (1977) tracked strain-rates along a flow-unit boundary for 1.5 km. Along this boundary, longitudinal foliation transposed from earlier structures, along with minor folds, developed (Figure 31). Measured strain-rate tensor orientations settled down to a near-45° relationship with foliation, as would be predicted if this structure was continuing to evolve in a simple shear regime. Actual values of the principal extending strain-rate were up to 0.14 a^{-1}. However, the relationship between foliation and strain-rate tensors is often unclear, as a similar experiment on White Glacier, Axel Heiberg Island, demonstrated an initial simple shear relationship that did not survive many

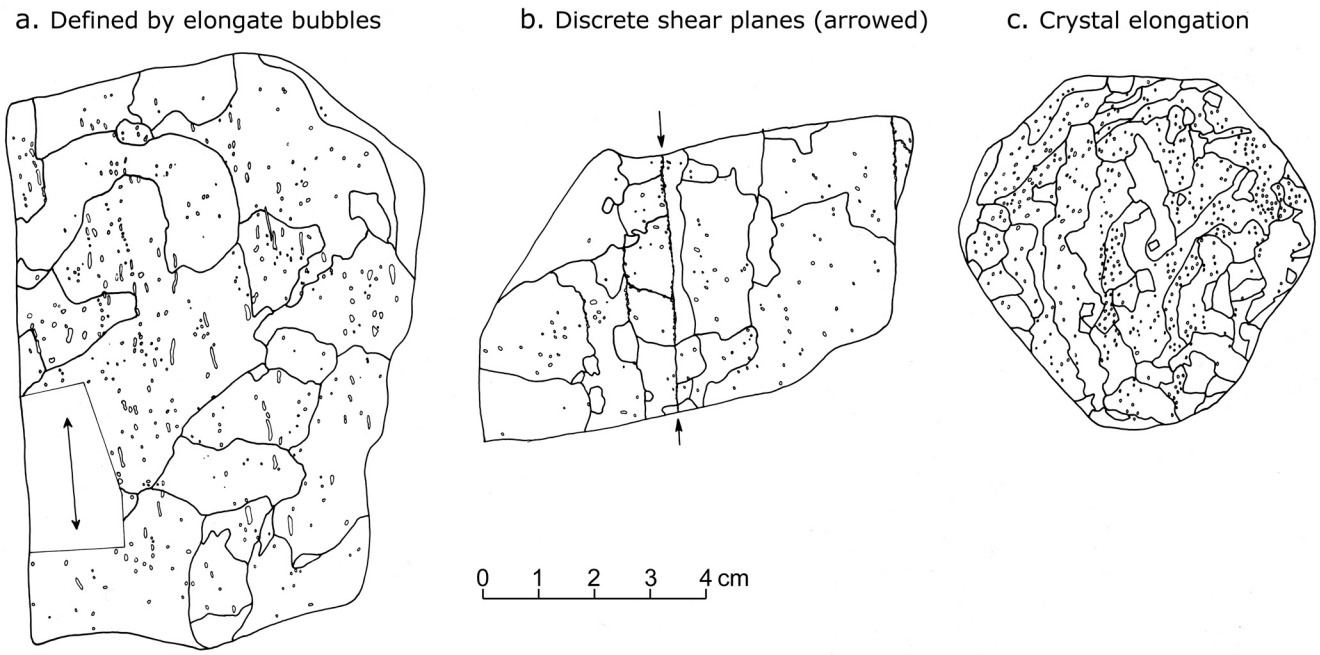

Figure 29. Crystal structure of different types of longitudinal foliation in polythermal White Glacier, Axel Heiberg Island, drawn from photographs of thin sections under cross-polarized light (modified from Hambrey & Müller, 1978).

meters below the flow-unit convergence zone (Hambrey & Müller, 1978). The main reason for this relationship is that, once developed, longitudinal foliation may be transported downglacier as a passive marker (Lawson, 1996), becoming deformed in different stress regimes. Thus the orientation of foliation no longer has any relation to the strain-rate tensors. It is therefore more advantageous to consider the formation and subsequent evolution of longitudinal foliation in relation to cumulative (finite) strain (i.e., taking into account the full strain history of "parcels" of ice). Cumulative strain has been determined by two methods: (a) visually, by tracking the change in shape of arbitrary circles from a velocity distribution and flow line map through use of Mohr circle constructions (Milnes & Hambrey, 1976); or (b) a finite element modeling approach (Clarke & Hambrey, 2019; Hambrey & Clarke, 2019; Hooke & Hudleston, 1978; Hubbard & Hubbard, 2000). These methods recognize that, in reality, longitudinal foliation is the product of continuous and often multiple phases of deformation (Hambrey et al., 1980). When longitudinal foliation first forms, a cumulative strain ellipse is initially oriented at 45° to the trend of foliation. If the foliation remains in a simple shear regime, the long axis (x-axis) of the strain ellipse will rotate toward parallelism with the foliation (Figure 32). This relationship has been demonstrated on Griesgletscher (Hambrey & Milnes, 1977; Hambrey et al., 1980) and Haute Glacier d'Arolla, Switzerland (Goodsell, Hambrey, Glasser, Nienow, & Mair, 2005; Hubbard & Hubbard, 2000), and Midtre Lovénbreen, Svalbard (Hambrey et al., 2005).

Unlike longitudinal foliation, arcuate (or transverse) foliation is primarily the result of crevasse traces passing into a longitudinally compressive stress regime (e.g., below an icefall), where the transverse layering is amplified (Allen et al., 1960; Gunn, 1964; Hambrey & Lawson, 2000; Hambrey & Milnes, 1977; Lawson, 1996). Arcuate foliation therefore develops in a pure shear regime where the foliation forms normal to the maximum compressive strain-rate and remains in this attitude as it travels through the glacier. In other words, the foliation forms and remains perpendicular to the short axis (z-axis) of the strain ellipse (Figure 32). Griesgletscher also demonstrates this relationship, but the magnitude of cumulative strain and subsequent strength of the arcuate foliation are substantially less than for longitudinal foliation (Hambrey & Milnes, 1977; Hambrey et al., 1980). However, the 3-D relationships between foliation and the strain ellipsoid have yet to be explored.

Both longitudinal and transverse foliation has been observed in surge-type glaciers, notably Variegated Glacier, Alaska (Lawson et al., 1994; Pfeffer, 1992). Longitudinal foliation forms during the quiescent phase when flow is predominantly ductile, in much the same way as it forms in non-surge-type glaciers.

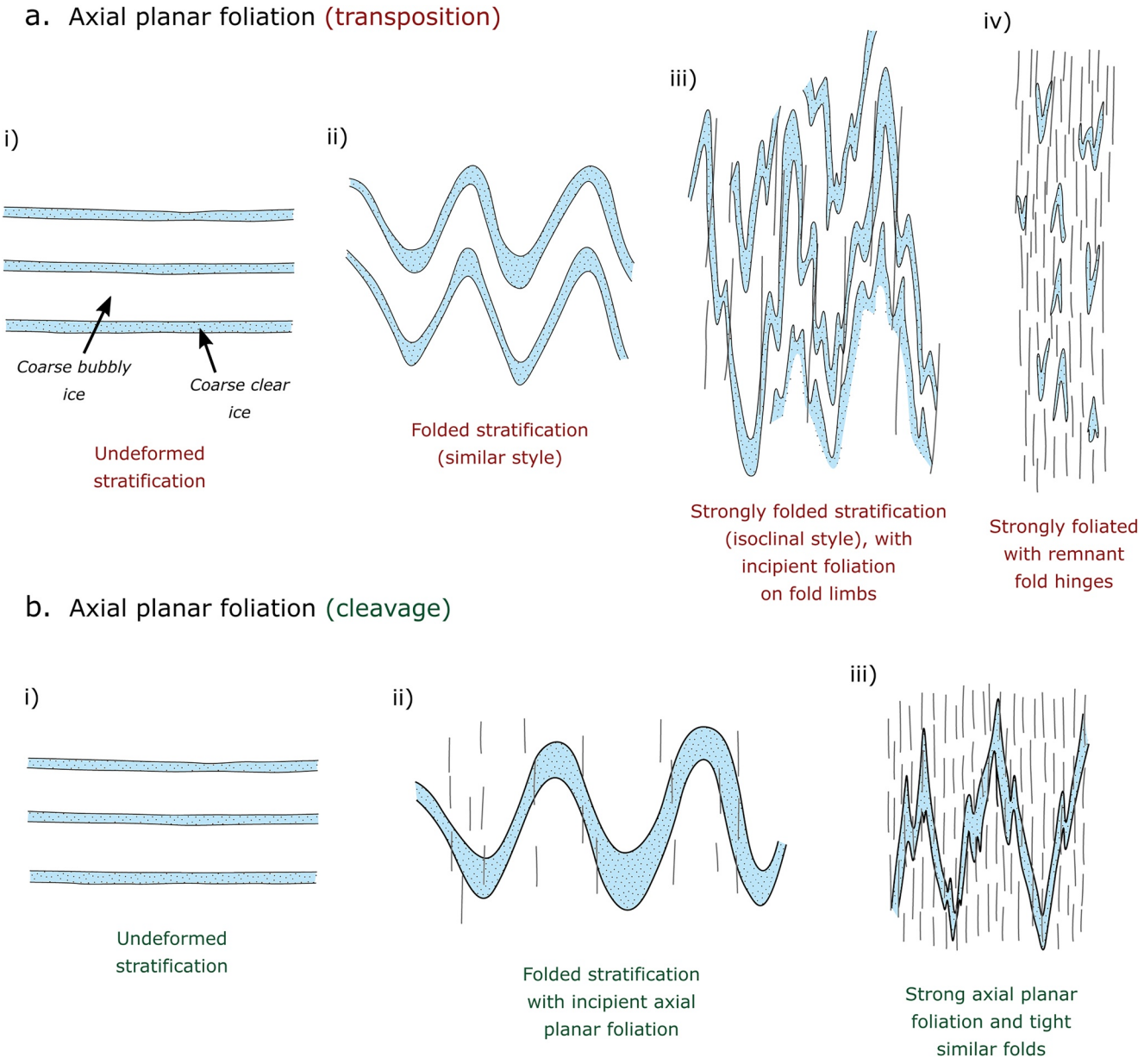

Figure 30. Schematic diagram to illustrate the relationship between foliation and folding. (a) Transposition from earlier layering such as stratification (modified from Hambrey, 1994). (b) Cleavage-like foliation in axial planar relationship with folded stratification.

In contrast, formation of transverse foliation is probably related to intense surge-related thrust-faulting and longitudinal shortening under a high compressive stress at the surge front (Hambrey & Lawson, 2000; Lawson et al., 1994; Pfeffer, 1992).

5.3.3. Boudinage Structures

Boudinage structures that are so characteristic of multi-layered deformed rocks also occur in glacier ice. They are the result of layer-parallel extension and pulling apart of a layer, or layers, of different rheology from the surrounding material (Fossen, 2010). Classic boudinage layers when viewed in cross-section resemble strings of sausages (hence the derivation of the term "boudin" from the French word for blood sausage). However, a range of boudin geometries exists, depending on the ice layer properties and the specific deformational environment (Fossen, 2010; Hambrey & Lawson, 2000; Hambrey & Milnes, 1975). Boudin shapes vary from rectangular through to pinch-and-swell structures depending upon the viscosity contrast

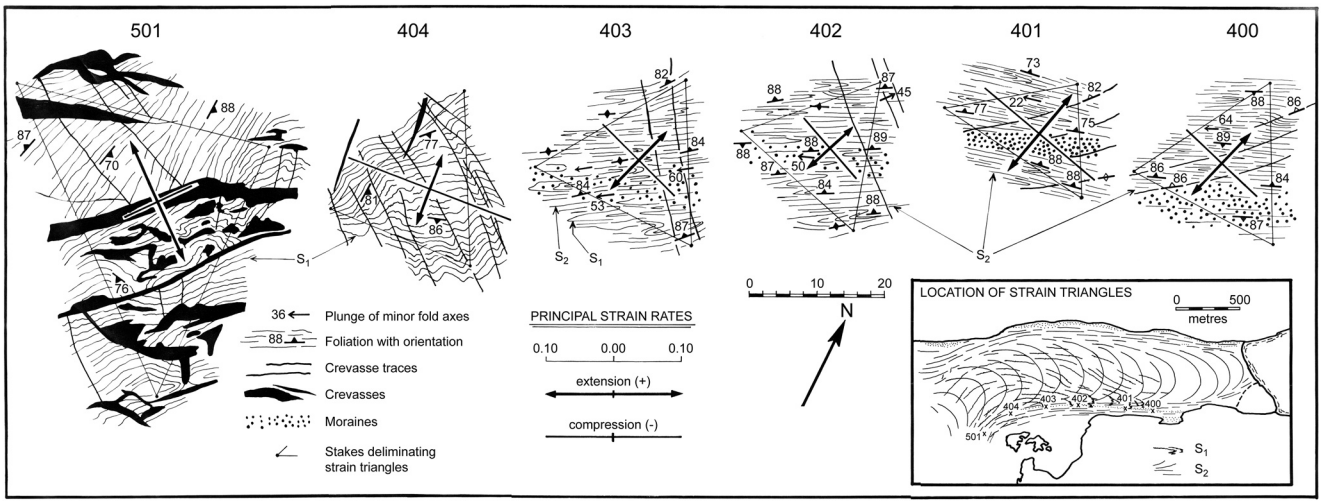

Figure 31. Strain-rate tensors measured using triangular stake arrays at six points across a flow-unit boundary in Griesgletscher, Switzerland, illustrating the relationship between actively forming foliation and simple shear (after Hambrey et al., 1980; reproduced with permission of the International Glaciological Society).

between the ice layers (Figure 33). Strongly competent layers (i.e., layers that are relatively more resistant to flow than the surrounding matrix or layers) form rectangular boudins by brittle deformation, while the surrounding less-competent materials deform by ductile deformation (Hambrey & Milnes, 1975). If the competence contrast between layers is less, the resulting boudins are more rounded or stretched out by ductile deformation. Less competent layers that have a low ductility contrast between adjacent ice types are termed pinch-and-swell structures (Fossen, 2010). Two main types of boudinage are found in glaciers: (a) competence contrast; and (b) foliation boudinage. Both types have been observed in temperate glaciers with scales

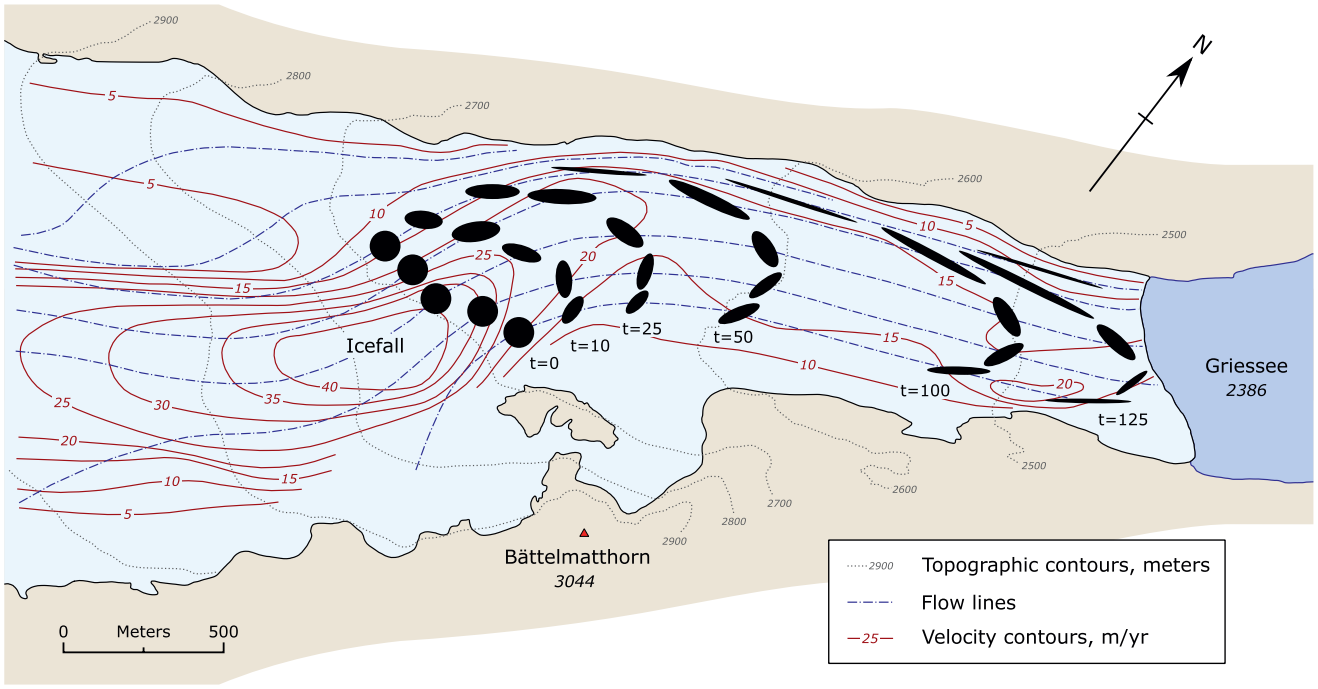

Figure 32. Strain ellipses calculated from a velocity contour/flow trajectory map on Griesgletscher, Switzerland, in the 1970s, prior to subsequent recession and stagnation. The *t*-numbers adjacent to ellipses on each transect are years taken for ice to reach those points from the base of the icefall, assuming steady-state flow (modified from Hambrey & Milnes, 1977).

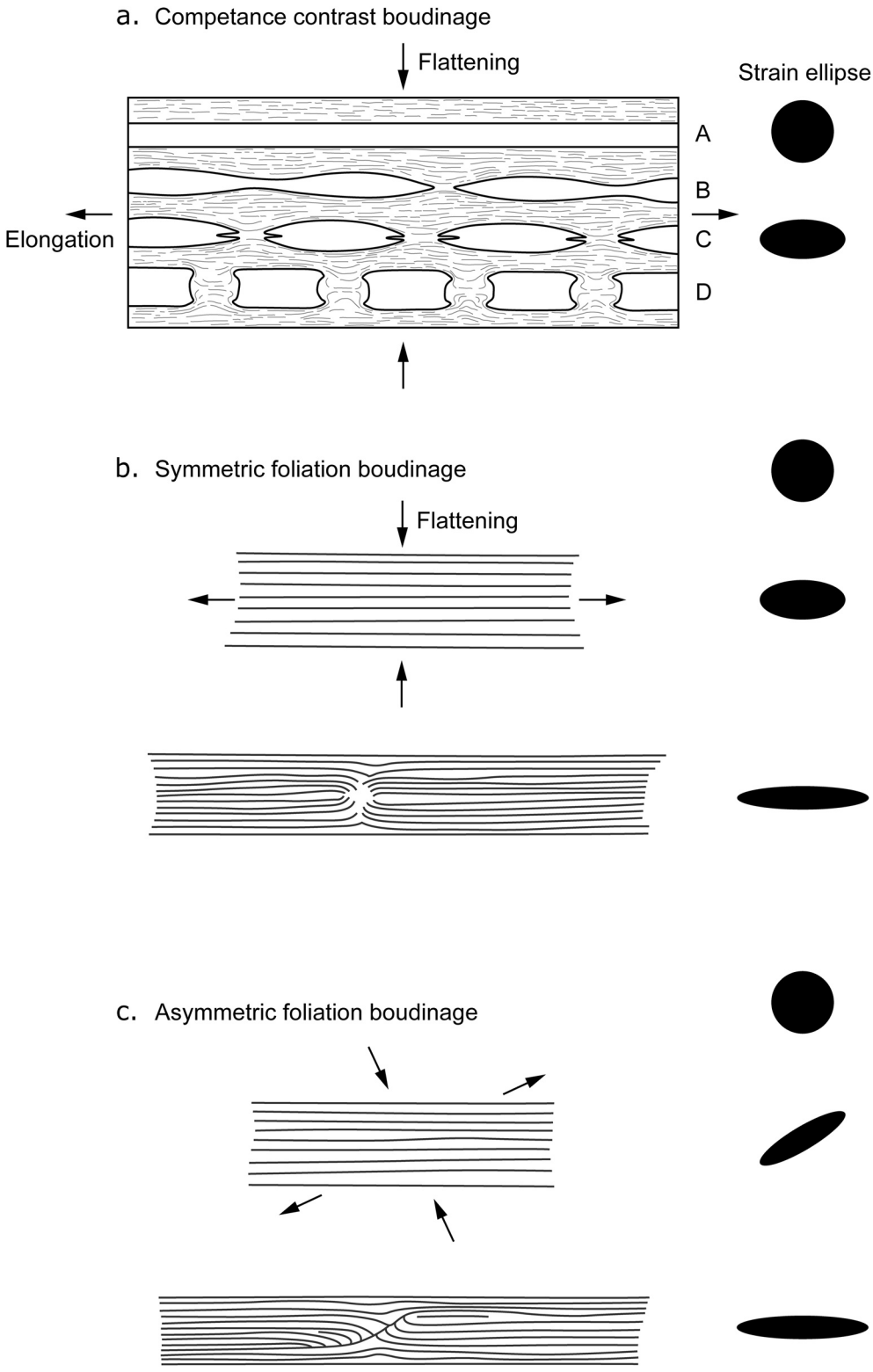

Figure 33. Schematic diagram to illustrate the development of different types of boudinage structure. (a) Competence-contrast boudinage. (b) Symmetric foliation boudinage. (c) Asymmetric foliation boudinage. The relationship with the strain ellipse is shown (after Hambrey & Milnes, 1975; reproduced with permission of the International Glaciological Society).

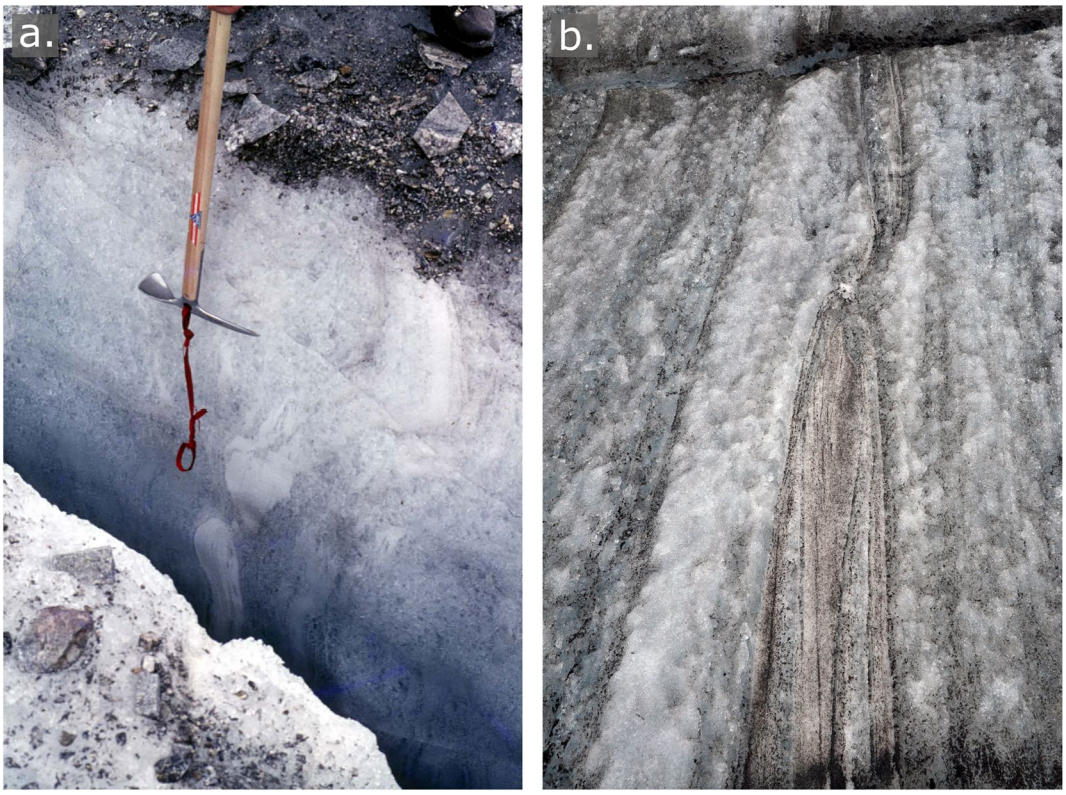

Figure 34. Examples of boudinage structures. (a) Competence-contrast boudinage (white ice) in longitudinal foliation in Vadrec da l'Albigna, Switzerland. (b) Asymmetric foliation boudinage in longitudinal foliation, Gulkana Glacier, Alaska.

ranging from centimeters through to several meters (Hambrey & Lawson, 2000; Hambrey & Milnes, 1975). However, in rocks, more complex yet uncommon boudinage geometries such as chocolate tablet boudinage can sometimes develop in nonplane-strain deformation regimes (Passchier & Druguet, 2002).

Competence contrast boudinage (Figure 33a) forms where a competent layer is extended, separating the layer into regularly spaced and shaped sections by ductile deformation, brittle deformation, or a combination of the two (Fossen, 2010). Examples of competence-contrast boudinage have been observed in Swiss glaciers, where packages of fine ice layers that are surrounded by coarse bubbly ice within foliation have become attenuated (Figure 34a) (Hambrey & Lawson, 2000; Hambrey & Milnes, 1975). The basal ice zone is also prone to boudinage formation. Debris-rich ice, or indeed entrained packages of sediment, are typically more competent than debris-free ice. However, it is worth noting that depending on factors such as debris concentration, temperature, and the presence or absence of water at crystal boundaries, debris-rich ice layers can either be strengthened or weakened in comparison to surrounding layers (cf. Moore, 2014); examples have been reported from the basal zone of cold glaciers in the Dry Valleys, Antarctica (Gow, 1972; Hambrey & Fitzsimons, 2010).

Foliation boudinage comprises two subcategories: (a) symmetric; or (b) asymmetric (Figures 33b and 33c). Both varieties are found in areas of strong longitudinal foliation, such as at the glacier margins or at the confluence of flow units; however, the latter is most common (Hambrey & Lawson, 2000; Hambrey & Milnes, 1975, 1977). Unlike competence contrast boudinage that develops in individual ice layers, foliation boudinage forms in foliated or multi-layered ice (Figure 34b). Despite individual ice layers being structurally anisotropic, because the boudins form across a number of layers, the foliation can be regarded as effectively having the same rheology inside and outside of the boudin (Fossen, 2010; Hambrey & Milnes, 1975). Consequently, the boudinage layer as a whole can be regarded as having no competence contrast with the surrounding ice (Hambrey & Milnes, 1975). Symmetrical foliation boudinage (Figure 33b) forms between tensile fractures. As the fractures open, the foliated ice becomes pinched toward the fracture and a void

develops between boudins. Observations of symmetrical foliation boudinage reveal that void structures between boudins become water-filled and subsequently freeze to produce large clear ice crystals that grow perpendicular to the void's edge (Hambrey & Milnes, 1975). Asymmetric foliation boudinage (Figure 33c) is strongly related to brittle shear fractures or ductile shear zones that cross-cut longitudinal foliation obliquely. Displacement along the shear fractures rotates the foliation, forming the boudin neck (Fossen, 2010; Hambrey & Lawson, 2000), and a rotational strain regime is envisaged. The formation of foliation boudinage occurs in response to longitudinal extension and simple shear acting in unison. Such conditions are found on the outside of a bend, and it has been suggested that fractures initially formed upglacier may act as planes of weakness that can be reactivated in this type of stress regime (Hambrey & Lawson, 2000; Lawson et al., 1994).

Boudin-like features may result from two separate phases of deformation. Tensile fractures develop in areas experiencing extension. Subsequent transport into a non-coaxial strain regime closes and rotates the fracture, also deforming the foliation lying perpendicular to the fracture (boudin neck) to form pairs of offset asymmetric hook folds or flanking structures (Figure 23), explained in Section 5.3.1 (Hambrey & Lawson, 2000; Hudleston, 1989). Equivalent flanking structures observed in rocks are indeed defined as an end-member type of foliation boudinage (Arslan et al., 2008).

5.4. Combined Brittle and Ductile Structures

5.4.1. Basal Ice

The basal ice layer can be distinguished from other types of glacier ice in that it has unique physical and chemical characteristics, notably high concentrations of debris, and a high proportion of regelation ice, especially in polythermal glaciers. The considerable research that has been undertaken on basal ice has been evaluated in several reviews (Alley et al., 1997; Hubbard & Sharp, 1989; Hubbard et al., 2009; Knight, 1997; Moore, 2014). Study of basal ice facies, exposed in marginal cliff sections, is important for deducing conditions and processes occurring at or near to the bed of a glacier or an ice sheet.

Several distinct basal ice types have been defined based on debris concentration, ice type, and air bubble content (Hubbard et al., 2009). The properties of these different facies impacts upon how they deform. For example, the mechanical and dynamic properties of debris-ice mixtures is affected by various factors, which complicates the relationship between debris content and deformation, see Section 3.5 (Moore, 2014).

Basal ice itself has many structural features, including micro-shears, isoclinal and similar folds (Figure 35a), and competence-contrast boudinage (Figure 35b), on a decimeter scale. Thus the ice and debris facies comprising basal ice are disrupted and made more complex by flow-related tectonic deformation (Waller et al., 2000). Flow over bumps and around obstacles induces recumbent folding (also known as "lee-side eddies"). The basal ice zone is thus one of intense shear where most of the glacier deformation is concentrated, and the folds can be regarded as the result of "perturbation of flow," as in geological shear zones (Alsop & Holdsworth, 2002).

From field observations, basal ice appears to be elevated to a higher level in a glacier by a combination of folding and thrust-faulting (Figure 35c). Recumbent folding on a scale of several meters commonly involves clean glacier ice above the basal debris layer, and a thrust-faulted lower limb in many cases implies a temporal progression from ductile deformation to brittle failure.

5.4.2. Thrust-Faulting and Recumbent Folding

Reference has been made in Section 5.2.4 to the common association of inferred thrust-faulting and recumbent folding. Examples include Kviárjökull in Iceland (Phillips et al., 2017), Tunabreen in Svalbard (Fleming et al., 2013), and Trapridge Glacier in the Yukon (Hambrey & Clarke, 2019). Typically, similar or isoclinal folds with axial planes parallel to thrust planes, and with fold axes normal to flow, occur in the basal several meters of glaciers that have experienced strong longitudinal compression. These relationships are best observed if ice cliffs are aligned approximately parallel to the ice-flow direction. Fold axes commonly are not straight, so when folds are observed face-on they are in the form of sheath folds, as, for example, described at Tunabreen in Svalbard (Fleming et al., 2013).

Figure 35. Structures in basal ice. (a) The basal ice zone of Fountain Glacier, Bylot Island, showing debris entrainment, isoclinal folding, and shear structures. The tape length is 1 m. (b) Competence-contrast boudinage structure near the base of Wright Lower Glacier, Victoria Land, Antarctica. The boudins are of fluvial sand, partially rotated, and surrounded by basal ice. (c) Debris-laden thrust faults and folded basal ice layers characterize the then-advancing (1975) snout of Thompson Glacier, Axel Heiberg Island, Canada.

The evolution of fold/thrust-fault relationships has been explored at Trapridge Glacier, Yukon, from both observational and numerical modeling perspectives (Clarke & Blake, 1991; Hambrey & Clarke, 2019). As observed in 2006, a slow-motion surge had reached the terminus a few years earlier, producing a cliff up to 15 m high (Figure 36a). This cliff revealed an assemblage of coarse-clear ice and debris layers, extending for tens of meters. Most layers dip down-glacier but less steeply than the underlying bed. These layers had an asymptotic relationship with the bed and with each other, with a prominent debris layer generating other debris layers above it in "piggy-back" fashion (Figure 20a). The debris itself has the sedimentological properties of basal ice sediment, melting out to produce a diamicton. Some debris layers lose their debris upwards, and others terminate abruptly. These debris layers are intimately associated with meter-scale recumbent folds of similar and isoclinal type, with fold axes sub-parallel to the ice front (Figures 36b and 36c). Some of the folds comprise debris layers as well. The lower limbs of many of these folds are truncated at a debris plane.

The debris layers represent thin zones of basal ice that have been raised from the glacier bed. The process described by Hudleston (1976) of recumbent folding triggered at bedrock bumps, appears to apply in this case. As a basal debris layer is folded within the body of the glacier, the fold becomes increasingly attenuated until the lower limb is "sheared off" (Figure 36d), which then develops into a thrust-fault. Many thrusts reach a high level in the ice cliffs, but few penetrate the surface, so are considered to be "blind." Distortion of fold axial planes and intersecting thrust-faults with debris give rise to structurally highly complex zones in the lower parts of the glacier cliffs (Figure 36e).

Since the folds and thrusts are observed only at the snout of the glacier, and not where they were formed, modeling their evolution during the slow-surge cycle is a challenge. However, a thermomechanical ice

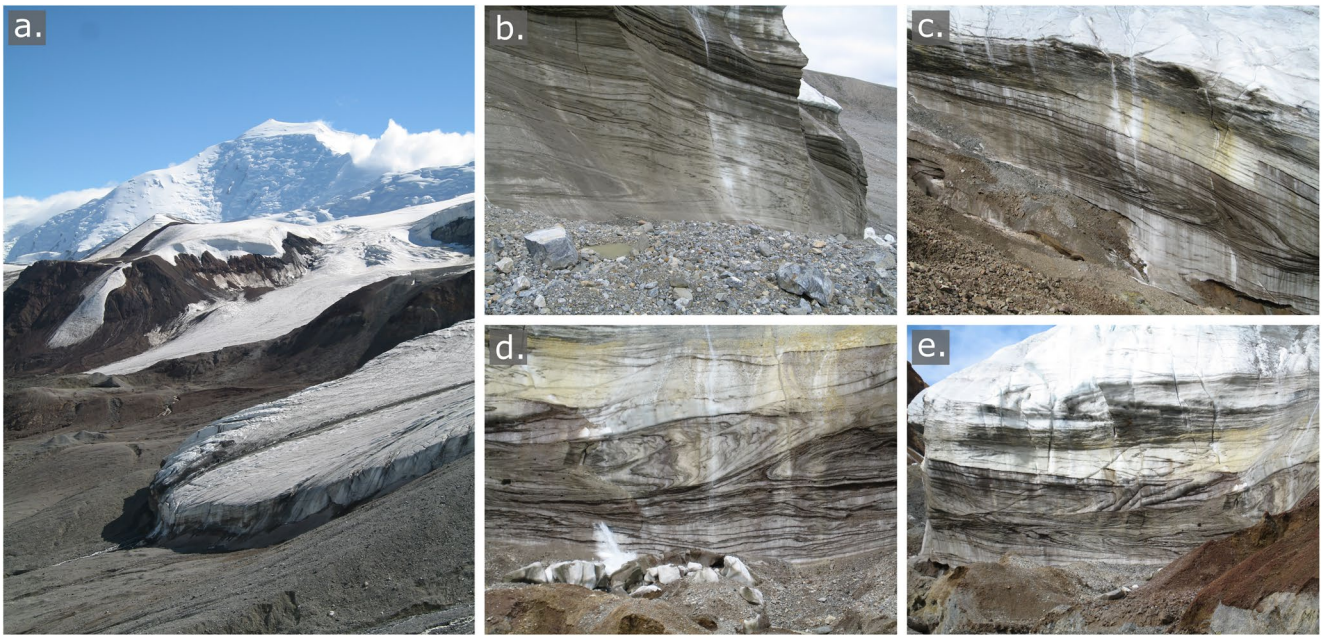

Figure 36. Fold and thrust-fault relationships in Trapridge Glacier, Yukon, following the development of a terminal cliff during a "slow surge." (a) Overview of the snout of the glacier, showing the terminal cliff in which folding, thrust-faulting, and debris-entrainment are prominent. (b) Meter-scale similar style folding with centimeter-scale parasitic folds and debris-laden thrusts. (c) Meter-scale isoclinal fold and layers containing basal debris; flow to the right. (d) Recumbent fold with "sheared off" lower limb, and other zones of shear and thrust-faulting; flow diagonally to the right. (e) Complex deformation to the full height of the 10 m-high glacier cliff, showing isoclinal and similar folding, thrust-faulting, shear zones, and basal ice layers: flow toward the camera position.

dynamics model has been developed using known ice thickness, temperature, and velocity field data, which then leads to quantification of tensors for velocity gradient, deformation rate, and deviatoric stress (Hambrey & Clarke, 2019). Modeling during a surge cycle indeed predicts that recumbent folds will form near bumps in the bed (cf. Hudleston, 1976) and toward the glacier snout. On the other hand, the numerical model was not able to resolve the intricate strain pattern that can result from a combination of folding and thrust-faulting. In a more generic case of a "Traplike" glacier, a simple scalar parameterization was proposed that aimed to identify strain conditions favoring folding during surging and nonsurging scenarios (Clarke & Hambrey, 2019). These authors showed that the nonsurging model was most conducive to folding, probably because creep deformation is greater than in surging models. However, it was not possible to simulate the combination of folding and thrusting in the surging model, a task that remains for future researchers.

5.4.3. Shear Zones

Discrete shear zones, exposed at the glacier surface, are linear or curvilinear structures that experience noticeably higher strain than the surrounding zones. They are often associated with thrust-faulting and foliation, but are also evident in crevassed areas (Hambrey & Lawson, 2000; Hudleston, 1989). A combination of ductile and brittle deformation is often seen in shear zones, with initial ductile deformation becoming superseded by brittle fracture when the brittle strength of the ice is exceeded. As in longitudinal foliation, simple shear may also subject the ice to cataclasis. However, ice crystal growth can also be promoted depending on the balance of constructive and destructive processes active during deformation. Discrete shear zones are primarily observed at flow unit boundaries in areas of strong longitudinal foliation, in areas of active crevasse formation and strike-slip faulting, or parallel to thrust-faults.

At the confluence of two flow units, enhanced simple shear tightly folds and transposes primary stratification into a strong longitudinally oriented transposition foliation (cf. Section 5.3.2). It is at or near to flow-unit boundaries that shear zones, composed of comparatively thin layers (sometimes called shear bands) of fine-grained white ice, can commonly be observed. The presence of fine-grained ice is evidence of crystallographic modification of pre-existing ice layers, as this ice facies is not derived from initial snowpack

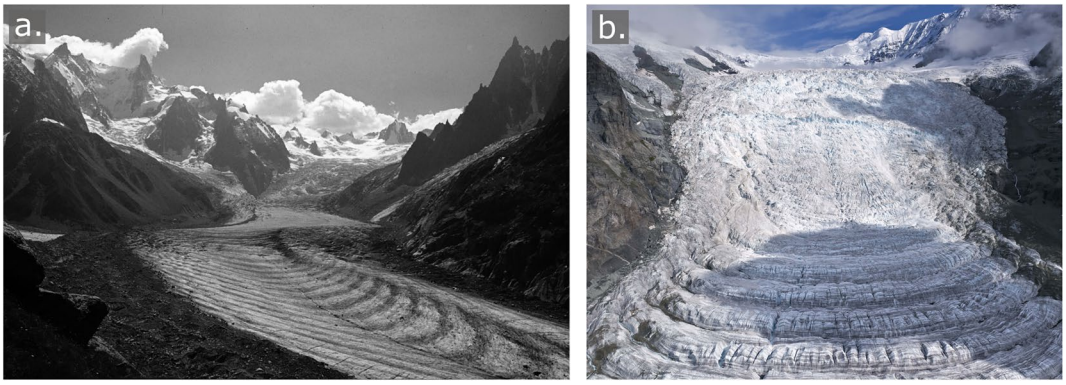

Figure 37. Characteristics of ogives. (a) Band ogives or Forbes' bands forming at the base of an icefall on Mer de Glace, France. (b) Wave ogives developing in the icefall of Ewigschneefeld, Grosser Aletschgletscher, Switzerland.

formation (cf. Wadham & Nuttall, 2002) or from the diagenesis of the snowpack into glacier ice (Hambrey, 1977a; Hambrey & Lawson, 2000; Jennings et al., 2014).

Shear zones are also observed where strike-slip faulting occurs in areas of active crevassing, or where crevasse traces are reactivated. Bending of passive marker layers (e.g., longitudinal foliation) within the shear zone occurs as a result of ductile deformation, displacing the layering and forming hook folds (sometimes called drag folds) that bend toward the fracture. Ductile deformation continues to displace layering until the brittle strength of the ice is exceeded and brittle fracture is initiated (Hambrey & Lawson, 2000).

Sheared ice is commonly observed parallel to thrust-faults, where ductile deformation deforms englacial layers (e.g., longitudinal foliation) before brittle fracture is initiated. Evidence of thrust-fault-related shear zones has been observed in surge-type glaciers in Svalbard (Hambrey et al., 1996), where transverse shear zones evident on the surface of Bakaninbreen reached several tens of meters in length at the surge front. Surging glaciers also develop shear zones at their margins. Although different from the aforementioned shear zones, they are zones of heavily fractured and brecciated ice that results from fast glacier flow against the valley side.

5.4.4. Ogives

Ogives are striking, but enigmatic alternating arcuate bands or waves that are occasionally seen below icefalls in valley glaciers. They have received considerable attention since the early pioneers James Forbes and Louis Agassiz studied these structures on the Mer de Glacier in the French Alps in the mid-19th century (Figure 37a; also Figure 1) (see review in Goodsell et al., 2002). These ogives were well-known to tourists in the 19th century, as a funicular railway was built to the station of Montenvers, which provided a dramatic view over the glacier. At the same location today, the glacier surface has down-wasted by several hundred meters and is strewn with rock debris, obscuring much of the structure. The convex down-glacier nature of ogives reflects ice-flow differences across the breadth of the glacier. Among the earliest systematic studies of ogives, those on three Icelandic glaciers are noteworthy in establishing an annual cycle of their formation, and identifying a possible role played by thrust-faulting of basal debris to form the dark bands (Ives & King, 1954; King & Ives, 1956).

Ogives are now considered to comprise two types: (a) band ogives; and (b) wave ogives. Band ogives are sometimes referred to as Forbes bands, or as "moraine ogives" (Gunn, 1964). Wave ogives (sometimes referred to as swell-and-swale ogives) are characterized by wave-like arcs. The two types are commonly juxtaposed (Goodsell et al., 2002; Hambrey & Lawson, 2000; Post & La Chapelle, 1971; Waddington, 1986). Band ogives consist of alternating dark bands of highly foliated debris-rich ice and light bands of coarse bubbly ice (Figure 37a), whereas wave ogives are arcuate surface undulations which have a maximum amplitude of c. 5 m directly below an icefall (Figure 37b) (Goodsell et al., 2002; Herbst et al., 2006). Band ogives have a 3-D geometry often compared to nested spoons with the dip of the layers oriented upglacier.

There is general acceptance that wave ogive formation is a result of seasonal variations in ablation as ice velocity increases when entering an icefall, creating a wave-and-trough morphology for each year's movement of ice through the icefall. Extension and the resulting thinning of the ice ensure that ice in the icefall has a larger surface area than for the rest of the glacier. Therefore, comparatively more ablation during the summer months is reflected in the surface being lowered to form the wave troughs, whereas ridges reflect passage through the icefall during the winter months when snow accumulates, reflect radiation, and therefore has a comparatively higher surface. This model has also been used to explain the formation of both wave and band ogives, with the troughs acting as sediment traps during the summer months to give the darker color (Nye, 1958, 1959b; Waddington, 1986). A refinement of this hypothesis is that the dark bands are a consequence of debris and refrozen water being concentrated in glacier-wide crevasses within the icefall in summer (King & Lewis, 1961). Using the assumption that each pair of ogives are formed annually, it has proved possible to determine velocity changes over time, as on the Mer de Glace (Lliboutry & Reynaud, 1981).

Band ogives are more structurally complex than the above interpretation implies, and internal deformation plays a crucial role. Among the many hypotheses, shearing was suggested by Chamberlin (1895), and "reverse faulting with associated drag folding" by Posamentier (1978). A detailed structural study of ogives was undertaken by Goodsell et al. (2002), who mapped in 3-D and undertook a ground-penetrating radar survey of ogives below the icefall of Bas Glacier d'Arolla in Switzerland. Modifying the Posamentier (1978) model, they proposed that dark ogive bands were the surface expression of intense up-glacier dipping (transverse) foliation formed at the base of an icefall. The foliation exposed at the surface was a manifestation of shear zones developed parallel to rotated and compressed crevasse traces, propagating from the bed. The basal connection is evident from local patches of debris (subrounded and subangular clasts) and basal ice in the dark layers at the glacier surface. The light bands represent glacier ice derived from firn, with relatively little contained debris. This shear hypothesis of ogive formation is further supported by research on the Icelandic glacier Kvíarjøkull, where ogive foliation is associated with thrust-faulting (Swift & Jones, 2018; Swift et al., 2006). These band ogives are the dominant structure in the glacier, extending from the base of an icefall across the width of the glacier to the snout (Phillips et al., 2017).

A curious feature of some ogives is the lack of relief between the light and dark ogive components, whereas one would expect differential ablation to be evident. This is true on the Mer de Glace, where Vincent et al. (2018) studied the mass balance of the individual light and dark bands. They found that the albedo was 40% lower in the darker bands than in the lighter ones, but that mass balances were similar. Variations in surface roughness were considered to be the reason for this result.

5.5. Hydrologically Derived Structures

The action of supraglacial, englacial, and subglacial streams leads to the erosion of channels, moulins, and canyons (St Germain & Moorman, 2019). Many of these drainage features are controlled by existing structures, such as crevasses, crevasse traces, and foliation. A well-illustrated account comes from Mikkaglaciären in northern Sweden (Stenborg, 1969). Channels and moulins are, in turn, healed with frozen water or snow, or close as a result of deformation of the ice, leaving distinctive structures, as described below. These features have received little attention, however. The importance of ice structures in influencing water-routing through a glacier is covered in Section 9.4.

5.5.1. Supraglacial Channel-Fills

Glaciers with convex cross-sectional profiles often have marginal streams where supraglacial water has drained to the lateral margins of the glacier, whereas glaciers with concave cross-sections usually develop supraglacial channels in the middle-reaches of the glacier (Hambrey, 1977c). Supraglacial meltwater channels are sometimes ephemeral features that close as a result of ice creep during the winter months, at least in dynamically active glaciers. They subsequently reform in a different location during the following melt-season. Channels are commonly deep (several meters) relative to their width, especially in slow-moving polythermal glaciers. Meandering channels with pools and riffles are common (Ferguson, 1973; Hambrey, 1977c; Knighton, 1972, 1981, 1985; Parker, 1975; Stenborg, 1969). In active ice, once abandoned, channels are healed as deformation results in closure, leaving curved traces at the glacier surface. In slow-moving

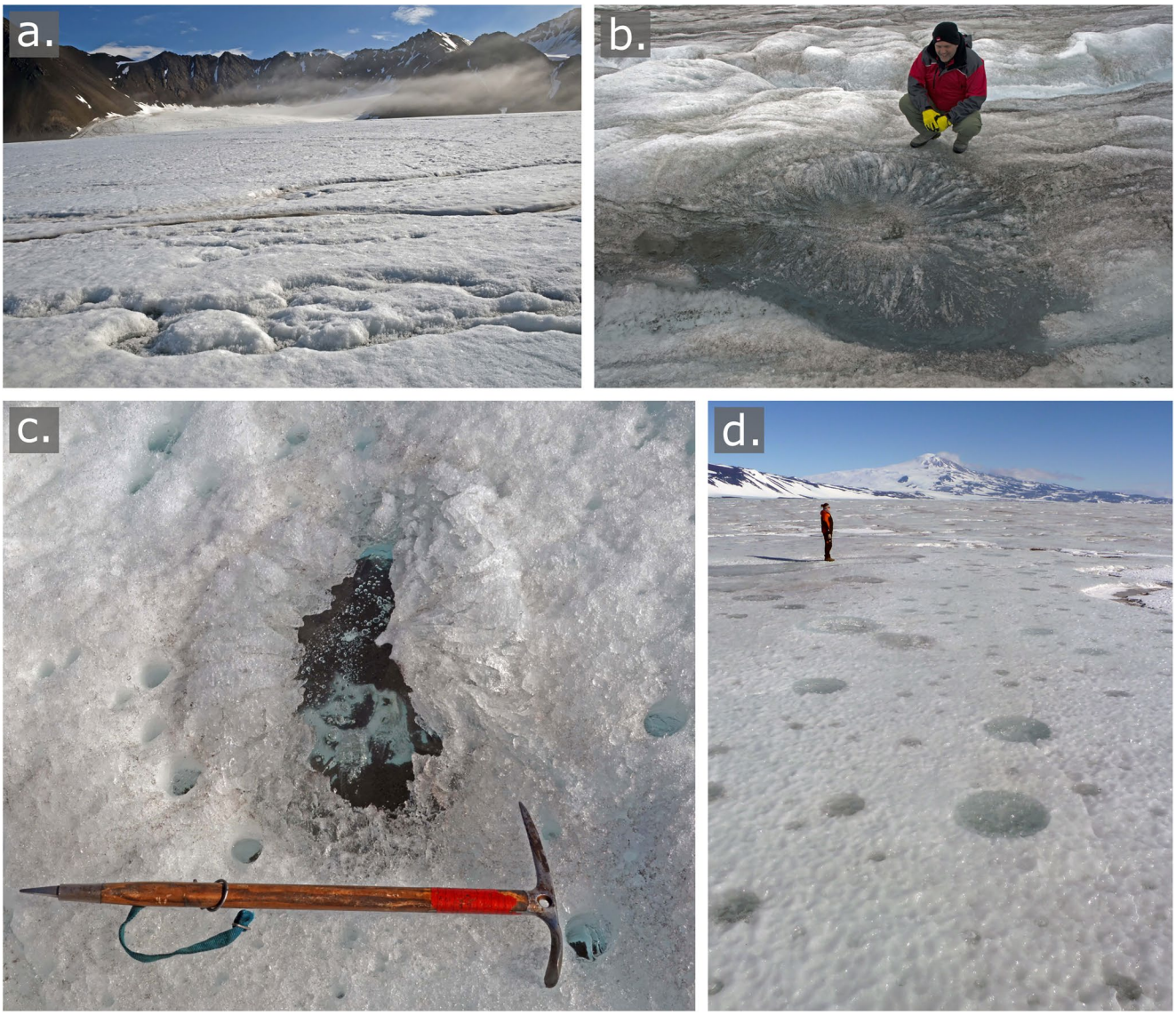

Figure 38. Examples of hydrologically derived structures. (a) Supraglacial channel-fills running right to left on Midtre Lovénbreen, Svalbard. (b) Large crystal quirk on Fountain Glacier, Bylot Island, Canada. (c) Cryoconite quirk on Fountain Glacier. (d) Healed crystal quirks, forming cylindrical clear ice bodies, in southern McMurdo Ice Shelf, Antarctica.

ice, channel closure is slow, allowing standing water to freeze, forming coarse clear ice channel fills, or filled by snow, forming firn or fine-grained ice fills (Figure 38a).

5.5.2. Cut-and-Closure Systems

A variant of the above develops where channel incision rates exceed surface melting of the surrounding ice, allowing perennial supraglacial channels to form (Rippin et al., 2015; St Germain & Moorman, 2019). The development of perennial supraglacial channels is favored in cool environments where surface ablation is relatively low, yet there is still a high surface discharge (i.e., where a channel drains a large catchment) to enable high incision rates. Typically, on polythermal glaciers, supraglacial streams can penetrate the surface at rates of 30 cm a day (Gulley, Benn, Müller, & Luckman, 2009), and develop into englacial conduits, for example, on Austre Brøggerbreen and Longyearbreen, Svalbard (Hansen et al., 2020; Kamintzis et al., 2017; Vatne, 2001). As supraglacial channels become deeply incised into the glacier, the roof of the conduit commonly closes as a result of ice creep, or become blocked by drifted snow or refrozen meltwater, a process known as "cut-and-closure" (Fountain & Walder, 1998; Gulley, Benn, Müller, & Luckman, 2009;

Irvine-Fynn et al., 2011; Rippin et al., 2015; St Germain & Moorman, 2019). Continuing channel incision through the ice mass may eventually allow the glacier bed to be reached. However, conduit blockages that result from infilling by snow, the refreezing of meltwater during the winter, or sediment delivery, can divert the course of the channel. Englacial conduits formed in this fashion are usually highly sinuous with shallow channel gradients separated by steep cliffs (knick-points) along their length (Hansen et al., 2020; Kamintzis et al., 2017). A prominent suture is usually present, running along the roof where the channel walls have closed in response to ice creep, whilst roof and wall collapse generate ice breccia, as on Khumbu Glacier (Gulley, Benn, Müller, & Luckman, 2009).

5.5.3. Crystal Quirks

Circular or elliptical void structures (crystal quirks) are commonly observed on the surface of glaciers (Holmlund, 1988; Irvine-Fynn et al., 2011; Stenborg, 1968). Voids are commonly water-filled or healed, and have diameters that range from a few decimeters to several meters. Healed crystal quirks consist of coarse clear ice crystals that grow from the edge of the structure, forming a radiating array of long crystals with a suture in the center (Figure 38b) (Jennings et al., 2014). Crystal quirks are the remnant voids of moulins and englacial conduits that have closed up (Goodsell, Hambrey, & Glasser, 2005; Jennings et al., 2014). Open voids commonly deform into elliptical shapes in 2-D before healing. Crystal quirks, having a lower albedo than the surrounding ice, commonly occur in depressions, thus allowing meltwater to accumulate. These stagnant pools effectively act as traps for eolian dust and microbial mats. It is common for prominent mounds of silt nodules to remain on the surface of a glacier when ablation of the surrounding ice melts-out a crystal quirk, revealing the sediment that was trapped within it.

5.5.4. Cryoconite Holes and Cryoconite Quirks

Following the removal of the winter snow cover, superimposed ice and slush, the glacier surface develops a weathering crust (Irvine-Fynn et al., 2011; Müller & Keeler, 1969). Dust and fine debris (cryoconite) alters the surface albedo, leading to differential ablation, and the debris melting down as cylindrical holes (MacDonell & Fitzsimons, 2008). The morphology of holes is influenced by variations in radiation (McIntyre, 1984), and there is a linear relationship between the mass of sediment in a hole and the surface area (Cook et al., 2010). Cryoconite holes provide a home for the growth of bacteria and other microbiological communities, which generate and absorb carbon dioxide (Wharton et al., 1985).

The morphology of cryoconite holes are commonly structurally controlled, such as where foliation results in straight edges, but these holes do not in themselves normally generate ice-structural features in temperate or polythermal glaciers. A rare exception is when temporary freezing of water-filled holes leads to the growth of radiating coarse clear ice crystals, several centimeters long that form an arched roof over the hole. These previously unreported features were observed on the polythermal Fountain Glacier on Bylot Island in 2014 by one of the authors (MJH), and are here named *cryoconite quirks* on account of their similarity to crystal quirks (Figure 38c). In colder regions, large cylindrical frozen cryoconite holes are present in late spring on McMurdo Ice Shelf, Antarctica (Figure 38d), where they reach diameters of half a meter, but thaw out in summer.

5.6. Microstructure and Crystal Fabric of Glacier Ice

Although this review focuses on macro- and meso-scale structures, which are visible at the surface of glaciers and ice sheets, a brief summary of micro-scale structures and crystal fabric is warranted. In geological terms, glacier ice can be considered to be both a mineral and a rock, deforming close to its melting point in both a brittle and ductile manner. The microstructure of glacier ice is defined as the arrangement of grains, grain boundaries, and any other material, such as sediment, that makes up the "rock" body. Analysis of ice crystal fabric, involves measuring the 3-D orientation of crystals, the nature of crystal boundaries, and air bubble content. Both microstructure and fabric control the mechanical properties of glacier ice, and their study helps contribute to the deduction of the history of the ice (Koehn & Bons, 2014).

Although there are many studies of ice microstructure and crystal fabric in glacier ice, only a small proportion of them have made the link with meso- and macro-scale glacier structures observable in the field. Several studies in a special issue of the *Journal of Structural Geology* discuss the current status of research

in various aspects of this field (Koehn & Bons, 2014). In a review of natural ice microstructures, Faria et al. (2014a) described how interest in this field was triggered by an expedition to Jungfraujoch near the upper reaches of Switzerland's largest glacier, the Grosser Aletschgletscher, under the leadership of Gerald Seligman, the founder of the International Glaciological Society. Seligman and his colleagues pioneered the use of thin sections of glacier ice, studied under polarized light, to investigate the transformation from snow, through firn, into glacier ice, followed by the effects of glacier flow. This was achieved by measuring ice crystal orientations and generating fabric diagrams that record their orientations in 3-D (Perutz & Seligman, 1939). These methods continue in use to this day, albeit the original universal stage method of measuring orientations (Rigsby, 1960) has been replaced by more sophisticated technology, such as using an automated fabric analyzer (Wilson et al., 2003).

Fabric patterns, with clusters of crystals of similar orientation, develop in response to slip on the lattice planes of ice crystals during deformation. In glaciers, slip on the basal plane is most important and, as a consequence, the planes rotate to become perpendicular to the maximum shortening direction (Hudleston, 2015). When poles to crystallographic axes (c-axes) are plotted on a stereographic projection, ice from a location of flow divergence, such as at the summit of an ice dome, has a pattern consisting of a small circle located around the axis of uniaxial compression. However, in zones of differential flow, the fabric patterns lack consistency, and reflect passage of ice through different stress fields with subsequent recrystallization. For example, girdle fabrics may evolve into multi-maxima (commonly fourfold) fabrics. The relationship with foliation typically is that the pole to the foliation is parallel to one of the c-axis maxima or to the center of multi-maxima fabrics (Hambrey, 1976a; Kamb, 1959). From a study at Griesgletscher, it was found that at some sites, the orientation of c-axis maxima was the same as that of the short axis of the cumulative strain ellipse. In other cases, there is no discernable relationship between foliation and fabric; this is perhaps unsurprising, given the extent to which ice recrystallizes near the glacier surface when exposed to ablation (Hambrey, 1979). Another factor is that during deformation, strain rate increases in parallel with temperature. Thus microstructures formed under steadily increasing deviatoric stress are superimposed (Wilson et al., 2014). These complications make it challenging to relate ice microstructure to the evolution of crystal fabric.

The analysis of microstructure and fabric in valley glaciers is constrained by the large size of crystals, which commonly reach tens of centimeters in temperate valley glaciers (Figure 39), hence the relatively low number of studies (Hellmann et al., 2020; Monz et al., 2021). The development of a crystallographic preferred orientation or crystal fabric in temperate coarse-grained natural ice is therefore poorly constrained, especially in shear-dominated regimes. To investigate crystal fabric patterns in coarse-grained temperate ice in the marginal zone of Storglaciären, Monz et al. (2021) employed cryo-electron backscatter diffraction (EBSD) to measure the crystallographic orientation of a- and c-axes in a shear-dominated setting. Even though the crystal fabric of ice is commonly defined by the preferred orientation of c-axes, slip on the basal plane may not necessarily be isotropic (Kamb, 1961), therefore the orientation of a-axes is also required to accurately characterize ice crystal orientations. In comparison with laboratory studies, shear strains in the marginal ice of Storglaciären are much higher, yet the ice is subjected to much lower natural strain rates. It is therefore likely that in natural settings, dynamic recrystallization is more evident, with the crystal orientation representing a smaller component of the overall shear history (Monz et al., 2021). Furthermore, Monz et al. (2021) concluded that previous studies investigating crystal fabric in coarse-grained ice may have incorrectly reported multimaxima fabrics as a result of limited samples sizes and sampling bias.

Much greater attention has focused on polar ice cores since they were first extracted from the Greenland and Antarctic ice sheets, largely because of their value in providing high-resolution climatic records, as reviewed by Faria et al. (2014a). In terms of understanding glacier flow and the creation of macrostructures, it is the deeper parts of these ice cores that are of most interest. Examples include the development of shear zones and recumbent folding at the base of the Greenland Ice Sheet, and the impact this deformation has on distorting the ice stratigraphy (Faria et al., 2014a). At a crystallographic level, thin sections of ice cores show subgrain development, and splitting of grains by "rotational recrystallization" to accommodate strain (Faria et al., 2014b). In addition, in high-impurity ice layers (which appear cloudy) microscopic grain-boundary sliding via microshears occurs. Also, nucleation of new grains can be observed at various depths under local concentrations of high strain, a process referred to as "dynamic recrystallization."

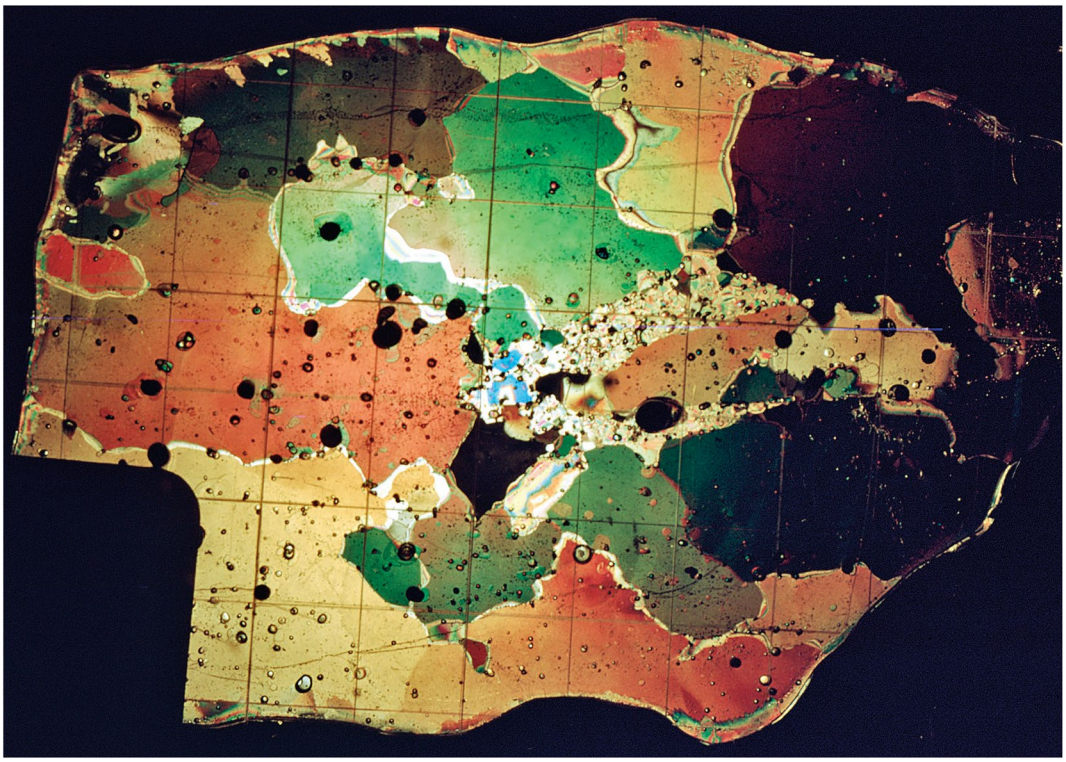

Figure 39. A large thin section of foliated coarse bubby ice from Charles Rabots Bre, Norway, illustrating how crystals can grow to several centimeters in length. The sample is viewed beneath cross-polarized plates on a universal stage. The rectangular grid squares have 1 cm sides.

5.7. Modeling Structural Evolution in Glaciers

Since the advent of computers, numerical modeling has played a major role in advancing most branches of glaciology. However, structural glaciology is a field where numerical modeling is less well developed than in other disciplines. Reasons for this are that models tend to focus on the areal extent, thickness, and response time of a glacier as inputs. Thus, the spatial resolution of glacier flow models is commonly insufficient to resolve processes at the scale of many ice structures. Nevertheless, a number of effective attempts have been made to model the development of individual structures, such as crevasses (Colgan et al., 2016; van der Veen, 1999), fractures previously alleged to be thrusts (Moore et al., 2010), foliation (Hambrey et al., 2005; Hooke & Hudleston, 1978; Hubbard & Hubbard, 2000), and folding (Hudleston, 1976), as discussed above.

For a more comprehensive overview of structural glaciological evolution, Trapridge Glacier in the Yukon has proved to be an ideal candidate, as some 30 years of ice dynamics data are available, allowing the development of a theoretical model that could be applied to a real glacier (Clarke & Hambrey, 2019; Hambrey & Clarke, 2019). This research provided an explanation of a range of structures to be found in a theoretical glacier that has experienced a slow surge. Clarke and Hambrey (2019) developed a thermomechanical numerical ice dynamics model in which passive transport and rotation during glacier flow could be combined with the accumulated effects of strain and episodic fracture. A particularly helpful approach was to define a "deformation gradient tensor" (F) because it encapsulates the total strain experienced by a parcel of ice. Evaluation of F involved ice trajectory calculations and integrations along these trajectories. The approach was used to explain patterns of medial moraines, stratification, foliation, folding, and crevasse traces in a theoretical "Traplike" glacier (Clarke & Hambrey, 2019).

The model was applied to the real Trapridge Glacier, by using data obtained in the field, notably subglacial topography, and 3-D orientation data of foliation and fractures (Hambrey & Clarke, 2019). Modeling of the real structures was successful in some respects, but not in others, as summarized below:

1. Medial moraine patterns are uncomplicated and could be readily simulated using a particle tracking approach;
2. Primary stratification (S_0) can be modeled using the assumption of isochronous layering and a semi-Lagrangian tracer method;
3. Longitudinal foliation (S_1) was associated with the orientation and flattening of strain ellipsoids and can be modeled effectively using the deformation gradient tensor, F;
4. Modeling results are consistent with the suggestion that transverse foliation (S_2) results from compression and rotation of transverse near-vertical cracks;
5. At the scale of the simulation model, folding is a subgrid process, but the introduction of a scalar "fold propensity index," based on a scalar invariant of the gradient of F, seemed to offer promise of better representing complicated deformation as a scalar parameter;
6. The representation of crevasse traces in the model did not compare well with the field data, probably because of oversimplification in the model;
7. Crack density simulations yielded an explanation for the counter-intuitive observation that the density of surface cracking has a decreasing trend in the downglacier direction.

Thus, although numerical modeling efforts have increasingly been able to simulate the formation of several types of brittle and ductile structures, this is a field that is, ripe for further development, especially when numerical modeling grid-size can match the scale of the structures.

6. Examples of Typical Structural Assemblages in Valley Glaciers

Each glacier is structurally unique and reflects the role played by deformation, which in turn is controlled by mass balance, the geometry of the bed, and thermal regime. A typical cirque glacier, for example, Vesl-Skautbreen in southwestern Norway (Grove, 1960a) has a simple structure, dominated by primary stratification and a few crevasses. Cirque glaciers may show signs of reactivation of this layering as thrusts, as demonstrated by Lachman Glacier on James Ross Island, Antarctica (Carrivick et al., 2012). Glaciers emerging from a cirque into a narrow tongue may reveal folding of stratification and the development of longitudinal foliation, as on Charles Rabots Bre, northern Norway (Hambrey, 1976b). Glaciers with multiple basins feeding a narrow tongue reveal several flow units, each with stratification that becomes increasingly tightly folded downglacier, and with longitudinal foliation developing at flow-unit boundaries, and inferred thrust-faults at the snout; examples are White Glacier on Axel Heiberg Island (Hambrey & Müller, 1978), Haut Glacier d'Arolla in Switzerland (Goodsell, Hambrey, Glasser, Nienow, & Mair, 2005), Midtre Lovénbreen in Svalbard (Hambrey et al., 2005), Vadrec del Forno in Switzerland (Jennings et al., 2014), and Kvíárjökull in Iceland (Phillips et al., 2017). Glaciers with icefalls reveal the early overprinting of stratification by crevasses and crevasse traces, which evolve into arcuate foliation and sometimes ogives, with longitudinal foliation at flow unit boundaries, and numerous minor folds representing remnants of earlier structures, as described at Pasterzenkees in Austria (Herbst & Neubauer, 2000; Schwarzacher & Untersteiner, 1953), Blue Glacier in Washington State (Allen et al., 1960), Griesgletscher in Switzerland (Hambrey & Milnes, 1977), Bas Glacier d'Arolla in Switzerland (Goodsell et al., 2002), and Kviárjökull in Iceland (Swift & Jones, 2018). Additional complications arise if the glacier is surge-type, and structures can be identified as originating from either the quiescent or active phase, a well-studied example being Variegated Glacier in Alaska (Lawson, 1996; Lawson et al., 1994).

Thus glaciers are characterized by multiple phases of deformation (i.e., polyphase deformation), producing several generations of planar structures that are labeled S_0, S_1, S_2 etc., with some examples being given in Table 1. Each phase affects a "parcel" of ice as it moves through the glacier, but is not temporarily constrained as is often assumed to be the case in structural geology. In order to appreciate the full range of structures in valley glaciers, a number of common morphological and dynamic types are described below.

6.1. Multiple Basins Feeding a Narrow Glacier Tongue

Many glaciers have this configuration, especially where the local relief is only moderate (1000 m or less). Examples that have been described in detail include Vadrec del Forno (Jennings et al., 2014) and Haut Glacier d'Arolla (Goodsell, Hambrey, Glasser, Nienow, & Mair, 2005) in the Swiss Alps, Ghiacciaio dei Forni

Reviews of Geophysics

10.1029/2021RG000743

Table 1
Sequential Development of Planar Structures and Folds in Studied Cirque and Valley Glaciers

	Norway	European Alps						Southern Alps, NZ	Svalbard, Norway			Alaska	West Greenland
Glacier/area	Charles Rabots Bre	Gries-gletscher	Vadrec del Forno	Bas Glacier d'Arolla	Haut Glacier d'Arolla	Vadret da Morteratsch	Glacier de St. Sorlin	Fox & Franz Josef glaciers	Midtre Lovénbreen	Austre Brøggerbreen	Hessbreen	Variegated Glacier	Kuannersiut Glacier
Thermal or dynamic type	Temperate	Temperate	Temperate	Temperate	Temperate	Temperate	Temperate	Temperate	Polythermal	Cold	Polythermal/ surge-type	Temperate/ surge-type	Polythermal/ surge-type
No. of flow units	2	2	6	1 (lower)	2	2	6	Multiple	4	6	4	3	?
Primary stratification	S_0	S_0	S_0	S_0	S_0	S_0	S_0	S_0	S_0	S_0	S_0	S_0	S_0
Folding; first phase	F_1	F_1	F_1	F_1	F_1	F_1	F_1		F_1	F_1	Not recognized	F_1	
Early crevasse traces											S_1		
Longitudinal foliation	S_1	S_1	S_1	S_1 (lower)	S_1	S_1	S_1	S_1	S_1	S_1	S_2	S_1	S_1
Transverse crevasse traces; first phase	–	S_2	S_2	S_2	S_2	S_2	S_2	S_2	S_2 Multiple sets	S_2 Multiple sets	S_2	–	S_2
Basal ice formation													S_3
Ogives	–	–	–	S_2	–	S_2	–		–	–		–	
Arcuate foliation	-	S_2	S_2	S_2	–	S_2	–		–	–		S_2	
Folding; second phase	–	F_2	–	F_2	–	F_2	–		F_2	–	F_2	F_2	
Transverse crevasse traces; second phase	–	S_3	–	–	–	S_3	–		–	Multiple sets			
Folding; third phase	–	–	–	–	–	F_3	–		–	–	F_3	–	
Thrust-faults/shear planes	–	S_4	–	–	S_3	–	S_3	S_3	S_3	–	S_3	S_3	S_4
Longitudinal/ splaying fractures	–	–	–	–	–	–	–		S_4	–			
Late crevasse traces	–	–	–	–	–	–	–		-	–	S_4	F_3	
Hydro-fracture and crevasse infilling													S_5
Reference	Hambrey (1977a)	Hambrey and Milnes (1977)	Jennings et al. (2014)	Goodsell et al. (2002)	Goodsell, Hambrey, Glasser, Nienow, and Mair (2005)	This study	Roberson (2008)	Appleby et al. (2017); Brook et al. (2017)	Hambrey et al. (2005)	Jennings et al. (2016)	Hambrey and Dowdeswell (1997)	Lawson et al. (1994)	Roberts et al. (2009)

Note. The sequential development of planar structures (S) and folds (F) in cirque (Charles Rabots Bre) and valley glaciers (the remainder) using standard structural geological notation. Transverse crevasse traces, arcuate foliation, and ogives are a family of related structures, S_2.

in the Italian Alps (Azzoni et al., 2017), Glacier de St. Sorlin in the French Alps (Roberson, 2008), Midtre Lovénbreen (Hambrey et al., 2005) and Austre Brøggerbreen (Jennings et al., 2016) in Svalbard, and Fox and Franz Josef glaciers in New Zealand (Appleby et al., 2017; Brook et al., 2017) (Table 1).

Vadrec del Forno may be regarded as representative (Jennings et al., 2014); it is c. 5.3 km in length and spans an altitudinal range of 2240–3,200 m.a.s.l. Two broad accumulation basins deliver six flow units in which primary stratification (S_0) becomes folded (F_1) in a zone of converging flow, with longitudinal foliation developing either by transposition from stratification, or as a cleavage-like structure, both having axial planar relationships with the folds (S_1). Simple shear, predominantly focused at flow unit boundaries, thus dominates the deformation in this glacier, with inferred strain ellipses rotating to parallelism with the longitudinal foliation. The dominant structure throughout the tongue of this glacier is foliation, but remnants of stratification are traceable a considerable distance downglacier (Figure 40). The foliation is intersected by numerous crevasse traces (S_2), but there are few open crevasses nowadays, reflecting contemporary rapid recession and low dynamic activity.

Other alpine valley glaciers that reveal similar assemblages of ductile structures are the Fox and Franz Josef glaciers in the Southern Alps of New Zealand (Appleby et al., 2017; Brook et al., 2017), each of which has multiple converging flow units. However, since both glaciers are fast-flowing on relatively steep gradients, they have an abundance of crevasses with many orientations. The structural sequence, starting with primary stratification and its evolution through to longitudinal foliation, as well as the development of crevasses and crevasse traces, ends at the snout with arcuate shear fractures or thrust-faults. Similarly, a well-mapped cirque glacier in the French Alps, the Glacier de St. Sorlin, also has multiple flow units that, where they converge, fold the stratification and transpose it into longitudinal foliation (Roberson, 2008). As discussed in Section 9.2, folding and foliation in all of these glaciers are implicated in debris entrainment.

This type of configuration also applies to much larger, topographically confined, ice masses which have multiple accumulation basins feeding a narrow glacier tongue, and which are best observed in satellite imagery. An example from the Canadian High-Arctic is Aktineq Glacier, on Bylot Island. This glacier is a c. 35 km-long land-terminating glacier, with 21 accumulation basins (further divided into 45 sub-accumulation basins) feeding a glacier tongue attaining a maximum width of c. 4 km (Jennings, 2017). The tongue of the glacier is dominated by pronounced longitudinal structures defined by alternating light and dark bands that become increasingly evident toward the snout. Comparatively thinner dark longitudinal structures are interpreted to be flow unit boundaries composed of strong longitudinal foliation, accentuated at the surface of the glacier by differential ablation, higher concentrations of trapped eolian-derived sediment, and the supraglacial exposure of entrained englacial and subglacial debris (Jennings, 2017). This style of foliation is also clearly visible in high-resolution oblique aerial photographs at nearby Sermilik Glacier (Figure 41a), and from ground observations on adjacent glaciers (Figure 41b).

6.2. Structural Assemblage Dominated by Icefall Processes

Valley glaciers with icefalls occur mainly in areas of high relief, typically of 2000 m or more, where bedrock irregularities result in the formation of icefalls. Extending flow above and within an icefall is followed by compressive flow at the base, and the resulting structural assemblage differs markedly from that described in Section 6.1. Well-studied examples include Griesgletscher and Bas Glacier d'Arolla in the Swiss Alps (Table 1), Blue Glacier in Washington State (Allen et al., 1960), Gulkana Glacier in Alaska (Ragan, 1969), Pasterzenkees in the Austrian Alps (Herbst & Neubauer, 2000), Kvíárjökull in Iceland (Phillips et al., 2017; Swift & Jones, 2018), Soler Glacier in the Northern Patagonian Icefield (Aniya & Naruse, 1987; Aniya et al., 1988), and Shackleton Glacier in the Canadian Rockies (Jiskoot et al., 2017). Severe recession of these glaciers has meant that many of the features described in the earlier (pre-2010) studies have now disappeared. Recent examples of glaciers with contrasting icefalls are described below.

6.2.1. Vadret da Morteratsch, Southeastern Switzerland

This temperate glacier has not previously been described from a structural perspective, but is taken as a typical example of an icefall-dominated structural assemblage (Figure 42). This glacier, along with its tributary, Vadret Pers, descends from c. 4,000 to c. 2,000 m.a.s.l. over a distance of 7 km. The main glacier contributes one major and one minor flow unit to the tongue. By 2014, Vadret Pers was nearly severed from the main

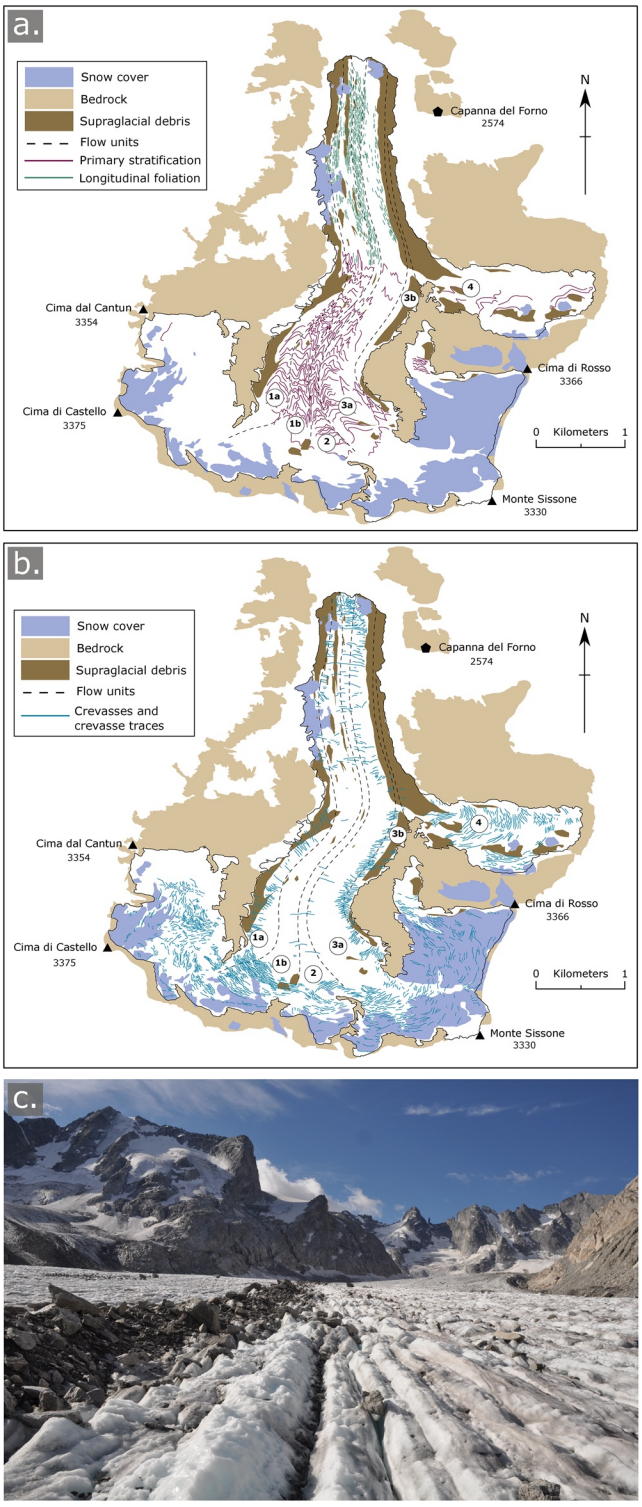

Figure 40. Paired structural maps of Vadrec del Forno, Switzerland, a valley glacier fed by multiple basins and comprising six flow units (numbered). (a) Stratification, with folding and longitudinal foliation. (b) Crevasses (a few only) and crevasse traces (modified from Jennings et al., 2014). (c) Upglacier view of longitudinal foliation and a medial moraine at the flow unit boundary between flow units 1a and 2 at the surface of Vadrec del Forno. More detailed maps of the lower glacier tongue area, with three-dimensional data plotted, are shown in Figure 8.

Figure 41. Longitudinal foliation related to flow unit boundaries in a large polythermal valley glacier. (a) Oblique aerial photograph of longitudinal foliation in Sermilik Glacier, Bylot Island, Canadian Arctic, illustrating the continuity of layering and low-amplitude folding as the ice reaches near to the snout. (b) Appearance of longitudinal foliation with continuous layering viewed at ground level for comparison; Stagnation Glacier, Bylot Island.

glacier as a consequence of ongoing rapid recession; however, the flow unit from this source still formed part of the tongue, albeit totally debris-mantled.

A massive icefall located just below the equilibrium line dominates Vadret da Morteratsch, and consequently little primary stratification (S_0) and early foliation (S_1) survive except as fold remnants with transverse axes at the foot of the icefall. The icefall is dominated by crevasses and crevasse traces of numerous orientations as well as séracs. In the zone of compression at the foot of the icefall these structures transform into arcuate foliation (S_2). The base of the icefall also generates wave ogives, parallel to the arcuate foliation, which evolve into band ogives downglacier. The arcuate foliation dips steeply upglacier at this point, and in places incorporates basal debris, indicating a connection to the glacier bed. A second phase of minor (meter-scale) folding (F_2) with axial planes parallel to the foliation is developed. Through comparison with Griesgletscher (Hambrey & Milnes, 1977), these structures are inferred to form under a pure shear regime, with the strain ellipse long axes developing parallel to the arcs. The outer limits of the arcs attain a longitudinal trend at the edges of the flow unit, where asymmetric foliation boudinage develops. The inferred regime here is one of simple shear, whereby strain ellipses develop at 45° to the structure and rotate toward parallelism with it. A transition from pure shear in mid flow unit to simple shear at the edges must exist in this type of structural regime.

Beginning with a steep (70°–80°) upglacier dip in the foliation at the base of the icefall, the centerline dip downglacier decreases to around 20° until it is intersected by an area of transverse and diagonal crevasses, comprising two main areas of extending flow (Figure 42). This zone yields a second set of transverse crevasse traces (S_3), with a centerline dip upglacier of c. 70°–85°, which cross-cut the earlier arcuate foliation and ogives (S_2). Drag folds (F_3) are associated with displacements along S_3. Both S_2 and S_3 continue to evolve downglacier, their centerline upglacier dips decreasing to 10°–20° at the snout. At the edges of this flow unit, under a cover of supraglacial debris, S_3 rotates into the plane of S_2, and dips are near vertical. Isoclinal and similar folds with axial planes parallel to this combined longitudinal foliation are evident if the debris cover is cleaned off.

6.2.2. Kviárjökull, Southeastern Iceland

The investigations of the tongue of the temperate glacier, Kviárjökull, in the zone below its icefall, have yielded contrasting interpretations of the dynamics of the glacier, by exploring the significance of different structures. The contribution by Phillips et al. (2017) sets a new standard in mapping fractures (crevasses) in considerable detail, by combined 3-D measurements of fractures in the field, with digital scanning of aerial photographs and photogrammetry, terrestrial LiDAR and digital elevation modeling, unmanned aerial vehicle (UAV) surveys, and ground-penetrating radar soundings. The structural "architecture" comprises a central corridor of elongate to lobate "domains" along the central axis of the glacier, enclosed within lateral

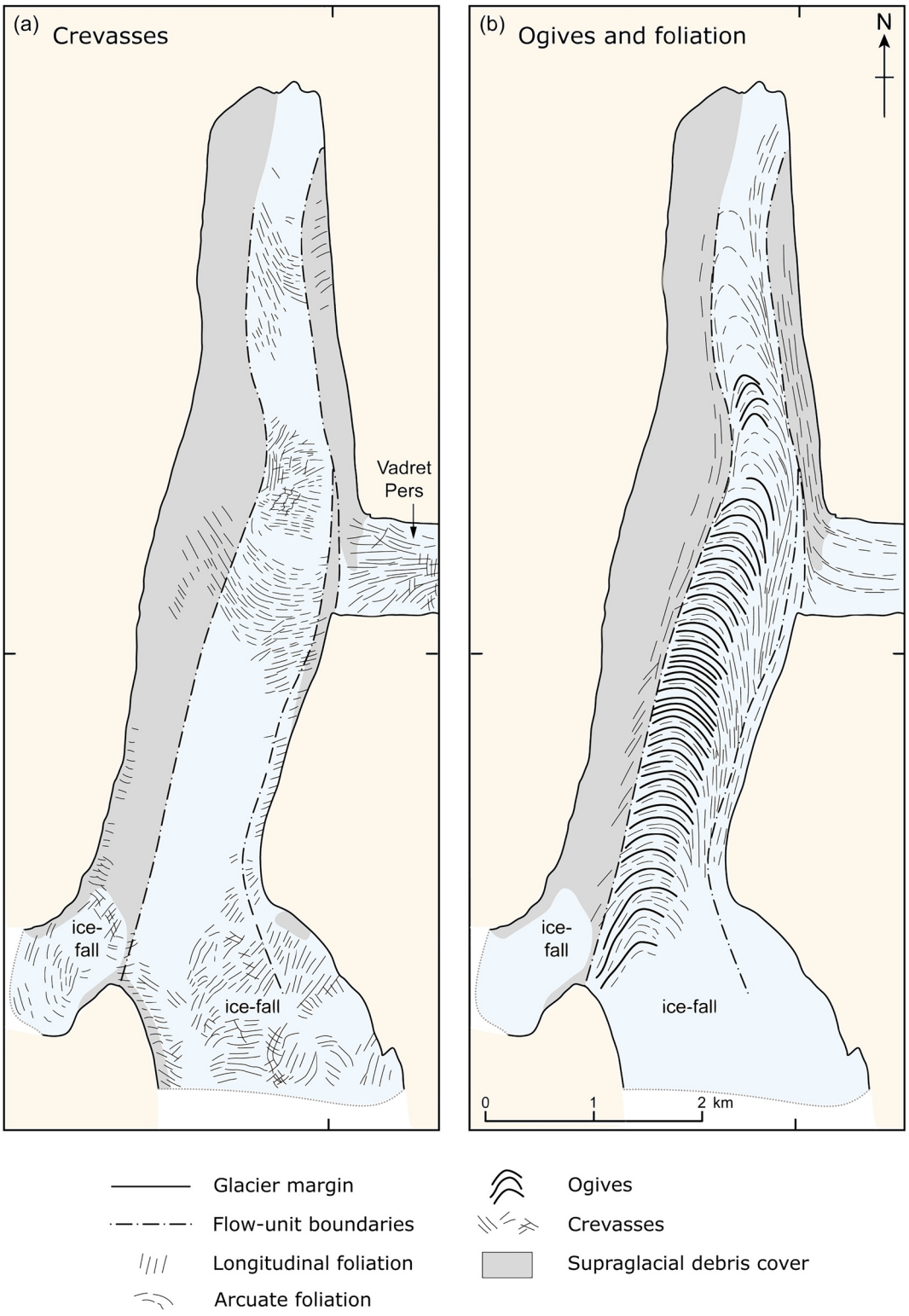

Figure 42. Paired structural maps of Vadret da Morteratsch, Switzerland, a valley glacier dominated by an icefall. The tributary glacier on the right (East) is Vadret Pers, which has recently been severed from the main glacier tongue. (a) Crevasses (open). (b) Arcuate and longitudinal foliation and associated ogives, and crevasse traces.

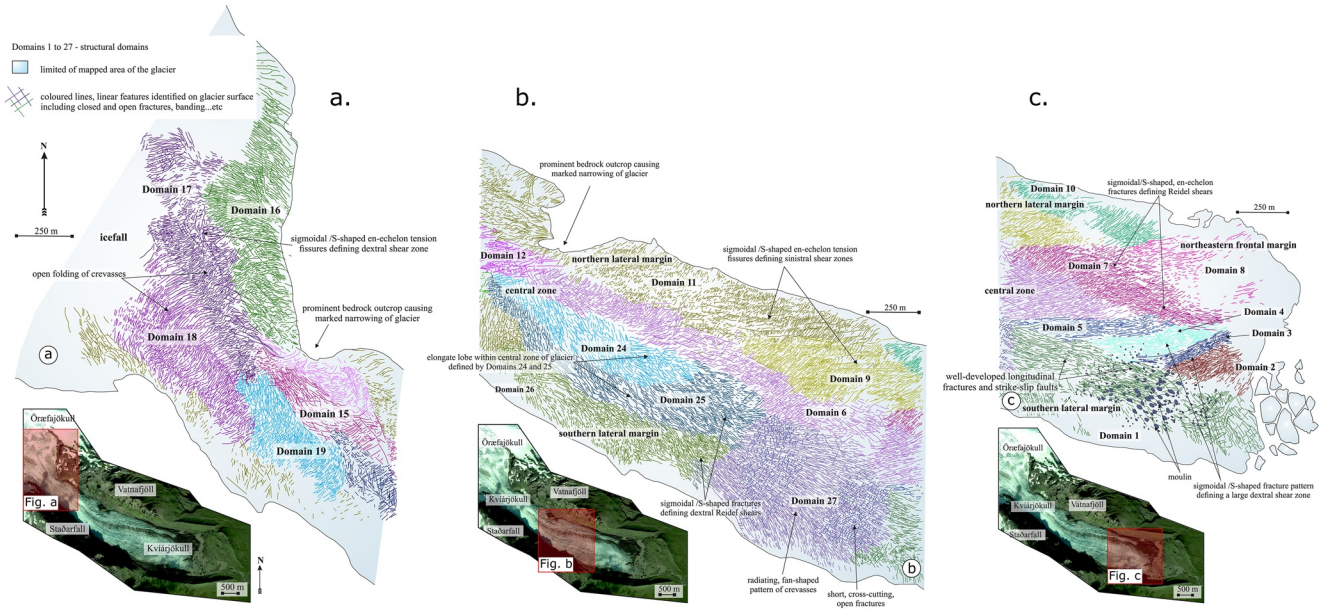

Figure 43. Structural maps of three contiguous sections of the tongue of Kviárjökull, Iceland (modified from Phillips et al., 2017). The maps illustrate crevasses, crevasse traces, and other fractures, which are grouped into distinctive structural domains (27 in total).

marginal zones (Figure 43). These domains were defined by crevasse patterns, supplemented by data on banding (i.e., foliation) and clean/dirty ice alternations (i.e., ogives or Forbes bands).

Crevasses have many orientations, but have been grouped into domains. Brittle shear zones dissect earlier fractures, and also reactivate them to form a series of short (10–50 m long) open sigmoidal-to-arcuate en echelon tension gashes, referred to as Riedel shears. Toward the snout, the banding is offset by a series of thrust-faults dipping at 15°–40°, and are the result of compressive flow against a reverse bedrock slope. The thrust-faults are associated with rare, tight asymmetrical folds, verging in the direction of ice-flow. The modern glacier has been divided in 27 domains (Figure 43), and their evolution examined with reference to a series of aerial photographs, taken between 1945 and 2014. The authors' interpretation of this structurally complex tongue is that it reflects changes in the stress regime spatially and temporally. Flow in the modern glacier is inferred to be concentrated along the central axis ("concentrated axial glacier flow"). The other domains are inferred to represent distinct pulses of ice flow.

Swift and Jones (2018) rejected the hypothesis of pulsed axial glacier flow on these grounds: (a) that crevasse patterns are simply an ice surface response to stresses generated by an uneven bedrock topography; (b) that there is a prominent transverse/arcuate foliation, formed in the icefall, which is associated with ogives; (c) this foliation is an earlier structure than the crevasses in the glacier tongue, yet maintains its integrity throughout the whole glacier tongue and is not disrupted by supposed pulses; (d) analysis of ice-surface displacement (feature-tracking) show a uniform flow field through the tongue. Thrust-faulting occurs along the darker ogive-parallel foliation as the ice approaches the terminus (Swift et al., 2006), indicating the availability of pre-existing weaknesses.

We conclude, without having personal experience of the glacier, that the Swift and Jones (2018) rejection of the pulsed axial flow hypothesis of Phillips et al. (2017) is plausible, and agree that normal uniform flow is evident from the arcuate foliation. Nevertheless, the domain maps are of significant interest, but perhaps are best interpreted as defining discrete zones of crevassing associated with bedrock bumps. These domains thus represent crevasses formed in situ and that these crevasses would not survive significant transport because of ablation.

6.2.3. Shackleton Glacier, Canadian Rockies

The largest temperate glacier in the Canadian Rockies, covering 40 km^2, is Shackleton Glacier. It has a complex morphology, characterized by multiple flow units, a channel that fluctuates in width, bedrocks

steps, and multiple icefalls (Jiskoot et al., 2017). A range of structures were identified, including crevasses, crevasse traces, ogives, longitudinal foliation, folded foliation, and thrust-faults. The study utilized a range of techniques, including direct field orientation measurements, velocity stakes, GPS for locations, and speckle-tracking using pairs of synthetic aperture radar images to determine displacement of surface ice and hence velocities.

The main focus of the study was on formation of crevasses where the main flow unit interacted with a tributary. The crevasses were classified using SPOT imagery. Five main groups of crevasse types were identified: (a) arcuate upglacier and transverse crevasses in zones of longitudinal extension as the ice approached an icefall and where the main trunk narrowed; (b) longitudinal and splaying crevasses indicative of lateral extension at the base of the icefalls; (c) short marginal crevasses forming at angle of 45° to the margins in zones of uniform velocity; (d) longer, upward-splaying crevasses where the glacier trunk enters a valley constriction and zone of longitudinal compressive flow; and (e) chevron and en echelon crevasses in rotating marginal bends. The SPOT imagery also allowed digitization of the density of crevasses to be determined (Jiskoot et al., 2017).

6.3. Structural Assemblage of Surge-Type Glaciers

Structurally, surge-type glaciers are even more complex than "normal" glaciers. The principal characteristic is the presence of striking "looped" moraines, representing pulses of ice that occurred at different times from tributaries into the main glacier tongue. Surge phases are characterized by velocities that are orders of magnitude faster than in quiescent stage flow. These two stages are represented predominantly by brittle surface structures, and ductile structures respectively. Surge cycles span as few as 10 years for temperate glaciers in Alaska to 100+ years for polythermal glaciers in Svalbard, and the surge phase itself lasts several months to several years respectively. Thus the structural assemblage observed on a surge-type glacier depends upon which part of the surge cycle is investigated. For a review of the processes and products, see M. Sharp (1988a, 1988b) and for an explanation of the physical processes of surge-type glaciers, see Cuffey and Paterson (2010, Ch. 12).

6.3.1. Temperate Glaciers

As a representative of surge-type temperate glaciers, Variegated Glacier in Alaska has been studied in most detail. The glacier has surged once more since it was subject to intensive investigation during and after the then-predicted 1982–1983 surge (which failed to reach the terminus), but those studies remain fundamental to understanding surges in general. The physical processes operating during the surge, which took place in two stages over an 18-month period, were synthesized by Kamb et al. (1985), and the structural attributes investigated by Sharp et al. (1988), Lawson et al. (1994, 2000), and Lawson (1996) immediately following the surge. Variegated Glacier is a temperate valley glacier that had undergone six known surges since 1900. It is 20 km long, flowing east to west on the south side of the St. Elias Mountains. With an altitudinal range of about 2,000 m, it has a gradient which varies from 1° to 8°, and lacks icefalls. W. Lawson (1996) prepared a series of structural maps, based on aerial photographs, to illustrate the evolution of longitudinal foliation, moraines, crevasses, and crevasse traces (S_2) during the quiescent period, through to the end of the surge. The structural evolution sequence (Table 1) is as follows. The foliation (S_1), associated folding (F_1), and moraines form loops and contortions that are clearly visible in aerial photographs of the glacier in its quiescent state, indicative of multiple flow instabilities. Furthermore, in a broader stagnant lobe, these structures are further subject to folding under longitudinal compression (F_3). Crevasses and crevasse traces (S_2) are present, but their geometry is then typical of nonsurge-type glaciers.

The 1982–1983 surge resulted in a total transformation of the ice surface into one where crevasses were dominant (Figure 44a). The surge stopped in the stagnant ice zone of compressively folded moraines. The glacier switched to plug flow, and its margins became zones of intense shear in which "P" shears, Riedel shears, a breccia zone, and tensional fractures occurred in sequence toward the glacier margin, over a distance of 50 m. This pattern of structural development corresponds to that associated with geological wrench-fault zones. Throughout the main body of the glacier, transverse and longitudinal fractures developed. As the surge propagated into stagnant ice in the terminal lobe, recumbent folds (commonly with

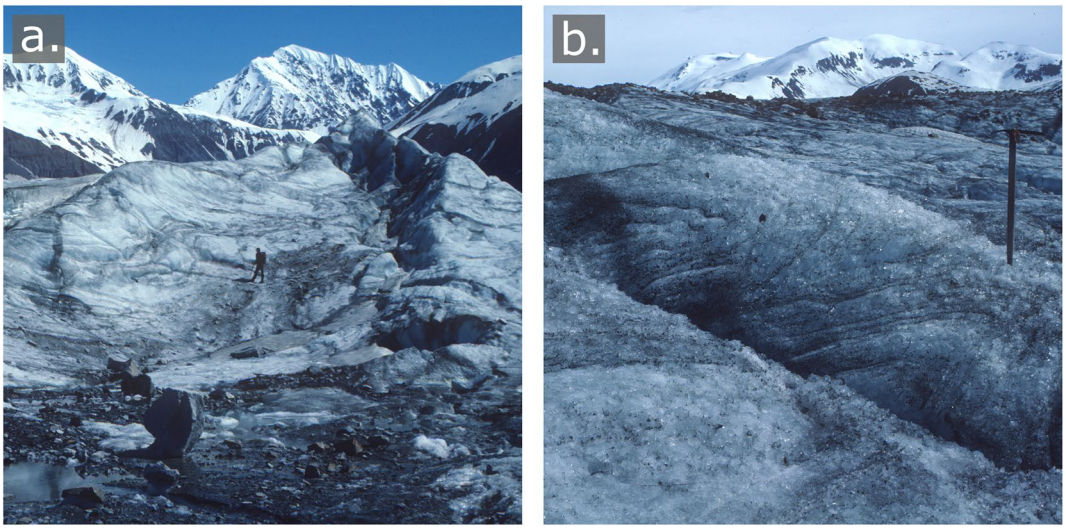

Figure 44. Surface structures of Variegated Glacier, Alaska in 1985, following the 1982–1983 surge. (a) High relief represents the remnants of the crevasses that formed during the surge. Thrust-faulting and folding verging in the direction of the passage of the surge front is evident to the left of the person. (b) Characteristic surface structure after the passage of the surge front, showing discrete planar fractures and shears, interpreted as thrusts (S_3), and overturned folds, verging in the direction of flow (F_3). Structural interpretation from Lawson et al. (1994).

sheared-off limbs) with axes perpendicular to flow (F_3), and convex downglacier thrust-faults (S_3) developed (Figure 44b) (Raymond et al., 1987; Sharp et al., 1988).

The strain history associated with this structural evolution (Lawson, 1996) is as follows:

1. During the 16-year quiescent period that preceded the 1982–1983 surge, the predominantly weakly compressive strain field was spatially static, and strain-rates associated with it increased over time. Quiescent phase flow was shear-dominated, and the magnitudes and orientations of principal strain-rates were similar to those in nonsurge-type glaciers. Deformation was coaxial in the middle of the glacier and noncoaxial toward the margins.
2. During the surge, the strain field continually evolved as the velocity peak associated with the surge front migrated downglacier and intensified. Displacements, measured from distinctive moraine features, averaged 3.1 km during the full surge cycle, of which 60% took place during the 18-month-long surge. The style of deformation and the magnitude of the cumulative strain that the ice experienced depended on its position relative to the surge nucleus and final position of the velocity peak. Ice which lay upglacier of the surge nucleus underwent continuous and cumulative longitudinal elongation. Ice which lay between the surge nucleus and the final position of the velocity peak experienced longitudinal shortening followed by elongation. Ice which lay below the position of the velocity peak experienced continuous and cumulative longitudinal shortening. During the surge phase, strains were generally coaxial across the width of the glacier, except that noncoaxial strains probably occurred near the margins early in the surge phase.

To understand the full cumulative strain history, it is necessary to consider the residence time of ice within the glacier (Lawson et al., 2000). A technique based on an evaluation of strain-rate fields derived from velocity gradients along the centerline, was applied using Equation 2. Ice exposed in the higher reaches of the ablation area, following the 1982–1983 surge had experienced one surge cycle and thus a relatively simple deformation history. In contrast, ice exposed at the terminal lobe at the same time, had experienced approximately 100 years of evolution through six surge cycles. Measures of cumulative strain in this case masked the effect of large but transient strain events, and also demonstrated that large cumulative strains can also be reversed. The structural assemblages do not fully reflect these strain complexities, as certain structures, notably crevasses and crevasse traces are reactivated several times during passage of ice through the glacier. Nevertheless, the structural sequence (Table 1) is a somewhat simplistic generalization of the range of deformational processes occurring in this glacier.

6.3.2. Polythermal Glaciers

Svalbard is a High-Arctic region containing a high proportion of surge-type glaciers, although percentage estimates vary enormously, from 13% (Jiskoot et al., 1998) to 90% (Lefauconnier & Hagen, 1991). This uncertainty is due to the fact that the quiescent phase, typically lasting 50–100 years, commonly exceeds the period that glaciers have been observed. Similarly, the surge phase itself is longer than those in temperate glaciers, lasting 3–15 years, rather than a year or less. Because timing of the onset of a surge is difficult to predict, few studies were made of Svalbard glaciers prior to the advent of satellite imagery. Now, with this tool, it is possible to trace the structural evolution through a full surge cycle. An example is a study of the 64.7 km^2 Comfortlessbreen, a partly tidewater glacier on the NW coast of Spitsbergen (Svalbard), the surge of which lasted from approximately 2002 to 2009 (Figure 45) (King et al., 2016). Using a combination of ASTER satellite data, aerial photography, and ground observations, the principal structural changes were documented. Pre-surge structures were dominated by stratification (partly folded) and foliation (Figure 45a), with active crevasses only present near the terminus, where calving took place into the sea. In contrast, during the surge, images show that the glacier surface was dominated by crevasses (Figures 45b and 45c) while, at the advancing snout, numerous thrust-faults (Figure 45d) and a few basal crevasses (Figure 45e) were associated with basal debris (till and glaciomarine sediment) being raised upwards (King et al., 2016).

Hessbreen is another surge-type glacier that has been studied structurally, but in its post-surge state, the surge being in 1947 (Hambrey & Dowdeswell, 1997). This glacier is typical of the many small land-terminating glaciers that flow from upland cirques in Svalbard. The structural sequence is summarized in Table 1. As with Variegated Glacier, the investigation of surge-type glaciers in Svalbard suggests that the evolution of ductile structures dominates during the quiescent stage, whereas brittle structures preferentially form during in a surge phase.

A more dramatic example of a polythermal glacier surging is the 1995–1998 surge of Kuannersuit Gletscher on Disko Island in West Greenland (Larsen et al., 2010; Roberts et al., 2009). This glacier emanates from the island's ice cap and the terminus advanced 10.5 km over this period, producing a 65 m-thick stacked sequence of debris-rich basal ice and meteoric glacier ice. The full structural sequence was defined by Roberts et al. (2009) (Table 1). In total, five phases of planar structure formation were documented (Figure 46). Thrust-faulting was the dominant process, with the development of three low-angle major thrusts beginning at the glacier bed and isolating four discrete structural zones. These were intersected by high-angle forward and reverse thrusts and crevasse traces. Previously formed recumbent folds had their limbs sheared off by the thrusts. Proglacial frozen meltwater, known as "*naled*" or "*Aufeis*," was incorporated by thrusting as the glacier advanced. The outer zone of the thrust-faulted sequence comprised thrust blocks of glaciofluvial sediments and ice, which were also affected by hydrofracturing that led to the formation of sills and dykes of clear ice (Roberts et al., 2009).

The thrust-faults formed early in the surge, and produced an overthrow of at least 200–300 m, leading to a 30 m-thick repetition of basal ice at the ice margin. As with some polythermal glaciers in Svalbard and the Yukon, thrust-faulting was thought to have been initiated at the boundary between warm ice in the thicker interior and cold ice at the snout. Unusually, basal debris-rich ice formed after the thrust-faulting phase. The debris comprised diamicton, which was predominantly entrained by freeze-on during conductive cooling and regelation (Roberts et al., 2009).

6.4. Structural Assemblages Observed in Cross-Section

It is normally only possible to investigate ice structures where they become exposed at the surface of a glacier, effectively providing an approximately horizontal plane that allows the 2-D spatial distribution of structures to be mapped and their surface 3-D characteristics to be measured in the field. These data allow the englacial geometry of ice structures to be inferred in 3-D. Incised supraglacial streams commonly offer a tantalizing glimpse of structures in 3-D where they become exposed in channel walls. However, small channels, on the order of several meters in depth, only offer limited exposures for study. Larger supraglacial channels potentially provided suitable sections for study, but access during the ablation season is problematic because of meltwater, and during the winter most channels become clogged by snow. In spite of this, it is occasionally possible to view structures in cross-section where terminal and lateral ice cliffs form, and

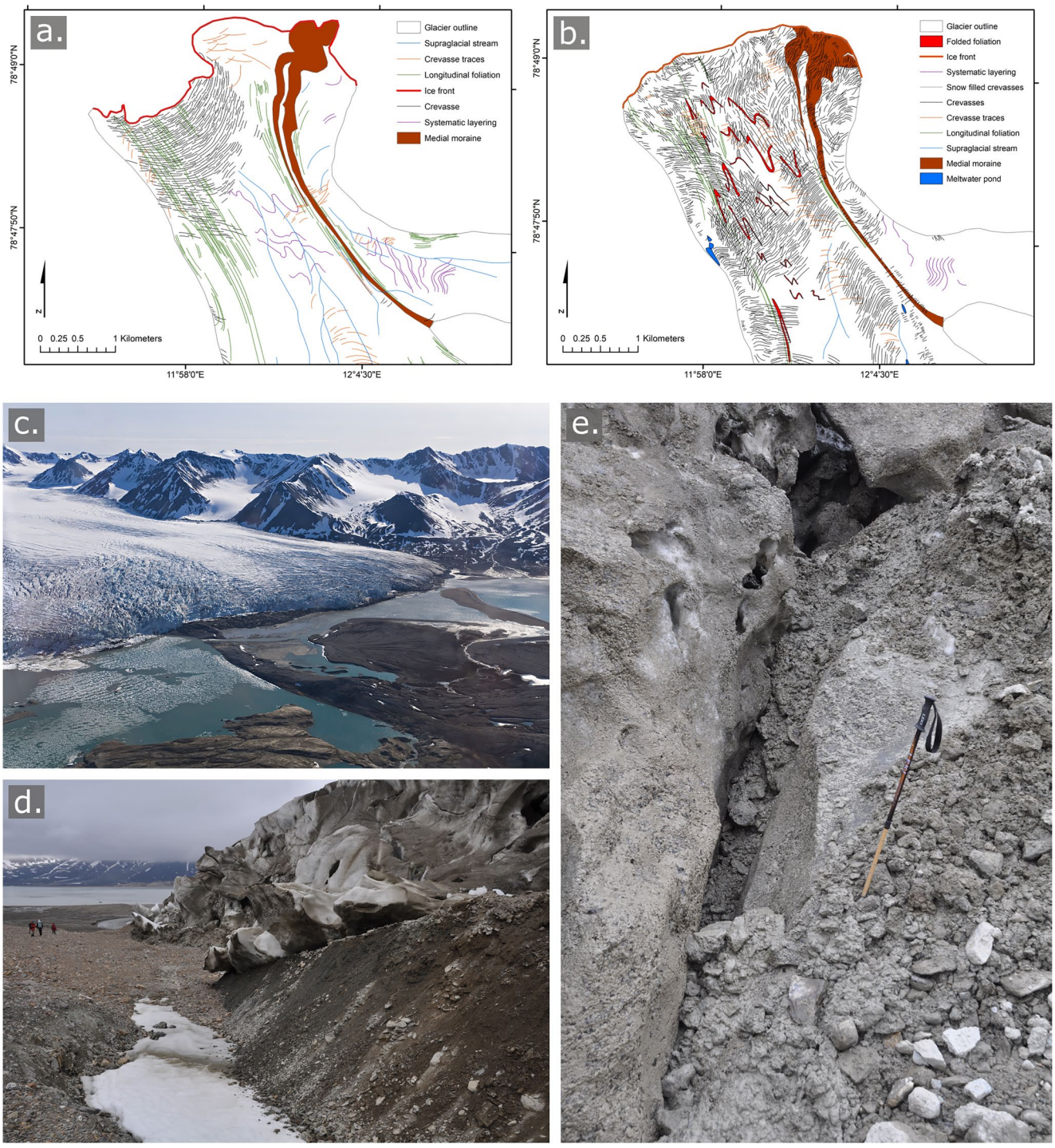

Figure 45. The 2002–2009 surge of Comfortlessbreen, NW Spitsbergen, Svalbard. Structural maps of the terminal area of Comfortlessbreen in: (a) 1990; and (b) 2009. (c) Aerial view of the terminal area in July 2009 shortly before the surge ceased. (d) Thrust-faulting at the true left margin of the glacier near the terminus, with relatively clean ice being actively displaced over sediment-laden ice. (e) Entrainment of basal debris into a basal crevasse near location (d) (after King et al., 2016).

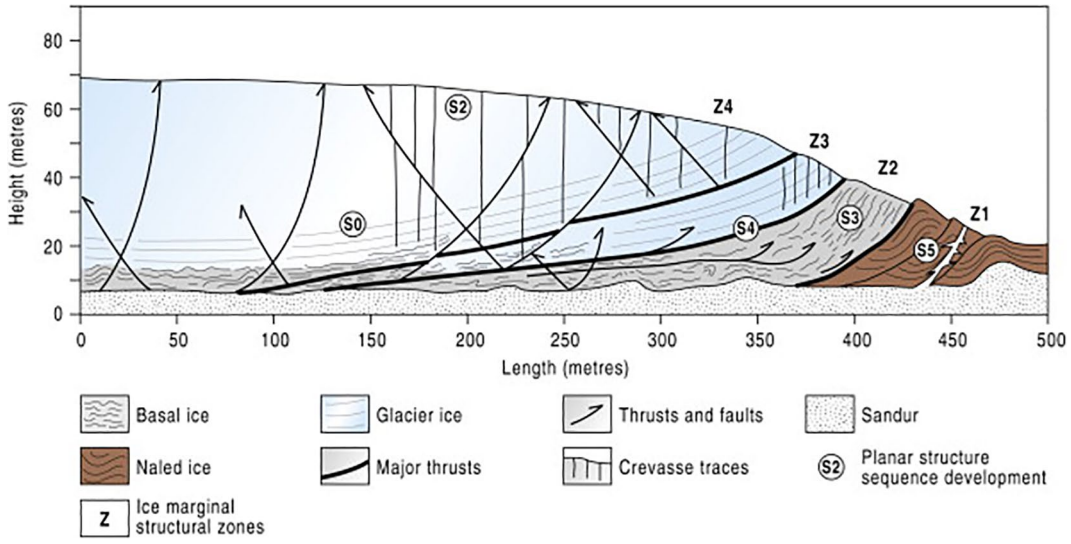

Figure 46. Schematic cross-section of the post-surge terminal zone of Kuannersuit Gletscher, Disko Island, West Greenland. The structures and their locations associated with the five phases of deformation are indicated (Roberts et al., 2009; reproduced with permission of Elsevier).

in the walls of frozen englacial hydrological channels and moulins, allowing the vertical characteristics of structures to be visually assessed.

6.4.1. Structures Viewed in Terminal Cliffs

Vertical cross-sections at glacier margins occur where a tidewater glacier calves into the sea, where a glacier terminates in a lake, and where a glacier terminus is undercut by lateral streams. Cold and polythermal glaciers also commonly have cliff faces resting on land if they have recently experienced an advance. Such glaciers provide good opportunities for establishing the continuity of surface structures at depth. Despite these opportunities, few investigators have examined ice cliffs in detail, but this is helpful in order to achieve a 3-D perspective of glacier structure. Here, we focus on examples from the Swiss Alps, including a relatively simple cirque glacier that terminates in a lake, and a suite of valley glaciers. Also described is a surge-type tidewater glacier in Svalbard.

The cirque glacier is nameless, but terminates in a lake named Griessee. Most of the surface is debris-covered as a consequence of rockfall from the steep headwall that rises to the summit of Clariden (3,267 m), but in 2018 the cliff provided an excellent cross-section of the glacier snout (Figure 47). Three discrete flow units can be identified, in each of which sedimentary stratification derived from snow in the accumulation area, along with buried supraglacial debris from rockfall, is arranged into three synclines. The boundaries between the flow units represent zones of strong deformation, where the stratification is transposed into foliation and shear zones.

Also in Switzerland, three structurally more complex valley glaciers, uniquely for a few years in the 1970s, developed terminal cliffs as a consequence of calving into newly formed reservoirs, followed by lake-lowering in winter as the water was used for hydro-electric power generation. The three Swiss valley glaciers: Griesgletscher, Oberaargletscher, and Vadrec da l'Albigna, developed cliffs that revealed the full ice thickness when the water-levels in the reservoirs were low (in early summer). The cliffs were photographed and the structures revealed were interpreted on the basis of surface observations. Each glacier revealed a broad synclinal structure of original transverse but rotated crevasse traces, remnants of longitudinal foliation (albeit folded), and thrust-faults with entrained basal debris (Figure 48) (Hambrey, 1977b). As a consequence of glacier recession, none of these ice cliffs remain today.

Tidewater glacier cliffs yield variable structural information depending on whether they terminate in shallow or deep water. The example from Svalbard is a valley glacier, Tunabreen, which originates from a highland icefield. Unusually for Svalbard, this glacier has surged four times within the last hundred years, and

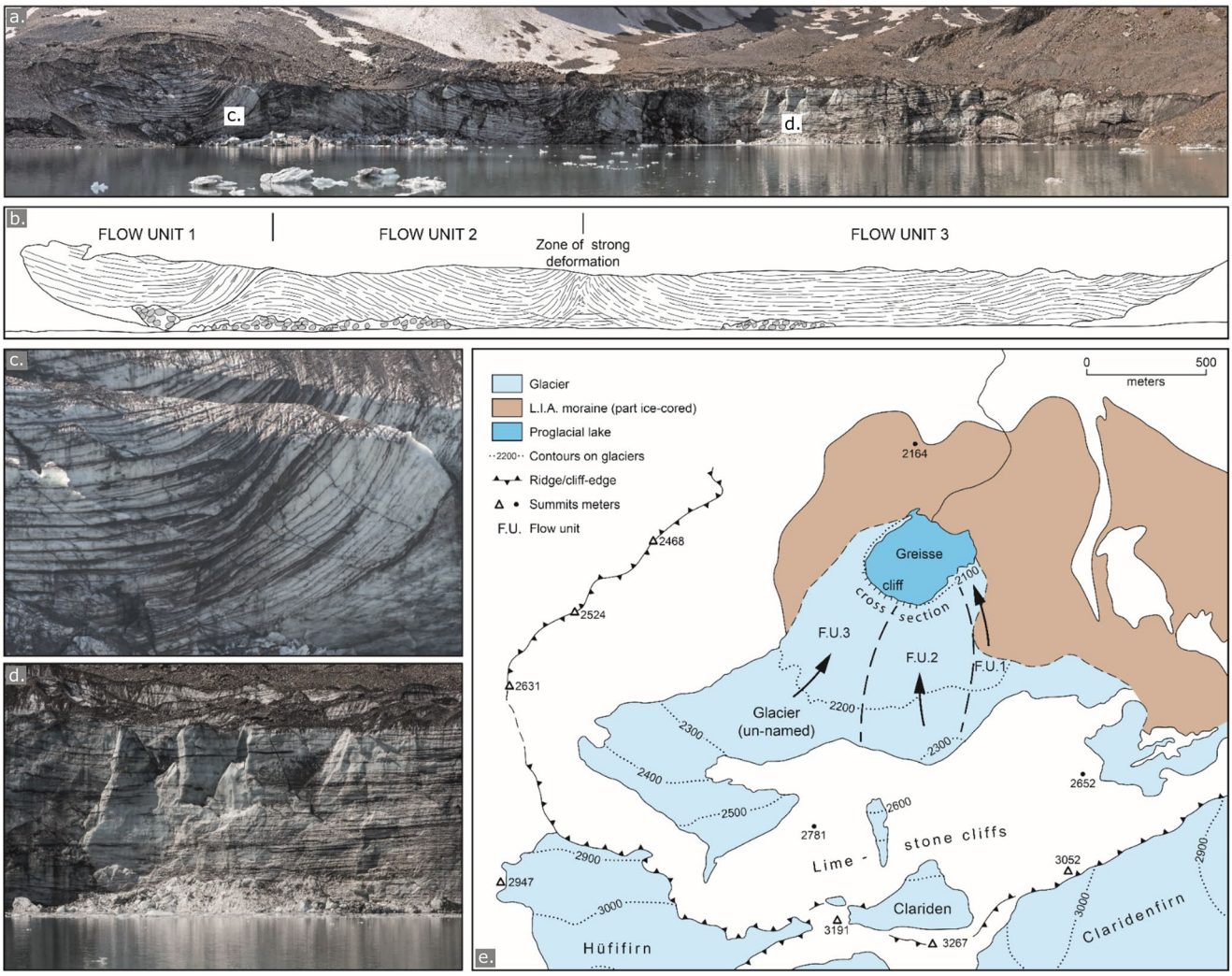

Figure 47. Structural interpretation of the terminal cliff of an unnamed glacier beneath the peak of Clariden, Klausenpass, Switzerland (August 2018). This composite cirque glacier terminates in a lake, Griessee, and the terminal cliff reveals a simple internal structure, dominated by primary stratification. (a) Stitched panorama of the glacier cliff. (b) Sketch of structures from the panorama showing discrete flow units, with strong deformation evident between flow units 2 and 3. (c) Telephoto of steeply inclined stratification merging into transposition foliation in the zone of strong deformation between flow units 2 and 3. (d) Telephoto of near-horizontal stratification in the middle of flow unit 3, emphasized by rockfall debris embedded with the stratification. (e) Simplified topographic map showing the form of the cirque glacier with its constituent flow units.

a structural interpretation of its ice cliff was made prior to the last surge that started in 2016 (Fleming et al., 2013). That study focused on the magnetic fabrics of basal ice (see also Section 9.2). The debris-rich ice was elevated to a high level from the soft deforming bed of marine sediment. Other structures included crevasses, normal faults, thrust-faults, and weakly foliated ice.

6.4.2. Structures Viewed in Englacial Channels and Moulins

A potentially fruitful, but as yet untapped means of investigating structures at depth, is the exploitation of englacial meltwater conduits for viewing structures in cross-section. At the end of the ablation season, meltwater drainage through englacial channels largely ceases, and conduits have yet to close as a result of ice deformation; therefore, englacial access is possible (Gulley, Benn, Screaton, & Martin, 2009). Glacier speleological investigations have primarily been employed to investigate the formation and evolution of englacial drainage networks to aid our understanding of meltwater routing through ice masses. These types of study have been successfully undertaken in a range of locations, including Svalbard (e.g., Benn et al., 2009; Gulley, Benn, Müller, & Luckman, 2009; Hansen et al., 2020; Kamintzis et al., 2017; Pulina, 1984; Vatne, 2001), the

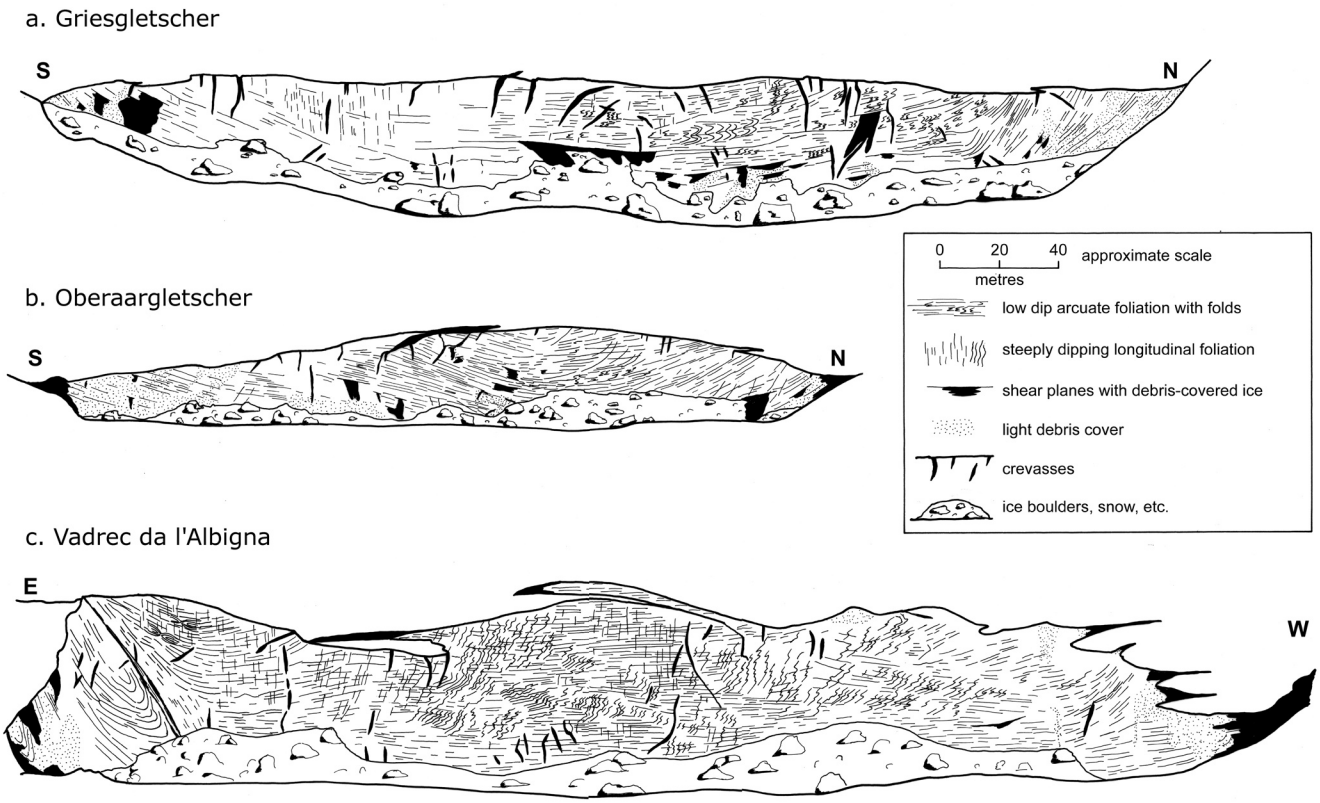

Figure 48. Structural assemblages, uniquely exposed in ice cliffs of three Swiss valley glaciers in 1974, soon after the creation of reservoirs that led to the development of temporary full-height calving cliffs. These represent cross-sections of the internal structure of typical valley glaciers, with crevasses, arcuate and longitudinal foliations, folds, and thrust-faults (some containing debris) evident (Hambrey, 1977b; reproduced with permission of the International Glaciological Society).

Alps (e.g., Piccini et al., 2002), the Himalaya (e.g., Benn et al., 2009, 2017; Gulley, Benn, Müller, & Luckman, 2009), Alaska (e.g., Benn et al., 2009; Gulley, 2009), and Patagonia (e.g., Badino & Piccini, 2002). However, even though the walls of moulins and englacial channels effectively act as windows into the interior of a glacier, often exposing ice structures in spectacular detail (Figure 49), this method of study has yet to be fully exploited.

In crevasse-free regions of polythermal glaciers, englacial channels can form by "cut-and-closure" (Gulley, Benn, Müller, & Luckman, 2009), which can incise through much of a glacier's thickness, and in some cases may reach the bed, potentially providing ice sections through the full ice depth. Closed channels form distinctive structures in their own right (Section 5.5.2), which commonly intersect older ductile structures.

Even though structures in conduit walls can occasionally be obscured by hoar frost, in contrast to supraglacial ice surfaces exposed during the ablation season, conduit walls normally lack a weathering crust, therefore exposing structures with remarkable clarity. Structures commonly visible in conduit walls include primary stratification, longitudinal foliation (Figures 49a and 49b), a variety of fractures (Figures 49a, 49b and 49e), as well as entrained debris and debris layers (Figures 49b–49d). The complex structures and ice facies evident (Figures 49c and 49d) illustrate an intricate record of polyphase deformation that is not fully observable at the surface of a glacier. The lack of supraglacial evidence is, in part, a result of the scarcity of basal ice exposed, combined with a reduced preservation potential associated with the development of a weathering crust.

The ablation of ice abandoned by receding glaciers can occasionally leave collapsed englacial conduits, which in areas of high sublimation may also reveal ice sections with extraordinary clarity, albeit in no longer active ice that is stagnating in situ.

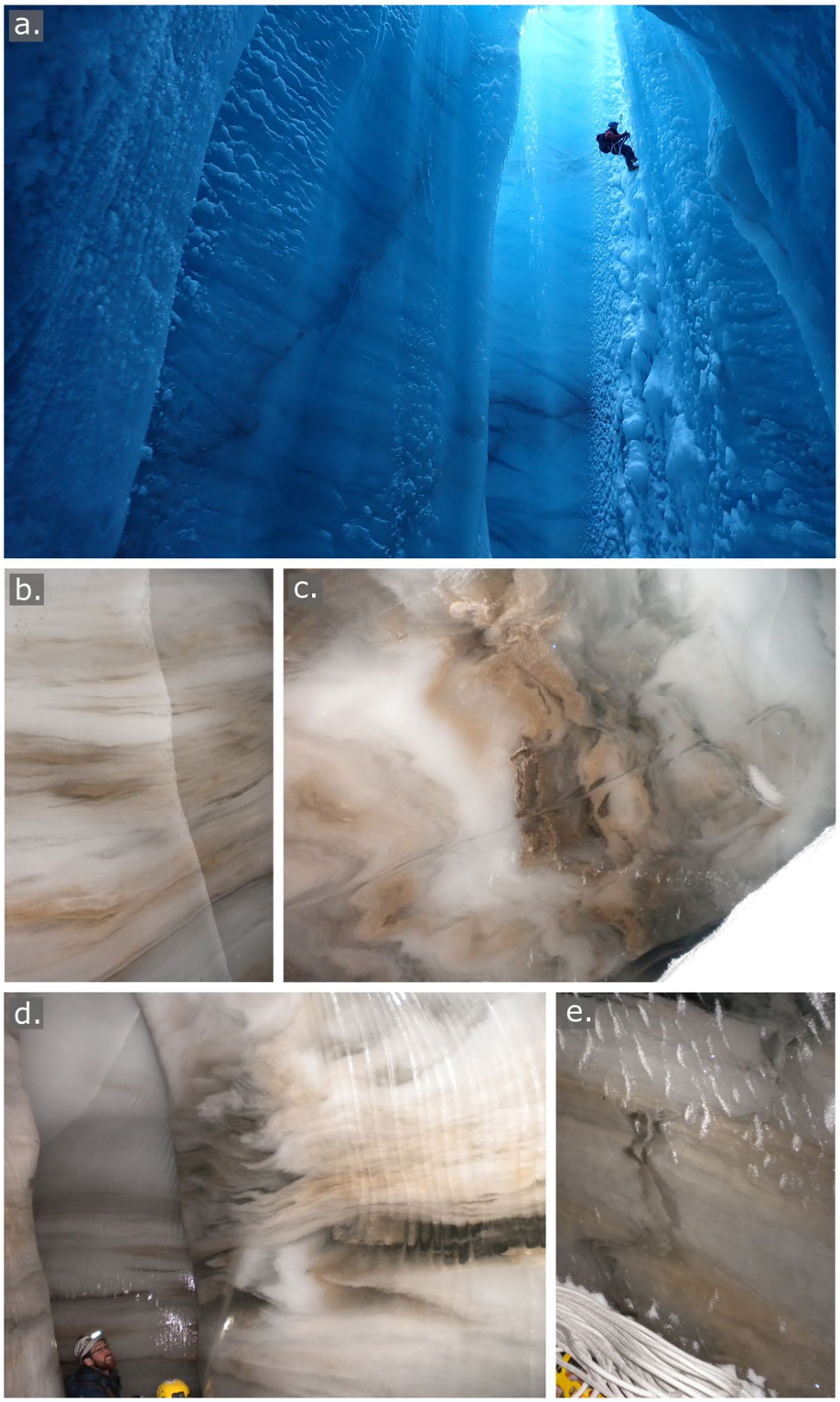

Figure 49.

7. Glaciers as an Analog for Deformation in Orogenic Belts

The application of structural geological principles to glaciology recognizes the similarity of structures in both deformed rocks and ice, although, as mentioned above, ice deforms several orders of magnitude faster than typical rocks in orogenic belts (Hambrey & Milnes, 1977). The following are the main equivalent structures:

1. Primary stratification represents the fundamental building blocks of both rocks and ice, whether they are destroyed or not by deformation and metamorphism.
2. Foliation in ice is equivalent to gneissosity, schistosity, or cleavage in rocks.
3. Folds of all types occur in glaciers as well as in rocks.
4. Fractures in ice have many of the characteristics of strike-slip, normal, and reverse faults in rocks.
5. Crevasses are equivalent to tensional fracturing in Earth's crust, and en echelon crevasses are the equivalent of tension gashes in rocks.
6. Crevasse traces are equivalent to tensional veins, for example, of quartz, in rocks.
7. Thrust faults in ice, particularly when associated with recumbent folding, are comparable to structures in fold-and-thrust tectonic belts.

Structural considerations in glaciers throw light on how deformation takes place in thrust belts. In studying deformed rocks, geologists face a situation where the evidence of strain history is limited to cumulative or finite strain, and the strain history is difficult to unravel. Generally, the sequential geological notation of planar structures and folds implies that each successive structure occurs temporally later than its predecessor. For example, in a thrust sheet it is assumed that motion occurs simultaneously throughout the body of rock, which conceptually is flawed. A glacier is a plausible model of a gravitationally driven thrust sheet. A key conclusion is that glaciers demonstrate that apparently "later" structures are forming at the same time as "earlier" structures, a finding that implies that motion is spatially variable within a thrust sheet.

Direct analogies between glacier and orogenic-belt structures have been made by various authors (Elliot, 1976; Hambrey & Milnes, 1977; Herbst & Neubauer, 2000; Hudleston, 1983, 2015). As an example, the diverse range of structures in the valley glacier Pasterzenkees in Austria has been evaluated (Herbst & Neubauer, 2000). These authors argued that this glacier represents "a natural model of an extensional allochthon formed on top of an orogenic wedge, and also a model for raft tectonics at passive continental margins." An extensional allochthon is a near-surface, gravity-driven mass with a basal low-angle normal fault. This mass represents the upper brittle crust and floats on a ductile lower crust.

The ablation area of Pasterzenkees comprises three main structural domains:

1. An upper domain with three individual flow units which flow in a near steady-state manner, mainly controlled by a lubricated, basal normal fault surface. Lateral shear margins, with longitudinal foliation, illustrate the character of the basal shear zone. The surface is characterized by tensional structures, reflecting brittle behavior under high tensile stresses.
2. A lower area with thrusts, which splay from the basal shear zone, and reflect decrease in velocity, that is, compression.
3. An extensional frontal wedge with normal faulting, formed from a combination of ablation by meltwater, topographic oversteepening, and destruction by meltwater-related basal erosion.

These attributes of Pasterzenkees are likened specifically by Herbst and Neubauer (2000) to the Neogene to Holocene Alpine-Carpathian tectonic system, whereby the formation of both bodies is guided by similar processes, as well as by temperature and rheological behavior.

Figure 49. Ice structures visible in the walls of moulins and englacial conduits. (a) The author (S. J. A. Jennings) ascending a vertical 48 meter moulin in Austre Brøggerbreen, Svalbard. Note the steeply dipping fracture traces in the moulin walls which are cross-cut by foliation. Photograph Blair Fyffe. (b) Strongly foliated ice with varying concentrations of fine-grained debris entrained in Larsbreen, Svalbard. Note the vertical fracture trace, demonstrating neither opening nor crystal growth, cross-cutting the foliation. (c) Highly deformed ice layers with varying concentrations of entrained debris in Larsbreen, Svalbard. The highly complex characteristics of the ice reflect several stages of deformation. Note the thin zone running sub-horizontally through the section, which represents a ductile shear zone with attenuated features. (d) Highly folded and foliated ice in Larsbreen, Svalbard. Note the polyphase deformation with parasitic folds superimposed on larger folds. Vertical ridges in the upper right corner of the image are related to the geometry of the conduit wall. (e) Folded water-healed crevasse cross-cutting foliation in Larsbreen, Svalbard. Note the coarse clear ice facies with suture running through the center. Photographs "b" to "e" S. J. A. Jennings.

8. Upscaling to Ice Sheets

Before the deployment of Earth-observing satellites, little was known about the structure of the Greenland and Antarctic ice sheets, and their constituent ice streams and ice shelves, except around their periphery. Satellites have subsequently provided unparalleled opportunities to investigate the manifold longitudinal structures and a wide variety of fractures at the ice sheet surface. Airborne geophysical surveys, notably ice-penetrating radar, complement the satellite observations, and have allowed the internal structure of the ice sheets to be investigated.

Even a cursory survey of ice sheet structures demonstrates how many are similar to those visible in valley glaciers. Since surveys of the latter have focused on the spatial and geometrical configuration of structures in exposed ice, and a good understanding of their mode of formation has been obtained, they provide an opportunity to "upscale" these observations to ice masses several orders of magnitude larger. This section, therefore, explores the commonality between a variety of structures, including longitudinal flow features, folding, crevasses, and other fractures, based on a variety of satellite and geophysical studies that have focused primarily on parts of the Antarctic Ice Sheet.

8.1. Interpretation of Longitudinal Flow Features

Longitudinal surface structures that are commonly found in Antarctica and Greenland are most prominent on the surface of fast-flowing ice streams, outlet glaciers, and ice shelves. In order to determine past and present dynamics of large ice masses, it is vital that the origin of these features is understood. However, their formation and significance have not been fully explored (Glasser & Gudmundsson, 2012; Glasser et al., 2015). A wide range of literature has referred to these features variously as flow lines (Crabtree & Doake, 1980; Orheim & Lucchitta, 1987), lineations (Crabtree & Doake, 1980), flow stripes (Casassa & Brecher, 1993; Gudmundsson et al., 1998), flow bands (Swithinbank et al., 1988) or flowbands (Jacobel et al., 1996), flow traces (Merry & Whillans, 1993), streaklines (Hulbe & Fahnestock, 2004, 2007; Raup et al., 2005), or simply longitudinal (surface) structures (Ely et al., 2017; Holt, Glasser, & Quincey, 2013; Holt, Glasser, Quincey, & Siegfried, 2013; Holt et al., 2014). The first of these terms is used in the following discussion, and evidence is presented that, in many cases, this feature is the surface manifestation of the 3-D structure longitudinal foliation, as reviewed by Glasser et al. (2015).

Most studies of flow lines have been based on satellite-image interpretation of Antarctic ice streams and ice shelves, but the concept applies equally to the Greenland Ice Sheet, and bear comparison with longitudinal structures in valley glaciers of all sizes. Detailed ground-based studies are only possible on relatively small valley glaciers; therefore, upscaling to larger ice masses relies on seeking out areas of exposed ice, combined with surface observations where possible. Early research that suggested that flow lines were longitudinal foliation was that of Reynolds (1988) and Reynolds and Hambrey (1988) on Wordie and George VI ice shelves in the Antarctic Peninsula respectively. In the latter case, detailed aerial photographs of the ice-shelf margin confirmed that two sets of elongated lakes were parallel to longitudinal foliation (flow lines) and crevasse traces.

Two studies have examined the flow line structure of the entire Antarctic Ice Sheet, as well as several representative glacier basins, using satellite imagery (Ely & Clark, 2016; Glasser et al., 2015). These features are commonly associated with converging flow and are focused in ice streams and their continuation into ice shelves. A striking characteristic of flow lines is their persistence for >100 km in ice shelves, such as in the Larsen B Ice Shelf (Figure 50) (Glasser & Scambos, 2008), and in ice streams (Ely & Clark, 2016; Glasser et al., 2015; Hambrey & Dowdeswell, 1994).

Three hypotheses concerning the origin of flow lines have been evaluated (Glasser et al., 2015):

1. They form as a result of lateral compression in topographic situations where glaciers flow from wide accumulation basins into a narrow tongue. The longitudinal features are interpreted as the surface expression of foliation formed as a result of folding and transposition of primary stratification, with flow-parallel axial planes. This solution is reminiscent of converging flow in valley glaciers (Ely et al., 2017; Hambrey & Glasser, 2003). These features also form at the confluence of glacier tributaries and in the

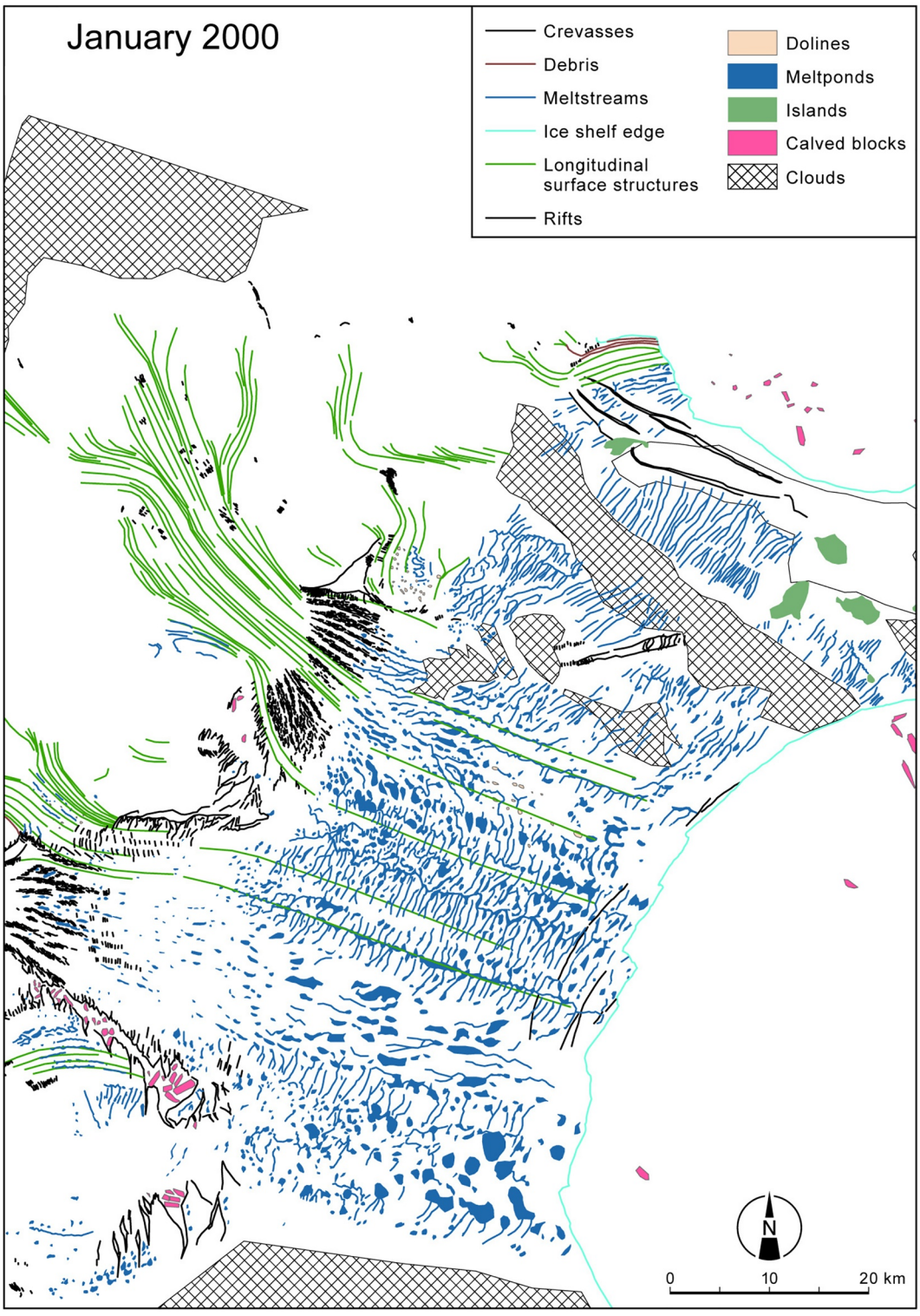

Figure 50. Structural glaciological map of the Larsen B Ice Shelf, Antarctic Peninsula, prior to its 2002 collapse, showing longitudinal surface structures, meltponds, and crevasses (Glasser & Scambos, 2008; reproduced with permission of the International Glaciological Society). The longitudinal surface structures are inferred to be foliation resulting from converging flow in the source glaciers, and the meltponds inferred to be aligned parallel to transverse crevasse traces.

lee of nunataks as a consequence of converging flow and longitudinal extension (Glasser & Gudmundsson, 2012). In both cases, the features represent 3-D structures.
2. They form where two ice stream or glacier tributaries converge and a zone of intense simple shear develops. The longitudinal structures represent aligned crystal bands related to shear (Hulbe & Whillans, 1997; Whillans & van der Veen, 1993).
3. They are the surface expression of perturbations at the bed of the ice mass, formed during sliding (Gudmundsson et al., 1998).

Of the above hypotheses, only the first has been tested by comparing satellite imagery with ground observations. The most convincing evidence that flow lines are the surface manifestation of longitudinal foliation is from the Lambert Glacier—Amery Ice Shelf system in East Antarctica (Figure 51). Arguably the biggest discrete glacier system in the world, its middle reaches consist of exposed ice in which the structure is clearly foliation, verified by ground observations at the margin (Glasser et al., 2015; Hambrey & Dowdeswell, 1994). Furthermore, penetration of ice into side valleys, results in distortion, so that the foliation acquires a curved, cross-flow unit configuration; in this situation the structure is rotated away from parallelism with flow. Perturbations in flow over time are also revealed in some locations, for example, the Ross Ice Shelf, where switching on and off of the constituent ice streams has taken place at different times (Fahnestock et al., 2000); by analogy with large valley glaciers, it is probable that many of these structures are also foliations. Flow lines resulting from converging flow have been recorded in several regions of Antarctica, including the SW Antarctic Peninsula region (e.g., Holt, Glasser, & Quincey, 2013), and ice streams feeding into the Ross and Ronne-Filchner ice shelves (Ely et al., 2017), although in these cases snow cover precludes confirmation that these too represent longitudinal foliation.

One of the first studies to combine detailed measurements of exposed structures in 3-D in the field with satellite interpretation, was on George VI Ice Shelf which forms a cap over the tectonic rift, separating the Antarctic Peninsula Ice Sheet from Alexander Island (Hambrey et al., 2015). Originating on the Peninsula, flow lines in the Bertram Glacier ice stream were observed to be parallel to ice-flow, crossed the ice shelf, and impinged on the far shore of Alexander Island, where they were folded in axial planar relationship with a new foliation derived in response to pure shear from transverse crevasse traces in the ice stream.

Although flow lines are interpreted unambiguously as foliation where bare ice is exposed, areas that are snow-covered preclude definitive solutions. On the Lambert-Amery system, C-band satellite radar imagery that penetrates the upper snow layer reveals well-defined flow lines, both in the component ice streams and in the coastal region. In between is a long reach of bare glacier ice with demonstrable longitudinal foliation of the same orientation. The conclusion is that foliation develops a surface topography that reflects differential ablation of the different ice types, is retained beneath snow cover, and is emphasized by oblique lighting.

In contrast to Antarctica, there are few similar studies of flow lines in the Greenland Ice Sheet. An aerial photographic survey of Jakobshavn Isbræ, a major ice stream on the west side of the ice sheet, well illustrates the nature of flow lines, manifested as persistent longitudinal troughs and ridges, and interpreted as shear zones (Mayer & Herzfeld, 2000). Similarly, another west Greenland outlet glacier, Isunguata Sermia, also displays flow lines (Jones et al., 2018). In both these cases the emphasis was on crevasses, but the flow lines themselves, exposed in bare ice, are probably longitudinal foliation.

8.2. Folding and Boudinage Structures

The widespread use of radio-echo sounding has revolutionized our understanding of the internal layering within ice sheets (Figure 52). Large-scale folding has been observed in the ice streams of West Antarctica (Arcone et al., 2004; Jacobel et al., 1993, 2000). In this case, shear folds developed at the margin of Ice Stream C (now known as Kamb Ice Stream), before it switched off (ceased to flow) and became buried. In the interior of the West Antarctic Ice Sheet, upstream of Byrd Station (Siegert et al., 2004), a distinctive fold structure demonstrated rotation of a 50-km-long axis through 45°, having started parallel to the ice-flow direction. The origin of this fold structure was not known, but it is conceivable that the fold formed as a result of converging flow, after the manner of flow from multiple basins in valley glaciers.

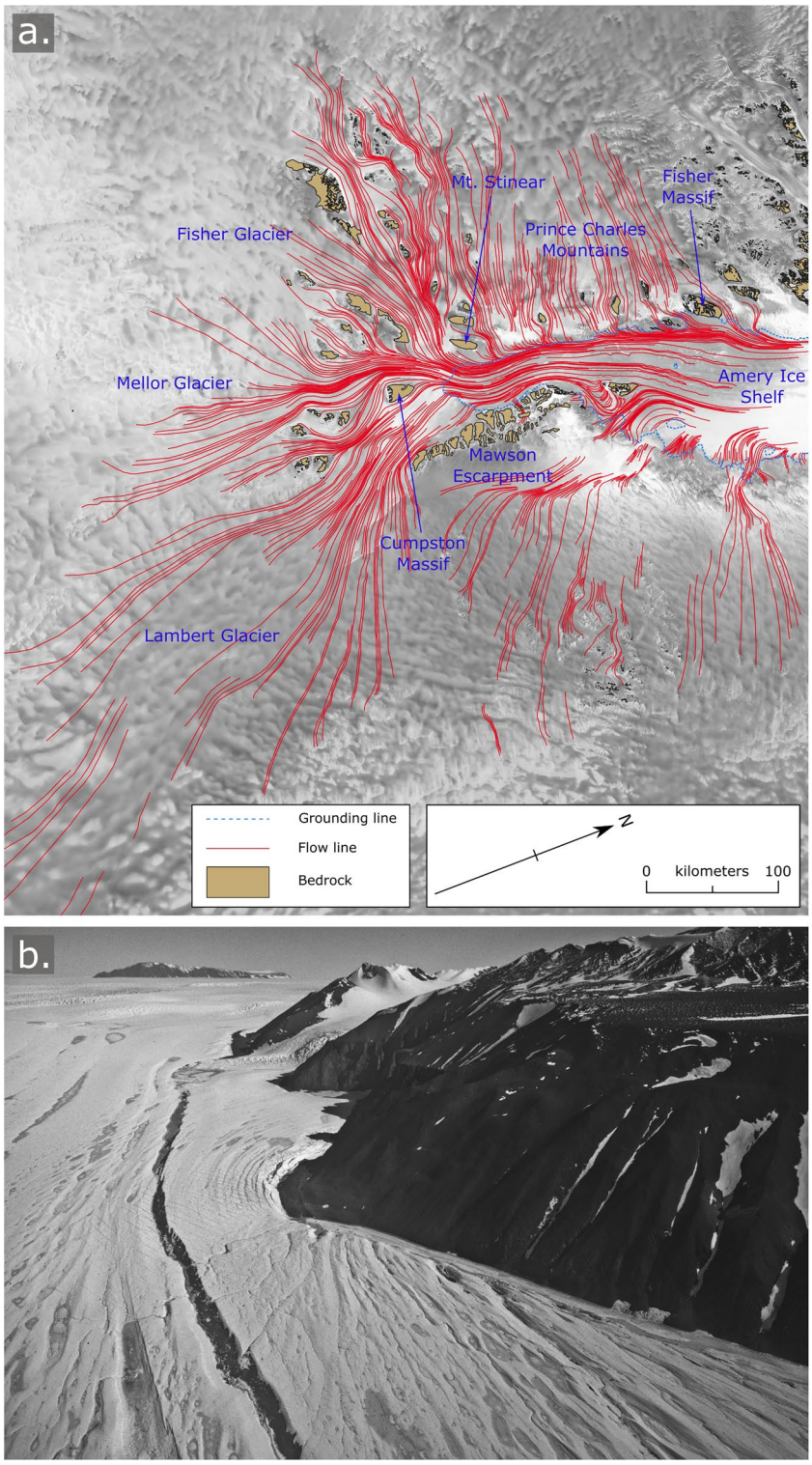

Figure 51. "Flow lines," interpreted as longitudinal foliation in part of the Lambert Glacier—Amery Ice Shelf System, East Antarctica. (a) Map of foliation (red lines), illustrating converging flow of three major glaciers—Lambert, Mellor, and Fisher glaciers, followed by the grounding-line (blue dashed line), with floating ice to the right, overlaid on RADARSAT satellite imagery (available from https://nsidc.org/data/radarsat/index.html) (modified from Jennings, 2017). (b) Aerial photograph of flow structures and local medial moraine at the west margin of Amery Ice Shelf at Fisher Massif; from ground observations of bare glacier ice these structures are unequivocally longitudinal foliation.

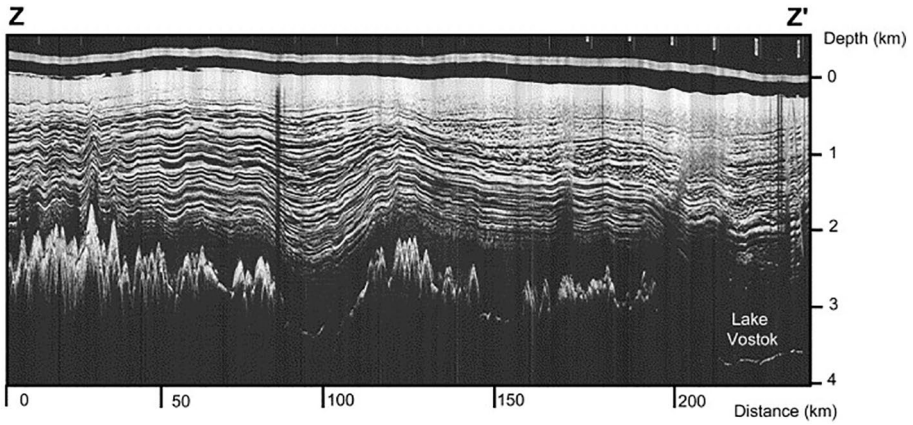

Figure 52. Ice-penetrating radar line parallel to ice-flow direction. Ice flow from the East Antarctic Ice Sheet divide at Ridge B to the site of the Vostok ice core, with subglacial Lake Vostok on the right (Siegert & Kwok, 2000; reproduced with permission of Elsevier).

The complexity of deep englacial structures in ice streams within the West Antarctic Ice Sheet has been demonstrated by an ice-penetrating radar investigation of the Möller and Institute ice streams (Ross et al., 2020). The technique enabled the identification of a zone of multiple highly reflective layers over 500 m thick, which are highly deformed and folded in areas of lateral convergence of the ice streams. The overall structure is a series of five anticlines and synclines, with a wavelength of 3–5 km. The zone was interpreted as a complex of deep-ice facies in which there are abrupt transitions in crystal orientation fabric. Deep ice of this nature is generated by three possible mechanisms: (a) water freezing to the ice sheet base and evolving during flow; (b) deformation of ice of varied lithology; or (c) entrainment of basal debris. The most prominent fold is associated with a flow stripe, observed in satellite imagery (Ross et al., 2020). This association of flow-parallel fold axes with a flow stripe is reminiscent of converging flow structures in the much smaller valley glaciers, where fieldworkers have mapped structures in 3-D. Thus, these Antarctic features may be regarded as foliation (the flow stripe) in axial planar relationship with folding (cf. Hambrey & Glasser, 2003).

Folding (or "bent flow lines") have been described from the Ross Ice Shelf, Antarctica, using satellite imagery (Fahnestock et al., 2000). The ice shelf comprises multiple flow units from the Transantarctic Mountains and ice streams of the West Antarctic Ice Sheet, which interact to create a highly complex structural pattern. The adjacent, but much smaller McMurdo Ice Shelf is noted for having areas of net ablation, and these reveal fold structures on the scale of hundreds of meters, defined by moraine ridges and elongated ponds, known as "The Swirls" (Figure 53). Polyphase deformation is evident, with three phases of folding. As there is no discernable movement in the ice shelf, the structures are interpreted as having formed during a former, more dynamic ice-flow regime (Glasser et al., 2014).

Folding has also been recognized using radio-echo sounding techniques near the base of the Greenland Ice Sheet. Overturned folds were detected by Dahl-Jensen et al. (2013), and large-scale disturbance in the layering of radio-echo reflectors by Drews et al. (2009). Complex structures that qualitatively resemble sheath folds have also been observed in the basal ice of the Greenland Ice Sheet (Figure 54) (MacGregor et al., 2015), which may have formed in relation to rheologically weak layers or slip surfaces (e.g., Reber et al., 2012), although these structures are commonly indistinct and difficult to map from ice-penetrating radar data (MacGregor et al., 2015).

Boudinage structures in valley glaciers are covered in Section 5.3.3. However, boudinage also develops on a much greater scale in large polar outlet glaciers and ice streams, as well as at depth in the middle of ice sheets (Cunningham & Waddington, 1990; Marmo & Wilson, 2000). Understanding boudinage structures on this scale is important, especially with regard to the stratigraphic disturbances boudins may have on deep ice cores (Cunningham & Waddington, 1990; Staffelbach et al., 1988). It is common to observe folds, kink bands, and shear zones near the lateral margins of ice sheets as a result of basal shear (Hudleston, 1976); however, the majority of ice sheet models predict that the stratigraphic layering near ice divides should

Figure 53. Aerial photograph of tightly folded moraines in the McMurdo Ice Shelf, Ross Embayment, Antarctica, with Mt Erebus in the background. These structures were described by Glasser et al. (2014).

be preserved in their correct chronological order (Waddington et al., 2001). Nevertheless, a lack of stratigraphic correlation between two deep ice cores from the center of the Greenland Ice Sheet has led some researchers to consider the role played by folding or boudinage at ice divides. For example, anisotropy in ice rheological properties may result in the development of "wrinkles," that could become overturned into recumbent folds, possibly introducing errors into deep ice-core stratigraphy (Drews et al., 2009; Waddington et al., 2001). Boudinage structures may also develop at or near ice divides, with the implication that ice layers may be interpreted as erroneously thick or thin depending on whether the ice core intersects the boudin neck or swell (Cunningham & Waddington, 1990). The formation of a "Raymond bump" beneath an ice divide has also been suggested, even under steady-state flow conditions. The development of a stratigraphic anticline at the ice divide results because vertical ice-flow velocities at the divide are lower than nearby adjacent areas (Raymond, 1983). The development of a vertical c-axis fabric further enhances anticline

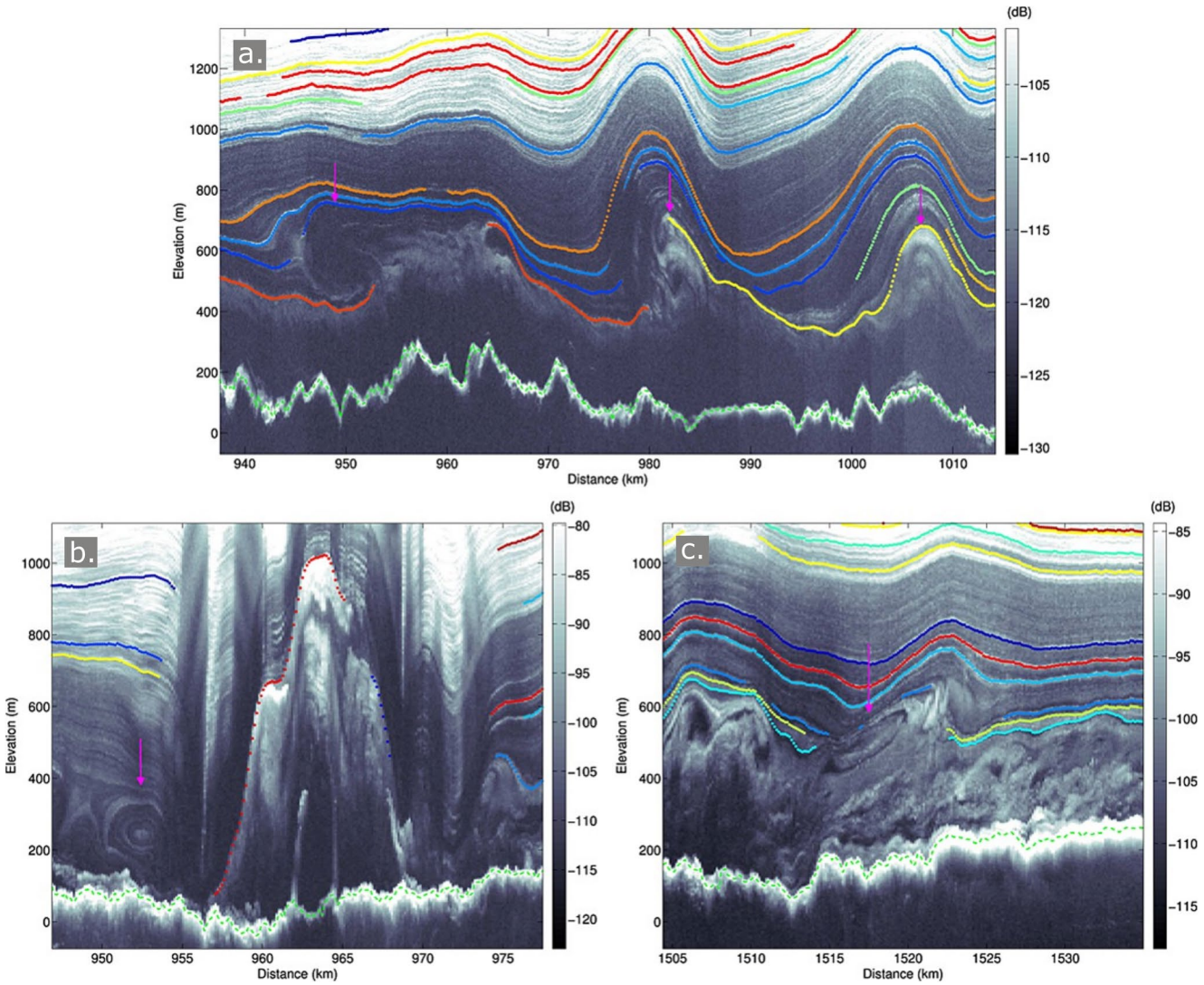

Figure 54. Radargrams from transects of the Greenland Ice Sheet illustrating complex deformation patterns in basal ice, collected on: (a) March 29, 2011; and (b and c) April 29, 2011. Potential sheath folds, visible as eye-like structures, are identified with magenta arrows. Colored radar reflections highlight folded primary stratification, which is increasingly deformed toward the bed. The various colors of individual reflections have no physical significance (MacGregor et al., 2015).

formation (Pettit et al., 2007), with the anisotropic rheology possibly leading to the development of central and flanking synclines (Martin et al., 2009). In nonsteady flow conditions, the migration of an ice divide could result in a previously formed anticline deforming into recumbent structures (Jacobson & Waddington, 2005). Therefore, numerical modeling of fold and boudinage occurrence and behavior (Cunningham & Waddington, 1990; Passchier & Druguet, 2002) is extremely important for identification of areas that should be avoided when coring.

8.3. Formation of Crevasses and Shear Margins in Ice Streams

On the Antarctic Ice Sheet, a major focus of studies of crevasse formation has been on ice streams, which are the main conduits for ice discharge into the Southern Ocean. Many ice streams flow into ice shelves, including those in West Antarctica, which flow into both the Ross Ice Shelf and the Ronne-Filchner Ice Shelf, and into the small ice shelves in the Antarctic Peninsula (Figure 55a). Other ice streams reach the coast but are flanked by ice shelves, such as Pine Island and Thwaites glaciers in the Amundsen Sea sector of West Antarctica (Figure 55b). Other ice streams, especially in East Antarctica, reach the coast and float

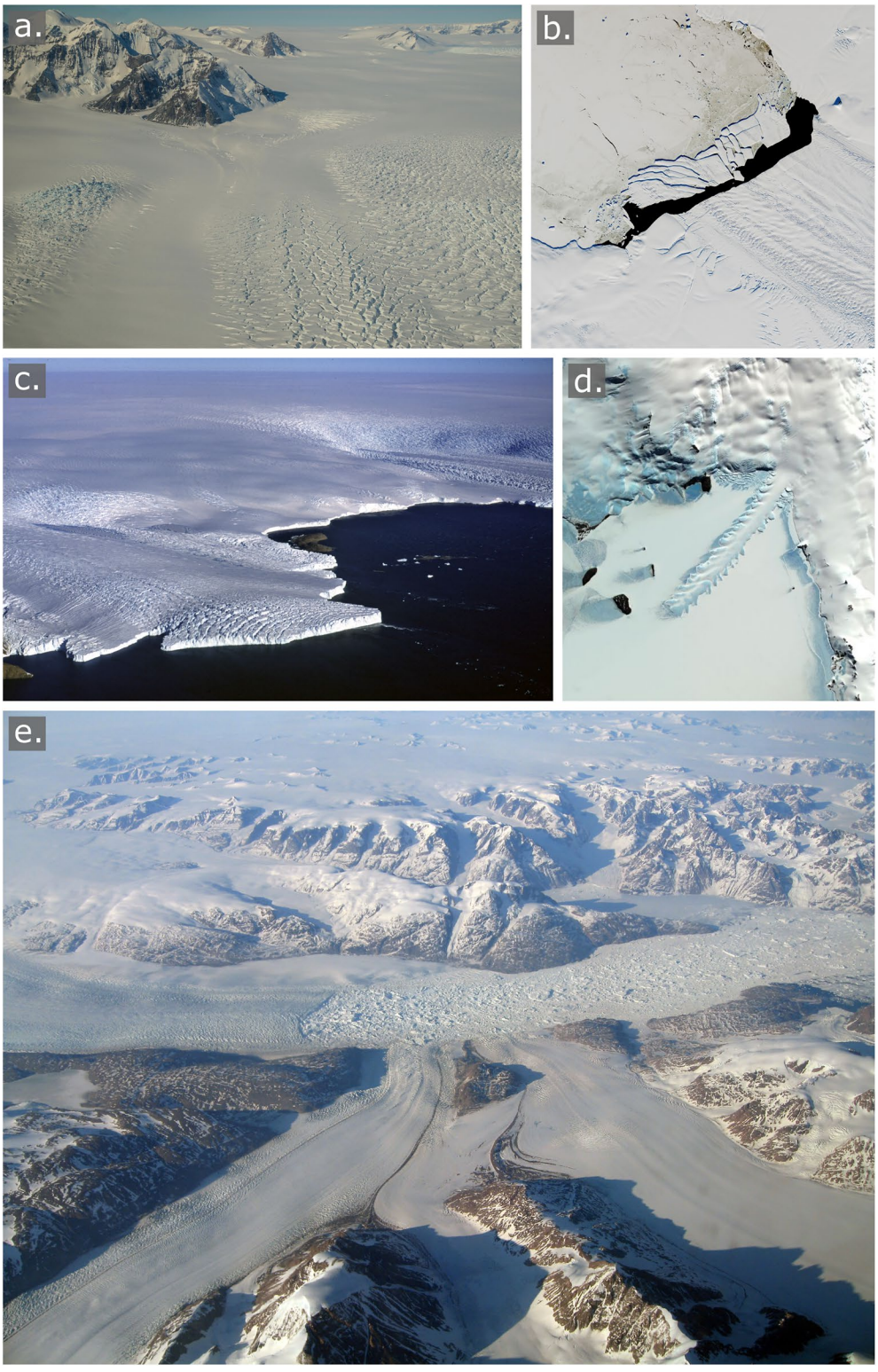

Figure 55.

(Figure 55c), or otherwise project from the coastline as long floating "glacier tongues." The best-known is Erebus Glacier Tongue (Figure 55d), but the largest is the Drygalski Ice Tongue, which extends about 100 km from the coast.

Using radio-echo sounding data, buried crevasses in Antarctica have been identified, and used to estimate the amount of time since the fractured ice had been exposed to areas of high stress (e.g., Clarke et al., 2000; Retzlaff & Bentley, 1993; Shabtaie & Bentley, 1987; Smith et al., 2002). This technique assumes that crevasses only develop at the ice surface and subsequently become buried when passively transported down-glacier. The depth of crevasse burial is then used to estimate the amount of time elapsed since that area of ice was exposed to sufficiently high stresses to initiate crevassing. However, it has been suggested that this assumption may be incorrect and subsurface as well as surface crevasse formation may be possible. Crevasse formation could occur at depths of several meters in areas lacking surface crevassing, and it has been demonstrated that starter cracks can form at depths of 10–30 m (Nath & Vaughan, 2003).

Unique crevasse patterns at the onset zone of Ice Stream B (now known as Whillans Ice Stream), in West Antarctica, with geometries resembling pairs of separating chromosomes (cf. Merry & Whillans, 1993; Vornberger & Whillans, 1986), have also been used to locate and track the upstream migration of the ice stream's onset zone over time (S. Price & Whillans, 2001). Whereas, comparatively smaller-scale observations of the McMurdo Shear Zone using ground-penetrating radar have been used to demonstrate that regions dominated by simple shear, and especially areas with higher shear strain rates, are more likely to have a greater number of crevasses (Kaluzienski et al., 2019). These observations are particularly useful for assessing local amounts of "damage," and therefore ice weakening, which has implications for calving and ice shelf breakup.

The importance of ice streams is emphasized by the fact that they are the conduit for the majority of ice-discharge from an ice sheet to the oceans (e.g., Rignot et al., 2011). Thus, many studies have investigated the variables that regulate ice stream dynamics (e.g., Arthern et al., 2015), as these factors have a direct impact on ice sheet mass balance. For example, lateral shear margins are comparatively narrow zones that separate bedrock, and slow-moving or stagnant ice, from the fast-flowing main body of an ice stream. Consequently, an ice stream experiences intense shear and high cumulative strains, providing a source of lateral drag that resists ice flow (Echelmeyer et al., 1994; Minchew et al., 2018). The down-flow evolution of ice rheology in shear margins is therefore an important control governing flow, as variations in rheology dictate the amount of lateral drag. Investigations of several Siple Coast ice streams have illustrated the importance of marginal processes in an ice stream for controlling flow. Examples include studies of the margins of Ice Stream B (now known as the Whillans Ice Stream) (Echelmeyer et al., 1994; Whillans et al., 1993), Ice Stream D (now known as the Bindschadler Ice Stream) (Scambos et al., 1994), and Ice Stream E (now known as the MacAyeal Ice Stream) (MacAyeal, 1992).

Changes in ice rheology are dependent upon a range of mechanisms, including damage, heating, melting, and the development of a preferred crystallographic fabric; however, the relative contributions of these mechanisms is still not clear (Cuffey & Paterson, 2010; Hudleston, 2015; Minchew et al., 2018). In an investigation of the Rutford Ice Stream, West Antarctica, Minchew et al. (2018) explored the processes controlling the evolution of ice rheology in the shear margins of the ice stream. They concluded that macro-scale surface crevassing had a negligible impact on the evolution of ice rheology, primarily because the fractures were confined to a shallow surface layer relative to the thickness of the ice column. However, crystallographic fabric was found to have a significant impact, effectively softening the ice by approximately an order of magnitude. Shear-heating was found to drive the meso-scale evolution of ice rheology. Even

Figure 55. Examples of ice streams. (a) Converging ice streams flowing past coastal mountains from the Antarctic Peninsula Ice Sheet in Graham Land toward the George VI Ice Shelf. (b) Calving of Pine Island Glacier, a major fast-flowing, thinning and receding ice stream in the West Antarctic Ice Sheet (USGS/NASA satellite image 2017349 December 17, 2017lrg). (c) Two small heavily crevassed ice streams bounded by less active ice at the edge of the East Antarctic Ice Sheet; the prominent ice stream in the foreground is Chaos Glacier. (d) The 12 km-long Erebus Glacier Tongue, which flows off the volcano Mt Erebus on Ross Island; in this image the tongue is surrounded by sea ice. The serrated edge is characteristic of such features (NASA ASTER satellite image—https://eoimages.gsfc.nasa.gov/images/imagerecords/4000/4965/aster_erebus_30nov01_15m.jpg). (e) A major ice stream, Kangerdlugssuaq Gletscher (upper left), draining part of the Greenland Ice Sheet, flows into Kangerdlugssuaq Fjord in East Greenland, as viewed from a commercial flight from London to Vancouver. The high density of icebergs mixed with sea ice, close to the floating glacier front, is referred to as "sikussaq".

though the study area lacked temperate ice, the importance of shear-heating in areas with temperate ice was emphasized as interstitial liquid water has a pronounced softening effect on ice (Minchew et al., 2018).

As in Antarctica, the Greenland Ice Sheet also has numerous ice streams, but these generally terminate in fjords, rather than flow into ice shelves (Figure 55e). Some are exceptionally fast-flowing, and Jakobshavn Isbræ for a period in the 2000s was the world's fastest glacier, flowing at 17 km a year, although it has since slowed down. The combination of fast flow, uneven or channel-like bedrock topography, and acceleration into the sea, gives rise to heavily crevassed ice stream surfaces, with multiple generations and domains of crevasses of different orientation (Echelmeyer et al., 1991; Jones et al., 2018; Mayer & Herzfeld, 2000, 2008). Jakobshavn Isbræ is dominated by shear crevasse patterns toward the margins, commonly intersecting the traces of older crevasses, while a central zone (or flow unit) is characterized mainly by closed crevasses (crevasse traces) (Mayer & Herzfeld, 2000). In contrast to the ice streams of West Antarctica, the comparatively high driving stresses of Jakobshavn Isbræ results in less localized crevasse patterns. Furthermore, as the glacier does not flow into an ice shelf, and therefore has a relatively unconfined terminus, Jakobshavn Isbræ is more akin to unbuttressed Antarctic ice streams, such as Pine Island and Thwaites glaciers (Echelmeyer et al., 1991).

8.4. Formation of Crevasses and Rifts in Ice Shelves

8.4.1. Causes and Impact of Ice Shelf Recession

Around the coastal margins of Antarctica, and especially the periphery of the Antarctic Peninsula and West Antarctic Ice Sheet, critical changes are taking place in response to climatic and oceanographic warming, resulting in the weakening and collapse of ice shelves (Vaughan & Doake, 1996). One of the earliest recorded ice-shelf collapses was that of the Wordie Ice Shelf (Doake & Vaughan, 1991). Crevasses extended to the bottom of the ice shelf to form rifts (large-scale full-depth fractures), and their development was enhanced by meltwater. Future ice-shelf collapses in this region were reported to be imminent, and this indeed was borne out. Scambos et al. (2000) explored the link between ice shelf collapse and climatic warming in the Antarctic Peninsula as a whole. They noted that the warming climate was leading to a longer melt season and an increase in the extent of ponding on the surface of an ice shelf. A clear link was found between melt ponds and enhanced retreat or collapse. Crevasse propagation by meltwater is a dominant mechanism by which ice shelves weaken and recede (Scambos et al., 2009). However, ice shelves in the Antarctic Peninsula are not alone in being vulnerable to meltwater-induced hydrofracturing. Remotely sensed mapping of fractures within ice shelves, combined with the application of fracture mechanics theory, has indicated that 60 ± 10% of all Antarctic ice shelves (by area) are susceptible to hydrofracture, particularly if they become inundated with supraglacial meltwater (Lai et al., 2020).

The disintegration of the Larsen A and B ice shelves on the East Antarctic Peninsula coast has received considerable attention (Cook & Vaughan, 2010). Larsen B Ice Shelf collapsed in dramatic fashion in little more than a month in 2002, losing an area of 3,000 km^2 and producing an armada of icebergs. The preceding longitudinal flow structures, crevasses, and rift patterns in relation to supraglacial melt-ponds were mapped by Glasser and Scambos (2008) (Figure 50). Breakup of ice shelves is of particular concern in the context of rising sea levels, since the flow of glaciers that once fed them accelerated following ice shelf breakup (De Rydt et al., 2015; Hulbe et al., 2008; Rignot et al., 2004; Rott et al., 2011; Scambos et al., 2004; Shuman et al., 2011). The removal of the buttressing effect provided by the ice shelves caused the interior ice streams to effectively surge, drawing down ice from the interior (De Angelis & Skvarca, 2003), a process that has led to widespread up-stream dynamic changes (Reese et al., 2018) and has contributed to sea-level rise. Similar dynamic changes caused by the weakening and recession of ice shelves around the periphery of the Antarctic Peninsula and West Antarctic Ice Sheet have had a direct impact on the mass balance of the ice sheet as a whole (Pritchard et al., 2012). Consequently, in recent years, research has focused on the mechanisms by which ice shelves fracture and breakup. In particular, the structural attributes of ice shelves have been investigated, as the internal structure of an ice shelf influences the formation and propagation of rifts.

8.4.2. Constitution of Ice Shelves

The internal structure of ice shelves varies, but generally comprises a combination of meteoric ice (derived from inland glaciers and ice streams), accreted marine ice, sea ice, and accumulated snow. At the grounding

line, the majority of Antarctic ice shelves remain structurally intact as coherent ice masses, formed by the coalescence of tributary glaciers and ice streams. However, a number of ice shelves, such as the Brunt Ice Shelf and Thwaites Glacier Tongue, do not retain their structural integrity, and therefore form as a conglomerate of meteoric ice blocks (icebergs) fused together by sea ice and accumulated drifted snow (King et al., 2018; Milnes et al., 2020).

In these circumstances, the longitudinal separation between icebergs is determined by the velocity of the source tributaries flowing from the interior. At the grounding line, fast flowing and comparatively thicker inflows of meteoric ice discharging from subglacial troughs fracture into closely packed icebergs separated by narrow transverse-to-flow channels (Figure 56a) (King et al., 2018). In contrast, thinner inflows discharging from subglacial ridges at a slower rate are unable to provide a sufficient supply of ice to match the velocity of the ice shelf (which is driven by the faster discharging tributaries). Consequently, icebergs are comparatively thinner, and are widely separated from one-another (Figure 56a). In both cases, the ice shelf develops as the expanses between meteoric icebergs become infilled by sea ice and collapsed blocks of meteoric ice, fusing the icebergs together (King et al., 2018).

As areas of sea ice between icebergs represent topographic lows at the surface of the ice shelf, snow accumulates via direct precipitation or by drifting, eventually compacting into firn. The continued accumulation of firn loads the sea ice, forcing it below sea level as a result of hydrostatic adjustment, allowing seawater to infiltrate the porous firn layers, which have not sufficiently compacted to the stage of pore close-off (Figure 56b). Repeated freezing cycles concentrates the salt to form a "brine reflector," which is evident in ice-penetrating radar surveys (Figure 57). Eventually, the infiltration of seawater ceases, despite continued firn accumulation driving the sea ice deeper below sea level. The mechanism by which this process terminates are not clear, but it is likely to involve an amalgamation of continued firn pore-closure combined with the freezing of seawater in interstitial cavities, ultimately reducing the permeability of the firn. Alternatively, the accumulation of marine ice at the base of the ice shelf may eventually form impermeable layers over time (King et al., 2018). The resulting structure is a form of primary stratification, but of a complex and unusual nature.

At the boundary between tributary inflows of meteoric ice that feed into the same ice shelf, suture zones develop, composed of a mélange of sea ice, marine ice, collapse debris from meteoric blocks, and in situ snowfall (Glasser et al., 2009; Jansen et al., 2013; McGrath et al., 2014). These suture zones bind neighboring tributaries, and often form in the lee of peninsulas, which can contribute a limited influx of meteoric blocks to the suture zone if the peninsula has a catchment area. Strain-thickening of the suture zone often occurs as comparatively thicker neighboring tributary inflows compress the suture as they laterally spread downstream (McGrath et al., 2014). Despite the heterogeneous nature of suture zones, they commonly appear smooth in visible imagery, as they lack the large-scale structural features such as crevasses and rifts that are commonly present in meteoric inflows (Glasser et al., 2009; Holland et al., 2009). Additionally, preferential surface accumulation of precipitated and drifted snow occurs in suture zones, which usually are defined by surface depressions in the ice shelf. Infilling by snow thus reduces the visibility of any surface variations (Leonard et al., 2008).

Marine ice develops below suture zones as buoyant ice shelf meltwater rises in plumes from the keels of comparatively deep meteoric inflows near to the grounding-line (Holland et al., 2009). Pressure-melting of meteoric ice near the grounding-line releases meltwater that becomes supercooled as it rises and the pressure decreases, refreezing to the ice shelf base at shallower depths in ice draft minima, usually found downstream of peninsulas (Holland et al., 2009; McGrath et al., 2014). Newly accreted marine ice is probably slushy, initially forming permeable layers, but subsequent accumulation of new layers and conductive heat flux toward the ice shelf surface consolidates the marine ice (Craven et al., 2009; Hubbard et al., 2012), further cementing neighboring meteoric tributary inflows into a cohesive mass (Glasser et al., 2009; Holland et al., 2009). A spatially limited variation of this process can occur in basal crevasses and rifts, whereby localized convection currents melt fracture walls, with the resulting meltwater refreezing as marine ice at shallower depths within the fracture (Hubbard et al., 2012; Jordan et al., 2014; Khazendar & Jenkins, 2003).

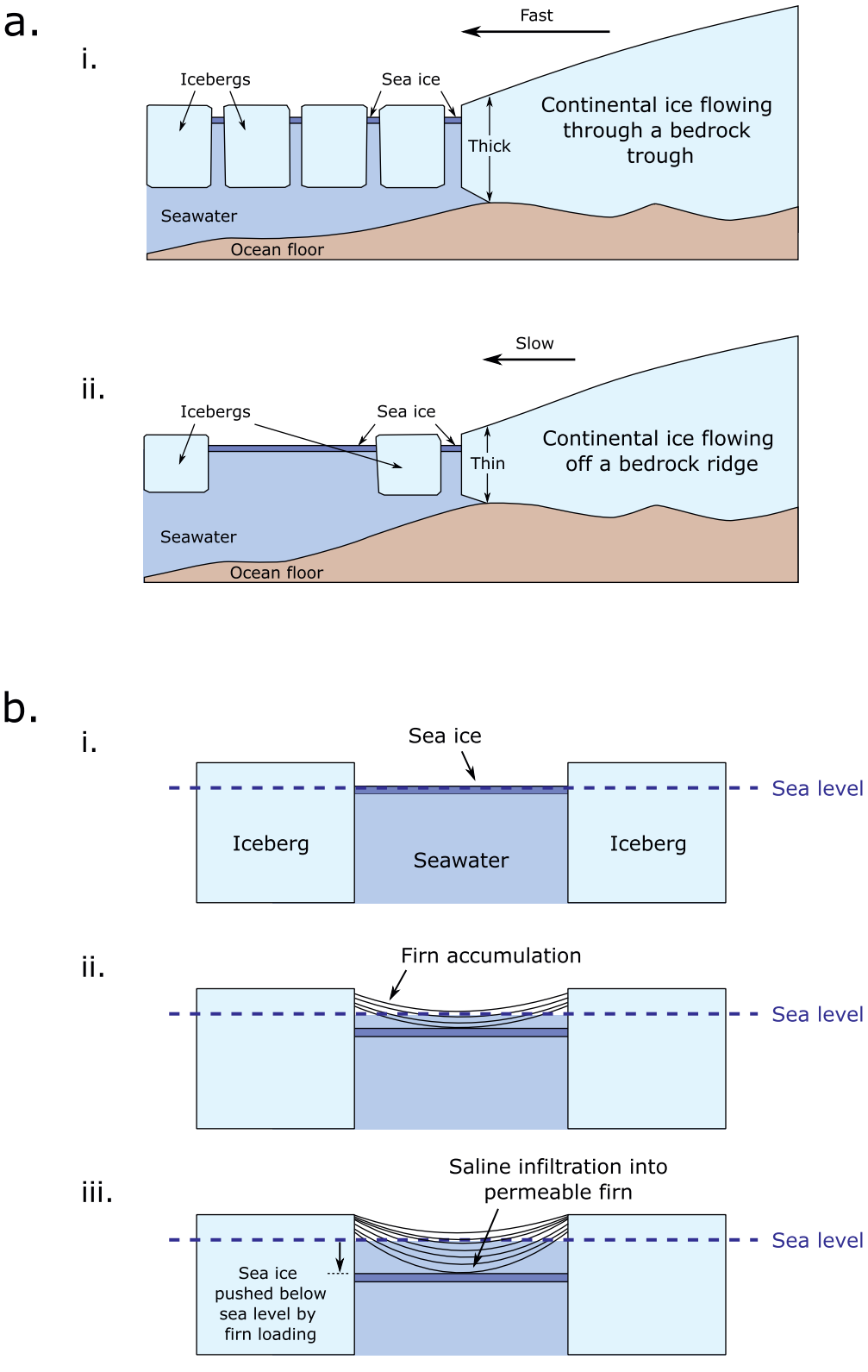
a.
i.
Fast
Icebergs
Sea ice
Thick
Continental ice flowing through a bedrock trough
Seawater
Ocean floor
ii.
Slow
Icebergs
Sea ice
Thin
Continental ice flowing off a bedrock ridge
Seawater
Ocean floor
b.
i.
Sea ice
Sea level
Iceberg
Seawater
Iceberg
ii.
Firn accumulation
Sea level
iii.
Saline infiltration into permeable firn
Sea level
Sea ice pushed below sea level by firn loading

Figure 56.

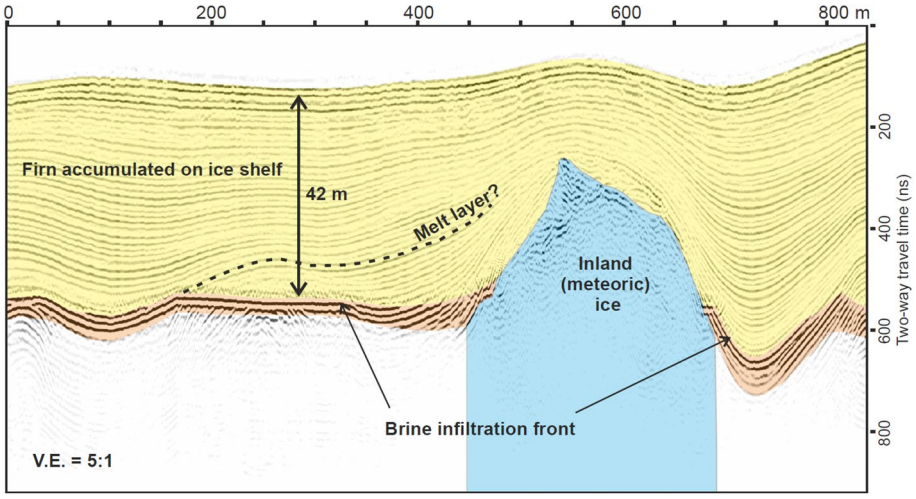

Figure 57. Detailed section of a radar profile from the Brunt Ice Shelf with overlying interpretation of the internal structure of the ice shelf. Continuous horizontal layering represents firn accumulation, which develops an anticline above the meteoric iceberg, and synclines adjacent to the iceberg. A brine infiltration front illustrates the level to which seawater has penetrated the firn as a result of firn loading of the sea ice, which, in places, cross-cuts firn layers (King et al., 2018).

8.4.3. Ice Shelf Fractures

The highly variable and heterogeneous composition of ice shelves has important implications for ice shelf fracture and disintegration (e.g., Glasser & Scambos, 2008) (Figure 50). Rheological and structural differences between interior-derived meteoric ice compared with the ice that forms in suture zones and between meteoric icebergs, act as a control on rift-propagation (Borstad et al., 2017). For example, it has been demonstrated that suture zones in the Larsen C Ice Shelf on the eastern coast of the Antarctic Peninsula, have a higher fracture toughness compared with adjacent meteoric inflows, despite being thinner and lacking a homogeneous structure (Jansen et al., 2013; Khazendar et al., 2011; McGrath et al., 2014). Ice shelf fracture is not a steady process, but is a consequence of sporadic rifting and interaction with other structures (crevasses and fracture traces), as demonstrated by an investigation of George VI Ice Shelf, Antarctic Peninsula (Holt, Glasser, Quincey, & Siegfried, 2013) and Pine Island Glacier, West Antarctica (Jeong et al., 2016).

Fractures in meteoric ice have been found to terminate at suture zones in the Ross Ice Shelf (Fahnestock et al., 2000), in the Ronne-Filchner Ice Shelf (Hulbe et al., 2010; Larour et al., 2004; Rignot & MacAyeal, 1998), and fracture propagation was demonstrated to alter direction multiple times when entering a suture zone on the Amery Ice Shelf (Walker et al., 2015). In the Larsen C Ice Shelf, fracture propagation through meteoric ice occurred at a higher rate than through suture zones (Borstad et al., 2017), with Hulbe et al. (2010) demonstrating that rift-propagation would continue if not hindered by the higher fracture toughness of the ice mélange in sutures, which would considerably increase future calving events. The resistive properties of suture zones to fracture propagation is likely to be a combination of temperature, heterogeneous composition, water content, and crystal fabric; however, the relative importance of these factors is as yet unknown (King et al., 2018; McGrath et al., 2014). Conversely, structural analyses of rift-propagation in the Brunt Ice Shelf has illustrated that the general trajectory of fracture-propagation is determined by the large-scale stress field, forming perpendicular to the maximum stress tensor (De Rydt et al., 2018; Gudmundsson

Figure 56. Schematic diagrams based on observations from the Brunt Ice Shelf illustrating the formation of different ice shelf structures. (a) The spacing of meteoric icebergs within ice shelves dictated by the comparative velocities of tributary glaciers. (i) Comparatively fast-flowing thick ice discharging from a subglacial trough breaks into numerous closely packed icebergs separated by narrow channels of sea ice which fuse the icebergs together. (ii) Comparatively slower-flowing thin ice discharging from a subglacial ridge at a velocity less than that of the ice shelf (which is driven by faster-flowing tributaries). Consequently, icebergs are widely spaced with large expanses of sea ice cementing them together. (b) Illustration of firn loading of sea ice, whereby sea ice between meteoric icebergs is forced below sea level, allowing saline infiltration. (i) Initial formation of sea ice between meteoric icebergs. (ii) Accumulation of in situ and drifted snow on the sea ice, which eventually compacts into firn. The continued accumulation of snow loads the sea ice, forcing it below sea level. (iii) Permeable firn layers allow the infiltration of seawater from below (modified from King et al., 2018).

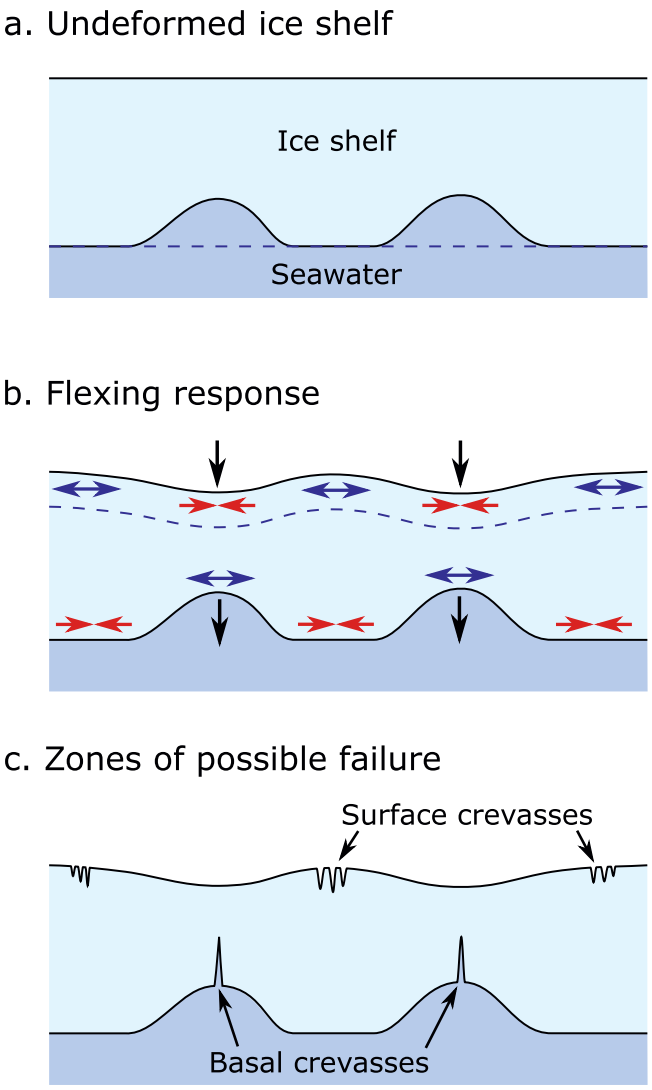

Figure 58. Schematic diagram based on observations from Pine Island Glacier, West Antarctica, illustrating the formation of surface and basal crevasses in an ice shelf based on thin-beam theory. (a) Undeformed ice shelf with uneven basal surface resulting from the continued melt of sub-ice shelf channels by ocean melting. (b) Sagging of the ice surface above the sub-ice shelf channels induces compressional (red arrows) and extensional (blue arrows) stresses in the ice shelf. (c) The formation of surface and basal crevasses in response to the stresses induced by flexing of the ice shelf (modified from Vaughan et al., 2012).

et al., 2017). However, at a smaller scale, rift trajectory is governed by the location and shape of meteoric blocks, with fractures preferentially propagating around icebergs, presumably exploiting pre-existing structural weaknesses in the ice mélange (E. King et al., 2018). In this case from the Brunt Ice Shelf, the rift was only observed to propagate through a meteoric block once, which corresponded with a period of considerably slower propagation rates (De Rydt et al., 2018). The contrasting behavior, especially with regard to fracture propagation rates through meteoric ice and ice mélange between different ice shelves, is a topic that requires further study to improve calving laws and models for accurately predicting ice shelf stability (Benn & Åström, 2018; King et al., 2018).

Basal (bottom) crevasses are fractures that penetrate upwards from the base of an ice mass (Jezek, 1984; van der Veen, 1998b). They have been identified in several ice shelves from geophysical surveys, for example, in the Ross Ice Shelf (Jezek & Bentley, 1983; Jezek et al., 1979), the Larsen C Ice Shelf (Luckman et al., 2012; McGrath, Steffen, Rajaram, et al., 2012; McGeath, Steffen, Scambos, et al., 2012), the Fimbul Ice Shelf (Humbert & Steinhage, 2011), the floating tongue of Pine Island Glacier (Vaughan et al., 2012), as well as in a large tabular iceberg calved from the Ross Ice Shelf (Peters et al., 2007). Despite early surveys suggesting that basal crevasses are likely to be abundant in Antarctic ice shelves (Shabtaie & Bentley, 1982), only comparatively recently have these structures been receiving significant attention (e.g., Luckman et al., 2012; McGrath, Steffen, Rajaram, et al., 2012; McGeath, Steffen, Scambos, et al., 2012; Vaughan et al., 2012). Basal fractures differ from surface fractures as they are water-filled, and can therefore penetrate through more than half of the ice thickness (Luckman et al., 2012). Consequently, basal crevasses are thought to be important structural elements for the stability of ice shelves (McGrath, Steffen, Scambos, et al., 2012).

In a study investigating basal crevasses in the Larsen C Ice shelf, McGrath, Steffen, Rajaram, et al. (2012) identified the main mechanisms by which basal fractures probably contribute to the disintegration of ice shelves: (a) the deformation of the ice shelf surface above the basal crevasse in response to modified buoyancy and gravitational forces, leading to the development of >10 m deep surface depressions in which meltwater can collect; (b) the initiation of surface crevassing as a result of bending stresses induced by the formation of basal crevasses, which form large (up to 40 m-wide) surface crevasses at the margins of the surface trough; and (c) the effective reduction of ice shelf thickness, decreasing the depth required to produce, and increasing the likelihood of a full-thickness rift.

Supraglacial troughs, induced by basal crevasses, are readily visible in remotely sensed imagery as surface undulations of parallel alternating light and dark bands, oriented transverse to flow (Luckman et al., 2012; McGrath, Steffen, Scambos, et al., 2012). Surface crevassing is generally lacking upstream of the undulations, but becomes more abundant downstream, with surface crevasse orientations remaining approximately parallel to the crests of the surface undulations (McGrath, Steffen, Scambos, et al., 2012). The formation of bands of surface crevasses on ridge crests in relation to basal crevasses has also been observed on the floating tongue of Pine Island Glacier, where it was hypothesized that they developed as a result of stresses derived from the hydrostatic relaxation of the ice shelf (Figure 58) (Vaughan et al., 2012). The surface expression of basal crevasses consequently controls the location and distribution of meltwater ponds at the surface of ice shelves, which develop along supraglacial depressions. The formation of surface crevasses in relation to basal crevasses, and therefore the close proximity to meltwater ponds, provides the initial

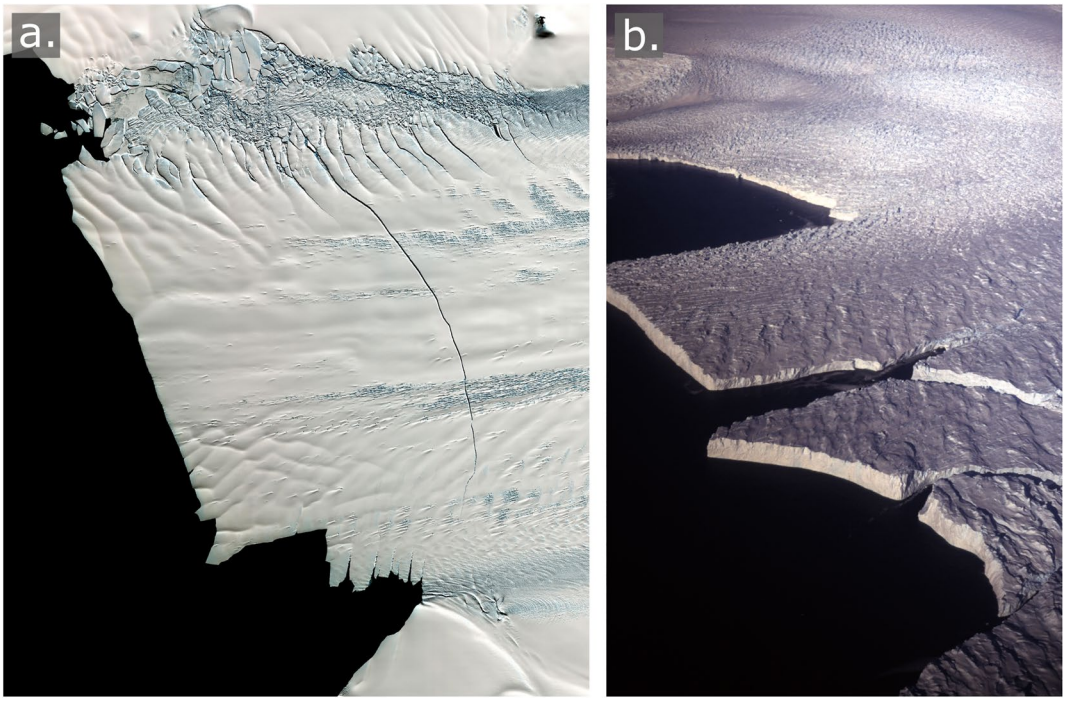

Figure 59. Rifting in ice shelves and iceberg production. (a) Rifting in Pine Island Glacier, a fast-flowing ice stream within an ice shelf in West Antarctica, which is being destabilized by oceanographic warming beneath and changing dynamics. This image also shows the birth of tabular berg B44 (area 185 km^2) in September 2017; width of image c. 55 km. Note the large lateral shear zone parallel to the top of the image consisting of a mélange of meteoric blocks, sea ice, in situ snow cover, and marine ice (https://eoimages.gsfc.nasa.gov/images/imagerecords/91000/91066/pineisland_oli_2017271_lrg.jpg) (see also Figure 55b). (b) Rifting and incipient tabular iceberg formation, Fimbul Ice Shelf, Princess Elizabeth Land, East Antarctica. The process is cyclic, with slow advance over many decades, followed by large break-outs.

fracture and necessary reservoir to initiate hydrofracture, increasing the likelihood of full-thickness crevasse penetration and rift formation (McGrath, Steffen, Scambos, et al., 2012).

8.4.4. Ice Shelf Calving

Calving from ice shelves can occur by a number of mechanisms, ranging from cyclic calving of large tabular icebergs, through to the catastrophic disintegration of entire ice shelves (Benn & Åström, 2018). Stable ice shelves that have been in a long-term steady state tend to experience multi-decadal growth punctuated by large infrequent calving events that produce icebergs ranging from several hundred square meters through to many hundreds, if not thousands, of square kilometers in size (Benn & Åström, 2018; Fricker et al., 2002; Liu et al., 2015). Large tabular icebergs are usually released from ice shelves via the slow propagation of rifts (Figure 59a). The formation of large-scale rifts is primarily determined by the stress field, forming perpendicular to the maximum stress tensor (De Rydt et al., 2018; Gudmundsson et al., 2017). However, the internal structure of an ice shelf influences fracture propagation, as discussed above, and comparatively thin ice shelves (<200 m thick) may also be prone to influence from ocean swells (Bassis & Walker, 2012; Benn & Åström, 2018) and ocean warming (Holt, Glasser, Quincey, & Siegfried, 2013).

Even though large calving events are part of a natural cycle for ice shelves (Figure 59b), the release of large icebergs can destabilize an ice shelf, leading to further recession, and potentially collapse. The possible destabilization of the Larsen C Ice Shelf following the calving in July 2017 of the 5,800 km^2, 200 m thick, A68 iceberg via a rapidly propagating rift is a good example of a rift-derived calving event (Jansen et al., 2015). However, even though rift-derived calving is common for Antarctic ice shelves, ongoing climatic and ocean warming are potentially increasing the formation of rifts. Observations from the floating tongue of Pine Island Glacier indicate that basal melting, combined with a changing stress regime resulting

from the disintegration of the ice mélange, are leading to the development of new rifts that are leading to calving events further upglacier than have previously been observed (Jeong et al., 2016).

8.4.5. Impact of Increasing Melt-Rates on Ice Shelf Hydrofracturing

The disintegration or collapse of ice shelves has been occurring in the northern Antarctic Peninsula over the last several decades (Cook & Vaughan, 2010), with implications for the velocity at which tributary glaciers and ice streams flow into the ocean (Reese et al., 2018). Several factors, such as thinning of ice shelves by increased surface and basal melt, structural weakening via fracturing (e.g., Jeong et al., 2016), and the development of impermeable surface layers, have all led to the preconditioning of ice shelves for collapse (Benn & Åström, 2018; Glasser & Scambos, 2008; Hubbard et al., 2016; Luckman et al., 2014; Scambos et al., 2000). Increasing accumulation of surface meltwater ponds can trigger rapid fracturing of ice shelves through hydrofracturing. Once initiated, hydrofracturing results in a positive feedback effect, whereby a chain-reaction of supraglacial lake drainage occurs as a result of lake-induced flexural stresses. This, in turn, causes neighboring lakes to also drain. Furthermore, the flexural stresses enable a fracture network with a sufficiently narrow horizontal spacing to induce capsize-driven breakup (Banwell et al., 2013; MacAyeal & Sergienko, 2013). However, it is becoming more apparent that, not only ice shelves inundated with supraglacial meltwater can collapse, but ice shelves in colder environments are vulnerable to oceanic currents that can initiate widespread fracturing and fragmentation (Bassis & Ma, 2015; Jeong et al., 2016; Vaughan et al., 2012).

Ice dolines are spatially limited structural features that are almost exclusively observed at the surface of ice shelves, which are found in areas of supraglacial meltwater ponds (Bindschadler et al., 2002; Moore, 1993). Ice dolines investigated on the Larsen B Ice Shelf, prior to its collapse, consisted of elongate surface depressions, generally oriented with the long-axis approximately parallel to ice flow. Dolines were commonly arranged in clusters, but isolated examples also occurred. The maximum horizontal dimensions observed reached c. 1 km in length by 500 m in width, yet dolines with horizontal dimensions of <100 m in either direction were also investigated. The maximum depth measured of a doline was 19 m, which meant that even the deepest dolines had floors that were several meters above estimated sea level (Bindschadler et al., 2002). It is likely that ice dolines formed when supraglacial meltwater ponds, which form above impermeable layers within the ice shelf, eventually drained through fractures into the interior of the ice shelf, thereby creating a subsurface void in the underlying firn. Subsequent collapse of the surface layer into the underlying cavity forms the doline, which appears to maintain a drainage connection to the underlying ocean. This was indicated by the observation that dolines and their surrounding area remain drained of supraglacial meltwater, even during the melt season. Initial fracture formation was attributed to the unequal loading of surface ice layers by meltwater ponds, creating tensile stresses that form fractures at the lake edge, enabling the water to drain (Bindschadler et al., 2002).

8.4.6. Contrasts With Arctic Ice Shelves

Arctic ice shelves are fewer in number and much smaller than their Antarctic counterparts, being confined to several High-Arctic archipelagos (Dowdeswell, 2017; Jeffries, 2017) and the fjords of northern Greenland (Reeh, 2017). In contrast to Antarctic ice shelves, the majority of Arctic ice shelves are not glacier fed, but predominantly comprise sea ice that develops in thickness (up to a few tens of meters) by the basal accretion of marine ice and the surface accumulation of snow (Jeffries, 1992; Mueller et al., 2003). The largest individual Arctic ice shelf at the turn of the century was the 443 km^2 Ward Hunt Ice Shelf, Nunavut, Canada, which began fragmenting in the period from 2000 to 2002 (Mueller et al., 2003). The largest Eurasian Arctic ice shelf, was the c. 240 km^2 Matusevich Ice Shelf, in the Russian High-Arctic archipelago of Severnaya Zemlya, prior to its collapse in 2012 (Dowdeswell, 2017). The differing composition of Arctic compared with Antarctic ice shelves (Dowdeswell & Jeffries, 2017), combined with their poleward flow-directions (Mueller et al., 2003), suggest that Arctic ice shelves may be particularly vulnerable to climatic warming. Decreasing accretion of marine ice and the warming of the ice shelves' landward margins may precondition Arctic ice shelves for increased recession and eventual collapse (Mueller et al., 2003).

The ice shelves of northernmost Ellesmere Island have a characteristic ribbed, or corrugated ridge-trough surface morphology, which have been referred to as “rolls” by some authors (e.g., Hattersley-Smith, 1957). This distinctive morphology has been used to help identify so called “ice islands” as tabular icebergs that

have calved into the Arctic Ocean (Dowdeswell & Jeffries, 2017; Jeffries, 1992). Similar ridge-trough ice surface morphologies that have been observed elsewhere (e.g., on lake ice) suggest that their formation is not directly related to internal ice shelf dynamics, with their origin more likely derived from prevailing winds that elongate pre-existing surface meltwater ponds (troughs) and winter snow drifts (ridges), initially forming in a similar manner to seif dunes in desert environments (Hattersley-Smith, 1957; see also Braun, 2017; Jeffries, 1987).

8.5. Thrust-Faulting and Recumbent Folding

The most dynamic parts of the Antarctic and Greenland ice sheets are heavily crevassed ice streams and outlet glaciers that terminate in the sea. Therefore, their internal structures are difficult to observe. However, in those areas where ice sheets terminate on land, there is the opportunity to investigate the nature of deformation at the base of large ice masses. The most detailed work has been undertaken in the Vestfold Hills and Bunger Hills that form oases at the edge of the East Antarctic Ice Sheet. At Bunger Hills, Fitzsimons and Colhoun, (1995) documented recumbent folding and thrusting, involving the entrainment of basal debris. At Vestfold Hills, basal freezing and entrainment of glaciomarine sediment along the lateral margin of a marine inlet revealed a complex of thrust-block moraines (Fitzsimons, 1996). "Controlled moraines" (formerly referred to as "inner moraines") are formed on the surface of the ice sheet where basal ice crops out (Evans, 2009). Upwarping of basal debris combined with net ablation, results in sinuous ice-cored moraines running approximately parallel to the ice margin. The basal ice and overlying clean ice reveal structures that range from slightly deformed layered ice to complex polyphase folding and shearing, with recumbent folds having an amplitude of >15 m (Evans, 2009; Fitzsimons, 2003). These ice-sheet marginal structures resemble those in the smaller-scale cold margins of polythermal valley glaciers in the Arctic, and give a good indication of the deformational processes that occur beneath much of these ice sheets.

9. Significance of Structural Glaciology for Other Glaciological Sub-Disciplines

9.1. Glacier Dynamical Changes Over Time

Structural glaciology may be used to infer changes in dynamics for the period in which ice has resided in a glacier. All glaciers retain structures that show a transition from headwall to terminus, a process that has led to the classifying of structures according to their order of formation, as outlined above. More specifically, most valley glaciers today are receding steadily, and as a result they are becoming less dynamic. Typically, this is manifested in the reduced number of crevasses, and the only indication of former activity may be the presence of numerous crevasse traces (Colgan et al., 2016; Hambrey & Lawson, 2000). One example of using structures to understand changing dynamics, in which structural mapping was combined with radar and cumulative strain modeling, is Midtre Lovénbreen in Svalbard (Hambrey et al., 2005). This glacier, like most of those in Svalbard, reached its greatest postglacial extent around 1900 CE, since when the snout has retreated and the glacier thinned. During this most dynamic phase, the glacier surface was heavily fractured, and extensive thrust-faulting occurred at the snout, generating moraines. As the glacier thins, so the proportion of frozen-to-wet bed increases and eventually this polythermal glacier will become cold-based. This transition has already happened at nearby Austre Brøggerbreen, which is now almost crevasse-free and is revealing its internal structure at the surface. There is now a glacier-wide network of intersecting crevasse traces, some of which contain frozen water, suggesting that the glacier may have once surged (Jennings et al., 2016).

Studies of changing dynamics over time are more readily resolvable in surge-type glaciers, especially if serial aerial photographs are available. This is especially the case in Alaska and the Yukon, where the surge cycle is typically a few decades or less. The most detailed study of surge evolution over time is a study of Variegated Glacier (Lawson, 1996), as described in Section 6.3, covering three surge cycles over half a century, with an average frequency of 14 years (Kamb et al., 1985). However, at least two other glaciers, the Susitna Glacier, Alaska, and the Lowell Glacier, Yukon, show particularly striking examples of a multiple surge history. The 35-km-long Susitna Glacier has spectacular looped moraines, well seen in an ASTER image from 2009 (Figure 60a). Clarke (1991) examined the surging history of this glacier, and inferred that there was an interaction of surging and non-surging tributaries. Surge cycles were 50–60 years long, the last

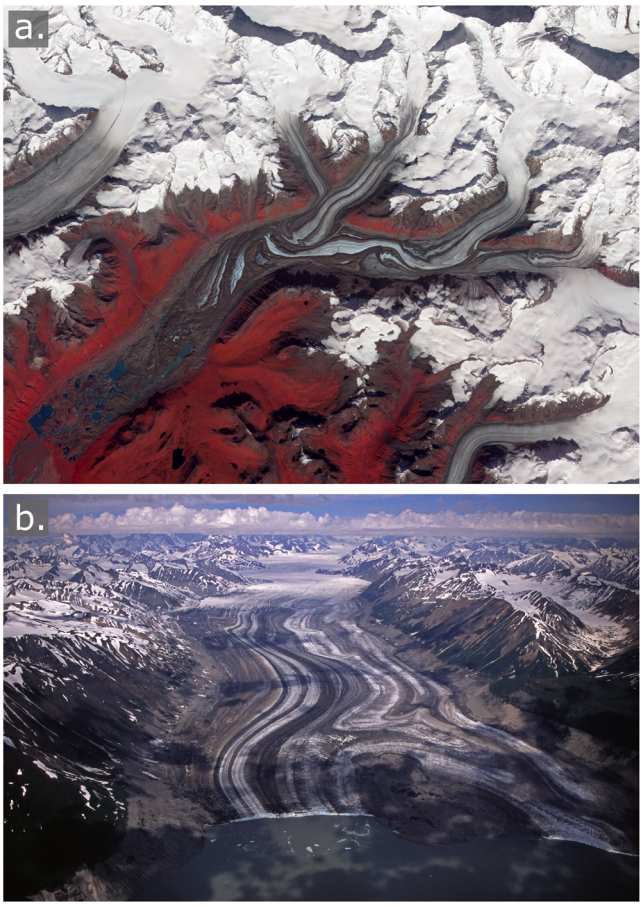

Figure 60. Glaciers with multiple surge histories. (a) An ASTER image of Susitna Glacier, Alaska, taken on August 27, 2009, during a quiescent stage in the surge cycle. This false-color image shows debris-covered ice as brown, and vegetation as red. Source: http://eoimages.gsfc.nasa.gov/images/imagerecords/46000/46449/susitna_ast_2009239_lrg.jpg. (b) Oblique aerial view of Lowell Glacier, Yukon, in August 2006, showing several surge loops distorting medial moraines and longitudinal foliation.

having occurred in 1987–1988. In the 2009 image, each looped moraine records a surge, but many other structures are also visible, including longitudinal foliation parallel to the moraines, arcuate foliation and weak ogives associated with icefalls, isoclinal and similar folds in addition to the surge loops, and abundant crevasse traces. Similarly, the 65-km-long Lowell Glacier has experienced five surges since 1948 (Bevington & Copland, 2014), reflected in several surge loops and deformed longitudinal foliation (Figure 60b). These structures reflect different stages in the surge cycle, but have yet to be resolved in detail.

Overall, despite radical changes in ice dynamics between surging and quiescent phases, some aspects of past structural history are preserved, notably deformed supraglacial moraines and deep-seated structures revealed by ablation, such as foliations. Brittle structures from prior surges, however, are less well-preserved as crevasse traces than in nonsurge-type glaciers. These structures tend to be short-lived and penetrate to comparatively shallow depths, and thus ablate away within several years.

In Svalbard, surges are also common (cf. Sevestre & Benn, 2015), but the surge cycle is so long that it is rare that more than one surge has been observed on a single glacier. As an example, Comfortlessbreen, whose 5-years surge terminated in 2010, had no prior record of surging, nor did it previously have any of the attributes normally ascribed to surge-type glaciers (Figure 45a) (King et al., 2016).

The correlation of deep ice cores with radiostratigraphic studies has enabled the internal structures of ice sheets to be age-depth constrained, allowing stratigraphic information to be extrapolated to much larger areas. Care must be taken when extrapolating isochrones away from ice core locations, as the disruption of englacial layering has been linked with enhanced ice-flow and increased strain (e.g., Rippin et al., 2003), as well as the preservation of buried eolian erosional surfaces that truncate the stratigraphic sequence (e.g., Cavitte et al., 2016). Nevertheless, radiostratigraphy is a useful tool for assessing past ice sheet dynamics and constraining ice sheet models. For example, decades worth of ice-penetrating radar surveys enabled the age structure and deep radiostratigraphy of the Greenland Ice Sheet to be comprehensively mapped (MacGregor et al., 2015). Despite the current peripheral thinning of the Greenland Ice Sheet, radiostratigraphy illustrated that the interior thickening of the ice sheet was related to dynamic changes resulting from rheological differences between Holocene ice and comparatively softer ice deposited during the last glacial period (MacGregor et al., 2016). Similarly, comparatively little is known about the past dynamic behavior of the Antarctic Ice Sheet prior to satellite observations, an understand of which is vital for assessing topics such as the stability of the West Antarctic Ice Sheet (Bodart et al., 2021). Stratification, visible as internal reflecting horizons in airborne radar data, preserves a cumulative record of accumulation, basal melt, past flow features, and ice dynamics, which if dated, can provide a dynamic record that spans the Quaternary Period. Such studies have been successfully undertaken for the West Antarctic Ice Sheet, which have deduced Holocene ice-flow dynamics across catchments with complex flow histories (e.g., Ashmore et al., 2020) and for major ice streams discharging into the ocean, such as Pine Island Glacier (Bodart et al., 2021), as well as the identification of isochrones spanning the Quaternary Period for large expanses of the East Antarctic Ice Sheet (e.g., A. Winter et al., 2019).

9.2. Debris Entrainment and Transfer

9.2.1. The Significance of Debris Entrainment

The sheer complexity of glacial sediments and landforms is a reflection of the wide range of processes involved in debris entrainment into, and deposition from, a glacier (cf. Benn & Evans, 2010). Assimilation of debris into glacier ice takes place via the surface and the bed. Surface debris-entrainment involves rockfall from exposed frost-affected cliffs, stonefall from exposed lateral moraines and scree slopes (Benn et al., 2003; Hambrey et al., 2008), rock-slope failure of over-steepened slopes (Ballantyne, & Stone, 2009; Jibson et al., 2006), and debris-flows (Deline et al., 2015; Kirkbride & Sugden, 1992).

Debris-entrainment at the base of a glacier occurs via the processes of regelation (Alley et al., 1997; Hubbard et al., 2009; Knight, 1997), glaciohydraulic supercooling (Alley et al., 1997; Cook et al., 2006; Swift et al., 2018; Tweed et al., 2005), net adfreezing (Christoffersen et al., 2005; Swift et al., 2018), and by reworking of old buried ice (Evans, 1989b; Everest & Bradwell, 2003; Moorman & Michel, 2000).

Once entrained within the body of the glacier, debris is subjected to the same range of glaciotectonic processes that affects clean ice, such as folding, faulting (especially thrust-faulting), shear, and ingestion by crevasses (Benn & Evans, 2010; Hambrey et al., 1999). An in-depth knowledge of these processes is needed if glacial landforms, such as moraines, are to be fully understood (see Section 9.3).

Several modes of debris entrainment have been recognized where ice deformation plays a prominent role, as discussed below.

9.2.2. Debris Entrainment at the Base of a Glacier

Incorporation of debris at the glacier base has long been identified as an important mechanism in developing a basal ice layer and transporting the sediment through the glacier system, ever since the pioneering studies of valley glaciers in Svalbard (Garwood & Gregory, 1898) and in Antarctica (Wright & Priestley, 1922). The first quantitative analyses and structural attributes of sediment within the basal zone of a polythermal glacier (Boulton, 1967, 1970) were also undertaken in Svalbard, and this research laid the foundations for modern glacial sedimentology. Over subsequent decades the complexity of ice and debris facies in the basal ice layer have been systematically defined in both temperate and polythermal glaciers (Hubbard & Sharp, 1989; Hubbard et al., 2009; Knight, 1997; Lawson et al., 1998). However, the structural complexity of this zone has received relatively little attention. One exception is an examination of surge-type Tunabreen in Svalbard (Fleming et al., 2013), which portrays a complex interplay between folding, thrust-faulting, and debris-entrainment via a diapiric-like process as well as regelation. These authors also pioneered the use of magnetic fabrics of sediment particles in basal ice, to provide a basis for the analysis of Quaternary, and even Neoproterozoic glacial sediments, using the same technique.

9.2.3. Incorporation of Angular Rockfall Material Within the Stratified Sequence of Snow and Firn, and Redistribution by Folding

The importance of the processes of high-level debris-entrainment and transfer to low levels in glaciers has been recognized for several decades (Boulton, 1978; Eyles & Rogerson, 1978; Small, 1983). More recently, the relevance of ice structure in explaining debris distribution has been demonstrated through systematic mapping in 3-D of stratification, foliation, and thrust-faults in several polythermal glaciers in Svalbard (Hambrey et al., 1999). The first of these processes, involves the incorporation of rockfall within a stratified sequence of snow, firn, and superimposed ice. It is followed by folding, particularly where a wide accumulation basin feeds a narrow tongue. Folding is most intense near flow-unit boundaries or at the glacier margins and is commonly associated with an axial planar foliation (Hambrey & Glasser, 2003; Hambrey et al., 2005; Jennings et al., 2016). The original rockfall debris re-emerges near the snout as a suite of medial moraines, whose traces define the hinges of the folds, and are thus parallel to flow (Figures 61 and 62a).

Other glaciers where angular rockfall-derived debris is folded to varying degrees within stratification include Bas Glacier d'Arolla in Switzerland (Goodsell, Hambrey, & Glasser, 2005), Vadrec del Forno in Switzerland (Jennings et al., 2014), Glacier de St. Sorlin in France (Roberson, 2008), and Fox Glacier, New Zealand (Appleby et al., 2017; Brook et al., 2017). In all cases, rockfall debris is tightly folded at flow-unit boundaries, where lateral compression results in high cumulative strains, and where medial moraines are

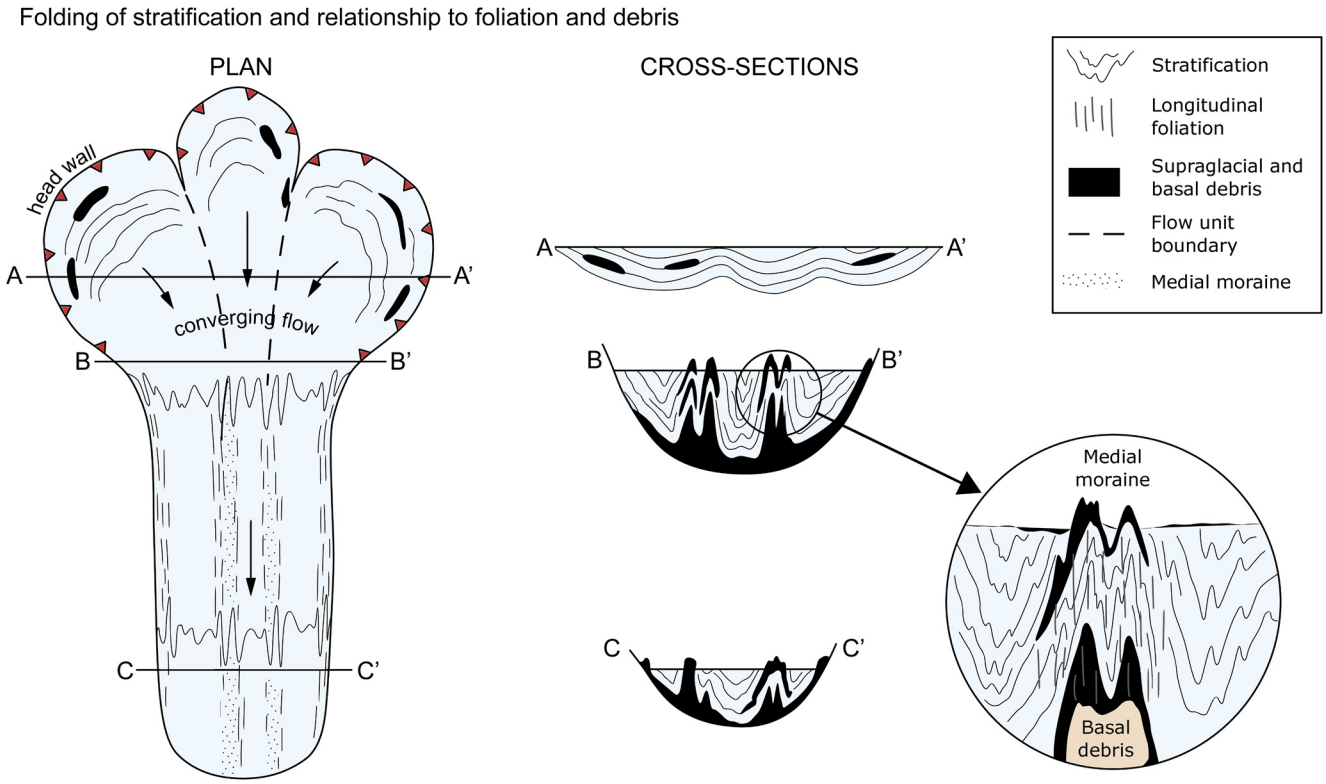

Figure 61. Conceptual model of debris-entrainment by folding of supraglacial debris and stratification as multiple flow units merge, and folding within the basal debris layer in association with the development of the related longitudinal foliation. This model is based on observations of valley glaciers in Svalbard (modified from Hambrey et al., 1999).

exposed. In these situations, fold axes are oriented in the direction of glacier flow, and folded angular debris has been transported at a high level within the glacier.

In each of the Svalbard, Alpine, and New Zealand glaciers referred to above, both supraglacial sediment and basal sediment are entrained by folding. In the former case, rockfall debris accumulates on snow in the accumulation area, and with converging flow units and lateral compression the debris is folded within primary stratification, such that the long axes of folds develop parallel to the flow direction. The same lateral compression also can produce folded zones within basal ice with fold axes similarly parallel to flow (Hambrey & Glasser, 2003). Consequently, folding draws basal debris into a higher level position within the glacier (Figure 62b). Thus some medial moraine ridges are a composite of supraglacially and basally derived debris, the two components being distinguished by their distinctive sedimentology. This process is focused primarily at flow-unit boundaries and glacier margins, and near the snout where ice at depth has become exposed by ablation (Hambrey et al., 1999).

9.2.4. Debris Incorporation by Thrust-Faulting and Related Processes

Of all the structural processes reviewed, the ability of thrust-faulting and shearing processes in glaciers to entrain debris from the bed has proved to be the most contentious issue. Regarding their geometry, fractures interpreted as thrust-faults form arcs across the glacier surface, and have an asymptotic relationship with the glacier bed, with dips ranging from low to high-angle (Figure 62c) or remaining near-parallel to the bed (Figure 62d). Large quantities of debris may be entrained within these fractures in polythermal glaciers. The debris is demonstrably derived from the basal ice zone or the glacier substrate, and include a variety of sedimentary facies, depending on what the glacier has recently overridden (Boulton et al., 1999; Garwood & Gregory, 1898; Goldthwait, 1951; Hambrey & Dowdeswell, 1997; Hambrey et al., 1996, 1999; Souchez, 1971; Swinzow, 1962; Zdanowicz et al., 1996).

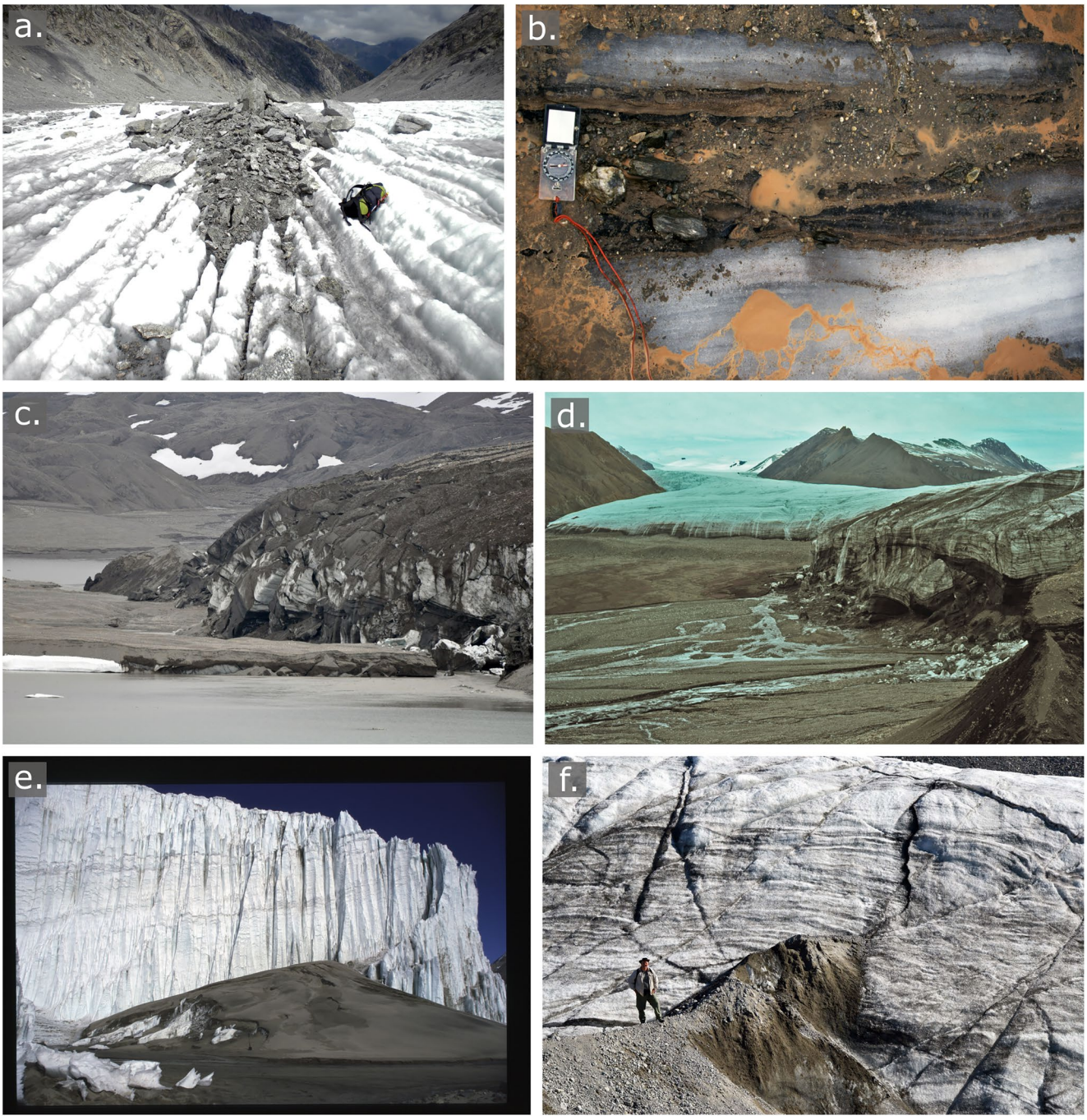

Figure 62. Debris entrainment processes: (a) Supraglacial debris which was incorporated in the snowpack in the accumulation area has become buried and folded during flow, remerging in the lower tongue as a foliation parallel ridge, with the ridge crest representing the fold axis, Vadrec del Forno, Switzerland. Photograph S. J. A. Jennings. (b) Basally derived debris incorporated in longitudinal foliation and exposed at the surface of Austre Brøggerbreen, Svalbard. (c) High-angle thrust-faulting at the snout of Comfortlessbreen near the end of a surge in 2010. All this debris is subglacially derived, and none was present on the ice surface prior to the surge. (d) Low-angle thrust-faulting with basal debris at the terminus of the then advancing Thompson Glacier, Axel Heiberg Island, Canadian Arctic, in 1975. (e) Thrust-faulting of a layer of fluvial sand in cold-based Wright Lower Glacier, Victoria Land, Antarctica. (f) Incipient recumbent folding with a "hanging anticline" and moderately high-angle thrust-fault, entraining sandy gravel exposed at the margin of Stagnation Glacier, Bylot Island, Canadian Arctic.

Similar entrainment mechanisms have also been recorded at the cold-ice margins of the East Antarctic Ice Sheet and individual glacier margins in the McMurdo Dry Valleys, Antarctica (Figure 62e). At the edge of the land-based East Antarctic Ice Sheet in the Vestfold Hills and Bunger Hills, debris entrainment involves not only thrust-faulting, but also recumbent folding. The result is the formation of thrust-block moraines that form a continuum with debris ridges derived from basal ice inland of the ice sheet edge (Fitzsimons, 1996, 2003; Souchez, 1967). Thrust-faulting also defines how the moraines form at the margins of cold outlet and valley glaciers in the Dry Valleys. The result is again a continuum from the ice margin, through mixed terrain of ice and sediment, to discrete morainic landforms. In these areas, sedimentary facies are dominated by glaciofluvial and eolian sand, and sandy gravel from prior glacial advances, all of which are entrained en bloc into the base of the glacier, and released as ramps and disorganized moraine heaps at the ice edge as the ice margin slowly recedes (Fitzsimons & Howarth, 2019; Hambrey & Fitzsimons, 2010).

Quantities of debris entrained by thrust-faulting in temperate glaciers (Figure 20c) are generally much less, as the basal debris load is comparatively light, sliding is the dominant mechanism of flow, and reworking of subglacial sediment by water is predominant. For example, at the Icelandic glacier, Svínafellsjökull, Swift et al. (2018) demonstrated the role of multiple sediment transfer processes associated with the reverse slope of an over-deepening (a glacially eroded basin), culminating in thrust-faulting. Small volumes of debris associated with thrust-faulting have also been recorded from Haut Glacier d'Arolla in the Swiss Alps (Goodsell, Hambrey, & Glasser, 2005), and the surge-type temperate Variegated Glacier in Alaska (Lawson et al., 1994; Sharp et al., 1988). However, except for Variegated Glacier, there are few documented examples where displacements can be unequivocally demonstrated on putative thrusts in temperate glaciers. The concepts of thrusting and possible alternative mechanisms to explain this specific geometry of debris-entrained features are developed further in Section 9.2.8.

A related conceptual model of debris entrainment was developed for Bas Glacier d'Arolla, Switzerland, where zones of shear associated with rotated crevasse traces at the base of an icefall, developed as an integral part of ogive formation. The darker ogive bands were associated with debris of basal origin (Goodsell et al., 2002; Goodsell, Hambrey, & Glasser, 2005). The same process of entrainment was also inferred on the Icelandic glaciers Kviárjökull (Swift et al., 2006), Tungnafellsjökull (Evans, 2010), and Svínafellsjökull (Swift et al., 2018) to explain the basal character of entrained debris. For example, in Svínafellsjökull, thrust-faulting is preferentially initiated along pre-existing foliation planes within the band ogives. The debris bands comprise "stratified facies ice" which is typical of the basal ice layer, and this interpretation is supported by stable isotope data. This ogive debris is considered to have been uplifted to a high level in the glacier by thrust-faulting, a process promoted in this case by flow against a reverse basal slope, inducing strong compression.

The same processes of simple shear or thrusting also apply to the debris-mantled Khumbu Glacier, Nepal, which although predominantly covered in supraglacial debris, also has zones of basal debris formed in association with ogives at the base of the Khumbu Icefall (Hambrey et al., 2008).

9.2.5. Entrainment by Recumbent/Sheath Folding at the Base of a Glacier

This process is widely observed where glaciers have marginal cliffs that display the internal structure. Although not specifically linked to debris entrainment, Hudleston (1976) explained this style of folding in the Barnes Ice Cap in the Canadian Arctic as being initiated when ice departs from steady-state flow as, for example, when the underlying bed is uneven, as explained in Section 5.3.1. Debris-rich basal ice is commonly entrained by this process in the cold margins of the East Antarctic Ice Sheet where it terminates on land (Fitzsimons, 2003), and also occurs widely in polythermal glaciers, especially when they surge (Figure 62c). In some cases, as observed in both polythermal and temperate glaciers, recumbent folding is followed by shearing off of the lower limb along a thrust-fault, thus demonstrating the interaction between ductile and brittle deformation (Figure 62f).

9.2.6. Ingestion of Debris by Crevasses

Surface crevasses commonly intersect supraglacial lateral and medial moraines, and thus are able to absorb characteristically angular debris to depths of a few tens of meters (Bennett & Evans, 2012). As the crevasses close, a vertical septum of debris is trapped in the ice, but ablation tends to remove this infilling over a period of several years (Gulley & Benn, 2007). Debris can also be entrained at the base of a glacier when

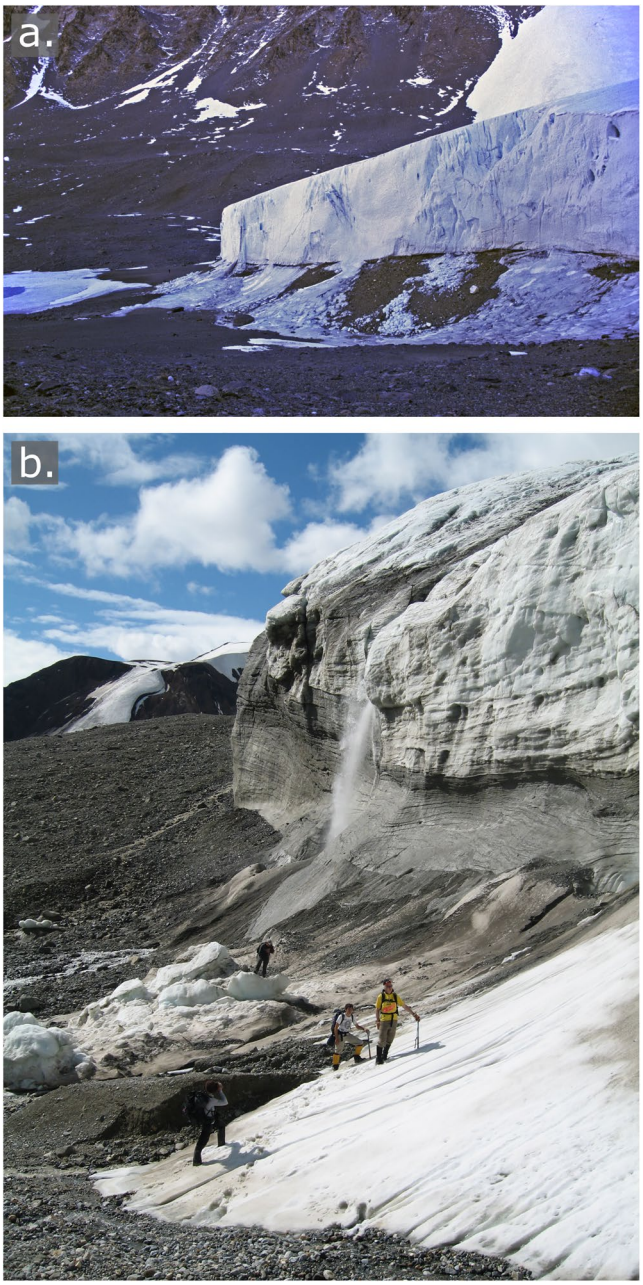

Figure 63. Examples of apron entrainment. (a) Typical cold glacier, Suess, in the Dry valleys of Antarctica. The apron is made up of dry-calved ice blocks and subglacial debris incorporated along a thrust plane. (b) Polythermal Trapridge Glacier, Yukon, Canada, showing a terminal cliff soon after cessation of a "slow surge" (2006). The apron consists of calved ice blocks, snow banks, and basally derived debris (much of it reworked by slumping and flowage).

basal crevasses form, typically during a surge on a soft deformable bed. Subglacial sediment (basal till) is squeezed into these crevasses as the glacier sinks into the bed as the surge ceases. Distinctive crevasse-fill ridges are consequently left when the ice disappears (Dowdeswell et al., 2016; Evans & Rea, 1999, 2003; Rea & Evans, 2011; Sharp, 1985).

9.2.7. Incorporation of Debris by Apron-Entrainment

This process occurs at the cliff-bounded terminal margins of polythermal and cold glaciers during an advancing phase. Accumulated dry-calved ice blocks and debris at the foot of a frontal cliff form an "apron" (Figure 63a) which, during an advance, is overridden and elevated by glaciotectonic processes within the ice mass under compressive flow. The mixed material is overwhelmed as the ice continues to advance, and is incorporated into the glacier by a process known as "apron-entrainment" (Evans, 1989b; Fitzsimons et al., 2008; Ó Cofaigh et al., 2003; Shaw, 1977). In polythermal glaciers, such as those in the Canadian High-Arctic, overridden and entrained aprons are recognizable in basal ice sequences where mosaics of individual clean ice blocks and debris are still evident, becoming increasingly attenuated into complex alternating debris-rich and debris-poor layers (Figure 63b) (Evans, 1989b; see also Benn & Evans, 2010). At the most extreme low end of the temperature range, such as in the advancing cliff at the margin of Victoria Upper Glacier in the Dry Valleys of Antarctica, the structure of an apron is highly complex. An inner element to the apron consisting of foliated ice, dipping steeply upglacier, and an outer element comprising permafrost ground, elements of basal ice, and normal glacier ice, along with refrozen meltwater. Foliation is inconsistently oriented, but with a downglacier, slope-parallel dip (Fitzsimons et al., 2008). At nearby Taylor Glacier, apron material is reworked by mass-flow processes during periods of melt (Shaw, 1977). Overall, aprons have a conglomeratic or breccia-like texture (Fitzsimons et al., 2008; Shaw, 1977).

9.2.8. The Problem of Thrust-Faulting

Of the above mechanisms, thrust-faulting has proved to be particularly controversial in the context of debris-entrainment. Differing views even exist concerning the same glacier. For example, Kongsvegen is a typical surge-type polythermal glacier in Svalbard, which last surged in 1948. A cliff section roughly aligned parallel to flow, revealed the contested debris layers in 3-D. Investigations by Bennett et al. (1996, 1999) and Glasser et al. (1998) emphasized the role of thrust-faulting in entraining basal debris. However, Woodward et al. (2002) argued that thrust-like features were, in fact, rotated basal crevasse-fills. Further investigation on Kongsvegen using ground-penetrating radar to evaluate the geometry of debris layers (Murray & Booth, 2010), reaffirmed the thrust-faulting hypothesis. Furthermore, an analysis of the oxygen/deuterium isotopic signature of ice in the debris layers confirmed a basal ice origin rather than a frozen infill of sediment (B. Hubbard et al., 2004), further supporting the thrust-faulting hypothesis.

A second glacier where the thrust-faulting and debris entrainment process has been questioned is Storglaciären in northern Sweden. The terminus of this marginally polythermal glacier has englacial debris layers that melt out to form curvilinear supraglacial ice-cored ridges (Jansson et al., 2000). Surface velocity was found to decrease sharply by 50% across the ridge line. Transport of debris was inferred to be in cold ice as a result of shearing of clean ice intercalated with debris layers, rather than along discrete "shear planes" (thrust-faults). Glasser et al. (2003)

also examined these ridges, in the context of the whole-glacier structure, combining structural glaciological, isotopic, and ground-penetrating radar studies. The debris ridges did not appear to be related to any pre-existing structural weaknesses, but were nevertheless inferred to represent thrust-faulting at the thermal boundary between cold marginal ice and active temperate ice. However, on theoretical grounds, it has been argued that thrust-faulting at Storglaciären was implausible (Moore et al., 2010), because numerically modeled compressive strain rates are six orders of magnitude too small to induce fracture. These authors acknowledge, however, that pre-existing structural weaknesses, such as crevasse traces in association with high-pressure water, do not preclude thrust-faulting. Nevertheless, they state that the conditions conducive to thrust-faulting in glaciers are rarely met, except possibly during surging, and that debris entrainment must take place by some other (unspecified) process.

Possible alternative mechanisms that have been proposed for elevating debris-rich basal ice and basal debris to the surface of some glaciers generally involves the entrainment of debris through regelation at the bed (e.g., Hubbard & Sharp, 1989; Hubbard et al., 2009; Iverson & Semmens, 1995; Shoemaker, 1990; Weertman, 1964). The subsequent elevation of the entrained debris near to the glacier terminus may then stem from the upward component of ice flow when experiencing longitudinal compression (Hudleston, 2015). The presence of debris-free superimposed ice below debris-laden layers cropping out near the margin of the Barnes Ice Cap was suggested to be derived from an advance of the ice cap (Hooke, 1973). Alternatively, folding at the boundary between a frozen and unfrozen bed has been proposed as a mechanism to elevate basal ice and subglacial debris, which is then revealed at the surface of the glacier as ablation melts out the debris layer (Moore et al., 2012). These mechanisms do not explain the presence of fractures in these situations. However, Hudleston (2015) concluded that if fractures are present, they are most likely to have formed as tensional rather than shear fractures.

Despite the theoretical arguments against thrust-faulting, on structural geological grounds, it is evident that debris-rich basal ice and even rafts of subglacial sediment can be uplifted into an englacial position within polythermal glaciers. Geometrical relationships of different structures suggest that thrust-faulting is the most likely mechanism for this, and is facilitated by the transition from ice that is, sliding on a lubricated bed, to ice that is, frozen to the bed (Clarke & Blake, 1991; Hambrey et al., 1999). Then, as the glacier surface ablates, lines or wedges of sediment commonly emerge at the ice surface, notably near the snout (Figure 18). The sedimentary facies are variable, typically consisting of diamicton (derived from basal till), sand and gravel (reworked from glaciofluvial sediment), and laminated mud and sand (of glaciolacustrine or glaciomarine affinity).

The main issue in identifying thrust-faults is that the homogeneous nature of the ice/sediment mix commonly precludes identification of discrete displacements. However, where displacements are visible, they are a convincing sign that thrust-faulting has taken place. Another consideration is that today's glaciers are in a general state of recession, and supposed thrust-faults are no longer actively forming, except in glaciers that are undergoing a surge. These arguments demonstrate the need for a multi-faceted approach to assess the viability of thrusting in glacier ice, combining 3-D measurements in the field, sedimentological studies of the entrained material, and geochemical and geophysical analysis.

9.3. Structurally Controlled Landform Development

9.3.1. Significance of Glacier Structure for Landform Development

The role played by glacier structures in producing depositional landforms have received considerable attention in the last few decades. The emphasis has been on characterizing the geometry of structures containing debris and their associated landforms, combined with detailed lithofacies analysis of the sediments. Pioneering investigations on Svalbard glaciers by Boulton (1967, 1970, 1978) laid the foundations for our modern understanding of both debris-entrainment and depositional processes in a geological context. Subsequent studies regarding debris transport as part of a larger scale glacial system (Boulton & Eyles, 1979; Drewry, 1972; Evans, 2003; 2009; Kirkbride, 1995; Small, 1987) advanced our knowledge of structure-debris relationships. More recent research has systematically linked 3-D structural geometry at the whole-glacier scale to sediment-landform assemblages associated with High-Arctic polythermal and cold-based glaciers that have developed since the Neoglacial maximum, particularly in Svalbard (Bennett et al., 1996; Boulton

et al., 1999; Hambrey & Glasser, 2003, 2012; Hambrey et al., 1996, 1999; 2005; Hubbard et al., 2004; Huddart & Hambrey, 1996; Lønne & Lauritsen, 1996; Lyså & Lønne, 2001; Midgley et al., 2013, 2018; Szuman & Kasprzak, 2010; Tonkin et al., 2016) and the Canadian High-Arctic (Evans, 1989a, 1989b; Ó Cofaigh et al., 2003; Shaw, 1977; Souchez, 1971). Similar application of these concepts to temperate alpine glaciers is even more recent (Appleby et al., 2010; Glasser & Hambrey, 2002; Goodsell, Hambrey, & Glasser, 2005; Jennings et al., 2014; Roberson, 2008).

Following the debris entrainment mechanisms outlined in Section 9.2, a number of distinctive landforms can be identified. The discussion which follows emphasizes the structural links with the glacier itself, rather than the modification processes that occur following deposition.

9.3.2. Deposition From the Basal Ice Layer

The sediment that forms part of the basal debris layer in a glacier reflects the substrate over which it flows, and reveals a complex association of structures, including shears and folds. However, following deposition, little evidence of the internal structure of the ice usually remains. The debris released from the basal layer has traditionally been split into lodgment till, meltout till, deformation till, and comminution till. However, it is more useful to use the term "subglacial traction till," which is defined as: "sediment deposited at a glacier sole, the sediment having been released directly from the ice and/or liberated from the substrate and then disaggregated and completely or largely homogenized during transport" (Evans et al., 2006). This all-embracing term reflects the fact that when sheets of till are deposited, they are the product of a mosaic of different processes. Innumerable investigations have been made of these processes (e.g., Benn & Evans, 2010; Bennett & Glasser, 2009; Evans, 2003, 2018).

9.3.3. Deposition From Debris Layers at the Glacier Margin (Controlled Moraines)

The term "controlled moraines," was introduced by Gravenor and Kupsch (1959) for landforms inferred to be influenced by ice structures in "live" (i.e., non-stagnant) ice. A modern definition is as follows: "supraglacially deposited hummocky debris concentrations that possess clear linearity when viewed in plan form due to the inheritance of the former pattern of debris concentration in the parent ice" (Evans, 2009). The debris is linked to crevasses and thrust-faults. In contrast, "uncontrolled moraines" do not reveal the former influence of ice flow.

The broadly similar term "inner moraines" has been applied to cold margins of the East Antarctic Ice Sheet (Fitzsimons, 2003; Souchez, 1967). Here, the term applies equally to features on the glacier or ice sheet surface, de-iced sediment accumulations in glacier forelands, and deglaciated landscapes. The moraine ridge morphology on the ice is dictated by englacial structures, such as foliation and debris layers. However, the morphology of the features on the glacier surface is not generally maintained after all the ice cores have melted; what is left behind are zones of hummocky moraine (Fitzsimons, 2003).

The interpretation of controlled moraines has been linked to specific processes which are viewed as the dominant control on subsequent morphology, such as: (a) englacial and proglacial thrust-faulting in polythermal glaciers in Svalbard, and cold "alpine" glaciers in Antarctica (Section 9.3.5); and (b) the non-structurally controlled process of glaciohydraulic supercooling in temperate glaciers in Alaska (Lawson et al., 1998) and Iceland (Roberts et al., 2002). However, although a single process may be largely responsible for some moraine morphologies soon after deposition, other processes are also at work that influence the character of controlled moraines in the glacial landsystem. As Evans (2009) highlights, the landform record consists of belts of hummocky moraine, chaotic in detail, but arranged in linear belts. Processes involved in creating the landform end-product include basal freeze-on, hydrofracture-infilling, apron-entrainment, folding, shearing, thrust-faulting, and ice/sediment stacking within the glacier. These processes are followed by slope failure, debris flowage, and reworking by fluvial activity after deposition. The volume of controlled moraines is influenced by the relative proportions of sediment and ice, which in turn is a function of glacier thermal regime and the distribution of sediment in relation to ice structure. The preservation potential of these moraines is dependent on the proportions of ice and sediment. Thus, controlled moraines are more likely to develop where debris-entrainment is greatest, as in polythermal glaciers. Such glaciers are commonly associated with permafrost environments where full deglaciation has not yet occurred and hence moraine linearity continues to be controlled by englacial debris patterns (Evans, 2009).

9.3.4. Recumbent Folding at the Base of a Glacier

The typical near bed-parallel orientation of the recumbent fold axial planes, and the amount of debris associated with the folding is generally insufficient to produce a distinctive landform when it melts out or is lodged at the glacier bed. Since the folding process involves basal ice, the sedimentary product is simply part of the sheet of till, as described above. Ice-marginal recumbent folding with debris entrainment has been described from the East Antarctic Ice Sheet margin in the Vestfold Hills (Fitzsimons, 2003), and from Trapridge Glacier in the Yukon (Hambrey & Clarke, 2019).

9.3.5. Thrust-Faulting Controls on Moraine Formation

Despite some views to the contrary (Moore et al., 2010; Woodward et al., 2002), the field evidence for thrust-faulting is unequivocal in many cases. Thrusting requires strong longitudinal compression at the snout of a glacier. Compression occurs: (a) where there is a down-slope switch from sliding to frozen bed conditions as in polythermal glaciers; (b) where there is a reverse bedrock slope; or (c) where flow is reduced when a glacier forms a piedmont lobe. It is inferred that basal debris is commonly incorporated englacially or elevated to the surface of the glacier along thrust-faults (Bennett et al., 1998; Boulton, 1970; Glasser & Hambrey, 2003; Glasser et al., 2003; Hambrey et al., 1999, 2005; Herbst & Neubauer, 2000; Herbst et al., 2006).

Basal debris may be elevated as slabs of debris-laden basal ice, and thrust over stagnant or slower moving ice. Alternatively, subglacial debris may be transported along thrust planes by simple shear, water flow, or sediment injection. The resulting debris-filled structures have been highly debated, and in some cases alternatively interpreted as crevasse fills (Evans & Rea, 1999; Sharp, 1985; Woodward et al., 2002). However, the presence of drag folds indicates that thrust-faulting was active during the formation of many of these structures. Similarly, as revealed by the oxygen isotope signature, it has been demonstrated that basal ice has been drawn to the surface along these features (Hubbard et al., 2004).

The question now arises: how are processes in the ice margin reflected in the adjacent landforms in the immediate proglacial zone? A close connection is most readily apparent where permafrost is found, for example, in association with cold and polythermal glaciers. In such cases, internal deformation within the glacier is propagated into subglacial frozen sediment and forwards into the proglacial area. Thus, there is a dynamic connection between glacier and sediment, allowing, for example, similar thrust-related structures to form in both ice or sediment, or a combination of both.

Thrust-faulting within the ice margin of polythermal glaciers in Svalbard has been inferred to give rise to an assemblage of several-meter-high moraines that have glacier-facing rectilinear slopes of constant angle. The moraines are thought to reflect a dynamic ice margin during deposition (Bennett et al., 1996, 1998; Hambrey & Huddart, 1995; Huddart & Hambrey, 1996). The term “moraine-mound complex” was applied to this assemblage of debris mounds, to differentiate it from a “hummocky moraine” assemblage that has an ice-stagnation connotation (Glasser & Hambrey, 2003; Hambrey et al., 1997). In this context, a moraine-mound complex is a form of controlled moraine, as defined by Evans (2009).

The thrust-faulting hypothesis, however, does not fully explain the morphology of moraine-mound complexes as some structural cross-sections reveal. For example, on examining the internal structure of such moraines by excavation at Midtre Lovénbreen in Svalbard, Midgley et al. (2007) found that both sediment facies associations and the internal structures were more complex than simply being the product of thrust-faulting. Facies included diamicton, sandy gravel, sand and mud, commonly arranged in sheets parallel to the glacier-facing moraine slope, with minor shears and faults evident within the sediment. At depth, ice facies had the characteristics of basal ice, and formed a core to the moraine mounds. Midgley et al. (2007) grouped moraine mounds into three types, of which the following two are applicable to many of the receding glaciers in Svalbard:

1. Mounds with a rectilinear and curvilinear ice-proximal face, with parallel inclined slabs of sediment, that reflect the orientation of thrusts within the ice margin. They are interpreted as representing a combination of freeze-on of subglacial sediment, followed by elevation along and above thrust-faults.
2. Rounded mounds and ridges that result from the stagnation of debris-bearing ice followed by topographic inversion, whereby thick debris-drapes in hollows retard ablation, and eventually become elevated

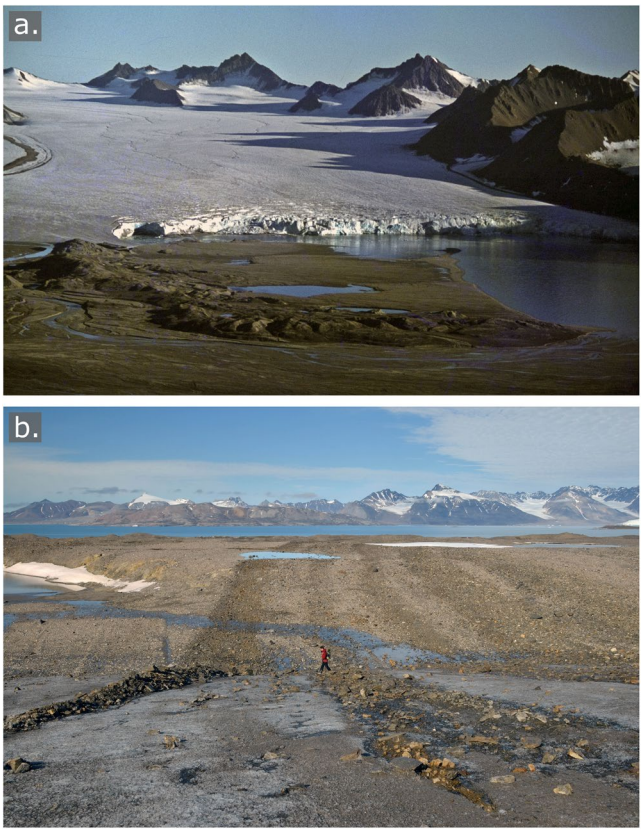

Figure 64. Examples of structurally controlled landforms. (a) A thrust moraine complex of Neoglacial and older age at pre-surge Comfortlessbreen, Svalbard. Sediments involved in thrust-faulting include basal glacial, glaciofluvial, and glaciomarine facies, and reworking by debris flowage and streams is common. The glacier in its pre-surge state was clean and terminated partly in the sea (cf. Figure 62c). (b) Supraglacial debris stripes running across the foreland of Midtre Lovénbreen, Svalbard. These ridges of angular debris are linked to the folded supraglacial debris layers in the source glacier in the foreground.

with respect to the surrounding terrain. This process is likely to indicate ice-marginal deposition and any relationship with glacier structure is incidental.

Thrust-faulting *beyond* the active ice margins of polythermal glaciers, where glacier deformation is propagated into frozen proglacial sediments, has given rise to highly distinctive ridge-like moraines, reaching heights exceeding 10 m and widths of several 100 m. These so-called thrust moraines (commonly, but inaccurately referred to as push moraines) are a feature of glaciers in Svalbard, especially the larger valley glaciers. Many examples have been described, notably moraines of Neoglacial age, here formed around 1900 CE (Bennett, 2001; Bennett et al., 1996; Boulton et al., 1999; Croot, 1988a; Etzelmüller et al., 1996; Hambrey & Huddart, 1995; Hart, 1998; Hart & Watts, 1997; Huddart & Hambrey, 1996; Midgley et al., 2013). In some of these cases, it is inferred that a basal décollement horizon or sole thrust occurs at the base of the permafrost layer. This hypothesis remains to be tested, however, but it is known that in Svalbard, the thickness of permafrost may be less than 100 m at the coast (where the moraines are located) to 500 m in the interior mountains, while beneath the thicker glaciers, the ground may be unfrozen (Humlum et al., 2003). Thus, in effect, the Neoglacial moraines are part of a continuum from englacial deformation, through contemporary ice-marginal processes, to deformed proglacial permafrost (Hambrey et al., 1997).

In the Canadian Arctic and Greenland, the term "thrust-block moraines" has been applied to related features. These moraines are the product of the interaction between a glacier and the adjacent permafrost terrain, and consist of a series of composite ridges that reflect thrust-propagation through frozen sediment, thereby uplifting tilted slabs of intact sediment, and stacking them in imbricate fashion (Aber et al., 1989; Evans, 1989b; Ó Cofaigh et al., 2003). Thrust-block moraines have also been linked to glacier surges (Evans & Rea, 2003).

In addition to thrust-faulting, shearing, and folding at the glacier terminus, other processes are at work to modify the morphology of moraines over time: bulldozing, squeezing, freeze-on, melt-out, and mass-flowage of sediment, resulting in a complex suite of landforms (Figure 64a). Contemporary moraines commonly have a core of stagnant glacier ice, or ice interbedded with sediment. If the sediment load is dominant, then the moraines will not degrade to the same extent as those with a high proportion of ice. Thus, the preservation potential of thrust moraines is exceedingly variable, and their identification in the Quaternary record can be challenging.

The same structural continuity between glaciers and proglacial landforms, especially with regard to thrust-faulting, is also evident in regions with cold-based glaciers, notably in Antarctica. Theoretical arguments discount thrust-faulting in such environments, yet this process is implicated in the formation of so-called "push moraines" associated with cold-based glaciers in the Dry Valleys of Antarctica. The term "push" usually applies to a bulldozing effect on proglacial sediment, so may not be entirely appropriate for moraines that are dominated by glaciotectonic processes (Benn & Evans, 2010). A study at Joyce Glacier in the Dry Valleys illustrated the dominance of glaciotectonic process in moraine formation (Fitzsimons & Howarth, 2019). This work, which involved surface mapping, sedimentary logging, and ground-penetrating radar, showed that at the ice margin a combination of ductile and brittle deformation occurs. Ductile deformation occurs in an ice-sediment mixture in which the ice content is more than 65% by volume, and brittle deformation occurs in which ice content is less than 65% (Fitzsimons & Howarth, 2019). The structural architecture comprises thrust-faults, low-angle listric faults, and recumbent folds, and four structural domains were identified: (a) a basal décollement and listric faults; (b) ice-cored ridges adjacent to the ice

margin, including folded debris-bearing ice; (c) ridges with thrusts dipping upglacier at 40°; and (d) forefield cracks indicative of small-scale thrust-faulting. As demonstrated at Joyce Glacier and at nearby Wright Lower Glacier (Hambrey & Fitzsimons, 2010), the interaction between clean ice, sediment-bearing ice, and sediment, gives rise to zones of considerable structural complexity, reflecting the different ways these materials respond to deformation.

As with polythermal glaciers, cold glaciers in the Dry Valleys show a continuum from ice to the recently deposited moraines. Fitzsimons (1996) explained that prominent moraines consist of blocks of sand, gravel, and organic silt, commonly preserving the original sedimentary structures from the overridden proglacial environment that included wind-blown sand and lacustrine sediment with algal mats. Unlike the thrust-block moraines of the Canadian High-Arctic, where studies stress the role of raised pore-water pressure, this cannot occur in the Dry Valleys because of the nature of the frozen sediment. The inferred process consists of block-entrainment of sediment with frozen-bed deformation, entrainment by overriding, and accretion of marginal ice and debris aprons; and transient wet-based conditions associated with the flow of glaciers into saline proglacial lakes (Fitzsimons, 1996).

On a larger scale, the cold margins of land-terminating parts of the East Antarctic Ice Sheet, as in the Vestfold Hills, also have thrust-block moraines. They reach heights of 20 m, especially along the lateral margins of outlet glaciers (Fitzsimons, 2003). The blocks include primarily stratified and massive diamicton with a shelly component, indicating that the original sediment was of glaciomarine origin, although this was raised above sea level and frozen by the time it was incorporated in the glacier ice.

Temperate glaciers, in contrast to polythermal and cold glaciers, do not demonstrate the same degree of continuity with the proglacial zone because the ground is not frozen. In Iceland, for example, "push moraines" show thrust-faulting, nappe formation and gravity sliding (Bennett et al., 2004; Croot, 1987, 1988b; Krüger, 1985), but these structures are independent of structural processes that occurred in the formerly adjacent glacier.

9.3.6. Deposition From Folded Stratification and Rockfall Debris

The characteristic folding style of stratified snow and firn, along with angular rockfall material from a glacier's headwall, disperses the debris into medial moraines that define fold axes parallel to flow. As the glacier recedes, the proglacial area becomes draped with this debris, each moraine delivering a distinctive lithology from the point source in the headwall (Figure 64b). This landform is referred to as "supraglacial debris-stripes" (Glasser & Hambrey, 2003; Hambrey et al., 1999). They form low-amplitude continuous stripes, several meters wide, but normally only one clast thick, and so are distinctive from flutes. There are few reports of these features from the Quaternary record, but these landforms are worth seeking out in upland landscapes where ice flow-unit boundaries can be inferred.

9.3.7. Deposition of Sediment From Crevasses and Geometrical Ridge Networks

It is unlikely that landforms associated with the filling of surface crevasses will survive ablation. In contrast, crevasse-squeeze ridges, created by the filling of basal crevasses with underlying till, are well-preserved in the Quaternary glacial record (Evans, Ewertowski, & Orton, 2016; Evans, Storrar, & Rea, 2016; Evans et al., 2007, 2020; Rea & Evans, 2011). These ridges commonly form sub-parallel sets, but some may intersect, as do surface crevasses. Debris ridges, formed by different processes, including crevasse-squeeze ridges, combine to form a "geometrical ridge network." Comparing with modern examples, crevasse-squeeze ridges seem to be mainly associated with glacier surges, where elevated basal water pressures and high stress gradients combine to produce small, but distinctive ridges on flat terrain. Several good examples of crevasse-squeeze ridge networks have been described from surge-type glacier margins in Iceland (Evans & Rea, 1999; Evans et al., 2007; Kruger, 1985; Sharp, 1985) and Svalbard (Christoffersen et al., 2005; Ottesen & Dowdeswell, 2006).

Geometrical ridge networks of a different structural origin reflect the interaction of thrust-faulting with debris-rich foliation, although this combination of processes has been rarely reported. The networks comprise cross-cutting ridges a few meters high. A well-exposed network was recognized in the proglacial zone of the surge-type glacier Kongsvegen in Svalbard (Bennett et al., 1996). Longitudinal ridges emerged from foliation that was associated with basal debris ("foliation-parallel ridges"), and these were in turn intersected

by transverse ridges that have the attributes of thrust-faults, but also comprising basal debris. The foliation-parallel ridges originated from foliation that was formed at depth as ductile structures, probably during the quiescent phase of glacier flow. In contrast, the thrust-related ridges formed during a previous surge (in 1948), when the surge-front passed through the glacier.

Geometric ridge networks have also been described from the proglacial area of two other surge-type glaciers in Svalbard, Tunabreen, and Von Postbreen, but a modified process of formation has been ascribed to them (Lovell, Fleming, Benn, Hubbard, Lukas, Rea, et al., 2015). Englacial structures include basal crevasse-squeezes containing deformation till. These debris-filled structures rotate with flow to produce an upglacier dip, and are then exploited by hydrofracturing under high basal water pressures, which initiates thrust-faulting. The structures melt out to form the ridge network. This conceptual model of multiple processes may go some way to reconciling the separate basal crevasse-fill and thrust models discussed above (Section 9.2.8).

9.4. Structural Controls on Hydrological Pathways

9.4.1. Structurally Controlled Hydrology of Valley Glaciers and Ice Caps

The hydrological systems of glaciers are strongly influenced by thermal regime, ice dynamics, and ice structure (Gulley, Benn, Screaton, & Martin, 2009). Temperate glaciers are generally free-draining internally, and water easily finds its way to the bed. Polythermal glaciers allow free internal drainage only in their temperate zones, and water tends to migrate toward the glacier margins or flow off snout, although some streams may enter an englacial position (Figure 65a). Cold glaciers, with frozen beds, only permit surface run-off. Surface drainage is controlled by glacier dynamics: a "healthy" active glacier tends to have a convex cross-valley profile forcing drainage toward the margins, whilst an "unhealthy" or stagnating glacier tends to develop a concave cross-valley profile, forcing the drainage toward the middle. An active glacier, furthermore, has numerous crevasses that capture surface drainage.

The relationship of surface drainage to ice structure boils down to differential weathering of different types of ice, structural weaknesses (e.g., fractures) in the ice, and the distribution of debris, particularly moraines. It is widely known that medial moraines, with their elevated relief, influence the routing of meltwater. Topography prevents streams crossing moraines, hence water is channeled into streams on either side, resulting in channel-incision and even the formation of "cryo-valleys" and canyons (Mölg et al., 2020).

The relationship between glacier structure and surface hydrology begins with the development of a weathering crust (Müller & Keeler, 1969; Schumsky, 1964). The crust is typically half a meter thick, unless removed by rainfall, and is peppered with cryoconite holes. Being dark, the cryoconite, a mixture of fine sediment and micro-organisms at the bottom of the hole, absorbs more radiation, and further enhances the weathering crust (Irvine-Fynn et al., 2011). However, weathering is dependent on the contrasting albedo of different ice types, typically coarse bubbly, coarse clear (or blue), and fine-grained ice (Allen et al., 1960; Meier, 1960). This shows the strongest differentiation in zones of prominent foliation; coarse bubbly and fine-grained ice facies are light-colored, and coarse clear ice is dark. The dip of the structure influences permeability, that is, it is greater if the structure is at a high-angle. Hydrologically, the weathered crust can facilitate transient water storage, and represents a depth-limited or confined aquifer (Irvine-Fynn et al., 2011).

Several authors have explored how fractures determine water-routing through a glacier. Supraglacial streams may be diverted or captured by crevasse traces (which are deep fractures acting as planes of weakness) or crevasses. It is at these locations that moulins (or glacier mills) occur, and these allow water to flow englacially or reach the glacier bed (Figure 65b) (Stenborg, 1968, 1969; 1973; see also Hambrey, 1977c; Jennings et al., 2014). Fountain and Walder (1998), in their wide-ranging review of the hydrology of temperate glaciers, speculated that water flow was directed along the bottom of crevasses. They noted how few data are available that show how water flux to moulins and crevasses is distributed over the glacier surface and how this evolves over time, yet these processes are fundamental to understanding the englacial part of the hydrological system. In an experimental study of englacial water passages on polythermal Swedish glacier, Storglaciären, flow was directed through a network of closed fractures, whilst flow in conduits was relatively rare (Fountain, Schlichting, et al., 2005). These fractures are probably crevasse traces, as many are exposed at the surface of this glacier (Glasser et al., 2003). Using speleological techniques, Gulley (2009) mapped 14

Figure 65. Hydrological pathways influenced by ice structures. (a) Surface water-flow during a day of high ablation on Fountain Glacier, a polythermal glacier on Bylot Island, Canadian Arctic. Some water emerges at transverse structures, which here are rotated low-angle crevasse traces, and is channeled downglacier along later longitudinal crevasse traces. (b) A moulin on temperate Gulkana Glacier, Alaska, which has formed at the crevasse visible to the left and behind the person. (c) Supraglacial stream following steeply dipping longitudinal foliation on polythermal Austre Lovénbreen, Svalbard. (d) A canyon which began as a supraglacial stream parallel to foliation, has attained meandering characteristics, and the relationship with this much larger stream no longer holds, Fountain Glacier. (e) Pressurized basal water, which built up at the base of Fountain Glacier during heavy rain, escaping along a longitudinal crevasse trace that is, connected to the bed.

englacial conduits on the temperate Matanuska Glacier in Alaska. He found that all conduits followed fractures in the ice, some of which formed by hydrostatic crevasse penetration where supraglacial streams were swallowed by longitudinal or shear crevasses. A particularly impressive example of a structurally controlled moulin and an englacial conduit was described from speleological studies at Austre Brøggerbreen, Svalbard (Vatne, 2001; see also Kamintzis et al., 2017). The entrance of one moulin, the initial 39 m deep shaft, and the subsequent diagonal channel were controlled by "tectonic structures," which are almost certainly one or several of the crevasse traces described by Jennings et al. (2016).

Meltwater in crevasses has been implicated in initiating the conditions necessary for a surge, following an examination of a surge in "Basin 3" in Austfonna, an ice cap in Svalbard (Gong et al., 2018). Ice velocities began increasing in the mid-1990s as a result of basal meltwater production and crevasse formation. The surge began across the whole basin in 2012, and reached its peak velocity of 6,500 m a^{-1} in January 2013. Crevasses were simulated by modeling basal friction and using observed surface velocity data. These parameters defined those areas where surface meltwater reached the bed. The data showed how stagnant ice at the marine terminus was activated ("unplugged") and the low-friction regions expanded. The resulting crevasse distribution was observed to reflect the basal friction pattern.

Hydraulically driven fracture propagation (hydrofracturing) was identified in the polythermal Svalbard glaciers, Hansbreen (Benn et al., 2009) and Hørbyebreen (Evans et al., 2012). It is now recognized as an important process beneath Arctic (e.g., Benn et al., 2009; Boon & Sharp, 2003) and temperate glaciers (e.g., Benn et al., 2009; Fountain, Jacobel, et al., 2005, Fountain, Schlichting, et al., 2005; Gulley, 2009; Le Heron & Etienne, 2005). This process requires a high meltwater supply, combined with ice under a high tensile stress, thereby allowing drainage to reach the bed. In contrast to hydrologically driven fracturing, in a compressive flow regime water exploits pre-existing fractures. Exploration and mapping has also been undertaken in extensive conduit systems on several debris-mantled polythermal glaciers in the Himalaya, including the Khumbu, Ngozumpa, Lhotse, and Ama Dablam glaciers. These conduits formed along debris-filled crevasse traces, although these channels migrated as they evolved until their roofs collapsed (Gulley & Benn, 2007; Gulley, Benn, Screaton, & Martin, 2009).

It is also common for supraglacial meltwater channels to form preferentially along favorably oriented penetrative ice structures, such as steeply dipping longitudinal foliation. This relationship has been documented on Charles Rabots Bre, Norway (Hambrey, 1977b) and Vadrec del Forno, Switzerland (Jennings et al., 2014). Foliation-parallel channels are linear and commonly incised to depths of several meters, especially in polythermal glaciers (Figure 65c). As supraglacial channel size increases, the control that ice structure has over channel morphology decreases (Figure 65d). Large meandering supraglacial channels are no longer controlled by layered structures such as longitudinal foliation (Hambrey, 1977c). Meandering results from a combination of hydrodynamic and differential heating, and meander wavelength is determined by channel width, depth, and Froude number (Parker, 1975). Also critical for meander formation is the generation of traveling waves of water-flow (Knighton, 1981). Both these effects override structural influences at some unknown critical level of discharge.

Structures, notably thrusts, have occasionally been observed to allow subglacial water to reach the surface, especially during glacier surges, such as on Bakaninbreen, Svalbard (Hambrey et al., 1996) and Skeiðarárjökull, Iceland (Bennett et al., 2000). Outflows of water along thrusts are commonly accompanied by entrainment of subglacial sediment. Vertical fractures (crevasse traces) have also provided routes for subglacial water to reach the surface at times of high basal water pressure (Bennett et al., 2000). For example, following a period of heavy rain, muddy water was observed flowing out of crevasse traces at the surface of Fountain Glacier, Bylot Island in July 2014 (Figure 65e). These crevasse traces could be followed to the base of the glacier, even cutting the basal ice layer.

Basal crevasses are known to play a role in subglacial hydrology and basal sliding from a study of Bench Glacier, Alaska (Harper et al., 2010). The subglacial environment is rarely accessible, but by using radar and seismic images, combined with in situ borehole measurements, the existence of numerous water-filled crevasses were revealed, with some extending tens of meters above the bed. The crevasses represent a store of water that can influence the rate at which the glacier slides on its bed. This study demonstrated that the

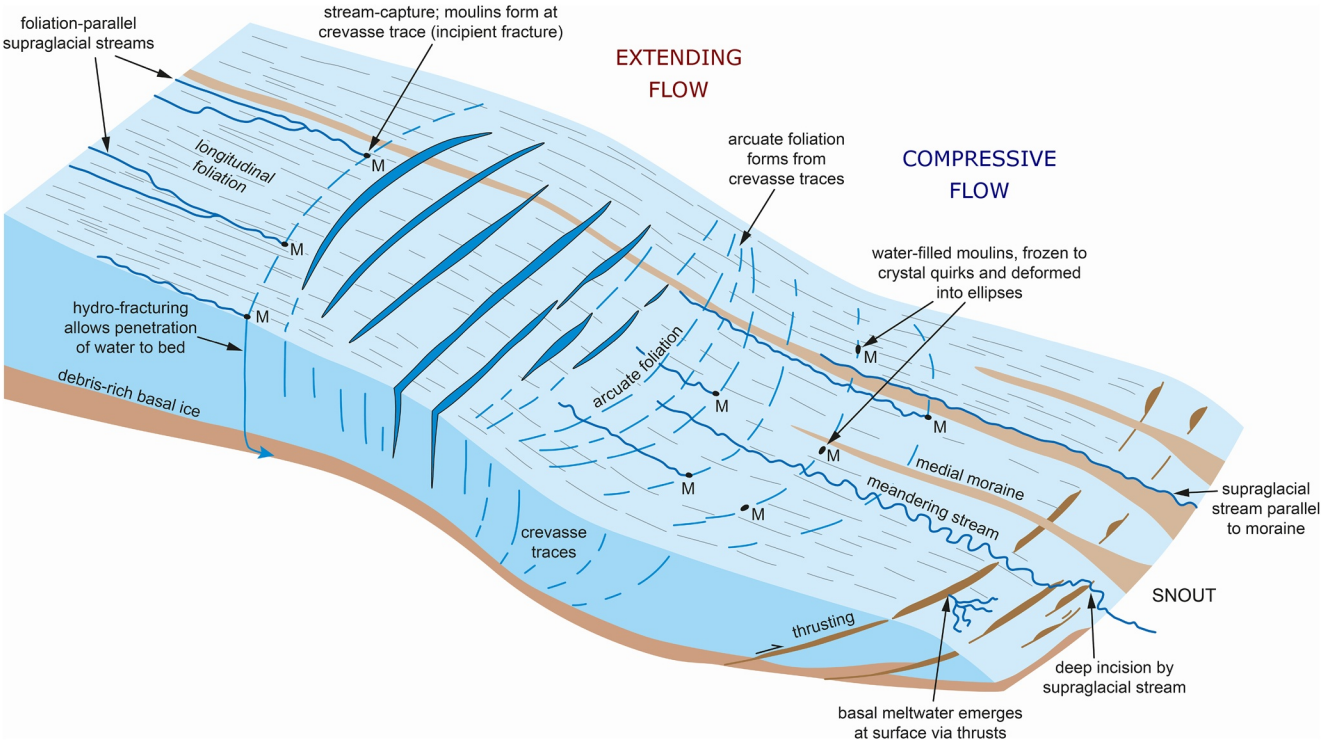

Figure 66. Conceptual model of a longitudinal segment of a valley glacier, showing the relationship between structure and drainage. Surface drainage is influenced by foliation, crevasses, and crevasse traces. Routing of water to and from the glacier bed via thrust-faults is also illustrated.

basal hydrological system can extend high into the overlying ice, but it is unknown how common it is for basal crevasses to influencing glacier hydrology.

In summary, the hydrological pathways in a valley glacier are influenced by the manner in which supraglacial streams interact with structure, including foliation, crevasses, and crevasse traces, while subglacial meltwater can also exploit structural weaknesses, such as basal crevasses and thrust-faulting (Figure 66).

9.4.2. Structurally Controlled Drainage in the Greenland Ice Sheet

Understanding the role of fractures in explaining the routing of water to the base of the Greenland Ice Sheet is a vitally important topic in glaciology. Water reaching the bed lubricates it, enabling the ice to flow faster, increase the discharge of icebergs through calving into the ocean, thus raising sea level. As a consequence, the ice sheet surface is drawn down, lowering the elevation of the ice surface, and making it even more prone to ablation. As Greenland's climate has warmed, the extent of supraglacial lakes and streams have expanded massively. The low albedo of lakes accelerates melting and down-wasting of the ice sheet surface. In many areas, the ice sheet surface displays multiple crevasse traces, which have the propensity to reopen as crevasses under high hydrostatic pressures. Moulins are commonly formed at crevasse traces, through which much of the meltwater drains to the bed.

In cold ice, such as makes up much of the Greenland Ice Sheet, water entering a crevasse can extend the fracture downwards to the bed by hydraulically driven fracturing or "hydrofracturing" (Chudley et al., 2020; Das et al., 2008; Doyle et al., 2013; van der Veen, 2007; Williamson et al., 2018). This situation is aided by in situ drainage of supraglacial lakes. An example of this processes was when an approximately 4 km^2 supraglacial lake drained rapidly through 1.1 km thick ice near the western margin of the ice sheet, via a c. 3 km long, 0.4 m wide fracture (Doyle et al., 2013). Drainage of multiple supraglacial lakes is often triggered at the same time when tensile-stress perturbations, induced by melting, propagate fractures in areas where fractures are normally absent or closed (Christoffersen et al., 2018). Given the abundance of crevasse traces in the ice sheet, it is likely that the tensile shock induced can propagate along these fractures.

The relationship between crevasses and surface stress has been examined at the outlet glacier Store Gletscher in West Greenland (Chudley et al., 2020). In a compressive flow regime, crevasses have a tendency to close and be water-filled, whereas in an extensional regime the crevasses are empty. These two states, controlled by the surface stress regime, have distinct thermal influences on the ice sheet, and thus delivery of water to the base of the ice sheet.

The process of hydrofracturing has been investigated theoretically using the "linear elastic fracture mechanics" method (van der Veen, 2007). Water-filled crevasses can penetrate cold glaciers within hours to days, depending on ice thickness and availability of supraglacial lakes. Once crevasse propagation is initiated, the growth rate is determined primarily by the rate at which water flows into the crevasse, not by the fracture toughness of the ice, nor by the magnitude of the tensile stress. A crevasse will penetrate to a depth where the stress intensity factor at the crevasse tip equals the fracture toughness of glacier ice. If water volumes are small, then the rate at which water in cold ice can freeze may prevent water reaching the bed (van der Veen, 2007).

The role played by hydrofracturing and crevasse formation in the context of calving has been explored theoretically using "continuum damage mechanics" in combination with numerical ice flow models (Duddu et al., 2020). The combination of meltwater in surface crevasses and sea water in basal crevasses promotes hydrofracturing.

9.5. Structural Glaciological Influences on Microbiology

In the last decade there has been remarkable growth in our understanding of living organisms on glaciers. In a wide-ranging review, Hodson et al. (2008) evaluated the physical, biogeochemical, and microbiological characteristics of microbial habitats on ice masses, and argued that ice masses must be considered as ecosystems in their own right. Indeed, Edwards et al. (2014) have argued that ice masses represent Earth's largest freshwater ecosystem, a view that is, supported by the abundance, activity, and diversity of life, and the importance of ice masses in global biogeochemical cycles. Glacier surfaces and the bed, or the "glacial biome," are both richly endowed with micro-organisms, notably bacteria, cyanobacteria, algae, fungi, and viruses (Anesio & Laybourn-Parry, 2012; Anesio et al., 2017; Cook et al., 2016; Hodson et al., 2008; Irvine-Fynn et al., 2015; Stibal et al., 2012). These micro-organisms are mostly associated with liquid water, but can also survive through the winter freeze-up and in the snowpack. Cryoconite holes, which are commonly structurally influenced, are a favored location for microbial activity as the micro-organisms can bind themselves to sediment particles (Cook et al., 2016).

At the crystallographic scale, water may occur at triple junctions where inter-locking crystal boundaries meet, even in ice well below pressure melting point, forming veins which provide a host of micro-organisms (Mader et al., 2006; Price, 2006). In the Greenland Ice Sheet, these veins contain pollen grains, fungal spores, viruses, and bacteria, which reside in highly acidic cold water, yet are able still to metabolize (Barletta et al., 2012). Micro-organisms have even been discovered at least 3,500 m below the surface of the East Antarctic Ice Sheet in the Vostok ice core (Price, 2000). There, it is proposed that liquid veins are interconnected along triple-ice-crystal boundaries, even though the temperature is well below zero, providing a habitat in which psychrophilic bacteria can move and obtain energy and carbon from ions in solution. Modeling the liquid vein system within polar ice sheets has the potential for defining microbial habitats in the vein system (Dani et al., 2012). However, the manner in which the vein structure relates to glacier or ice sheet structure has not yet been determined.

At the macroscopic scale, the relationship between ice structure and the distribution of micro-organism-bearing cryoconite has been noted by Hodson et al. (2008). These authors showed a strong linear distribution of cryoconite in streams parallel to longitudinal foliation on polythermal glaciers in Svalbard, and also strings of cryoconite holes parallel to the foliation. Similarly, we have observed cryoconite associated with crevasse traces, and structurally controlled abandoned channels and moulins. However, no systematic studies have been undertaken, as far as we know, on the relationship between cryoconite and structure, and this is clearly a potentially fruitful field for research.

9.6. Application of Structural Glaciological Principles to Glacier-Like Forms on Mars

Near-surface water ice, either pure or mixed with regolith, forms a widespread suite of distinctive landforms in the mid-latitudes on Mars. These landforms are in many cases sufficiently similar to cryospheric features on Earth to allow analog-based comparisons to be made. Since evidence for mid-latitude ice-rich and glacier-like flows on Mars was first presented (e.g., Head & Marchant, 2003; Lucchitta, 1981), there has been growing interest in the landforms and dynamic significance of these glacier-like features (e.g., Dickson et al., 2008; Hepburn et al., 2019; Souness & Hubbard, 2012). Although little is known concerning the thermal and physical structure of Martian glacier-like features, many reveal structural phenomena that are strongly suggestive of ice masses with a debris cover, which have deformed in a similar manner to those on Earth (e.g., Brough et al., 2016).

In the mid-latitude belt of Mars, many features resembling valley glaciers on Earth occur, and have become known as "glacier-like forms" (B. Hubbard et al., 2011) and "viscous flow features" (Hepburn et al., 2019). More than 1300 glacier-like forms have been identified, and the morphological and sedimentological characteristics of several have been described (Dickson et al., 2008; Hubbard et al., 2014; Souness et al., 2012). Features of a structural glaciological nature include longitudinal structures interpreted as foliation, flow unit boundaries, compressional/extensional ridges, crevasses, and crevasse traces (Brough et al., 2016, 2019; Souness et al., 2012). Multiple phases of glaciation have been inferred from the superimposition of glacier-like forms, illustrated by complex flow patterns of multiple flow units (Hepburn et al., 2019).

Glacier-like landforms have also been identified. Using high-resolution Context Camera (CTX—6 m per pixel) imagery of several glacier-like forms, Dickson et al. (2008) documented moraines and flow lineaments to reconstruct a glacier recession sequence, focusing mainly on ice-marginal landforms. In a second example they provided an interpretative map, which indicates a trimline on the eastern flank, flow lineaments, and a piedmont lobe within a crater. This lobe is bounded by a moraine, beyond which is a "lineated valley-fill." However, from a structural glaciology perspective, a slightly different interpretation may be offered. This valley-constrained glacier-like form shows flow units, crevasses (probably dust-filled), and flow stripes that are similar to longitudinal foliation. In this example (Figure 67), the "ice" appears to converge from an "ice cap" at the head and along the flanks of the valley. After passing through the valley, debris-mantled "ice" spreads out as a piedmont lobe at the valley mouth, where an end-moraine separates it from a highly contorted zone reminiscent of moraines on the surface of surge-type glaciers.

Whether these interpretations are correct is not possible to verify at present, but there are no other analogous features on Earth that have this assemblage of characteristics. In the analysis of Martian glacier-like forms, a new generation of high-resolution imagery, which is superior to that available for many glaciers on Earth, offers considerable potential for the application of structural glaciological principles to understanding the flow dynamics of these forms. One example of this approach is the production of a structural glaciological map to document flow paths in a glaciologically complex basin in the Protonilus Mensae region, using both CTX and the High Resolution Imaging Science Experiment (HiRISE) camera, which has 30 cm per pixel resolution (Souness & Hubbard, 2013). In addition to streamlined mounds and moraine-like features, several types of longitudinal structures were recognized, and interpreted as longitudinal foliation, flow stripes, and debris stripes, as on Earth (Figure 68). The higher resolution led to an alternate interpretation of flow paths to that originally defined by Dickson et al. (2008).

This recently developed approach to investigating Martian glaciology, complements the geomorphological studies of hydrological features and periglacial phenomena, where the McMurdo Dry Valley region in Antarctica is considered to be an appropriate analog (Head & Marchant, 2014).

10. Structural Glaciology: A Summary

Summarizing the key structural attributes of glaciers, there are two main classes of structures:

1. *Primary structures* that are the product of accumulation and accretion without deformation, of which sedimentary stratification is the most important, but which also includes ice lenses and layers within snow, firn, and ice, as well as regelation ice at the base of a glacier.

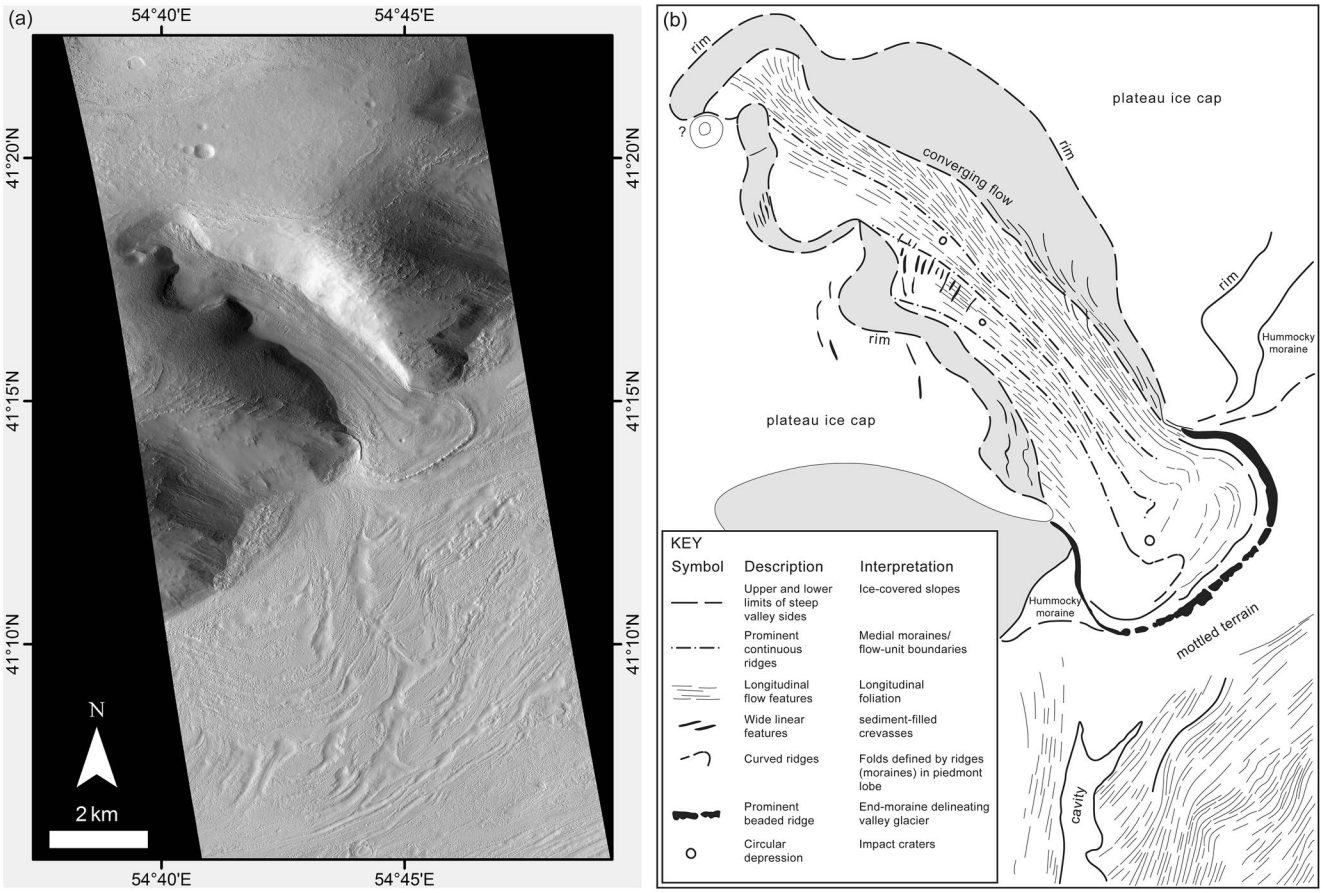

Figure 67. A Martian glacier-like feature with distinctive structural attributes. (a) A view of the Protonilus Mensae-Coloe Fossae region of the northern mid-latitudes on Mars, from a Thermal Emission Imaging System (THEMIS) image mosaic (Dickson et al., 2008). The lobe is approximately 2 km wide. (b) Structural interpretation, based on understanding of valley glaciers on Earth.

2. *Secondary structures* that are the product of deformation and further subdivided into brittle and ductile. Brittle structures include crevasses, faults, fractures, and crevasse traces. The most important ductile structures are foliation and folds, with boudinage structures being less common.

Some brittle structures, notably crevasses and crevasse traces, form where ice is under tension and the strain-rate exceeds a threshold value that varies for different glaciers. Other brittle structures form under a transpressive regime (oblique convergence with strike-slip faulting) or a compressive flow regime (thrusts). Ductile structures form in pure shear and simple shear regimes, and reflect the cumulative strain history. Many of these structures cross-cut one another, and the resulting structural assemblages may be complex, but recurring relationships may be identified according to different glacier geometries (Figure 69). Untangling this wide range of structures allows the structural history of a glacier to be determined. Strain ellipses are generally used to express this history, and are best derived using numerical modeling approaches. Satellite images and data now have sufficient resolution to infer that many flow structures in ice sheets and ice shelves are, in fact, foliation and crevasse traces.

Structural glaciological principles have been successfully applied in recent years to understanding how debris is entrained and transported through a glacier. These results may be used to explain how certain depositional landforms develop, although there is an ongoing debate, not only concerning the genetic terminology of moraines, but also about the multiplicity of processes involved in their formation. An example is the formation of controlled moraines and thrust-moraines, each of which is related to glacier structures to varying degrees, but which are also modified by non-structural processes.

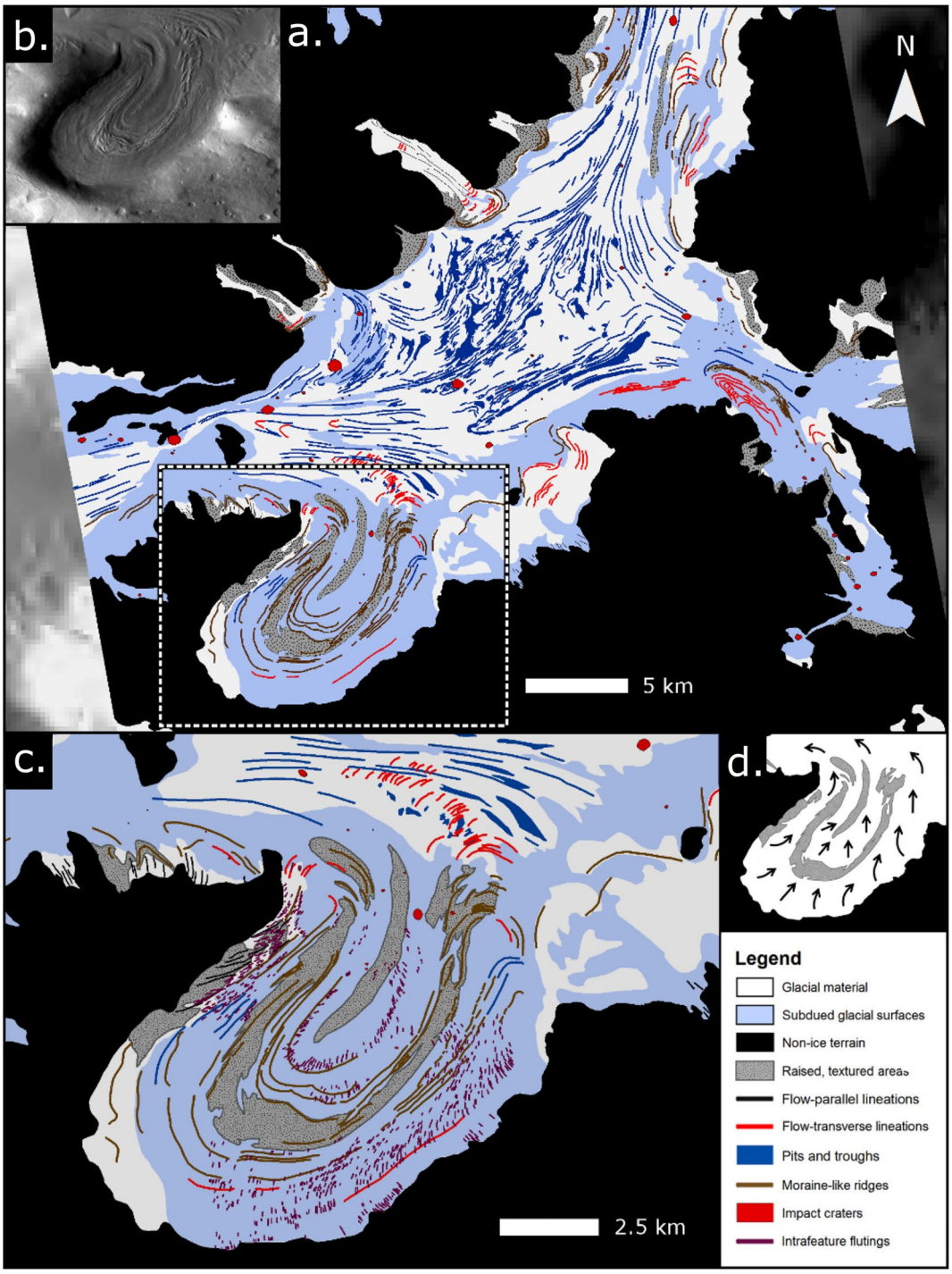

Figure 68. Structural glaciological and geomorphological maps showing the landform and surface texture assemblages observed and classified on the surface of a complex Martian glacier-like feature and its parent catchment. (a) Landforms and surfaces classified at a catchment scale, with (b) a context image (CTX image 22_009455_2214_XN_41N305W). (c) Expanded detail of the "alcove" (identified in "a" by a dashed box). (d) Reconstructed flow directions, interpreted from the landforms, slopes, and textures mapped in ("a" and "c") (modified from Souness & Hubbard, 2013).

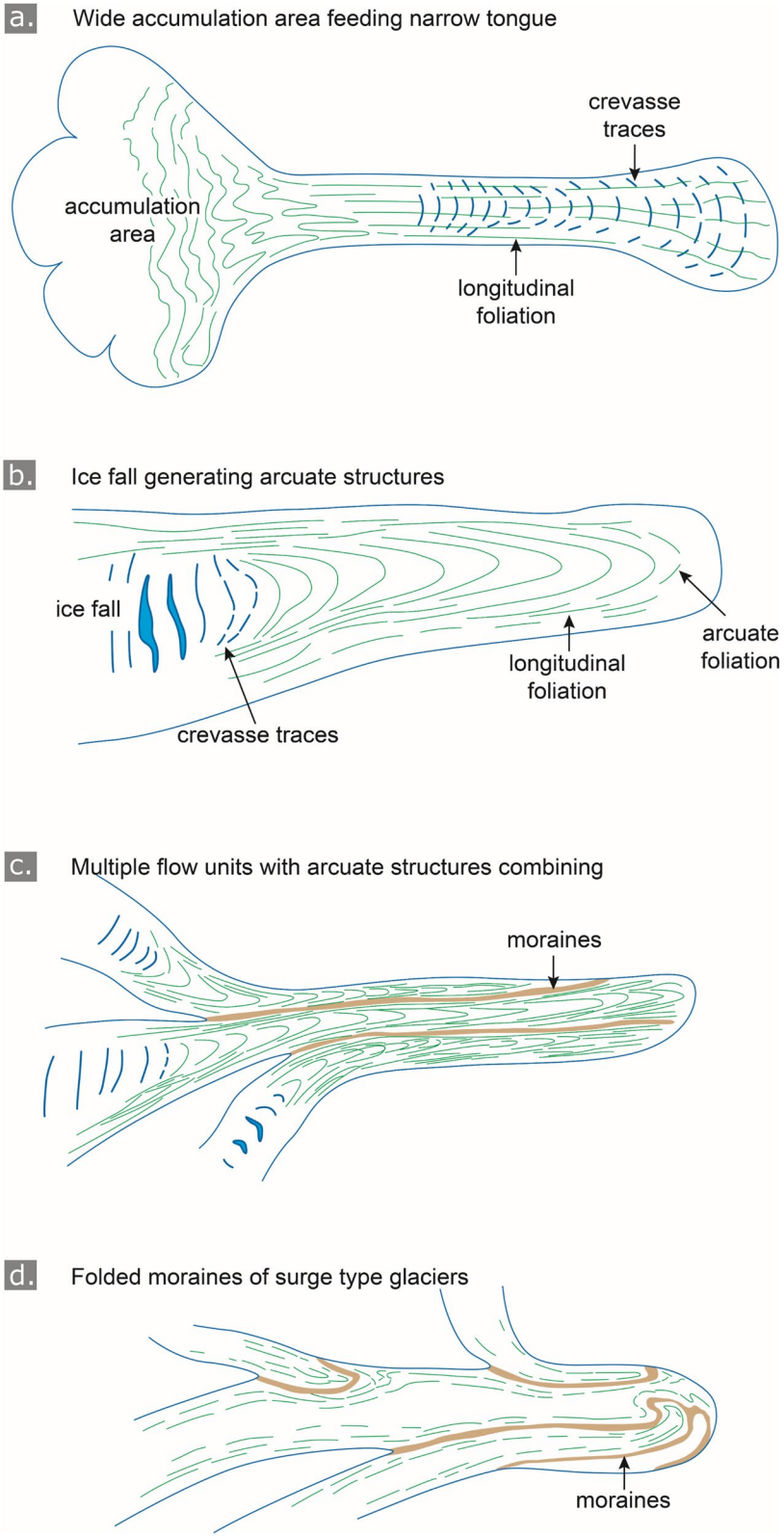

Figure 69. Schematic representation of structures associated with a variety of glacier geometries and ice dynamics.

A less well-developed area of research is the relationship between the vitally important field of glacier hydrology and structure, yet it is clear that features such as crevasses, crevasse traces, thrusts, and foliation all play a role in facilitating the routing of water through a glacier or an ice sheet. Lastly, newly emerging research fields, including microbiology and Martian glaciology, would benefit from adopting a structural geological approach.

11. Current Status and Future Research Directions

Structural glaciology is a field of cryospheric studies that has seen a surge of interest in the last decade, as it is recognized as fundamental to the understanding of glacier and ice sheet dynamics on different timescales. Therefore, the goal of this study has been to review our current knowledge of ice-deformational processes that lead to the wide range of structures observable on the surface of ice masses, and increasingly their interiors as geophysical techniques become more refined.

Until recently, the reasons why glacier structures were commonly overlooked in glaciology included: (a) the complexity and wide range of structural features in glaciers; (b) the difficulty of envisaging these structures in 3-D; (c) the need to apply unfamiliar structural geological approaches to understanding structures; (d) a lack of understanding of the relevance of cumulative strain and how this influences structural development over centuries and millennia; and (e) the need to devote considerable time and energy to document structures in 3-D in the field. It is hoped, therefore, that this comprehensive review of the field of structural glaciology will be of value to all glaciologists and to students interested in how glaciers interact with the landscape. Furthermore, since glaciers in effect may be considered as models of rock deformation, but deforming at rates that are measurable, we hope that this study will stimulate interaction between structural geologists and glaciologists.

The major uncertainties in structural glaciology, and how these may be applied to other sub-disciplines of glaciology are highlighted below.

1. *Relationship between ductile structures and strain*. Advances in this field have demonstrated how ductile structures such as foliation, folds, and boudinage are related to the cumulative strain ellipse. These advances have been achieved through assessing the movement and change of representative circles using surface flow path and velocity-distribution data, or through numerical modeling. To date all these studies have been in two dimensions, and now there is a need to model structural development in 3-D to determine the relationship with the strain ellipsoid. Foliation especially remains partially unexplained, for example, why does it form by transposition from stratification in some cases, but as a cleavage-like structure in others? Also we have not yet fully established the relationship between that second type of foliation and crystal structure.
2. *Relationship between brittle structures and stress*. It is known that crevasses form at a variety of strain-rates, which in turn are related to stress, but there is no reliable fracture criterion for glacier ice. Similarly thrust-faults form in locations near the snout of a glacier where the analysis of ice physics suggests that they should not. This may be partly because from the moment ice is formed it has pre-existing planes of weakness, and their role in initiating new fractures has not, as yet, been defined physically. A related structure, crevasse traces that form as tensional veins, is particularly interesting, because crystal growth takes place at a rate equal to wall separation. These structures are more widespread than crevasses, and the manner in which they form could have bearing on how similar features form in rocks. In all these cases the challenge is how to explain their formation quantitatively, when most physical equations assume that ice is homogeneous.
3. *How glacier structures inform us about ice dynamical changes over time*. Several studies have demonstrated how the evaluation of structures, such as moraines, foliation, folds, and crevasse traces provide evidence of past glacier dynamics. Applications of this approach range from assessing changes prior to, and during a surge, or considering how dynamics have changed since Neoglacial maxima. All studies of glacier dynamics would benefit from an assessment of structural changes over centuries to millennia.
4. *The role of numerical modeling in evaluating glacier structures*. Modeling to date has proved successful when associated with efforts to simulate kinematic structures that depend on the flow velocity field and its derivatives, notably crevasses and foliation. On the other hand, because of problems of their small

scale and not being considered in current ice dynamic models, attempts to simulate folding, crevasse trace orientation, and thrusts have been less successful, and highlight a need for further model development.

5. *Application of structural glaciology to glacial geomorphology*. Whereas structures such as thrust-faults and shear zones, and basal processes, have long been of interest to glaciologists, the role played by foliation and folding has received attention only in the last two decades. Whilst the character of basal debris figures prominently in geomorphological investigations of till, the relationship between supraglacial and basal debris within foliation and within thrusts has yet to be considered by most glacial geomorphologists. However, many glacier forefields are characterized by landforms that clearly relate to these processes. Therefore, not only is there a need to document carefully how debris emerges from glacier structures on forefields during glacier recession, it is also important to evaluate their preservation potential once the ice has melted.
6. *Upscaling to ice sheets*. Ice shelves and ice streams in Antarctica and Greenland are too large to allow 3-D mapping of surface structures in the field. However, satellite imagery is proving to be an excellent resource, and many features are common to both valley glaciers and large ice masses. Particularly significant is the recognition that so-called "flow lines" in ice sheets are, in many cases, the surface expression of longitudinal foliation. As yet, few studies have been made of the evolution of flow lines and foliation, and other structures in the Antarctic Ice Sheet in relation to strain, and even fewer on the Greenland Ice Sheet. Specifically, questions concerning longevity of these glacier structures, and the effectiveness and rates of their overprinting, have yet to be addressed. Feature-tracking and interferometric techniques are commonly used to determine velocity fields, but extending their application to determine cumulative strain histories would enable us to develop a better understanding of the long-term dynamics of these large ice masses.
7. *The influence of structure on iceberg calving*. The discharge of icebergs into the oceans accounts for a large proportion of mass loss from the Greenland and Antarctic ice sheets, with large-scale calving events significantly influencing the dynamics and structural integrity of ice shelves that buttress inland ice. Even though the collapse of ice shelves affects glacier flow, little is known about the mechanisms that drive rift formation, the influence of ice rheology on fracture propagation, and the structural controls on ice-cliff failure. Further study of the structural and rheological evolution of ice streams and ice shelves is necessary to aid the parameterization of calving models. Furthermore, the relationship between deep-penetrating structural weaknesses, such as crevasse traces that develop much further upglacier, and large-scale calving has yet to be ascertained.
8. *Application to glacier hydrology*. In the study of valley glaciers, the clear relationship between supraglacial streams and structure has been investigated on only a handful of glaciers. We know, for example, that streams follow longitudinal foliation, and are captured by moulins that form at crevasse traces. Key questions that remain include: what are the hydrological conditions that cause a switch from structurally controlled to non-structurally controlled channel development; and what extent is the pool-and-riffle morphology of channels controlled by structure? On a larger scale, the relationship between glacier flow, particularly the sliding component, remains one of the major unknown factors in quantifying the response of ice sheets to climate change. From published research and satellite imagery, it is clear that in the Greenland Ice Sheet there is a relationship between fractures and routing of supraglacial drainage to the bed, yet few in-depth studies of the relationship between glacier structure and hydrology have been undertaken. An important question here is, how is supraglacial lake drainage initiated? The process itself causes hydrofracturing, but do pre-existing crevasse traces provide the planes of weakness, as satellite imagery suggests?
9. *The role of structure in microbiological investigations*. Also connected with glacier hydrology, much emphasis has been placed on the microbiological communities found in cryoconite holes. The fact that morphology of these holes is determined in many cases by glacier structure, notably longitudinal foliation, is generally disregarded. Differential weathering of the different ice types that make up foliation means that more rapid weathering is focused on coarse clear ice layers, which melt more rapidly, rather than coarse bubbly or fine-grained ice layers. Similarly, sediment and cryoconite may be trapped in the coarse clear ice layers of crevasse traces or water-healed crevasses. On the crystallographic scale, structures explain the morphology of crystal boundaries, which are the focus of water-vein networks, and thus are the focus of microbiological activity *within* the ice. All these relationships remain to be explored.

10. *Applying structural geological concepts to Mars.* Remote Martian exploration has yielded higher resolution imagery than that which covers many glacierized regions on Earth. With the increasing recognition, especially in mid-latitudes, that flow features have many of the hallmarks of topographically constrained glaciers, a number of studies have highlighted the similarity between surface features on these "glacier-like forms" and the surrounding landforms, and glacier systems on Earth. Structural glaciological approaches may be used to recognize foliation, crevasses, and moraines, albeit draped in dust, and the potential exists for exploring the past dynamics of these features.

In summary, the field of structural glaciology offers many opportunities to investigate a wide range of glaciological problems. The approach to date has been mainly geological and qualitative. There is now a need for more rigorous quantitative, physical based and modeling approaches that recognize the complexities of structures in ice masses.

12. Glossary

The following definitions are adapted mainly from the "Color Atlas of Glacial Phenomena", compiled by Hambrey and Alean (2017). Other terms in this review can also be found in that volume.

Anastomosing: The property of connecting and diverging of two or more things, typically veins or streams. In the case of glacier ice, this applies to veins or layers of different types of ice, typically in foliation.

Boudin(age): A sausage-shaped block of less ductile material separated by a short distance from its neighbors within a more ductile medium. Where different ice types or layers of sediment are involved, the term "competence-contrast boudinage" is used, with fine-grained ice or sediment-rich ice typically being less ductile than surrounding coarse bubbly ice. These boudins normally form perpendicular to the maximum compressive strain, but if rotated, a shear component may also be involved. Some boudins occur within a mass of ice with strong deformation layering (foliation), and are referred to as "foliation boudinage."

Calving: The process of detachment of blocks of ice from a glacier, ice sheet, or ice shelf into water, producing icebergs. Where glaciers enter the sea or lake an ice cliff usually forms, referred to as the calving front. This can either be floating (typically for cold or polythermal glaciers terminating in deep water) or grounded (all thermal glacier types). Melting below the waterline by warm ocean waters may produce a notch that facilitates ice-cliff collapse. Large tabular icebergs are calved from ice shelves as a consequence of full-depth rifting.

Cirque glacier: A glacier occupying a highland amphitheater known as a cirque. The glacier is bordered by steep sides and a back-wall of exposed bedrock. A rotational component to glacier flow facilitates erosion of the cirque floor, which commonly contains a lake when the ice has receded.

Crevasse: A deep V-shaped cleft, tens or hundreds of meters in length, formed in the upper "brittle" part of a glacier, or at the glacier bed, which is generated when tensile stresses exceed the tensile strength of the ice. This occurs when the ice is undergoing extension, such as in the accumulation area, at the margins, when it flows over a rock step, or enters a water-body. Crevasses in temperate glaciers reach a few tens of meters in depth, but if filled with water they can propagate to greater depths. In cold glaciers, crevasse depths may be much greater. There is a wide range of geometrical arrangements of crevasses: arcuate, basal, chevron, concentric, en echelon, longitudinal, low angle, marginal, splaying, and transverse.

Crevasse trace: A fracture trace that extends across the surface of a glacier for tens or hundreds of meters. There are two main types: (a) a long vein of clear ice a few centimeters wide, formed as a result of fracture and recrystallization of ice under tension without separation of the two walls; this structure commonly forms parallel to an open crevasse or extends laterally into one. This type of crevasse trace is analogous to a tensional vein in deformed rocks. (b) A thicker vein of clear ice

resulting from the freezing of standing water in an open crevasse is also called a crevasse trace. Groups of crevasse traces may be extensively developed in a glacier, and different generations may intersect one another.

Cryoconite: Dark fine-grained sediment on the surface of a glacier. Since it absorbs more radiation than the surrounding ice, it melts downwards at a faster rate, producing "cryoconite holes." Cryoconite provides a host for microbial activity, such as algae, which bind the sediment particles into larger granule-sized grains.

Cryostatic pressure: (Also referred to as "**hydrostatic pressure**" or "**lithostatic pressure**" by some authors). The mean normal stress at a specific point within an ice mass. Normal stresses within a glacier act in all direction, primarily as a result of the ice spreading under its own weight. It can therefore be useful to compare how any given normal stress deviates from this value (see "**deviatoric stress**").

Cumulative strain: (Also referred to as "**total strain**" and "**finite strain**"). The total amount of strain that a material (e.g., rock or ice) has undergone, usually in response to the prolonged application of stress. In diagrammatic form, cumulative strain is expressed in the form of strain ellipses.

Deviatoric stress: The amount that a normal stress deviates from the cryostatic pressure at any given point. In certain circumstances the deviatoric stress may be tensile, despite the component normal stresses being compressive.

Firn (névé): Dense, old snow in which the crystals are partly joined together, but in which the air pockets are still linked. Firn usually refers to snow that has survived one melt-season or more. The density of firn ranges from 400 to 830 kg m^{-3}.

Flow lines: (Also referred to as "**flow stripes**," "**flow bands**," and "**streaklines**"). Longitudinal ice-surface features, particularly associated with ice sheets, and their constituent ice streams and ice shelves. Flow lines are generally parallel to ice-flow direction, and individual flow lines may be traced for over 1,000 km. They are visible both in areas of snow cover and bare glacier ice. There is evidence to suggest that many flow line sets are the surface manifestation of the 3-D structure longitudinal foliation, and that their relationship with flow direction may break down. Flow lines may also be evident in valley glaciers with strongly convergent flow; as snow cover melts during the ablation season, they are also revealed to be longitudinal foliation.

Flow unit: An individual component of glacier flow emanating from a distinct basin. In valley glaciers, multiple basins may result in several flow units merging, but their structural integrity can be recognized by medial moraines or strong longitudinal foliation at their boundaries, and by the preservation of arcuate structures within some of them. Flow units are also recognizable in ice sheets, especially within their component ice streams and ice shelves, as defined by flow lines.

Fold: Layers of ice that have been deformed into curved forms by flow at depth within a glacier. The key attributes of a fold are its axial plane, fold axis, limbs, and hinge (Figure 21). Common types of fold in glaciers are isoclinal, similar, chevron, sheath (eyed), and refolded. A wide variety of folds also occur in glacial sediments, formed especially when the sediment was wet and pressurized.

Foliation: Groups of closely spaced, often discontinuous, layers of coarse bubbly, coarse clear, and fine-grained ice, formed as a result of shear or compression at depth within a glacier. Foliation occurs in most glaciers, and there are two main types: longitudinal foliation and arcuate (or transverse) foliation. Foliation is commonly the product of transposition of earlier layering by increasingly tight folding, or as a new cleavage-like structure.

Fracture: A sharp planar discontinuity and weakness within a material. Fractures may be "open" or "closed" depending on if the fracture walls are in contact or have been separated. Fractures can form by several modes depending on the stress configuration during formation, however, tensional "opening" fracturing is the most common formation mode in glaciers.

Glacier: A perennial mass of ice, irrespective of size, originating on land by the recrystallization of snow to firn and then ice. A glacier also shows evidence of past or present flow. Glaciers are classified by size and morphology, including ice sheet (at the largest scale, defined as >50,000 km^2 in area), ice cap or ice dome, glacier complex, highland icefield, alpine (or valley) glacier, cirque glacier, ice apron or mountain apron glacier, niche glacier, hanging glacier, reconstituted/regenerated/rejuvenated glacier, expanded foot/piedmont glacier, and glacieret. Glaciers which interact with water bodies include ice shelf, calving glacier, tidewater glacier, and freshwater glacier. Glaciers may also be classified according their thermal regime. A glacier that is, at the pressure melting point throughout is referred to as a temperate or warm glacier. A cold or dry-based glacier has ice that is, below the pressure melting point, and is frozen to its bed. A polythermal glacier is a hybrid of the two types, typically having warm ice at the base where it is thickest (as a result of warming from geothermal heat), whilst the margins and upper parts are cold. The terms polar glacier and subpolar glacier were previously used to describe cold and polythermal glaciers, respectively, but these terms are no longer favored because of their geographical connotations.

Grounding-line: The line or zone where a glacier, ice stream, or ice shelf meets the sea. One type is where the line or zone separates a grounded glacier from its floating part, as in the case of cold and polythermal glaciers. Another type is where a grounded glacier rests on the sea floor without a floating extension, which is more typical of temperate glaciers.

Hydrofracturing: Within glacier ice, hydrofracturing is associated with the drainage of supraglacial lakes, often via crack-propagation in water-filled crevasses; it is widely known from the Greenland Ice Sheet where large lakes form on the glacier surface. Hydrofracturing can also affect sediments at the base of a glacier, whereby water under high pressure can fracture the underlying sediment. Fracturing may take place along bedding surfaces, or cut through the strata, allowing sediment to be injected in the form of clastic dykes.

Ice mélange: (Also referred to as "**sikussaq**"). The floating accumulation of calved icebergs, bergy bits, and brash ice that amass in front of tidewater glaciers and ice shelves, or develop in ice shelf suture zones between blocks of meteoric ice, either as a mass of free-floating ice debris, or fused together by sea ice. In some cases, ice mélange in front of calving ice masses can provide a buttressing effect.

Marine ice: Ice that commonly forms beneath sea ice and ice shelves by the freezing and accretion of buoyant meltwater that rises in plumes from the keels of comparatively deep meteoric icebergs and inflows. Pressure-melting of meteoric ice at depth releases meltwater that becomes supercooled as it rises and the pressure decreases, refreezing at shallower depths in ice draft minima. Newly accreted marine ice is probably slushy, initially forming permeable layers, but subsequent accumulation of new layers and conductive heat loss to the atmosphere consolidates the marine ice. A spatially limited variation of this process can occur in basal crevasses and rifts, whereby localized convection currents melt fracture walls, with the resulting meltwater refreezing as marine ice at shallower depths within the fracture.

Meteoric ice: Ice derived from the accumulation of snow that undergoes metamorphism into firn and eventual diagenesis into glacier ice. The term is most commonly used when referring to the composition of ice shelves, which comprise ice derived from multiple origins other than from tributary glaciers (e.g., "**sea ice**" and "**marine ice**").

Nappe: A structural geological term for a large sheet-like body of rock that has been displaced horizontally by a few to many kilometers above a thrust-fault. Similar structures in glaciers has a gravity-driven structural process, but at a smaller scale. They are characterized by recumbent folding with a thrust typically along

	the lower fold limb. The folding and thrusting process commonly allows debris in basal ice to be entrained to a higher level in the glacier.
Ogive:	Arcuate waves or bands, with their apices pointing down-glacier, which develop in an icefall. Wave ogives form first and comprise low-amplitude arcuate waves with a wavelength of tens of meters. Wave ogives commonly pass into band ogives (also known as Forbes' bands), which are arcuate light and dark stripes crossing a glacier surface, and are a type of arcuate foliation. A pair of waves and light and dark bands represent one year's movement through an icefall in a dynamically active glacier.
Rift:	A fracture that penetrates the full depth of an ice column. The term "rift" usually refers to a full-depth fracture in an ice shelf. The development of rifts in ice shelves are an important mechanism by which ice shelves calve, producing large tabular icebergs that at their largest can span many hundreds, if not thousands, of square kilometers in size. Stable ice shelves tend to experience multi-decadal growth punctuated by large infrequent calving events, controlled via the slow propagation of rifts. However, the release of large icebergs can destabilize an ice shelf, leading to further recession, and potentially collapse.
Sea ice:	Ice that forms as sea water freezes, which can reach many meters in thickness. "Sea ice" is a broad term that covers many different classifications and morphologies of sea-derived ice, but sea ice is most relevant from a structural glaciological perspective for its role in the formation of ice shelves. The development of sea ice in inter-meteoric block spaces is the initial process that binds inflowing tributary glaciers and icebergs to form a cohesive ice shelf. In contrast to Antarctic ice shelves that are predominantly glacier-fed, the few surviving Arctic ice shelves are primarily composed of a combination of sea ice, accreted marine ice, and in situ snow accumulation.
Sedimentary (primary) stratification:	The annual layering that forms from the accumulation of snow on a glacier, and which is preserved in firn and in glacier ice as continuous layers of coarse bubbly ice, with coarse clear/dirty ice representing the summer surface. During glacier flow, stratification is subject to folding and over-printing by other structures.
Superimposed ice:	Ice formed at the surface of a glacier by the freezing of rainwater or water-saturated snow. This ice facies is typically opaque, containing air bubbles, albeit fewer than contained in coarse bubbly ice facies derived directly from snow. Superimposed ice is most commonly associated with polythermal glaciers, and in some cases, can be the principal contributor to glacier mass gain.
Surge:	A short-lived phase of accelerated glacier flow during which the surface becomes broken up into a maze of crevasses. A surge may last a few months or several years and may end abruptly. Surges are separated by longer periods of relative inactivity, referred to as quiescence. The shortest quiescent phases last just over a decade, but most last for several decades. During a surge, ice is transferred from a reservoir area to a receiving area, sometimes with a bulge (representing a kinematic wave) moving rapidly through the glacier. Surges are related to changes in the basal hydrological or subglacial sediment regime, and are not directly related to climatic change.
Thermal regime:	The state of a glacier as determined by its temperature distribution. Three types are normally defined: temperate glacier with ice at the pressure-melting point throughout, cold glacier where all the ice is below the melting point and is thus frozen to the bed, and polythermal glacier which is a combination of these attributes.
Thrust-fault:	A low-angle fault, usually formed where the ice is under compression. Thrusts commonly extend from the bed and are associated with debris and overturned folds (see also "**nappe**"). Thrust-faults carrying abundant debris are particularly common in polythermal glaciers. Thrust-faults have been observed actually

forming in glaciers that are surging. The validity of thrusting as a process in glaciers is dismissed by some authors.

Tidewater glacier: A glacier that terminates in the sea, usually in a fjord or bay. The term usually applies to glaciers with termini that are grounded on the sea bottom, although it is also sometimes used for floating glacier tongues.

Data Availability Statement

All data used in this study are embedded in the text or in the cited studies.

Acknowledgments
The contributions of each author to this study are approximately equal. All photographs were taken by M. J. Hambrey, except where otherwise stated. Both authors provided new line drawings and S. J. A. Jennings and A. Smith undertook final drafting. S. Brough kindly provided and annotated the high-resolution image of a glacier-like feature on Mars. S. J. A. Jennings acknowledges funding for his Ph.D. program from 2012 to 2016 from the UK Natural Environment Research Council at Aberystwyth University (Reference no. J65727D), and further support from the Operational Program Research, Development, and Education—Project Postdoc@MUNI (No. CZ.02.2.69/0.0/0.0/16_027/0008360) at Masaryk University. Additional field support from the University Center in Svalbard (UNIS); the UK Arctic Research Station, Ny-Ålesund, Svalbard; Tarfala Research Station, Sweden; and the Czech J. G. Mendel Research Station, James Ross Island, Antarctica, are gratefully acknowledged. M. J. Hambrey acknowledges his early mentors, Wilfred Theakstone as PhD supervisor for introducing him to structural glaciology in the early 1970s, and Geoffrey Milnes as post-doctoral supervisor for teaching him structural geological principles. M. J. Hambrey has benefitted from the expertize and field collaboration of innumerable colleagues over a period of 50 years, and the support of his home institutions: the University of Manchester (1970–1974), ETH Zurich (1974–1977), the University of Cambridge (1977–1989), Liverpool John Moores University (1989–1996), and Aberystwyth University (1996-present). In addition, Fellowships at the universities of Otago, Wellington, and British Columbia, and the Alfred Wegener Institute in Germany, provided access to glaciers and ice sheets in otherwise inaccessible regions of the world. Funding has come from many sources, notably: the UK Natural Environment Research Council, the Swiss Nationalfond, the Royal Society (London), Antarctica New Zealand (via Peter Barrett and Sean Fitzsimons),

References

Aber, J. S., Croot, D. G., & Fenton, M. M. (1989). Large Composite-Ridges. *In Glaciotectonic landforms and structures. Glaciology and quaternary geology* (Vol. 5). Springer. https://doi.org/10.1007/978-94-015-6841-8_3

Agassiz, L. (1840). *Etudes sur les glaciers*. Jent et Gassmann. Retrieved from https://archive.org/details/tudessurlesgla00agas

Aliha, M. R. M., Ayatollahi, M. R., & Akbardoost, J. (2012). Typical upper bound-lower bound mixed mode fracture resistance envelopes for rock material. *Rock Mechanics and Rock Engineering*, *45*, 65–74. https://doi.org/10.1007/s00603-011-0167-0

Allen, C. R., Kamb, W. B., Meier, M. F., & Sharp, R. P. (1960). Structure of the lower Blue Glacier, Washington. *The Journal of Geology*, *68*, 601–625. https://doi.org/10.1086/626700

Alley, R. B., Cuffey, K. M., Evenson, E. B., Strasser, J. C., Lawson, D. E., & Larson, G. J. (1997). How glaciers entrain and transport basal sediments: Physical constraints. *Quaternary Science Reviews*, *16*, 1017–1038. https://doi.org/10.1016/S0277-3791(97)00034-6

Alley, R. B., Dupont, T. K., Parizek, B. R., & Anandakrishnan, S. (2005). Access of surface meltwater to beds of sub-freezing glaciers: Preliminary insights. *Annals of Glaciology*, *40*, 8–14. https://doi.org/10.3189/172756405781813483

Alsop, G. I., & Holdsworth, R. E. (1999). Vergence and facing patters in large-scale sheath folds. *Journal of Structural Geology*, *21*(10), 1335–1349. https://doi.org/10.1016/S0191-8141(99)00099-1

Alsop, G. I., & Holdsworth, R. E. (2002). The geometry and kinematics of flow perturbation folds. *Tectonophysics*, *350*(2), 99–125. https://doi.org/10.1016/S0040-1951(02)00084-7

Alsop, G. I., & Holdsworth, R. E. (2007). Flow perturbation folding in shear zones. In A. C. Ries, R. W. H. Butler, & R. H. Graham (Eds.), *Deformation of the continental crust: The legacy of mike Coward* (Vol. 272, pp. 75–101). Geological Society London Special Publications. https://doi.org/10.1144/GSL.SP.2007.272.01.06

Ambach, W. (1968). The formation of crevasses in relation to the measured distribution of strain-rates and stresses. *Archiv für Meteorologie, Geophysik und Bioklimatologie, Serie A*, *17*, 78–87. https://doi.org/10.1007/BF02250793

Amundson, J. M., Fahnestock, M., Truffer, M., Brown, J., Lüthi, M. P., & Motyka, R. J. (2010). Ice mélange dynamics and implications for terminus stability, Jakobshavn Isbræ, Greenland. *Journal of Geophysical Research*, *115*, F01005. https://doi.org/10.1029/2009JF001405

Anderton, P. W. (1973). *Structural glaciology of a glacier confluence, Kaskawulsh Glacier Yukon Territory, Canada (Institute of Polar Studies Report No. 26)*. Research Foundation and the Institute of Polar Studies, The Ohio State University.

Anesio, A. M., & Laybourn-Parry, J. (2012). Glaciers and ice sheets as a biome. *Trends in Ecology & Evolution*, *27*, 219–225. https://doi.org/10.1016/j.tree.2011.09.012

Anesio, A. M., Lutz, S., Chrismas, N. A. M., & Benning, L. G. (2017). The microbiome of glaciers and ice sheets. *npj Biofilms and Microbiomes*, *3*, 10. https://doi.org/10.1038/s41522-017-0019-0

Aniya, M., Casassa, G., & Naruse, R. (1988). Morphology, surface characteristics, and flow velocity of Soler Glacier, Patagonia. *Arctic and Alpine Research*, *20*(4), 414–421. https://doi.org/10.1080/00040851.1988.12002694

Aniya, M., & Naruse, R. (1987). Structural and morphological characteristics of Soler Glacier, Patagonia. *Bulletin of Glacier Research*, *4*, 69–77.

Appleby, J. R., Brook, M. S., Horton, T. W., Fuller, I. C., Holt, K. A., & Quincey, D. J. (2017). Stable isotope (δD–$\delta^{18}O$) relationships of ice facies and glaciological structures within the mid-latitude maritime Fox Glacier, New Zealand. *Annals of Glaciology*, *58*(75pt2), 155–165. https://doi.org/10.1017/aog.2017.11

Appleby, J. R., Brook, M. S., Vale, S. S., & MacDonald-Creevey, A. M. (2010). Structural glaciology of a temperate maritime glacier: Lower Fox Glacier, New Zealand. *Geografiska Annaler*, *92*(A), 451–467. https://doi.org/10.1111/j.1468-0459.2010.00407.x

Arcone, S. A., Spikes, V. B., Hamilton, G. S., & Mayewski, P. A. (2004). Stratigraphic continuity in 400-MHz radar profiles in West Antarctica. *Annals of Glaciology*, *39*, 195–200. https://doi.org/10.3189/172756404781813925

Arslan, A., Passchier, C. W., & Koehn, D. (2008). Foliation boudinage. *Journal of Structural Geology*, *30*(3), 291–309. https://doi.org/10.1016/j.jsg.2007.11.004

Arthern, R. J., Hindmarsh, R. C. A., & Williams, C. R. (2015). Flow speed within the Antarctic ice sheet and its controls inferred from satellite observations. *Journal of Geophysical Research: Earth Surface*, *120*(7), 1171–1188. https://doi.org/10.1002/2014JF003239

Ashmore, D. W., Bingham, R. G., Ross, N., Siegert, M. J., Jordan, T. A., & Mair, D. W. F. (2020). Englacial architecture and age-depth constraints across the West Antarctic Ice Sheet. *Geophysical Research Letters*, *47*(6), e2019GL086663. https://doi.org/10.1029/2019GL086663

Ashmore, D. W., Hubbard, B., Luckman, A., Kulessa, B., Bevan, S., Booth, A., et al. (2017). Ice and firn heterogeneity within Larsen C Ice Shelf from borehole optical televiewing. *Journal of Geophysical Research: Earth Surface*, *122*(5), 1139–1153. https://doi.org/10.1002/2016JF004047

Azzoni, R. S., Fugazza, D., Zennaro, M., Zucali, M., D'Agata, C., Maragno, D., et al. (2017). Recent structural evolution of Forni Glacier tongue (Ortles-Cevedale Group, Central Italian Alps). *Journal of Maps*, *13*(2), 870–878. https://doi.org/10.1080/17445647.2017.1394227

Badino, G., & Piccini, L. (2002). Englacial water fluctuation in moulins: An example from Tyndall Glacier (Patagonia, Chile). *Nimbus*, *23–24*, 125–129.

Ballantyne, C. K., & Stone, J. O. (2009). Rock-slope failure at Baosbheinn, Western Ross, NW Scotland: Age and interpretation. *Scottish Journal of Geology*, *45*, 177–181. https://doi.org/10.1144/0036-9276/01-388

the Australian National Antarctic Research Expeditions (via the late Barrie McKelvey), the U.S. Antarctic Program (via Peter Webb), University of British Columbia (via Garry Clarke), the University of Calgary (via Brian Moorman), McGill University/ETH (via Fritz Müller), the European Center for Arctic Environmental Research, and the Climate Change Consortium of Wales. Colleagues at the Center for Glaciology at Aberystwyth University reviewed an earlier version of this study: S. Brough (Mars), N. Glasser (all), T. Holt (all), B. Hubbard (all), and T. Irvine-Fynn (hydrology and microbiology). The authors also thank D. Nývlt, the reviewers David J. A. Evans and Peter L. Moore, the Editor Fabio Florindo, the Associate Editor Robert G. Bingham, and an anonymous editor, for their valued insights that have helped strengthen this study. There is no funding for this article.

Banwell, A. F., MacAyeal, D. R., & Sergienko, O. V. (2013). Breakup of the Larsen B Ice Shelf triggered by chain reaction drainage of supraglacial lakes. *Geophysical Research Letters*, *40*(22), 5872–5876. https://doi.org/10.1002/2013GL057694

Barletta, R. E., Priscu, J. C., Mader, H. M., Jones, W. L., & Roe, C. H. (2012). Chemical analysis of ice vein microenvironments: II. Analysis of glacial samples from Greenland and Antarctica. *Journal of Glaciology*, *58*, 1109–1118. https://doi.org/10.3189/2012JoG12J112

Bassis, J. N., & Ma, Y. (2015). Evolution of basal crevasses links ice shelf stability to ocean forcing. *Earth and Planetary Science Letters*, *409*, 203–211. https://doi.org/10.1016/j.epsl.2014.11.003

Bassis, J. N., & Walker, C. C. (2012). Upper and lower limits on the stability of calving glaciers from the yield strength envelope of ice. *Proceedings of the Royal Society A*, *468*, 913–931. https://doi.org/10.1098/rspa.2011.0422

Benn, D. I., & Åström, J. A. (2018). Calving glaciers and ice shelves. *Advances in Physics: X*, *3*(1), 1513819. https://doi.org/10.1080/23746149.2018.1513819

Benn, D. I., Bolch, T., Hands, K., Gulley, J., Luckman, A., Nicholson, L. I., et al. (2012). Response of debris-covered glaciers in the Mount Everest region to recent warming, and implications for outburst flood hazards. *Earth-Science Reviews*, *114*, 156–174. https://doi.org/10.1016/j.earscirev.2012.03.008

Benn, D. I., & Evans, D. J. A. (2010). *Glaciers and glaciation*. Hodder Education.

Benn, D. I., Gulley, J., Luckman, A., Adamek, A., & Glowacki, P. S. (2009). Englacial drainage systems formed by hydrologically driven crevasse propagation. *Journal of Glaciology*, *55*(191), 513–523. https://doi.org/10.3189/002214309788816669

Benn, D. I., Hulton, N. R. J., & Mottram, R. H. (2007). "Calving laws", "sliding laws" and the stability of tidewater glaciers. *Annals of Glaciology*, *46*, 123–130. https://doi.org/10.3189/172756407782871161

Benn, D. I., Kirkbride, M. P., Owen, L. A., & Brazier, V. (2003). Glaciated valley landsystems. In D. J. A. Evans (Ed.), *Glacial Landsystems* (pp. 372–406). Arnold.

Benn, D. I., Thompson, S., Gulley, J., Mertes, J., Luckman, A., & Nicholson, L. (2017). Structure and evolution of the drainage system of a Himalayan debris-covered glacier, and its relationship with patterns of mass loss. *The Cryosphere*, *11*, 2247–2264. https://doi.org/10.5194/tc-11-2247-2017

Benn, D. I., Warren, C. R., & Mottram, R. H. (2007). Calving processes and the dynamics of calving glaciers. *Earth-Science Reviews*, *82*, 143–179. https://doi.org/10.1016/j.earscirev.2007.02.002

Bennett, G. L., & Evans, D. J. A. (2012). Glacier retreat and landform production on an overdeepened glacier foreland: the debris-charged glacier landsystem at Kviárjökull, Iceland. *Earth Surface Processes and Landforms*, *37*(15), 1584–1602. https://doi.org/10.1002/esp.3259

Bennett, M. R. (2001). The morphology, structural evolution and significance of push moraines. *Earth Science Reviews*, *53*, 197–236. https://doi.org/10.1016/S0012-8252(00)00039-8

Bennett, M. R., & Glasser, N. F. (2009). *Glacial geology: Ice sheets and landforms*. Wiley-Blackwell.

Bennett, M. R., Hambrey, M. J., Huddart, D., & Ghienne, J. F. (1996). The formation of a geometrical ridge network by the surge-type glacier Kongsvegen, Svalbard. *Journal of Quaternary Science*, *11*, 430–438. https://doi.org/10.1002/(SICI)1099-1417(199611/12)11:6<437::AID-JQS269>3.0.CO;2-J

Bennett, M. R., Hambrey, M. J., Huddart, D., & Glasser, N. F. (1998). Glacial thrusting and moraine-mound formation in Svalbard and Britain: The example of Coire a'Cheund-chnoic (Valley of a Hundred Hills), Torridon, Scotland. In L. A. Owen (Ed.), *Mountain glaciation* (pp. 17–34). Wiley & Sons.

Bennett, M. R., Hambrey, M. J., Huddart, D., Glasser, N. F., & Crawford, K. (1999). The landform and sediment assemblage produced by a tidewater glacier surge in Kongsfjorden, Svalbard. *Quaternary Science Reviews*, *18*, 1213–1246. https://doi.org/10.1016/S0277-3791(98)90041-5

Bennett, M. R., Huddart, D., & Waller, R. I. (2000). Glaciofluvial crevasse and conduit fills as indicators of supraglacial dewatering during a surge, Skeiðarárjökull, Iceland. *Journal of Glaciology*, *46*, 25–34. https://doi.org/10.3189/172756500781833232

Bennett, M. R., Huddart, D., Waller, R. I., Cassidy, N., Tomio, A., Zukowskyj, P., et al. (2004). Sedimentary and tectonic architecture of a large push moraine: A case study from Hagafellsjökull-Eystri, Iceland. *Sedimentary Geology*, *172*, 269–292. https://doi.org/10.1016/j.sedgeo.2004.10.002

Bentley, C. R., Shabtaie, S., Blankenship, D. D., Rooney, S. T., Schultz, D. G., Anandakrishnan, S., & Alley, R. B. (1987). Remote sensing of the Ross ice streams and adjacent Ross ice shelf, Antarctica. *Annals of Glaciology*, *9*, 20–29. https://doi.org/10.3189/S0260305500200700

Bevington, A., & Copland, L. (2014). Characteristics of the last five surges of Lowell Glacier, Yukon, Canada, since 1948. *Journal of Glaciology*, *60*, 113–123. https://doi.org/10.3189/2014JoG13J134

Bhardwaj, A., Sam, L., Bhardwaj, A., & Martín-Torres, F. J. (2016). LiDAR remote sensing of the cryosphere: Present applications and future prospects. *Remote Sensing of Environment*, *177*, 125–143. https://doi.org/10.1016/j.rse.2016.02.031

Bindschadler, R., Scambos, T. A., Rott, H., Skvarca, P., & Vornberger, P. (2002). Ice dolines on Larsen ice shelf, Antarctica. *Annals of Glaciology*, *34*, 283–290. https://doi.org/10.3189/172756402781817996

Bindschadler, R. A., & Scambos, T. A. (1991). Satellite-image-derived velocity field of an Antarctic ice stream. *Science*, *252*(5003), 242–246. https://doi.org/10.1126/science.252.5003.242

Blatter, H. (1995). Velocity and stress fields in grounded glaciers: A simple algorithm for including deviatoric stress gradients. *Journal of Glaciology*, *41*, 333–344. https://doi.org/10.3189/S002214300001621X

Bodart, J. A., Bingham, R. G., Ashmore, D. W., Karlsson, N. B., Hein, A. S., & Vaughan, D. G. (2021). Age-depth stratigraphy of Pine Island Glacier inferred from airborne radar and ice-core chronology. *Journal of Geophysical Research: Earth Surface*, *126*(4), e2020JF005927. https://doi.org/10.1029/2020JF005927

Boon, S., & Sharp, M. (2003). The role of hydrologically-driven ice fracture in drainage system evolution on an Arctic glacier. *Geophysical Research Letters*, *30*(18). https://doi.org/10.1029/2003GL018034

Borstad, C., McGrath, D., & Pope, A. (2017). Fracture propagation and stability of ice shelves governed by ice shelf heterogeneity. *Geophysical Research Letters*, *44*, 4186–4194. https://doi.org/10.1002/2017GL072648

Boulton, G. S. (1967). The development of a complex supraglacial moraine at the margin of Sørbreen, Ny Friesland, Vestspitzbergen. *Journal of Glaciology*, *6*, 717–735. https://doi.org/10.3189/S0022143000019961

Boulton, G. S. (1970). On the origin and transport of englacial debris in Svalbard glaciers. *Journal of Glaciology*, *9*, 213–229. https://doi.org/10.3189/S0022143000023534

Boulton, G. S. (1978). Boulder shapes and grain size distributions of debris as indicators of transport paths through a glacier and till genesis. *Sedimentology*, *25*, 773–799. https://doi.org/10.1111/j.1365-3091.1978.tb00329.x

Boulton, G. S., & Eyles, N. (1979). Sedimentation by valley glaciers: A model and genetic classification. In C. Schlüchter (Ed.), *Moraines and Varves*. Balkema.

Boulton, G. S., van der Meer, J. J. M., Beets, D. J., Hart, K. J., & Ruegg, G. H. J. (1999). The sedimentary and structural evolution of a recent push moraine complex: Holmströmbreen, Spitsbergen. *Quaternary Science Reviews*, *18*, 339–371. https://doi.org/10.1016/S0277-3791(98)00068-7

Braun, C. (2017). The surface mass balance of the Ward Hunt Ice Shelf and Ward Hunt Ice Rise, Ellesmere Island, Nunavut, Canada. In L. Copland, & D. Mueller (Eds.), *Arctic ice shelves and ice islands* (pp. 149–183). Springer. https://doi.org/10.1007/978-94-024-1101-0_6

Brook, M., Hagg, W., & Winkler, S. (2017). Contrasting medial moraine development at adjacent temperate, maritime glaciers: Fox and Franz Josef Glaciers, South Westland, New Zealand. *Geomorphology*, *290*, 58–68. https://doi.org/10.1016/j.geomorph.2017.04.015

Brough, S., Hubbard, B., & Hubbard, A. (2019). Area and volume of mid-latitude glacier-like forms on Mars. *Earth and Planetary Science Letters*, *507*, 10–20. https://doi.org/10.1016/j.epsl.2018.11.031

Brough, S., Hubbard, B., Souness, C., Grindrod, P. M., & Davis, J. (2016). Landscapes of polyphase glaciation: Eastern Hellas Planitia, Mars. *Journal of Maps*, *12*, 530–542. https://doi.org/10.1080/17445647.2015.1047907

Burton, J. C., Amundson, J. M., Cassotto, R., Kuo, C.-C., & Dennin, M. (2018). Quantifying flow and stress in ice mélange, the world's largest granular material. *Proceedings of the National Academy of Sciences*, *115*(20), 5105–5110. https://doi.org/10.1073/pnas.1715136115

Campbell, S., Roy, S., Kreutz, K., Arcone, S. A., Osterberg, E. C., & Koons, P. (2013). Strain-rate estimates for crevasse formation at an alpine ice divide: Mount Hunter, Alaska. *Annals of Glaciology*, *54*, 200–208. https://doi.org/10.3189/2013AoG63A266

Carrivick, J. L., Davies, B. J., Glasser, N. F., Nývlt, D., & Hambrey, M. J. (2012). Late-Holocene changes in character and behaviour of land-terminating glaciers on James Ross Island, Antarctica. *Journal of Glaciology*, *58*, 1176–1190. https://doi.org/10.3189/2012JoG11J148

Casassa, G., & Brecher, H. H. (1993). Relief and decay of flow stripes on Byrd Glacier, Antarctica. *Annals of Glaciology*, *17*, 255–261. https://doi.org/10.3189/S0260305500012933

Cavitte, M. G. P., Blankenship, D. D., Young, D. A., Schroeder, D. M., Parrenin, F., Lemeur, E., et al. (2016). Deep radiostratigraphy of the East Antarctic plateau: Connecting the Dome C and Vostok ice core sites. *Journal of Glaciology*, *62*(232), 323–334. https://doi.org/10.1017/jog.2016.11

Chamberlin, T. C. (1895). The classification of American glacial deposits. *The Journal of Geology*, *3*, 270–277. https://doi.org/10.1086/607182

Christoffersen, P., Bougamont, M., Hubbard, A., Doyle, S. H., Grigsby, S., & Pettersson, R. (2018). Cascading lake drainage on the Greenland ice sheet triggered by tensile shock and fracture. *Nature Communications*, *9*, 1064. https://doi.org/10.1038/s41467-018-03420-8

Christoffersen, P., Piotrowski, J. A., & Larsen, N. K. (2005). Basal processes beneath an Arctic glacier and their geomorphic imprint after a surge, Elisebreen, Svalbard. *Quaternary Research*, *64*, 125–137. https://doi.org/10.1016/j.yqres.2005.05.009

Chudley, T. R., Christoffersen, P., Doyle, S. H., Dowling, T. P. F., Law, R., Schoonman, C. M., et al. (2020). Structural controls on the hydrology of crevasses on the Greenland ice sheet. *Journal of Geophysical Research: Earth Surface*. https://doi.org/10.1002/essoar.10502979.1

Clark, J. M., & Lewis, W. V. (1951). Rotational movement in cirques and valley glaciers. *The Journal of Geology*, *59*(6), 546–566. https://doi.org/10.1086/625911

Clarke, G. K. C., & Blake, E. W. (1991). Geometric and thermal evolution of a surge-type glacier in its quiescent state, Trapridge Glacier, Yukon Territory, Canada 1969–89. *Journal of Glaciology*, *37*, 158–169. https://doi.org/10.3189/S002214300004291X

Clarke, G. K. C., & Hambrey, M. J. (2019). Structural evolution during cyclic glacier surges: 2. Numerical modeling. *Journal of Geophysical Research*, *124*, 495–525. https://doi.org/10.1029/2018JF004870

Clarke, T. S. (1991). Glacier dynamics in the Susitna River basin, Alaska, USA. *Journal of Glaciology*, *37*, 97–106. https://doi.org/10.3189/S0022143000042842

Clarke, T. S., Liu, C., Lord, N. E., & Bentley, C. R. (2000). Evidence for a recently abandoned shear margin adjacent to ice stream B2, Antarctica, from ice-penetrating radar measurements. *Journal of Geophysical Research*, *105*, 13409–13422. https://doi.org/10.1029/2000JB900037

Colgan, W., Rajaram, H., Abdalati, W., McCutchan, C., Mottram, R., Moussavi, M. S., & Grigsby, S. (2016). Glacier crevasses: Observations, models, and mass balance implications. *Reviews of Geophysics*, *54*, 119–161. https://doi.org/10.1002/2015RG000504

Cook, A. J., & Vaughan, D. G. (2010). Overview of areal changes of the ice shelves on the Antarctic Peninsula over the past 50 years. *The Cryosphere*, *4*(1), 77–98. https://doi.org/10.5194/tc-4-77-2010

Cook, J., Edwards, A., Takeuchi, N., & Irvine-Fynn, T. (2016). Cryoconite: The dark biological secret of the cryosphere. *Progress in Physical Geography: Earth and Environment*, *140*(1), 66–111. https://doi.org/10.1177/0309133315616574

Cook, J., Hodson, A., Telling, J., Anesio, A., Irvine-Fynn, T., & Bellas, C. (2010). The mass-area relationship within cryoconite holes and its implications for primary production. *Annals of Glaciology*, *51*, 106–110. https://doi.org/10.3189/172756411795932038

Cook, J. C. (1956). Some observations in a northwest Greenland crevasse. *Eos, Transactions, American Geophysical Union*, *37*(6), 715–718. https://doi.org/10.1029/TR037i006p00715

Cook, S. J., Waller, R. I., & Knight, P. G. (2006). Glaciohydraulic supercooling: The process and its significance. *Progress in Physical Geography: Earth and Environment*, *30*(5), 577–588. https://doi.org/10.1177/0309133306071141

Crabtree, R. D., & Doake, C. S. M. (1980). Flow lines on Antarctic ice shelves. *Polar Record*, *20*, 31–37. https://doi.org/10.1017/S0032247400002898

Craven, M., Allison, I., Fricker, H. A., & Warner, R. (2009). Properties of a marine ice layer under the Amery Ice Shelf, East Antarctica. *Journal of Glaciology*, *55*(192), 717–728. https://doi.org/10.3189/002214309789470941

Croot, D. G. (1987). Glacio-tectonic structures: A mesoscale model of thin-skinned thrust sheets? *Journal of Structural Geology*, *9*, 797–808. https://doi.org/10.1016/0191-8141(87)90081-2

Croot, D. G. (1988a). Glaciotectonics and surging glaciers: A correlation based on Vestspitsbergen, Svalbard, Norway. In D. G. Croot (Ed.), *Glaciotectonics: Forms and processes* (pp. 49–61). Balkema.

Croot, D. G. (1988b). Morphological, structural and mechanical analysis of Neoglacial ice-pushed ridges in Iceland. In D. G. Croot (Ed.), *Glaciotectonics: Forms and processes* (pp. 33–47). Balkema.

Cuffey, K. M., & Paterson, W. S. B. (2010). *The physics of glaciers*. Elsevier.

Cunningham, J., & Waddington, E. D. (1990). Boudinage: A source of stratigraphic disturbance in glacial ice in central Greenland. *Journal of Glaciology*, *36*(124), 269–272. https://doi.org/10.3189/002214390793701336

Dahl-Jensen, D., Albert, M. R., Aldahan, A., Azuma, N., Balslev-Clausen, D., Baumgartner, M., et al. (2013). Eemian interglacial reconstructed from a Greenland folded ice core. *Nature*, *493*, 489–494. https://doi.org/10.1038/nature11789

Dani, K. G. S., Mader, H. M., Wolff, E. W., & Wadham, J. L. (2012). Modeling the liquid-water veins system within polar ice sheets as a potential microbial habitat. *Earth and Planetary Science Letters*, *333–334*, 238–249. https://doi.org/10.1016/j.epsl.2012.04.009

Das, S., Joughin, I., Behn, M., Howat, I., King, M., Lizarralde, D., & Bhatia, M. (2008). Fracture propagation to the base of the Greenland ice sheet during supraglacial lake drainage. *Science*, *320*, 778–781. https://doi.org/10.1126/science.1153360

De Angelis, H., & Skvarca, P. (2003). Glacier surge after ice shelf collapse. *Science*, *299*, 1560–1562. https://doi.org/10.1126/science.1077987

Deline, P., Hewitt, K., Reznichenko, N., & Shugar, D. (2015). Rock avalanches onto glaciers. In T. Davies (Ed.), *Landslide hazards, risks and disasters* (pp. 263–319). Elsevier. https://doi.org/10.1016/b978-0-12-396452-6.00009-4
De Rydt, J., Gudmundsson, G. H., Nagler, T., Wuite, J., & King, E. C. (2018). Recent rift formation and impact on the structural integrity of the Brunt Ice Shelf, East Antarctica. *The Cryosphere*, *12*, 505–520. https://doi.org/10.5194/tc-12-505-2018
De Rydt, J., Gudmundsson, G. H., Rott, H., & Bamber, J. L. (2015). Modeling the instantaneous response of glaciers after the collapse of the Larsen B ice shelf. *Geophysical Research Letters*, *42*(13), 5355–5363. https://doi.org/10.1002/2015GL064355
Dickson, J. l., Head, J. W., & Marchant, D. R. (2008). Late Amazonian glaciation at the dichotomy boundary on Mars: Evidence for glacial thickness maxima and multiple glacial phases. *Geology*, *36*, 411–414. https://doi.org/10.1130/G24382A.1
Doake, C. S. M., & Vaughan, D. G. (1991). Rapid disintegration of Wordie ice shelf in response to atmospheric warming. *Nature*, *350*, 328–330. https://doi.org/10.1038/350328a0
Dowdeswell, J. A. (2017). Eurasian Arctic ice shelves and tidewater ice margins. In L. Copland, & D. Mueller (Eds.), *Arctic ice shelves and ice islands* (pp. 55–74). Springer. https://doi.org/10.1007/978-94-024-1101-0_3
Dowdeswell, J. A., & Jeffries, M. O. (2017). Arctic ice shelves: An introduction. In L. Copland, & D. Mueller (Eds.), *Arctic ice shelves and ice islands* (pp. 3–21). Springer. https://doi.org/10.1007/978-94-024-1101-0_1
Dowdeswell, J. A., Solheim, A., & Ottesen, D. (2016). Rhombohedral crevasse-fill ridges at the marine margin of a surging Svalbard ice cap. In J. A. Dowdeswell, M. Canals, M. Jakobsson, B. J. Todd, E. K. Dowdeswell, & K. A. Hogan (Eds.), *Atlas of submarine glacial landforms: Modern, quaternary and ancient* (Vol. 46, pp. 73–74). Geological Society. https://doi.org/10.1144/M46.62
Dowdeswell, J. A., & Williams, M. (1997). Surge-type glaciers in the Russian High Arctic identified from digital satellite imagery. *Journal of Glaciology*, *43*, 489–494. https://doi.org/10.3189/S0022143000035097
Doyle, S. H., Hubbard, A. L., Dow, C. F., Jones, G. A., Fitzpatrick, A., Gusmeroli, A., et al. (2013). Ice tectonic deformation during the rapid in situ drainage of a supraglacial lake on the Greenland Ice Sheet. *The Cryosphere*, *7*, 129–140. https://doi.org/10.5194/tc-7-129-2013
Drewry, D. J. (1972). A quantitative assessment of dirt-cone dynamics. *Journal of Glaciology*, *11*(63), 431–446. https://doi.org/10.3189/S0022143000022383
Drews, R., Eisen, O., Weikusat, I., Kipfstuhl, S., Lambrecht, A., Steinhage, D., et al. (2009). Layer disturbances and the radio-echo free zone in ice sheets. *The Cryosphere*, *3*, 195–203. https://doi.org/10.5194/tc-3-195-2009
Driscoll, F. G. (1980). Formation of the neoglacial surge moraines of the Klutlan Glacier, Yukon Territory, Canada. *Quaternary Research*, *14*, 19–30. https://doi.org/10.1016/0033-5894(80)90004-6
Duddu, R., Jiménez, S., & Bassis, J. (2020). A non-local continuum poro-damage mechanics model for hydrofracturing of surface crevasses in grounded glaciers. *Journal of Glaciology*, *66*(257), 415–429. https://doi.org/10.1017/jog.2020.16
Durney, D. W., & Ramsey, J. G. (1973). Incremental strains measured by syntectonic crystal growths. In K. A. De Jong, & R. Scholten (Eds.), *Gravity and tectonics*. Wiley.
Echelmeyer, K., Clarke, T. S., & Harrison, W. D. (1991). Surficial glaciology of Jakobshavn Isbræ, West Greenland: Part I. Surface morphology. *Journal of Glaciology*, *37*(127), 368–382. https://doi.org/10.3189/S0022143000005803
Echelmeyer, K. A., Harrison, W. D., Larsen, C., & Mitchell, J. E. (1994). The role of the margins in the dynamics of an active ice stream. *Journal of Glaciology*, *40*(136), 527–538. https://doi.org/10.3189/S0022143000012417
Edwards, A., Irvine-Fynn, T., Mitchell, A. C., & Rassner, S. M. E. (2014). A germ theory for glacial systems? *WIREs Water*, *1*, 331–340. https://doi.org/10.1002/wat2.1029
Elliot, D. (1976). The motion of thrust sheets. *Journal of Geophysical Research*, *81*(5), 949–963. https://doi.org/10.1029/JB081i005p00949
Ely, J. C., & Clark, C. D. (2016). Flow-stripes and foliations of the Antarctic ice sheet. *Journal of Maps*, *12*(2), 249–259. https://doi.org/10.1080/17445647.2015.1010617
Ely, J. C., Clark, C. D., Ng, R. S. L., & Spagnolo, M. (2017). Insights on the formation of longitudinal surface structures on ice sheets from analysis of their spacing, spatial distribution, and relationship to ice thickness and flow. *Journal of Geophysical Research: Earth Surface*, *122*, 961–972. https://doi.org/10.1002/2016JF004071
Ensminger, S. L., Alley, R. B., Evenson, E. B., Lawson, D. E., & Larson, G. J. (2001). Basal-crevasse-fill origin of laminated debris bands at Matanuska Glacier, Alaska, USA. *Journal of Glaciology*, *47*(158), 412–422. https://doi.org/10.3189/172756501781832007
Epstein, S., & Sharp, R. P. (1959). Oxygen-isotope variations in the Malaspina and Saskatchewan glaciers. *The Journal of Geology*, *67*(1), 88–102. https://doi.org/10.1086/626559
Etzelmüller, B., Hagen, J. O., Vatne, G., Ødegård, R., & Sollid, J. L. (1996). Glacier debris accumulation and sediment deformation influenced by permafrost: Examples from Svalbard. *Annals of Glaciology*, *22*, 53–62. https://doi.org/10.3189/1996AoG22-1-53-62
Etzelmüller, B., Vatne, G., Ødegård, R. S., & Sollid, J. (1993). Mass balance and changes of surface slope, crevasse and flow pattern of Erikbreen, northern Spitsbergen: An application of geographical information systems (GIS). *Polar Research*, *12*, 131–146. https://doi.org/10.3402/polar.v12i2.6709
Evans, D. J. A. (1989a). The nature of glacitectonic structures and sediments at subpolar glacier margins, northwest Ellesmere Island, Canada. *Geografiska Annaler*, *71A*, 113–123. https://doi.org/10.1080/04353676.1989.11880280
Evans, D. J. A. (1989b). Apron entrainment at the margins of sub-polar glaciers, northwest Ellesmere Island, Canadian High Arctic. *Journal of Glaciology*, *35*(121), 317–324. https://doi.org/10.3189/S0022143000009230
Evans, D. J. A. (2003). *Glacial landsystems*. Arnold.
Evans, D. J. A. (2009). Controlled moraines: Origins, characteristics and palaeoglaciological implications. *Quaternary Science Reviews*, *28*, 183–208. https://doi.org/10.1016/j.quascirev.2008.10.024
Evans, D. J. A. (2010). Controlled moraine development and debris transport pathways in polythermal plateau icefields: Examples from Tungnafellsjökull, Iceland. *Earth Surface Processes and Landforms*, *35*, 1430–1444. https://doi.org/10.1002/esp.1984
Evans, D. J. A. (2018). *Glaciation: A very short introduction*. Oxford University Press.
Evans, D. J. A., Atkinson, N., & Phillips, E. (2020). Glacial geomorphology of the Neutral Hills Uplands, southeast Alberta, Canada: The process-form imprints of dynamic ice streams and surging ice lobes. *Geomorphology*, *350*, 106910. https://doi.org/10.1016/j.geomorph.2019.106910
Evans, D. J. A., Ewertowski, M., & Orton, C. (2016). Fláajökull (north lobe), Iceland: Active temperate piedmont lobe glacier landsystem. *Journal of Maps*, *12*(5), 777–789. https://doi.org/10.1080/17445647.2015.1073185
Evans, D. J. A., Phillips, E. R., Hiemstra, J. F., & Auton, C. A. (2006). Subglacial till: Formation, sedimentary characteristics and classification. *Earth-Science Reviews*, *78*, 115–176. https://doi.org/10.1016/j.earscirev.2006.04.001
Evans, D. J. A., & Rea, B. R. (1999). Geomorphology and sedimentology of surging glaciers: A landsystems approach. *Annals of Glaciology*, *28*, 75–82. https://doi.org/10.3189/172756499781821823
Evans, D. J. A., & Rea, B. R. (2003). Surging glacier landsystem. In D. J. A. Evans (Ed.), *Glacial landsystems*. Arnold.

Evans, D. J. A., Storrar, R. D., & Rea, B. R. (2016). Crevasse-squeeze ridge corridors: Diagnostic features of late-stage palaeo-ice stream activity. *Geomorphology*, *258*, 40–50. https://doi.org/10.1016/j.geomorph.2016.01.017
Evans, D. J. A., Strzelecki, M., Milledge, D. G., & Orton, C. (2012). Hørbyebreen polythermal glacial landsystem, Svalbard. *Journal of Maps*, *8*(2), 146–156. https://doi.org/10.1080/17445647.2012.680776
Evans, D. J. A., Twigg, D. R., Rea, B. R., & Shand, M. (2007). Surficial geology and geomorphology of the Bruarjökull surging glacier landsystem. *Journal of Maps*, *3*(1), 349–367. https://doi.org/10.1080/jom.2007.9710850
Everest, J., & Bradwell, T. (2003). Buried glacier ice in southern Iceland and its wider significance. *Geomorphology*, *52*(3–4), 347–358. https://doi.org/10.1016/S0169-555X(02)00277-5
Eyles, N., & Rogerson, R. J. (1978). A framework for the investigation of medial moraine formation: Austerdalsbreen, Norway and Berenden Glacier, British Columbia, Canada. *Journal of Glaciology*, *20*, 99–113. https://doi.org/10.3189/S0022143000021249
Fahnestock, M. A., Scambos, T. A., Bindschadler, R. A., & Kvaran, G. (2000). A millennium of variable ice flow recorded by the Ross Ice Shelf, Antarctica. *Journal of Glaciology*, *46*, 652–664. https://doi.org/10.3189/172756500781832693
Faria, S. H., Weikusat, I., & Azuma, N. (2014a). The microstructure of polar ice. Part I: Highlights from ice core research. *Journal of Structural Geology*, *61*, 2–20. https://doi.org/10.1016/j.jsg.2013.09.010
Faria, S. H., Weikusat, I., & Azuma, N. (2014b). The microstructure of polar ice. Part II: State of the art. *Journal of Structural Geology*, *61*, 21–49. https://doi.org/10.1016/j.jsg.2013.11.003
Ferguson, R. I. (1973). Sinuosity of supraglacial streams. *Bulletin of the Geological Society of America*, *84*(1), 251–256. https://doi.org/10.1130/0016-7606(1973)
Fitzsimons, S. (2003). Ice-marginal terrestrial landsystems: Polar-continental glacier margins. In D. J. A. Evans (Ed.), *Glacial landsystems* (pp. 89–110). Arnold.
Fitzsimons, S., & Howarth, J. (2019). Development of push moraines in deeply frozen sediment adjacent to a cold-based glacier in the McMurdo Dry Valleys, Antarctica. *Earth Surface Processes and Landforms*, *45*(3), 622–637. https://doi.org/10.1002/esp.4759
Fitzsimons, S., Webb, N., Mager, S., MacDonell, S., Lorrain, R., & Samyn, D. (2008). Mechanisms of basal ice formation in polar glaciers: An evaluation of the apron entrainment model. *Journal of Geophysical Research*, *113*(F2), F02010. https://doi.org/10.1029/2006JF000698
Fitzsimons, S. J. (1996). Formation of thrust-block moraines at the margins of dry-based glaciers, south Victoria Land, Antarctica. *Annals of Glaciology*, *22*, 68–74. https://doi.org/10.3189/1996AoG22-1-68-74
Fitzsimons, S. J., & Colhoun, E. A. (1995). Form, structure and stability of the margin of the Antarctic ice sheet, Vestfold Hills and Bunger Hills, East Antarctica. *Antarctic Science*, *2*, 171–179. https://doi.org/10.1017/S095410209500023X
Fleming, E., Lovell, H., Stevenson, C., Petronis, M., Benn, D., Hambrey, M., & Fairchild, I. J. (2013). Magnetic fabrics in the basal ice of a surge-type glacier. *Journal of Geophysical Research: Earth Surface*, *118*, 1–2278. https://doi.org/10.1002/jgrf.20144
Forbes, J. D. (1859). *Occasional papers on the theory of glaciers*. Adam and Charles Black. Retrieved from https://archive.org/stream/occasionalpapers00forbrich#page/n7/mode/2up
Forbes, J. D. (1900). *Travels through the Alps*. Adam and Charles Black.
Forster, R. R., Rignot, E., Isacks, B. L., & Jezek, K. C. (1999). Interferometric radar observations of glaciares Europa and Penguin, Hielo Patagónico Sur, Chile. *Journal of Glaciology*, *45*, 325–337. https://doi.org/10.3189/S0022143000001829
Fossen, H. (2010). *Structural geology*. Cambridge University Press.
Fountain, A. G., Jacobel, R. W., Schlichting, R., & Jansson, P. (2005). Fractures as the main pathways of water flow in temperate glaciers. *Letters to Nature*, *433*, 618–621. https://doi.org/10.1038/nature03296
Fountain, A. G., Schlichting, R. B., Jansson, P., & Jacobel, R. W. (2005). Observations of englacial water passages: A fracture-dominated system. *Annals of Glaciology*, *40*, 25–30. https://doi.org/10.3189/172756405781813762
Fountain, A. G., & Walder, J. (1998). Water flow through temperate glaciers. *Reviews of Geophysics*, *36*, 299–328. https://doi.org/10.1029/97RG03579
Frappé-Sénéclauze, T.-P., & Clarke, G. K. C. (2007). Slow surge of Trapridge Glacier, Yukon Territory, Canada. *Journal of Geophysical Research*, *112*, F03S32. https://doi.org/10.1029/2006JF0040607
Fricker, H. A., Young, N. W., Allison, I., & Coleman, R. (2002). Iceberg calving from the Amery ice shelf, East Antarctica. *Annals of Glaciology*, *34*, 241–246. https://doi.org/10.3189/172756402781817581
Gaffey, C., & Bhardwaj, A. (2020). Applications of unmanned aerial vehicles in cryosphere: Latest advances and prospects. *Remote Sensing*, *12*(6), 948. https://doi.org/10.3390/rs12060948
Garwood, E. J., & Gregory, J. W. (1898). Contribution to the glacial geology of Spitsbergen. *Quarterly Journal of the Geological Society*, *54*, 197–227. https://doi.org/10.1144/GSL.JGS.1898.054.01-04.18
Glasser, N. F., & Gudmundsson, G. H. (2012). Longitudinal surface structures (flowstripes) on Antarctic glaciers. *The Cryosphere*, *6*, 383–391. https://doi.org/10.5194/tc-6-383-2012
Glasser, N. F., & Hambrey, M. J. (2002). Sedimentary facies and landform genesis at a temperate outlet glacier: Soler Glacier, North Patagonian Icefield. *Sedimentology*, *49*, 43–64. https://doi.org/10.1046/j.1365-3091.2002.00431.x
Glasser, N. F., & Hambrey, M. J. (2003). Ice-marginal terrestrial landsystems: Svalbard polythermal glaciers. In D. J. A. Evans (Ed.), *Glacial landsystems* (pp. 65–88). Arnold.
Glasser, N. F., Hambrey, M. J., Crawford, K. R., Bennett, M. R., & Huddart, D. (1998). The structural glaciology of Kongsvegen, Svalbard, and its role in landform genesis. *Journal of Glaciology*, *44*, 136–148. https://doi.org/10.3189/S0022143000002422
Glasser, N. F., Hambrey, M. J., Etienne, L., Jansson, P., & Pettersson, R. (2003). The origin and significance of debris-charged ridges at the surface of Storglaciären, northern Sweden. *Geografiska Annaler*, *85*(A), 127–147. https://doi.org/10.1111/1468-0459.00194
Glasser, N. F., Holt, T., Fleming, E., & Stevenson, C. (2014). Ice shelf history determined from deformation styles in surface debris. *Antarctic Science*, *26*(6), 661–673. https://doi.org/10.1017/S0954102014000376
Glasser, N. F., Jennings, S. J. A., Hambrey, M. J., & Hubbard, B. (2015). Origin and dynamic significance of longitudinal structures ("flow stripes") in the Antarctic ice sheet. *Earth Surface Dynamics*, *3*, 239–249. https://doi.org/10.5194/esurf-3-239-2015
Glasser, N. F., Kulessa, B., Luckman, A., Jansen, D., King, E. C., Sammonds, P. R., et al. (2009). Surface structure and stability of the Larsen C ice shelf, Antarctic Peninsula. *Journal of Glaciology*, *55*(191), 400–410. https://doi.org/10.3189/002214309788816597
Glasser, N. F., & Scambos, T. A. (2008). A structural glaciological analysis of the 2002 Larsen B Ice Shelf collapse. *Journal of Glaciology*, *54*, 3–16. https://doi.org/10.3189/002214308784409017
Glasser, N. F., Scambos, T. A., Bohlander, J., Truffer, M., Pettit, E., & Davies, B. J. (2011). From ice-shelf tributary to tidewater glacier: Continued rapid recession, acceleration and thinning of Röhss Glacier following the 1995 collapse of the Prince Gustav Ice Shelf, Antarctic Peninsula. *Journal of Glaciology*, *57*, 397–406. https://doi.org/10.3189/002214311796905578

Glen, J. W. (1955). The creep of polycrystalline ice. *Proceedings of the Royal Society London, Series A*, *228*, 519–538. https://doi.org/10.1098/rspa.1955.0066
Goldthwait, R. P. (1951). Development of end moraines in east-central Baffin Island. *The Journal of Geology*, *59*, 567–577. https://doi.org/10.1086/625912
Gong, Y., Zwinger, T., Åström, J., Altena, B., Schellenberger, T., Gladstone, R., & Moore, J. (2018). Simulating the roles of crevasse routing of surface water and basal friction on the surge evolution of Basin 3, Austfonna ice cap. *The Cryosphere*, *12*(5), 1563–1577. https://doi.org/10.5194/tc-12-1563-2018
Goodsell, B., Hambrey, M. J., & Glasser, N. F. (2002). Formation of band ogives and associated structures at Bas Glacier d'Arolla, Valais, Switzerland. *Journal of Glaciology*, *48*, 287–300. https://doi.org/10.3189/172756502781831494
Goodsell, B., Hambrey, M. J., & Glasser, N. F. (2005). Debris transport in a temperate valley glacier: Haut Glacier d'Arolla, Valais, Switzerland. *Journal of Glaciology*, *51*, 139–146. https://doi.org/10.3189/172756505781829647
Goodsell, B., Hambrey, M. J., Glasser, N. F., Nienow, P., & Mair, D. (2005). The structural glaciology of a temperate valley glacier: Haut Glacier d'Arolla, Valais, Switzerland. *Arctic Antarctic and Alpine Research*, *37*, 218–232. https://doi.org/10.1657/1523-0430(2005)037[0218:TSGOAT]2.0.CO;2
Gow, A. J. (1972). Glaciological investigations of Antarctica. *Antarctic Journal of the United States*, *7*, 100–101.
Gravenor, C. P., & Kupsch, W. O. (1959). Ice-disintegration features in western Canada. *The Journal of Geology*, *67*(1), 48–64. https://doi.org/10.1086/626557
Gray, M. B., & Mitra, G. (1993). Migration of deformation fronts during progressive deformation: Evidence from detailed structural studies in the Pennsylvania Anthracite region, USA. *Journal of Structural Geology*, *15*, 435–449. https://doi.org/10.1016/0191-8141(93)90139-2
Grönvold, K., Óskarsson, N., Johnsen, S. J., Clausen, H. B., Hammer, C. U., Bond, G., & Bard, E. (1995). Ash layers from Iceland in the Greenland GRIP ice core correlated with oceanic and land sediments. *Earth and Planetary Science Letters*, *135*(1–4), 149–155. https://doi.org/10.1016/0012-821X(95)00145-3
Grove, J. M. (1960a). A study of Veslgjuv-breen. In W. V. Lewis (Ed.), *Norwegian cirque glaciers, Royal Geographical Society Research Series* (pp. 69–82). Royal Geographical Society.
Grove, J. M. (1960b). The bands and layers of Vesl-Skautbreen. In W. V. Lewis (Ed.), *Norwegian cirque glaciers, Royal Geographical SocietyRresearch Series* (pp. 69–82). Royal Geographical Society.
Gudmundsson, G. H., De Rydt, J., & Nagler, T. (2017). Five decades of strong temporal variability in the flow of Brunt ice shelf. *Journal of Glaciology*, *63*, 165–175. https://doi.org/10.1017/jog.2016.132
Gudmundsson, G. H., Iken, A., & Funk, M. (1997). Measurements of ice deformation at the confluence area of Unteraargletscher, Bernese Alps, Switzerland. *Journal of Glaciology*, *43*, 548–556. https://doi.org/10.3189/S0022143000035152
Gudmundsson, G. H., Raymond, C. F., & Bindschadler, R. (1998). The origin and longevity of flow-stripes on Antarctic ice streams. *Annals of Glaciology*, *27*, 145–152. https://doi.org/10.3189/1998AoG27-1-145-152
Gulley, J. (2009). Structural control of englacial conduits in the temperate Matanuska Glacier, Alaska, USA. *Journal of Glaciology*, *55*(192), 681–690. https://doi.org/10.3189/002214309789470860
Gulley, J., & Benn, D. I. (2007). Structural control of englacial drainage systems in Himalayan debris-covered glaciers. *Journal of Glaciology*, *53*(182), 399–412. https://doi.org/10.3189/002214307783258378
Gulley, J. D., Benn, D. I., Müller, D., & Luckman, A. (2009). A cut-and-closure origin from englacial conduits in uncrevassed regions of polythermal glaciers. *Journal of Glaciology*, *55*, 66–80. https://doi.org/10.3189/002214309788608930
Gulley, J. D., Benn, D. I., Screaton, L., & Martin, J. (2009). Mechanisms of englacial conduit formation and implications for subglacial recharge. *Quaternary Science Reviews*, *28*, 1984–1999. https://doi.org/10.1016/j.quascirev.2009.04.002
Gunn, B. (1964). Flow rates and secondary structures of Fox and Franz Josef glaciers, New Zealand. *Journal of Glaciology*, *5*(38), 173–190. https://doi.org/10.3189/S0022143000028768
Hambrey, M. J. (1974). Oxygen isotope studies at Charles Rabots Bre, Okstindan, northern Norway. *Geografiska Annaler—Series A: Physical Geography*, *56*(3–4), 147–158. https://doi.org/10.1080/04353676.1974.11879896
Hambrey, M. J. (1975). The origin of foliation in glaciers: Evidence from some Norwegian examples. *Journal of Glaciology*, *14*, 181–185. https://doi.org/10.3189/S0022143000013496
Hambrey, M. J. (1976a). Debris, bubble and crystal fabric characteristics of foliated glacier ice, Charles Rabots Bre, Okstindan, Norway. *Arctic and Alpine Research*, *8*, 49–60. https://doi.org/10.1080/00040851.1976.12003861
Hambrey, M. J. (1976b). Structure of the glacier Charles Rabots Bre, Norway. *The Geological Society of America Bulletin*, *87*, 1629–1637. https://doi.org/10.1130/0016-7606(1976)87%3C1629:SOTGCR%3E2.0.CO;2
Hambrey, M. J. (1977a). Foliation, minor folds and strain in glacier ice. *Tectonophysics*, *39*, 397–416. https://doi.org/10.1016/0040-1951(77)90106-8
Hambrey, M. J. (1977b). Structures in ice cliffs at the snouts of three Swiss glaciers. *Journal of Glaciology*, *18*, 407–414. https://doi.org/10.3189/S0022143000021080
Hambrey, M. J. (1977c). Supraglacial drainage and its relationship to structure with particular reference to Charles Rabots Bre, Okstindan, Norway. *Norsk Geogrrafisk Tidsskrift*, *31*, 69–77. https://doi.org/10.1080/00291957708545319
Hambrey, M. J. (1979). Crystal orientation fabrics in relation to structures and strain, Griesgletscher, Switzerland. *Zeitskrift für Gletscherkunde und Glazialgeologie*, *15*, 73–86.
Hambrey, M. J. (1994). *Glacial environments*. UCL Press.
Hambrey, M. J., & Alean, J. C. (2017). *Colour Atlas of glacial phenomena*. CRC Press.
Hambrey, M. J., Bennett, M. R., Dowdeswell, J. A., Glasser, N. F., & Huddart, D. (1999). Debris entrainment and transfer in polythermal valley glaciers. *Journal of Glaciology*, *45*, 69–86. https://doi.org/10.3189/S0022143000003051
Hambrey, M. J., & Clarke, G. K. C. (2019). Structural evolution during cyclic glacier surges: 1. Structural glaciology of Trapridge Glacier, Yukon, Canada. *Journal of Geophysical Research: Earth Surface*, *124*(2), 464–494. https://doi.org/10.1029/2018JF004870
Hambrey, M. J., Davies, B. J., Glasser, N. F., Holt, T. O., Smellie, J. L., & Carrivick, J. L. (2015). Structure and sedimentology of George VI ice shelf, Antarctic Peninsula: Implications for ice-sheet dynamics and landform development. *Journal of the Geological Society*, *172*(5), 599–613. https://doi.org/10.1144/jgs2014-134
Hambrey, M. J., & Dowdeswell, J. A. (1994). Flow regime of the Lambert Glacier-Amery ice shelf system, Antarctica: Structural evidence from Landsat imagery. *Annals of Glaciology*, *20*, 401–406. https://doi.org/10.3189/1994AoG20-1-401-406
Hambrey, M. J., & Dowdeswell, J. A. (1997). Structural evolution of a surge-type polythermal glacier: Hessbreen, Svalbard. *Annals of Glaciology*, *24*, 375–381. https://doi.org/10.3189/S0260305500012477

Hambrey, M. J., Dowdeswell, J. A., Murray, T., & Porter, P. R. (1996). Thrusting and debris entrainment in a surging glacier, Bakaninbreen, Svalbard. *Annals of Glaciology*, *22*, 241–248. https://doi.org/10.3189/1996AoG22-1-241-248
Hambrey, M. J., & Fitzsimons, S. J. (2010). Development of sediment-landform associations at cold glacier margins, Dry Valleys, Antarctica. *Sedimentology*, *57*, 857–882. https://doi.org/10.1111/j.1365-3091.2009.01123.x
Hambrey, M. J., & Glasser, N. F. (2003). The role of folding and foliation development in the genesis of medial moraines: Examples from Svalbard Glaciers. *The Journal of Geology*, *111*, 471–485. https://doi.org/10.1086/375281
Hambrey, M. J., & Glasser, N. F. (2012). Discriminating glacier thermal and dynamic regimes in the sedimentary record. *Sedimentary Geology*, *251*, 1–33. https://doi.org/10.1016/j.sedgeo.2012.01.008
Hambrey, M. J., & Huddart, D. (1995). Englacial and proglacial glaciotectonic processes at the snout of a thermally complex glacier in Svalbard. *Journal of Quaternary Science*, *10*, 313–326. https://doi.org/10.1002/jqs.3390100402
Hambrey, M. J., Huddart, D., Bennett, M. R., & Glasser, N. F. (1997). Genesis of "hummocky moraines" by thrusting in glacier ice: Evidence from Svalbard and Britain. *Journal of the Geological Society*, *154*, 623–632. https://doi.org/10.1144/gsjgs.154.4.0623
Hambrey, M. J., & Lawson, W. (2000). Structural styles and deformation fields in glaciers: A review. In A. J. Maltman, B. Hubbard, & M. J. Hambrey (Eds.), *Deformation of glacial materials* (Vol. 176, pp. 59–83). Geological Society London Special Publications. https://doi.org/10.1144/GSL.SP.2000.176.01.06
Hambrey, M. J., & Milnes, A. G. (1975). Boudinage in glacier ice—Some examples. *Journal of Glaciology*, *14*, 383–393. https://doi.org/10.3189/S0022143000021912
Hambrey, M. J., & Milnes, A. G. (1977). Structural geology of an Alpine glacier (Griesgletscher, Valais, Switzerland). *Eclogae Geologicae Helvetia*, *70*, 667–684.
Hambrey, M. J., Milnes, A. G., & Siegenthaler, H. (1980). Dynamics and structure of Griesgletscher, Switzerland. *Journal of Glaciology*, *25*, 215–228. https://doi.org/10.3189/S0022143000010455
Hambrey, M. J., & Müller, F. (1978). Structures and ice deformation in the White Glacier, Axel Heiberg Island, North West Territories, Canada. *Journal of Glaciology*, *20*, 41–66. https://doi.org/10.3189/S0022143000021213
Hambrey, M. J., Murray, T., Glasser, N. F., Hubbard, A., Hubbard, B., Stuart, G., et al. (2005). Structure and changing dynamics of a polythermal valley glacier on a centennial timescale: Midre Lovénbreen, Svalbard. *Journal of Geophysical Research*, *110*, R01006. https://doi.org/10.1029/2004JR000128
Hambrey, M. J., Quincey, D. J., Glasser, N. F., Reynolds, J. M., Richardson, S. J., & Clemmens, S. (2008). Sedimentological, geomorphological and dynamic context of debris-mantled glaciers, Mount Everest (Sagarmatha) region, Nepal. *Quaternary Science Reviews*, *27*, 2361–2389. https://doi.org/10.1016/j.quascirev.2008.08.010
Hansen, L. U., Piotrowski, J. A., Benn, D. I., & Sevestre, H. (2020). A cross-validated three-dimensional model of an englacial and subglacial drainage system in a High-Arctic glacier. *Journal of Glaciology*, *66*(256), 278–290. https://doi.org/10.1017/jog.2020.1
Harper, J., Bradford, J., Humphrey, N., & Meierbachtol, T. (2010). Vertical extension of the subglacial drainage system into basal crevasses. *Nature*, *467*, 579–582. https://doi.org/10.1038/nature09398
Harper, J. T., Humphreys, N. F., & Pfeffer, W. T. (1998). Crevasse patterns and the strain-rate tensor: A high-resolution comparison. *Journal of Glaciology*, *44*, 68–76. https://doi.org/10.3189/S0022143000002367
Harper, J. T., Humphreys, N. F., Pfeffer, W. T., Huzurbazar, S. V., Bahr, D. B., & Welch, B. C. (2001). Spatial variability in the flow of a valley glacier: Deformation of a large array of boreholes. *Journal of Geophysical Research: Solid Earth*, *106*, 8547–8562. https://doi.org/10.1029/2000JB900440
Hart, J. K. (1998). The deforming bed/debris-rich basal ice continuum and its implications for the formation of glacial landforms (flutes) and sediments (melt-out till). *Quaternary Science Reviews*, *17*(8), 737–754. https://doi.org/10.1016/S0277-3791(98)00065-6
Hart, J. K., & Watts, R. J. (1997). A comparison of the styles of deformation associated with two recent push moraines, South Van Keulenfjorden, Svalbard. *Earth Surface Processes and Landforms*, *22*, 1089–1107. https://doi.org/10.1002/(SICI)1096-9837(199712)22:12<1089::AID-ESP804>3.0.CO;2-8
Hattersley-Smith, G. (1957). The rolls on the Ellesmere ice shelf. *Arctic*, *10*(1), 32–44. https://doi.org/10.14430/arctic3753
Head, J. W., & Marchant, D. R. (2003). Cold-based mountain glaciers on Mars: Western Arsia Mons. *Geology*, *31*, 641–644. https://doi.org/10.1130/0091-7613(2003)031<0641:CMGOMW>2.0.CO;2
Head, J. W., & Marchant, D. R. (2014). The climate history of early Mars: Insights from the Antarctic McMurdo Dry Valleys hydrologic system. *Antarctic Science*, *26*, 774–800. https://doi.org/10.1017/S0954102014000686
Hellmann, S., Kerch, J., Weikusat, I., Bauder, A., Grab, M., Jouvet, G., et al. (2020). Crystallographic analysis of temperate ice on Rhonegletscher, Swiss Alps. *The Cryosphere*, *15*(2), 677–694. https://doi.org/10.5194/tc-2020-133
Hepburn, A. J., Ng, F. S. L., Livingstone, S. J., Holt, T. O., & Hubbard, B. (2019). Polyphase mid-latitude glaciation on Mars: Chronology of the formation of superposed glacier-like forms from crater-count dating. *Journal of Geophysical Research: Planets*, *125*(2), e2019JE006102. https://doi.org/10.1029/2019JE006102
Herbst, P., & Neubauer, F. (2000). The Pasterze glacier, Austria: An analogue of an extensional allochthon. In A. J. Maltman, B. Hubbard, & M. J. Hambrey (Eds.), *Deformation of glacial materials* (Vol. 176, pp. 159–168). Geological Society London Special Publications. https://doi.org/10.1144/GSL.SP.2000.176.01.12
Herbst, P., Neubauer, F., & Schöpfer, M. P. J. (2006). The development of brittle structures in an alpine valley glacier: Pasterzenkees, Austria, 1887–1997. *Journal of Glaciology*, *52*, 128–136. https://doi.org/10.3189/172756506781828872
Herzfeld, U. C., Clarke, G. K. C., Mayer, H., & Greve, R. (2004). Derivation of deformation characteristics in fast-moving glaciers. *Computers & Geosciences*, *30*, 291–302. https://doi.org/10.1016/j.cageo.2003.10.012
Herzfeld, U. C., & Mayer, H. (1997). Surge of Bering Glacier and Bagley Ice Field, Alaska: An update to August 1995 and an interpretation of brittle-deformation patterns. *Journal of Glaciology*, *43*(145), 427–434. https://doi.org/10.3189/S0022143000035012
Hobbs, B. E., Means, W. D., & Williams, P. F. (1976). *An outline of structural geology*. John Wiley and Sons.
Hodgkins, R., & Dowdeswell, J. A. (1994). Tectonic processes in Svalbard tide-water glacier surges: Evidence from structural glaciology. *Journal of Glaciology*, *40*(136), 553–560. https://doi.org/10.3189/S0022143000012430
Hodson, A., Anesio, A. M., Tranter, M., Fountain, A. G., Osborn, M., Priscu, J. C., et al. (2008). Glacial ecosystems. *Ecological Monographs*, *78*(1), 41–67. https://doi.org/10.1890/07-0187.1
Holdsworth, G. (1969). Primary transverse crevasses. *Journal of Glaciology*, *8*(52), 107–129. https://doi.org/10.3189/S0022143000020797
Holland, P. R., Corr, H. F. J., Vaughan, D. G., Jenkins, A., & Skvarca, P. (2009). Marine ice in Larsen Ice Shelf. *Geophysical Research Letters*, *36*, L11604. https://doi.org/10.1029/2009gl038162
Holmlund, P. (1988). Internal geometry and evolution of moulins, Storglaciären, Sweden. *Journal of Glaciology*, *34*, 242–248. https://doi.org/10.3189/S0022143000032305

Holt, T., Glasser, N., & Quincey, D. (2013). The structural glaciology of southwest Antarctic Peninsula ice shelves. *Journal of Maps*, *9*(4), 523–531. https://doi.org/10.1080/17445647.2013.822836
Holt, T. O., Glasser, N. F., Fricker, H. A., Padman, L., Luckman, A., King, O., et al. (2014). The structural and dynamic responses of Stange ice shelf to recent environmental change. *Antarctic Science*, *26*(6), 646–660. https://doi.org/10.1017/S095410201400039X
Holt, T. O., Glasser, N. F., Quincey, D., & Siegfried, M. R. (2013). Speedup and fracturing of George VI ice shelf, Antarctic Peninsula. *The Cryosphere*, *7*, 797–816. https://doi.org/10.5194/tcd-7-373-2013
Hooke, R. L. B. (1973). Flow near the margin of the Barnes Ice Cap, and the development of ice-cored moraines. *The Geological Society of America Bulletin*, *84*(12), 3929–3948. https://doi.org/10.1130/0016-7606(1973)84<3929:FNTMOT>2.0.CO;2
Hooke, R. L. B. (2019). *Principles of glacier mechanics*. Cambridge University Press.
Hooke, R. L. B., & Hudleston, P. (1978). Origin of foliation in glaciers. *Journal of Glaciology*, *20*, 285–299. https://doi.org/10.3189/S0022143000013848
Hopkins, W. (1862). On the theory of the motion of glaciers. *Philosophical Transactions of the Royal Society London*, *152*, 677–745. https://doi.org/10.1098/rstl.1862.0034
Hubbard, A., Blatter, H., Nienow, P., Mair, D., & Hubbard, B. (1998). Comparison of a three-dimensional model for glacier flow with field data at Haut Glacier d'Arolla, Switzerland. *Journal of Glaciology*, *44*, 368–378. https://doi.org/10.3189/S0022143000002690
Hubbard, A., & Hubbard, B. (2000). The potential contribution of high-resolution glacier flow modelling to structural glaciology. In A. J. Maltman, B. Hubbard, & M. J. Hambrey (Eds.), *Deformation of glacial materials* (Vol. 176, pp. 133–146). Geological Society London Special Publications. https://doi.org/10.1144/GSL.SP.2000.176.01.10
Hubbard, B., Christoffersen, P., Doyle, S. H., Chudley, T. R., Schoonman, C. M., Law, R., & Bougamont, M. (2021). Boreholde-based characterization of deep mixed-mode crevasses at a Greenlandic outlet glacier. *AGU Advances*, *2*(2), e2020AV000291. https://doi.org/10.1029/2020AV000291
Hubbard, B., Cook, S., & Coulson, H. (2009). Basal ice facies: A review and unifying approach. *Quaternary Science Reviews*, *28*, 1956–1969. https://doi.org/10.1016/j.quascirev.2009.03.005
Hubbard, B., Glasser, N., Hambrey, M., & Etienne, J. (2004). A sedimentological and isotopic study of the origin of supraglacial debris bands: Kongsfjorden, Svalbard. *Journal of Glaciology*, *50*, 157–170. https://doi.org/10.3189/172756504781830114
Hubbard, B., Luckman, A., Ashmore, D. W., Bevan, S., Kulessa, B., Munneke, P. K., et al. (2016). Massive subsurface ice formed by refreezing of ice-shelf ponds. *Nature Communications*, *7*, 11897. https://doi.org/10.1038/ncomms11897
Hubbard, B., & Malone, T. (2013). Optical-televiewer-based logging of the uppermost 630 m of the NEEM deep ice borehole, Greenland. *Annals of Glaciology*, *54*(64), 83–89. https://doi.org/10.3189/2013AoG64A201
Hubbard, B., Milliken, R. E., Kargel, J. S., Limaye, A., & Souness, C. (2011). Geomorphological characterisation and interpretation of a mid-latitude glacier-like form: Hellas Planitia, Mars. *Icarus*, *211*, 330–346. https://doi.org/10.1016/j.icarus.2010.10.021
Hubbard, B., Roberson, S., Samyn, D., & Merton-Lyn, D. (2008). Digital optical televiewing of ice boreholes. *Journal of Glaciology*, *54*(188), 823–830. https://doi.org/10.3189/002214308787779988
Hubbard, B., & Sharp, M. (1989). Basal ice formation and deformation: A review. *Progress in Physical Geography*, *13*, 529–558. https://doi.org/10.1177/030913338901300403
Hubbard, B., & Sharp, M. (1993). Weertman regelation, multiple refreezing events and the isotopic evolution of the basal ice layer. *Journal of Glaciology*, *39*(132), 275–291. https://doi.org/10.3189/S002214300001594X
Hubbard, B., & Sharp, M. (1995). Basal ice facies and their formation in the western Alps. *Arctic and Alpine Research*, *27*(4), 301–310. https://doi.org/10.1080/00040851.1995.12003127
Hubbard, B., Souness, C., & Brough, S. (2014). Glacier-like forms on Mars. *The Cryosphere*, *8*, 2047–2061. https://doi.org/10.5194/tc-8-2047-2014
Hubbard, B., Tison, J.-L., Pattyn, F., Dierckx, M., Boereboom, T., & Samyn, D. (2012). Optical-televiewer-based identification and characterization of material facies associated with an Antarctic ice-shelf rift. *Annals of Glaciology*, *53*(60), 137–146. https://doi.org/10.3189/2012AoG60A045
Huddart, D., & Hambrey, M. J. (1996). Sedimentary and tectonic development of a high-Arctic, thrust-moraine complex: Comfortlessbreen, Svalbard. *Boreas*, *25*, 227–243. https://doi.org/10.1111/j.1502-3885.1996.tb00639.x
Hudleston, P. J. (1976). Recumbent folding in the base of the Barnes Ice Cap, Baffin Island, Northwest Territories, Canada. *The Geological Society of America Bulletin*, *87*(12), 1684–1692. https://doi.org/10.1130/0016-7606(1976)87%3C1684:RFITBO%3E2.0.CO;2
Hudleston, P. J. (1977). Similar folds, recumbent folds, and gravity tectonics in ice and rocks. *The Journal of Geology*, *85*(1), 113–122. https://doi.org/10.1086/628272
Hudleston, P. J. (1983). Strain patterns in an ice cap and implications for strain variations in shear zones. *Journal of Structural Geology*, *5*, 455–463. https://doi.org/10.1016/B978-0-08-030273-7.50024-0
Hudleston, P. J. (1989). The association of folds and veins in shear zones. *Journal of Structural Geology*, *11*, 949–957. https://doi.org/10.1016/0191-8141(89)90046-1
Hudleston, P. J. (2015). Structures and fabrics in glacial ice: A review. *Journal of Structural Geology*, *81*, 1–27. https://doi.org/10.1016/j.jsg.2015.09.003
Hudleston, P. J., & Hooke, R. L. B. (1980). Cumulative deformation in the Barnes Ice Cap, and implications for the development of foliation. *Tectonophysics*, *66*, 127–146. https://doi.org/10.1016/0040-1951(80)90042-6
Hudleston, P. J., & Treagus, S. H. (2010). Information from folds: A review. *Journal of Structural Geology*, *32*(12), 2042–2071. https://doi.org/10.1016/j.jsg.2010.08.001
Hulbe, C. L., & Fahnestock, M. A. (2004). West Antarctic ice-stream discharge variability: Mechanism, controls and pattern of grounding-line retreat. *Journal of Glaciology*, *50*, 471–484. https://doi.org/10.3189/172756504781829738
Hulbe, C. L., & Fahnestock, M. A. (2007). Century-scale discharge stagnation and reactivation of the Ross ice streams, West Antarctica. *Journal of Geophysical Research*, *112*, F03S27. https://doi.org/10.1029/2006JF000603
Hulbe, C. L., LeDoux, C., & Cruikshank, K. (2010). Propagation of long fractures in the Ronne Ice Shelf, Antarctica, investigated using a numerical model of fracture propagation. *Journal of Glaciology*, *56*(197), 459–472. https://doi.org/10.3189/002214310792447743
Hulbe, C. L., Scambos, T. A., Youngberg, T., & Lamb, A. K. (2008). Patterns of glacier response to disintegration of the Larsen B ice shelf, Antarctic Peninsula. *Global and Planetary Change*, *63*(1), 1–8. https://doi.org/10.1016/j.gloplacha.2008.04.001
Hulbe, C. L., & Whillans, I. M. (1997). Weak bands within Ice Stream B, West Antarctica. *Journal of Glaciology*, *43*, 377–386. https://doi.org/10.3189/S002214300003495X
Humbert, A., & Steinhage, D. (2011). The evolution of the western rift area of the Fimbul Ice Shelf, Antarctica. *The Cryosphere*, *5*(4), 931–944. https://doi.org/10.5194/tc-5-931-2011

Humlum, O., Instanes, A., & Sollid, J. L. (2003). Permafrost in Svalbard: A review of research history, climatic background and engineering challenges. *Polar Research*, *22*(2), 191–215. https://doi.org/10.1111/j.1751-8369.2003.tb00107.x
Irvine-Fynn, T., Edwards, A., & Mitchell, A. (2015). Is there life on glaciers? *Geography Review*, *28*, 38–41.
Irvine-Fynn, T. D. L., Hodson, A. J., Moorman, B. J., Vatne, G., & Hubbard, A. L. (2011). Polythermal glacier hydrology: A review. *Reviews in Geophysics*, *49*, RG4002. https://doi.org/10.1029/2010RG000350
Iverson, N. R., & Semmens, D. J. (1995). Intrusion of ice into porous media by regelation: A mechanism of sediment entrainment by glaciers. *Journal of Geophysical Research*, *100*(B6), 10219–10230. https://doi.org/10.1029/95JB00043
Ives, J. D., & King, C. A. M. (1954). Glaciological observations on Morsárjökull S.W. Vatnajökull. *Journal of Glaciology*, *2*(16), 423–423. https://doi.org/10.3189/002214354793702443
Jacobel, R. W., Gades, A. M., Gottschling, D. L., Hodge, S. M., & Wright, D. L. (1993). Interpretation of radar-detected internal layer folding in West Antarctic ice streams. *Journal of Glaciology*, *39*, 528–537. https://doi.org/10.3189/S0022143000016427
Jacobel, R. W., Scambos, T. A., Nereson, N. A., & Raymond, C. F. (2000). Changes in the margin of ice stream C, Antarctica. *Journal of Glaciology*, *46*, 102–110. https://doi.org/10.3189/172756500781833485
Jacobel, R. W., Scambos, T. A., Raymond, C. R., & Gades, A. M. (1996). Changes in the configuration of ice stream flow from the West Antarctic Ice Sheet. *Journal of Geophysical Research*, *101*(B3), 5499–5504. https://doi.org/10.1029/95JB03735
Jacobson, H. P., & Waddington, E. D. (2005). Recumbent folding of divide arches in response to unsteady ice-divide migration. *Journal of Glaciology*, *51*(173), 201–209. https://doi.org/10.3189/172756505781829412
Jansen, D., Luckman, A., Kulessa, B., Holland, P. R., & King, E. C. (2013). Marine ice formation in a suture zone on the Larsen C ice shelf and its influence on ice shelf dynamics. *Journal of Geophysical Research: Earth Surface*, *118*, 1628–1640. https://doi.org/10.1002/jgrf.20120
Jansen, D., Luckman, A. J., Cook, A., Bevan, S., Kulessa, B., Hubbard, B., & Holland, P. R. (2015). Brief communication: Newly developing rift in Larsen C ice shelf presents significant risk to stability. *The Cryosphere*, *9*, 1223–1227. https://doi.org/10.5194/tc-9-1223-2015
Jansson, P., Näslund, J.-O., Pettersson, R., Richardson-Näslund, C., & Holmlund, P. (2000). Debris entrainment and polythermal structure in the terminus of Storglaciären. In M. Nakawo, C. F. Raymond, & A. Fountain (Eds.), *Debris-covered glaciers* (Vol. 264, pp. 143–151). IASH PublicationIAHS Press.
Jeffries, M. O. (1987). The growth, structure and disintegration of Arctic ice shelves. *Polar Record*, *23*(147), 631–649. https://doi.org/10.1017/s0032247400008342
Jeffries, M. O. (1992). Arctic ice shelves and ice islands: Origin, growth and disintegration, physical characteristics, structural-stratigraphic variability, and dynamics. *Reviews of Geophysics*, *30*, 245–267. https://doi.org/10.1029/92RG00956
Jeffries, M. O. (2017). The Ellesmere ice shelves, Nunavut, Canada. In L. Copland, & D. Mueller (Eds.), *Arctic ice shelves and ice islands* (pp. 23–54). Springer. https://doi.org/10.1007/978-94-024-1101-0_2
Jennings, S. J. A. (2017). *Origins of foliations and related phenomena in valley glaciers and ice sheets (Doctoral dissertation)*. Aberystwyth University. https://doi.org/10.13140/RG.2.2.33305.75361
Jennings, S. J. A., Hambrey, M. J., & Glasser, N. F. (2014). Ice flow-unit influence on glacier structure, debris entrainment and transport. *Earth Surface Processes and Landforms*, *39*(10), 1279–1292. https://doi.org/10.1002/esp.3521
Jennings, S. J. A., Hambrey, M. J., Glasser, N. F., James, T. D., & Hubbard, B. (2016). Structural glaciology of Austre Brøggerbreen, northwest Svalbard. *Journal of Maps*, *12*(5), 790–796. https://doi.org/10.1080/17445647.2015.1076744
Jeong, S., Howat, I. M., & Bassis, J. N. (2016). Accelerated ice shelf rifting and retreat at Pine Island Glacier, West Antarctica. *Geophysical Research Letters*, *43*, 11720–11725. https://doi.org/10.1002/2016GL071360
Jezek, K. C. (1984). Recent changes in the dynamic condition of the Ross ice shelf, Antarctica. *Journal of Geophysical Research*, *89*(BI), 409–416. https://doi.org/10.1029/JB089iB01p00409
Jezek, K. C., & Bentley, C. R. (1983). Field studies of bottom crevasses in the Ross ice shelf, Antarctica. *Journal of Glaciology*, *29*(101), 118–126. https://doi.org/10.3189/S0022143000005189
Jezek, K. C., Bentley, C. R., & Clough, J. W. (1979). Electromagnetic sounding of bottom crevasses on the Ross ice shelf, Antarctica. *Journal of Glaciology*, *24*(90), 321–330. https://doi.org/10.3189/S0022143000014842
Jibson, R. W., Harp, E. L., Schulz, W., & Keefer, D. K. (2006). Large rock avalanches triggered by the M 7.9 Denali Fault, Alaska, earthquake of 3 November 2002. *Engineering Geology*, *83*(1–3), 144–160. https://doi.org/10.1016/j.enggeo.2005.06.029
Jiskoot, H., Boyle, P., & Murray, T. (1998). The incidence of glacier surging in Svalbard: Evidence from multivariate statistics. *Computers & Geosciences*, *24*(4), 387–399. https://doi.org/10.1016/S0098-3004(98)00033-8
Jiskoot, H., Fox, T. A., & Van Wychen, W. (2017). Flow and structure in a dendritic glacier with bedrock steps. *Journal of Glaciology*, *63*(241), 912–928. https://doi.org/10.1017/jog.2017.58
Jones, C., Ryan, J., Holt, T., & Hubbard, A. (2018). Structural glaciology of Isunguata Sermia, West Greenland. *Journal of Maps*, *14*(2), 517–527. https://doi.org/10.1080/17445647.2018.1507952
Jordan, J. R., Holland, P. R., Jenkins, A., Piggott, M. D., & Kimura, S. (2014). Modeling ice-ocean interactions in ice-shelf crevasses. *Journal of Geophysical Research: Oceans*, *119*(2), 995–1008. https://doi.org/10.1002/2013JC009208
Kaluzienski, L., Koons, P., Enderlin, E., Hamilton, G., Courville, Z., & Arcone, S. (2019). Crevasse initiation and history within the McMurdo Shear Zone, Antarctica. *Journal of Glaciology*, *65*(254), 989–999. https://doi.org/10.1017/jog.2019.65
Kamb, B., Raymond, C. F., Harrison, W. D., Engelhardt, H., Echelmeyer, K. A., Humphrey, N., et al. (1985). Glacier surge mechanism: 1982–1983 surge of Variegated Glacier, Alaska. *Science*, *227*, 469–479. https://doi.org/10.1126/science.227.4686.469
Kamb, W. B. (1959). Ice petrofabric observations from Blue Glacier, Washington, in relation to theory and experiment. *Journal of Geophysical Research*, *64*(11), 1891–1909. https://doi.org/10.1029/JZ064i011p01891
Kamb, W. B. (1961). The glide direction in ice. *Journal of Glaciology*, *3*(30), 1097–1106. https://doi.org/10.3189/S0022143000017500
Kamintzis, J. E., Jones, J. P. P., Irvine-Fynn, T. D. L., Holt, T. O., Bunting, P., Jennings, S. J. A., et al. (2017). Assessing the applicability of terrestrial laser scanning for mapping englacial conduits. *Journal of Glaciology*, *64*(243), 37–48. https://doi.org/10.1017/jog.2017.81
Kehle, R. O. (1964). Deformation of the Ross ice shelf, Antarctica. *The Geological Society of America Bulletin*, *75*, 259–286. https://doi.org/10.1130/0016-7606(1964)75[259:DOTRIS]2.0.CO;2
Kellerer-Pirklbauer, A., & Kulmer, B. (2019). The evolution of brittle and ductile structures at the surface of a partly debris-covered, rapidly thinning and slowly moving glacier in 1998–2012 (Pasterze Glacier, Austria). *Earth Surface Processes and Landforms*, *44*, 1034–1049. https://doi.org/10.1002/esp.4552
Khazendar, A., & Jenkins, A. (2003). A model of marine ice formation within Antarctic ice shelf rifts. *Journal of Geophysical Research*, *108*, 3235. https://doi.org/10.1029/2002JC001673

Khazendar, A., Rignot, E., & Larour, E. (2011). Acceleration and spatial rheology of Larsen C Ice Shelf, Antarctic Peninsula. *Geophysical Research Letters*, *38*, L09502. https://doi.org/10.1029/2011GL046775
King, C. A. M., & Ives, J. D. (1956). Glaciological observations on some of the outlet glaciers of south-west Vatnajökull, Iceland, 1954: Part II: Ogives. *Journal of Glaciology*, *2*(19), 646–651. https://doi.org/10.3189/S0022143000033098
King, C. A. M., & Lewis, W. V. (1961). A tentative theory of ogive formation. *Journal of Glaciology*, *3*(29), 912–939. https://doi.org/10.3189/S0022143000027283
King, E. C., De Rydt, J., & Gudmundsson, H. (2018). The internal structure on the Brunt Ice Shelf from ice-penetrating radar analysis and implications for ice shelf fracture. *The Cryosphere*, *12*, 3361–3372. https://doi.org/10.5194/tc-12-3361-2018
King, O., Hambrey, M. J., Irvine-Fynn, T. D. L., & Holt, T. O. (2016). The structural, geometric and volumetric changes of a polythermal Arctic glacier during a surge cycle: Comfortlessbreen, Svalbard. *Earth Surface Processes and Landforms*, *41*(2), 162–177. https://doi.org/10.1002/esp.3796
Kirkbride, M. P. (1995). Processes of transportation. In J. Menzies (Ed.), *Modern glacial environments: Processes, dynamics and sediments. Volume 1. Glacial environments*. Butterworth-Heinemann.
Kirkbride, M. P., & Sugden, D. (1992). New Zealand loses its top. *Geographical Magazine*, *64*(7), 30–34.
Knight, P. G. (1992). Ice deformation very close to the ice-sheet margin in West Greenland. *Journal of Glaciology*, *38*(128), 3–8. https://doi.org/10.3189/S0022143000009539
Knight, P. G. (1997). The basal ice layer of glaciers and ice sheets. *Quaternary Science Reviews*, *16*, 975–993. https://doi.org/10.1016/S0277-3791(97)00033-4
Knighton, A. D. (1972). Meandering habit of supraglacial streams. *The Geological Society of America Bulletin*, *83*, 201–204. https://doi.org/10.1130/0016-7606(1972)83[201:MHOSS]2.0.CO;2
Knighton, A. D. (1981). Channel form and flow characteristics of supraglacial streams, Austre Okstindbreen, Norway. *Arctic and Alpine Research*, *13*(3), 295–306. https://doi.org/10.1080/00040851.1981.12004250
Knighton, A. D. (1985). Channel form adjustment in supraglacial streams, Austre Okstindbreen, Norway. *Arctic and Alpine Research*, *17*(4), 451–466. https://doi.org/10.1080/00040851.1985.12004052
Koehn, D., & Bons, P. D. (2014). Micro-dynamics of ice. *Journal of Structural Geology*, *61*, 1. https://doi.org/10.1016/j.jsg.2013.12.001
Kozarski, S., & Szupryczynski, J. (1973). Glacial forms and deposits in the Sidujökull deglaciation area. *Geographia Polonica*, *26*, 255–311.
Krüger, J. (1985). Formation of push moraines at the margin of Hofdabrekkujokull, South Iceland. *Geografiska Annaler*, *67*(A), 199–212. https://doi.org/10.1080/04353676.1985.11880146
Lai, C.-Y., Kingslake, J., Wearing, M. G., Chen, P.-H. C., Gentine, P., Li, H., et al. (2020). Vulnerablility of Antarctica's ice shelves to meltwater-driven fracture. *Nature*, *584*, 574–578. https://doi.org/10.1038/s41586-020-2627-8
Larour, E., Rignot, E., & Aubry, D. (2004). Modelling of rift propagation on Ronne ice shelf, Antarctica, and sensitivity to climate change. *Geophysical Research Letters*, *31*, L16404. https://doi.org/10.1029/2004GL020077
Larsen, N. K., Kronborg, C., Yde, J. C., & Knudsen, N. T. (2010). Debris entrainment by basal freeze-on and thrusting during the 1995–1998 surge of Kuannersuit Glacier on Disko Island, west Greenland. *Earth Surface Processes and Landforms*, *35*(5), 561. https://doi.org/10.1002/esp.1945
Lawson, D. E. (1979). A comparison of the pebble orientations in ice and deposits of the Matanuska Glacier, Alaska. *The Journal of Geology*, *87*(6), 629–645. https://doi.org/10.1086/628457
Lawson, D. E., & Kulla, J. B. (1978). An oxygen isotope investigation of the origin of the basal zone of the Matanuska Glacier, Alaska. *The Journal of Geology*, *86*(6), 673–685. https://doi.org/10.1086/649736
Lawson, D. E., Strasser, J. C., Evenson, E. B., Alley, R. B., Larson, G. J., & Arcone, S. A. (1998). Glaciohydraulic supercooling: A freeze-on mechanism to create stratified, debris-rich basal ice: I. Field evidence. *Journal of Glaciology*, *44*(148), 547–562. https://doi.org/10.3189/S0022143000002069
Lawson, W. (1990). *The structural evolution of variegated Glacier, Alaska (Doctoral dissertation)*. University of Cambridge.
Lawson, W. (1996). Structural evolution of variegated glacier, Alaska, USA, since 1948. *Journal of Glaciology*, *42*, 261–270. https://doi.org/10.3189/S0022143000004123
Lawson, W., Sharp, M. J., & Hambrey, M. J. (2000). Deformation histories and structural assemblages of glacier ice in a non-steady flow regime. In A. J. Maltman, B. Hubbard, & M. J. Hambrey (Eds.), *Deformation of glacial materials* (Vol. 176, pp. 85–96). Geological Society London Special Publications. https://doi.org/10.1144/GSL.SP.2000.176.01.07
Lawson, W. J., Sharp, M. J., & Hambrey, M. J. (1994). The structural geology of a surge-type glacier. *Journal of Structural Geology*, *16*, 1447–1462. https://doi.org/10.1016/0191-8141(94)90008-6
Lee, M. J., Kyle, P. R., Iverson, N. A., Lee, J. I., & Han, Y. (2019). Rittmann volcano, Antarctica as the source of a widespread 1252 ± 2 CE tephra layer in Antarctica ice. *Earth and Planetary Science Letters*, *521*, 169–176. https://doi.org/10.1016/j.epsl.2019.06.002
Lefauconnier, B., & Hagen, J. O. (1991). *Surging and calving glaciers in eastern Svalbard. Norsk Polarinstitutts Meddelelser 116*. Norsk Polarinstitutt.
Le Heron, D. P., & Etienne, J. L. (2005). A complex subglacial clastic dyke swarm, Sólheimajökull, Southern Iceland. *Sedimentary Geology*, *181*(1–2), 25–37. https://doi.org/10.1016/j.sedgeo.2005.06.012
Leonard, K. C., Tremblay, L.-B., MacAyeal, D. R., & Jacobs, S. S. (2008). Interactions of wind-transported snow with a rift in the Ross ice shelf, Antarctica. *Geophysical Research Letters*, *35*(5), L05501. https://doi.org/10.1029/2007GL033005
Lewis, W. V. (Ed.), (1960). *Norwegian cirque glaciers*. Royal Geographical Society Research Series.
Li, T., Zhang, B., Xiao, W., Cheng, X., Li, Z., & Zhao, J. (2020). UAV-based photogrammetry and LiDAR for the characterization of ice morphology evolution. *IEEE Journal of Selected Topics in Applied Earth Observations and Remote Sensing*, *13*, 4188–4199. https://doi.org/10.1109/JSTARS.2020.3010069
Liu, Y., Moore, J. C., Cheng, X., Gladstone, R. M., Bassis, J. N., Liu, H., et al. (2015). Iceberg calving of Antarctic ice shelves. *Proceedings of the National Academy of Sciences*, *112*(11), 3263–3268. https://doi.org/10.1073/pnas.1415137112
Lliboutry, L., & Reynaud, L. (1981). "Global dynamics" of a temperate valley glacier, Mer de Glace, and past velocities deduced from Forbes' bands. *Journal of Glaciology*, *27*(96), 207–226. https://doi.org/10.3189/S0022143000015367
Lønne, I., & Lauritsen, T. (1996). The architecture of a modern push- moraine at Svalbard as inferred from ground-penetrating radar measurements. *Arctic and Alpine Research*, *28*, 488–495. https://doi.org/10.1080/00040851.1996.12003201
Lovell, H., Fleming, E. J., Benn, D. I., Hubbard, B., Lukas, S., & Naegeli, K. (2015). Former dynamic behavior of a cold-based valley glacier on Svalbard revealed by basal ice and structural glaciology investigations. *Journal of Glaciology*, *61*(226), 309–328. https://doi.org/10.3189/2015JoG14J120

Lovell, H., Fleming, E. J., Benn, D. I., Hubbard, B., Lukas, S., Rea, B. R., Noormets, R., et al. (2015). Debris entrainment and landform genesis during tidewater glacier surges. *Journal of Geophysical Research*, *120*(8), 1574–1595. https://doi.org/10.1002/2015JF003509

Lucchitta, B. K. (1981). Mars and Earth: Comparison of cold-climate features. *Icarus*, *45*, 264–303. https://doi.org/10.1016/0019-1035(81)90035-X

Luckman, A., Elvidge, A., Jansen, D., Kulessa, B., Munneke, P. K., King, J., & Barrand, N. E. (2014). Surface melt and ponding on Larsen C ice shelf and the impact of föhn winds. *Antarctic Science*, *26*(6), 625–635. https://doi.org/10.1017/S0954102014000339

Luckman, A., Jansen, D., Kulessa, B., King, E., Sammonds, P., & Benn, D. I. (2012). Basal crevasses in Larsen C ice shelf and implications for their global abundance. *The Cryosphere*, *6*(1), 113–123. https://doi.org/10.5194/tc-6-113-2012

Luckman, A., Murray, T., & Strozzi, T. (2002). Surface flow evolution throughout a glacier surge measured by satellite radar interferometry. *Geophysical Research Letters*, *29*(23), 10-1–10-4. https://doi.org/10.1029/2001GL014570

Lüthi, M. P., Funk, M., & Iken, A. (2003). Indication of active overthrust faulting along the Holocene-Wisconsin transition in the marginal zone of Jakobshavn Isbræ. *Journal of Geophysical Research*, *108*(B11), 2543. https://doi.org/10.1029/2003JB002505

Lysså, A., & Lønne, I. (2001). Moraine development at a small high-Arctic valley glacier: Rieperbreen, Svalbard. *Journal of Quaternary Science*, *16*(6), 519–529. https://doi.org/10.1002/jqs.613

MacAyeal, D. R. (1985). Optimal measurement of ice-sheet deformation from surface-marker arrays. *Journal of Glaciology*, *31*(107), 54–59. https://doi.org/10.3189/S0022143000004998

MacAyeal, D. R. (1992). The basal stress distribution of ice stream E, Antarctica, inferred by control methods. *Journal of Geophysical Research*, *97*(B1), 595–603. https://doi.org/10.1029/91JB02454

MacAyeal, D. R., & Sergienko, O. V. (2013). The flexural dynamics of melting ice shelves. *Annals of Glaciology*, *54*(63), 1–10. https://doi.org/10.3189/2013AoG63A256

MacDonell, S., & Fitzsimons, S. (2008). The formation and hydrological significance of cryoconite holes. *Progress in Physical Geography*, *32*, 595–610. https://doi.org/10.1177/0309133308101382

MacGregor, J. A., Colgan, W. T., Fahnestock, M. A., Morlighem, M., Catania, G. A., Paden, J. D., & Gogineni, S. P. (2016). Holocene deceleration of the Greenland Ice Sheet. *Science*, *351*(6273), 590–593. https://doi.org/10.1126/science.aab1702

MacGregor, J. A., Fahnestock, M. A., Catania, G. A., Paden, J. D., Gogineni, S. P., Young, S. K., et al. (2015). Radiostratigraphy and age structure of the Greenland ice sheet. *Journal of Geophysical Research: Earth Surface*, *120*(2), 212–241. https://doi.org/10.1002/2014JF003215

MacGregor, J. A., Fahnestock, M. A., Colgan, W. T., Larsen, N. K., Kjeldsen, K. K., & Welker, J. M. (2020). The age of surface-exposed ice along the northern margin of the Greenland Ice Sheet. *Journal of Glaciology*, *66*(258), 667–684. https://doi.org/10.1017/jog.2020.62

Mader, H., Pettitt, M. E., Wadham, J. L., Wolff, E. W., & Parkes, R. J. (2006). Subsurface ice as a microbial habitat. *Geology*, *34*, 169–172. https://doi.org/10.1130/G22096.1

Mansell, D., Luckman, A., & Murray, T. (2012). Dynamics of tidewater surge-type glaciers in northwest Svalbard. *Journal of Glaciology*, *58*(207), 110–118. https://doi.org/10.3189/2012JoG11J058

Marmo, B. A., & Wilson, C. J. L. (1998). Strain localization and incremental deformation within ice masses, Framnes Mountains, east Antarctica. *Journal of Structural Geology*, *20*(2–3), 149–162. https://doi.org/10.1016/S191-8141(97)00073-4

Marmo, B. A., & Wilson, C. J. L. (2000). The stress distribution related to the boudinage of a visco-elastic material: Examples from a polar outlet glacier. In A. J. Maltman, B. Hubbard, & M. J. Hambrey (Eds.), *Deformation of glacial materials* (Vol. 176, pp. 115–134). Geological Society London Special Publications. https://doi.org/10.1144/GSL.SP.2000.176.01.09

Martin, C., Gudmundsson, G. H., Pritchard, H. D., & Gagliardini, O. (2009). On the effects of anisotropic rheology on ice flow, internal structure, and the age-depth relationship at ice divides. *Journal of Geophysical Research*, *114*, F04001. https://doi.org/10.1029/2008JF001204

Mayer, H., & Herzfeld, U. C. (2000). Structural glaciology of the fast-moving Jakobshavn Isbræ, Greenland, compared to the surging Bering Glacier, Alaska, USA. *Annals of Glaciology*, *30*, 243–249. https://doi.org/10.3189/172756400781820543

Mayer, H., & Herzfeld, U. C. (2008). The rapid retreat of Jakobshavn Isbræ, west Greenland: Field observations of 2005 and structural analysis of its evolution. *Natural Resources Research*, *17*(3), 167–179. https://doi.org/10.1007/s11053-008-9076-7

McCall, J. G. (1960). The flow characteristics of a cirque glacier and their effect on glacial structure and cirque formation. In W. V. Lewis (Ed.), *Norwegian cirque glaciers, Royal Geographical Society Research Series* (Vol. 4, pp. 39–62). Royal Geographical Society.

McGrath, D., Steffen, K., Holland, P. R., Scambos, T., Rajaram, H., Abdalati, W., & Rignot, E. (2014). The structure and effect of suture zones in the Larsen C Ice Shelf, Antarctica. *Journal of Geophysical Research: Earth Surface*, *119*, 588–602. https://doi.org/10.1002/2013jf002935

McGrath, D., Steffen, K., Rajaram, H., Scambos, T., Abdalati, W., & Rignot, E. (2012). Basal crevasses on the Larsen C ice shelf, Antarctica: Implications for meltwater ponding and hydrofracture. *Geophysical Research Letters*, *39*(16), L16504. https://doi.org/10.1029/2012GL052413

McGrath, D., Steffen, K., Scambos, T., Rajaram, H., Casassa, G., & Rodrigues Lagos, J. L. (2012). Basal crevasses and associated surface crevassing on the Larsen C ice shelf, Antarctica, and their role in ice-shelf instability. *Annals of Glaciology*, *58*(60), 10–18. https://doi.org/10.3189/2012AoG60A005

McIntyre, N. F. (1984). Cryoconite hole thermodynamics. *Canadian Journal of Earth Sciences*, *21*, 152–156. https://doi.org/10.1139/e84-016

Medrzycka, D., Copland, L., Van Wychen, W., & Burgess, D. (2019). Seven decades of uninterrupted advance of Good Friday glacier, Axel Heiberg Island, Arctic Canada. *Journal of Glaciology*, *65*(251), 440–452. https://doi.org/10.1017/jog.2019.21

Meier, M. F. (1958). *The mechanics of crevasse formation (Symposium at Toronto 1957—Snow and Ice)* (Vol. 46, pp. 500–508). IASH Publication.

Meier, M. F. (1960). *Mode of flow of Saskatchewan Glacier*. US Geological Survey Professional Paper.

Meier, M. F., Kamb, B., Allen, C. R., & Sharp, R. P. (1974). Flow of Blue glacier, Olympic Mountains, Washington, USA. *Journal of Glaciology*, *13*, 187–212. https://doi.org/10.3189/S0022143000023029

Meier, M. F., & Post, A. (1969). What are glacier surges? *Canadian Journal of Earth Sciences*, *6*, 807–817. https://doi.org/10.1139/e69-081

Merry, C. J., & Whillans, I. M. (1993). Ice-flow features on ice stream B, Antarctica, revealed by SPOT HRV imagery. *Journal of Glaciology*, *39*, 515–527. https://doi.org/10.3189/S0022143000016415

Mickelson, D. M., & Berkson, J. M. (1974). Till ridges presently forming above and below sea level in Wachusett Inlet, Glacier Bay, Alaska. *Geografiska Annaler*, *56*(A), 111–119. https://doi.org/10.2307/520432

Midgley, N. G., Cook, S. J., Graham, D. J., & Tonkin, T. N. (2013). Origin, evolution and dynamic context of a Neoglacial lateral-frontal moraine at Austre Lovénbreen, Svalbard. *Geomorphology*, *198*, 96–106. https://doi.org/10.1016/j.geomorph.2013.05.017

Midgley, N. G., Glasser, N. F., & Hambrey, M. J. (2007). Sedimentology, structural characteristics and morphology of a high-Arctic moraine-mound complex: Midre Lovénbreen, Svalbard. In M. J. Hambrey, P. Christoffersen, N. F. Glasser, & B. Hubbard (Eds.), *Glacial sedimentary processes and products* (Vol. 39, pp. 11–22). Special Publication of the International Association of Sedimentologists. https://doi.org/10.1002/9781444304435

Midgley, N. G., Tonkin, T. N., Graham, D. J., & Cook, S. J. (2018). Evolution of high-Arctic glacial landforms during deglaciation. *Geomorphology*, *311*, 63–75. https://doi.org/10.1016/j.geomorph.2015.12.019

Milnes, A. G., & Hambrey, M. J. (1976). A method of determining approximate cumulative strains in glacier ice. *Tectonophysics*, *34*, T23–T27. https://doi.org/10.1016/0040-1951(76)90090-1

Milnes, B. W. J., Stokes, C. R., Jenkins, A., Jordan, J. R., Jamieson, S. S. R., & Gudmundsson, G. H. (2020). Intermittent structural weakening and acceleration of the Thwaites Glacier Tongue between 2000 and 2018. *Journal of Glaciology*, *66*(257), 485–495. https://doi.org/10.1017/jog.2020.20

Minchew, B. M., Meyer, C. R., Robel, A. A., Gudmundsson, G. H., & Simons, M. (2018). Processes controlling the downstream evolution of ice rheology in glacier shear margins: Case study on Rutford Ice Stream, West Antarctica. *Journal of Glaciology*, *64*(246), 583–594. https://doi.org/10.1017/jog.2018.47

Mölg, N., Ferguson, J., Bolch, T., & Vieli, A. (2020). On the influence of debris cover on glacier morphology: How high-relief structures evolve from smooth surfaces. *Geomorphology*, *357*, 107092. https://doi.org/10.1016/j.geomorph.2020.107092

Monz, M. E., Hudleston, P. J., Prior, D. J., Michels, Z., Fan, S., Negrini, M., et al. (2021). Full crystallographic orientation (c and a axes) of warm, coarse-grained ice in a shear-dominated setting: A case study, Storglaciären, Sweden. *The Cryosphere*, *15*, 303–324. https://doi.org/10.5194/tc-15-303-2021

Moore, J. (1993). Ice blisters and ice dolines. *Journal of Glaciology*, *39*(133), 714–716. https://doi.org/10.3189/S002214300001666X

Moore, P. L. (2014). Deformation of debris-ice mixtures. *Reviews in Geophysics*, *52*, 435–467. https://doi.org/10.1002/2014RG000453

Moore, P. L., Iverson, N. R., Brugger, K. A., Cohen, D., Hooyer, T. S., & Jansson, P. (2011). Effect of a cold margin on ice flow at the terminus of Storglaciären, Sweden: Implications for sediment transport. *Journal of Glaciology*, *57*(201), 77–87. https://doi.org/10.3189/002214311795306583

Moore, P. L., Iverson, N. R., & Cohen, D. (2010). Conditions for thrust faulting in a glacier. *Journal of Geophysical Research*, *115*, F02005. https://doi.org/10.1029/2009JF001307

Moore, P. L., Iverson, N. R., Uno, K. T., Dettinger, M. P., Brugger, K. A., & Jansson, P. (2012). Entrainment and emplacement of englacial debris bands near the margin of Storglaciären, Sweden. *Boreas*, *42*(1), 71–83. https://doi.org/10.1111/j.1502-3885.2012.00274.x

Moorman, B. J., & Michel, F. A. (2000). The burial of ice in the proglacial environment on Bylot Island, Arctic Canada. *Permafrost and Periglacial Processes*, *11*(3), 161–175. https://doi.org/10.1002/1099-1530(200007/09)11:3%3C161

Mortensen, A. K., Bigler, M., Grönvold, K., Steffensen, J. P., & Johnsen, S. J. (2005). Volcanic ash layers from the Last Glacial Terminations in the NGRIP ice core. *Journal of Quaternary Science*, *20*(3), 209–219. https://doi.org/10.1002/jqs.908

Mottram, R. H., & Benn, D. I. (2009). Testing crevasse-depth models: A field study at Breiðamerkurjökull, Iceland. *Journal of Glaciology*, *55*(192), 746–752. https://doi.org/10.3189/002214309789470905

Mueller, D. R., Vincent, W. F., & Jeffries, M. O. (2003). Break-up of the largest Arctic ice shelf and associated loss of an epishelf lake. *Geophysical Research Letters*, *30*(20), 2031. https://doi.org/10.1029/2003GL017931

Mukherjee, S. (2014). Review of flanking structures in meso- and micro-scales. *Geological Magazine*, *151*(6), 957–974. https://doi.org/10.1017/S0016756813001088

Müller, F., & Keeler, C. M. (1969). Errors in short-term ablation measurements on melting ice surfaces. *Journal of Glaciology*, *8*, 91–105. https://doi.org/10.3189/S0022143000020785

Murray, T., & Booth, A. D. (2010). Imaging glacial sediment inclusions in 3-D using ground-penetrating radar at Kongsvegen, Svalbard. *Journal of Quaternary Science*, *25*(5), 754–761. https://doi.org/10.1002/jqs.1351

Murray, T., Dowdeswell, J. A., Drewry, D. J., & Frearson, I. (1998). Geometric evolution and ice dynamics during a surge of Bakaninbreen, Svalbard. *Journal of Glaciology*, *44*, 263–272. https://doi.org/10.3189/S0022143000002604

Murray, T., Gooch, D. L., & Stuart, G. W. (1997). Structures within the surge front at Bakaninbreen, Svalbard, using ground-penetrating radar. *Annals of Glaciology*, *24*, 122–129. https://doi.org/10.3189/S0260305500012040

Murray, T., Luckman, A., Strozzi, T., & Nuttall, A. (2003). The initiation of glacier surging at Fridtjovbreen, Svalbard. *Annals of Glaciology*, *36*, 110–116. https://doi.org/10.3189/172756403781816275

Murray, T., Strozzi, T., Luckman, A., Jiskoot, H., & Christakos, P. (2003). Is there a single surge mechanism? Contrasts in dynamics between glacier surges in Svalbard and other regions. *Journal of Geophysical Research*, *108*(B5), 2237. https://doi.org/10.1029/2002JB001906

Murray, T., Stuart, G. W., Miller, P. J., Woodward, J., Smith, A. M., Porter, P. R., & Jiskoot, H. (2000). Glacier surge propagation by thermal evolution at the bed. *Journal of Geophysical Research*, *105*, 13491–13507. https://doi.org/10.1029/2000JB900066

Nath, P. C., & Vaughan, D. G. (2003). Subsurface crevasse formation in glaciers and ice sheets. *Journal of Geophysical Research*, *108*(B1), 7–1. https://doi.org/10.1029/2001JB000453

Nye, J. F. (1952). The mechanics of glacier flow. *Journal of Glaciology*, *2*, 82–93. https://doi.org/10.3189/S0022143000033967

Nye, J. F. (1953). The flow law of ice from measurements in glacier tunnels, laboratory experiments, and the Jungfraufirn borehole experiment. *Proceedings of the Royal Society of London*, *219*, 477–489. https://doi.org/10.1098/rspa.1953.0161

Nye, J. F. (1955). Comments on Dr. Loewe's letter and notes on crevasses. *Journal of Glaciology*, *2*, 512–514. https://doi.org/10.3189/S0022143000032652

Nye, J. F. (1957). The distribution of stress and velocity in glaciers and ice sheets. *Proceedings of the Royal Society of London*, *239*, 113–133. https://doi.org/10.1098/rspa.1957.0026

Nye, J. F. (1958). *A theory of wave formation in glaciers (Cambridge Austerdalsbre Expedition) Symposium at Chamonix 1958—Physics of the Movement of Ice)* (Vol. 47, pp. 139–154). International Association of Scientific Hydrology Publication.

Nye, J. F. (1959a). A method of determining the strain-rate tensor at the surface of a glacier. *Journal of Glaciology*, *3*, 409–419. https://doi.org/10.3189/S0022143000017093

Nye, J. F. (1959b). The deformation of a glacier below an ice fall. *Journal of Glaciology*, *3*, 387–408. https://doi.org/10.3189/S0022143000017081

Ó Cofaigh, C., Evans, D. J. A., & England, J. (2003). Ice-marginal terrestrial landsystems: Sub-polar glacier margins of the Canadian and Greenland high-Arctic. In D. J. A. Evans (Ed.), *Glacial landsystems* (pp. 44–64). Arnold.

Oerlemans, J., Giesen, R. H., & van den Broeke, M. R. (2009). Retreating alpine glaciers: Increased melt rates due to accumulation of dust (Vadret da Morteratsch, Switzerland). *Journal of Glaciology*, *55*, 729–736. https://doi.org/10.3189/002214309789470969

Orheim, O., & Lucchitta, B. K. (1987). Snow and ice studies by thematic mapper and multispectral scanner Landsat images. *Annals of Glaciology*, *9*, 109–118. https://doi.org/10.3189/S0260305500000483

Ottesen, D., & Dowdeswell, J. A. (2006). Assemblages of submarine landforms produced by tidewater glaciers in Svalbard. *Journal of Geophysical Research*, *111*, F01016. https://doi.org/10.1029/2005JF000330

Parker, G. (1975). Meandering of supraglacial melt streams. *Water Resources Research*, *11*, 551–552. https://doi.org/10.1029/WR011i004p00551
Passchier, C. W. (2001). Flanking structures. *Journal of Structural Geology*, *23*(6–7), 951–962. https://doi.org/10.1016/S0191-8141(00)00166-8
Passchier, C. W., & Druguet, E. (2002). Numerical modelling of asymmetric boudinage. *Journal of Structural Geology*, *24*, 1789–1803. https://doi.org/10.1016/S0191-8141(01)00163-8
Patrick, B. A., Corvino, A. F., & Wilson, C. J. L. (2003). Ice-flow measurements and deformation at marginal shear zones on Sørsdal Glacier, Ingrid Christensen Coast, east Antarctica. *Annals of Glaciology*, *37*, 60–68. https://doi.org/10.3189/172756403781815933
Perutz, M. F., & Seligman, G. (1939). A crystallographic investigation of glacier structure and the mechanism of glacier flow. *Proceedings of the Royal Society, Series A*, *172*(950), 335–360. https://doi.org/10.1098/rspa.1939.0108
Peters, M. E., Blankenship, D. D., Smith, D. E., Holt, J. W., & Kempf, S. D. (2007). The distribution and classification of bottom crevasses from radar sounding of a large tabular iceberg. *IEEE Geoscience and Remote Sensing Letters*, *4*(1), 142–146. https://doi.org/10.1109/LGRS.2006.887057
Pettit, E. C., Thorsteinsson, T., Jacobson, H. P., & Waddington, E. D. (2007). The role of crystal fabric in flow near and ice divide. *Journal of Glaciology*, *53*(181), 277–288. https://doi.org/10.3189/172756507782202766
Pfeffer, W. T. (1992). Stress-induced foliation in the terminus of the Variegated glacier, USA, formed during the 1982–83 surge. *Journal of Glaciology*, *38*, 213–222. https://doi.org/10.3189/S0022143000003622
Pfeffer, W. T., Humphrey, N. F., Amadei, B., Harper, J., & Wegmann, J. (2000). In situ stress tensor measured in an Alaskan glacier. *Annals of Glaciology*, *31*, 229–235. https://doi.org/10.3189/172756400781820354
Phillips, E., Everest, J., Evans, D. J. A., Finlayson, A., Ewertowski, M., Guild, A., & Jones, L. (2017). Concentrated, "pulsed" axial glacier flow: Structural glaciological evidence from Kviárjökull in SE Iceland. *Earth Surface Processes and Landforms*, *42*(13), 1901–1922. https://doi.org/10.1002/esp.4145
Phillips, E., Finlayson, A., Bradwell, T., Everest, J., & Jones, L. (2014). Structural evolution triggers a dynamic reduction in active glacier length during rapid retreat: Evidence from Falljökull, SE Iceland. *Journal of Geophysical Research: Earth Surface*, *119*(10), 2194–2208. https://doi.org/10.1002/2014JF003165
Phillips, E., Finlayson, A., & Jones, L. (2013). Fracturing, block faulting, and moulin development associated with progressive collapse and retreat of a maritime glacier: Falljökull, SE Iceland. *Journal of Geophysical Research: Earth Surface*, *118*(3), 1545–1561. https://doi.org/10.1002/jgrf.20116
Piccini, L., Romeo, A., & Badino, G. (2002). Moulins and marginal contact caves in the Gornergletscher, Switzerland. *Nimbus*, *23–24*, 94–99.
Pohjola, V. A. (1996). Simulation of particle paths and deformation of ice structures along a flow-line on Storglaciären, Sweden. *Geografiska Annaler—Series A: Physical Geography*, *78*(2–3), 181–192. https://doi.org/10.1080/04353676.1996.11880464
Posamentier, H. W. (1978). Thoughts on ogive formation. *Journal of Glaciology*, *20*, 218–220. https://doi.org/10.3189/S0022143000198120
Post, A. (1972). Periodic surge origin of folded medial moraines on Bering Piedmont glacier, Alaska. *Journal of Glaciology*, *11*, 219–226. https://doi.org/10.3189/S0022143000022218
Post, A., & LaChapelle, E. R. (1971). *Glacier Ice*. The Mountaineers and University of Washington Press.
Pralong, A., & Funk, M. (2005). Dynamic damage model of crevasse opening and application to glacier calving. *Journal of Geophysical Research*, *110*(B1), B01309. https://doi.org/10.1029/2004JB003104
Price, P. B. (2000). A habitat for psychrophiles in deep Antarctic ice. *Proceedings of the National Academy of Sciences*, *97*, 1247–1251. https://doi.org/10.1073/pnas.97.3.1247
Price, P. B. (2006). Microbial life in glacial ice and implications for the cold origin of life. *FEMS Microbiology Ecology*, *5*, 217–231. https://doi.org/10.1111/j.1574-6941.2006.00234.x
Price, S. F., & Whillans, I. M. (2001). Crevasse patterns at the onset to ice stream B, West Antarctica. *Journal of Glaciology*, *47*(156), 29–36. https://doi.org/10.3189/172756501781832494
Pritchard, H., Murray, T., Luckman, A., Strozzi, T., & Barr, S. (2005). Glacier surge dynamics of Sortebræ, East Greenland, from synthetic aperture radar feature tracking. *Journal of Geophysical Research*, *110*, F03005. https://doi.org/10.1029/2004JF000233
Pritchard, H. D., Ligtenberg, S. R. M., Fricker, H. A., Vaughan, D. G., van den Broeke, M. R., & Padman, L. (2012). Antarctic ice-sheet loss driven by basal melting of ice shelves. *Nature*, *484*, 502–505. https://doi.org/10.1038/nature10968
Pulina, M. (1984). Glacierkarst phenomena in Spitsbergen. *Norsk Geografisk Tidsskrift*, *38*(3–4), 163–168. https://doi.org/10.1080/00291958408552121
Quincey, D. J., Luckman, A., & Benn, D. (2009). Quantification of Everest region glacier velocities between 1992 and 2002, using satellite radar interferometry and feature tracking. *Journal of Glaciology*, *55*(192), 596–606. https://doi.org/10.3189/002214309789470987
Ragan, D. M. (1969). Structures at the base of an icefall. *The Journal of Geology*, *77*, 647–667. https://doi.org/10.1086/627463
Ramberg, H. (1964). Note on model studies of folding moraines in piedmont glaciers. *Journal of Glaciology*, *5*(38), 207–218. https://doi.org/10.3189/S0022143000028781
Ramsay, J. G. (1967). *Folding and fracturing of rocks*. McGraw-Hill.
Ramsay, J. G. (1980). The crack-seal mechanism of rock deformation. *Nature*, *284*, 135–139. https://doi.org/10.1038/284135a0
Ramsay, J. G., & Huber, M. I. (1983). *The techniques of modern structural geology. Folds and Fractures* (Vol. 2). Academic Press.
Raup, B. H., Scambos, T. A., & Haran, T. (2005). Topography of streak-lines on an Antarctic ice shelf from photoclinometry applied to a single Advanced Land Imager (ALI) image. *IEEE Transactions on Geoscience and Remote Sensing*, *43*, 736–742. https://doi.org/10.1109/TGRS.2005.843953
Raymond, C., Johannesson, T., Pfeffer, T., & Sharp, M. (1987). Propagation of a glacier surge into stagnant ice. *Journal of Geophysical Research*, *92*(B9), 9037–9049. https://doi.org/10.1029/JB092iB09p09037
Raymond, C. F. (1983). Deformation in the vicinity of ice divides. *Journal of Glaciology*, *29*(103), 357–373. https://doi.org/10.3189/S0022143000030288
Rea, B. R., & Evans, D. J. A. (2011). An assessment of surge-induced crevassing and the formation of crevasse squeeze ridges. *Journal of Geophysical Research*, *116*, F04005. https://doi.org/10.1029/2011JF001970
Reber, J. E., Dabrowski, M., & Schmid, D. W. (2012). Sheath fold formation around slip surfaces. *Terra Nova*, *24*(5), 417–421. https://doi.org/10.1111/j.1365-3121.2012.01081.x
Reeh, N. (2017). Greenland ice shelves and ice tongues. In L. Copland, & D. Mueller (Eds.), *Arctic ice shelves and ice islands* (pp. 75–106). Springer. https://doi.org/10.1007/978-94-024-1101-0_4
Reese, R., Gudmundsson, G. H., Levermann, A., & Winkelmann, R. (2018). The far reach of ice-shelf thinning in Antarctica. *Nature Climate Change*, *8*, 53–57. https://doi.org/10.1038/s41558-017-0020-x

Retzlaff, R., & Bentley, C. R. (1993). Timing of stagnation of ice stream C, West Antarctica, from short pulse radar studies of buried surface crevasses. *Journal of Glaciology*, *39*, 495–506. https://doi.org/10.3189/S0022143000016440
Reynolds, J. M. (1988). The structure of the Wordie ice shelf, Antarctic Peninsula. *British Antarctic Survey Bulletin*, *80*, 57–64.
Reynolds, J. M., & Hambrey, M. J. (1988). The structural glaciology of George VI ice shelf, Antarctic Peninsula. *British Antarctic Survey Bulletin*, *79*, 79–95.
Rignot, E., Casassa, G., Gogineni, P., Krabill, W., Rivera, A., & Thomas, R. (2004). Accelerated ice discharge from the Antarctic Peninsula following the collapse of Larsen B ice shelf. *Geophysical Research Letters*, *31*, L18401. https://doi.org/10.1029/2004gl020697
Rignot, E., & MacAyeal, D. R. (1998). Ice-shelf dynamics near the front of the Filchner-Ronne Ice Shelf, Antarctica, reveal by SAR interferometry. *Journal of Glaciology*, *44*(147), 405–418. https://doi.org/10.3189/S0022143000002732
Rignot, E., Mouginot, J., & Scheuchl, B. (2011). Ice flow of the Antarctic ice sheet. *Science*, *333*(6048), 1427–1430. https://doi.org/10.1126/science.1208336
Rigsby, G. P. (1960). Crystal orientation in glacier and in experimentally deformed ice. *Journal of Glaciology*, *3*(27), 589–606. https://doi.org/10.3189/S0022143000023716
Rippin, D. M., Pomfret, A., & King, N. (2015). High resolution mapping of supra-glacial drainage pathways reveals link between micro-channel drainage density, surface roughness and surface reflectance. *Earth Surface Processes and Landforms*, *40*(10), 1279–1290. https://doi.org/10.1002/esp.3719
Rippin, D. M., Siegert, M. J., & Bamber, J. L. (2003). The englacial stratigraphy of Wilkes Land, East Antarctica, as revealed by internal radio-echo sounding layering, and its relationship with balance velocities. *Annals of Glaciology*, *36*, 189–196. https://doi.org/10.3189/172756403781816356
Roberson, S. (2008). Structural composition and sediment transfer in a composite cirque glacier: Glacier de St. Sorlin, France. *Earth Surface Processes and Landforms*, *33*, 1931–1947. https://doi.org/10.1002/esp.1635
Roberson, S., & Hubbard, B. (2010). Application of borehole optical televiewing to investigating the 3-D structure of glaciers: Implications for the formation of longitudinal debris ridges, midre Lovénbreen, Svalbard. *Journal of Glaciology*, *56*(195), 143–156. https://doi.org/10.3189/002214310791190802
Roberts, D. H., Yde, J. C., Knudsen, N. T., Long, A. J., Lloyd, J. M., & Lloyd, J. M. (2009). Ice marginal dynamics during surge activity, Kuannersuit Glacier, Disko Island, West Greenland. *Quaternary Science Reviews*, *28*(3–4), 209–222. https://doi.org/10.1016/j.quascirev.2008.10.022
Roberts, M. J., Russell, A. J., Tweed, F. S., & Kundsen, Ó. (2000). Ice fracturing during jökulhlaups: Implications for englacial floodwater routing and outlet development. *Earth Surface Processes and Landforms*, *25*, 1429–1446. https://doi.org/10.1002/1096-9837(200012)25:13<1429::aid-esp151>3.0.co;2-k
Roberts, M. J., Tweed, F. S., Russell, A. J., Knudsen, Ó., Lawson, D. E., Larson, G. J., et al. (2002). Glaciohydraulic supercooling in Iceland. *Geology*, *30*(5), 439–442. https://doi.org/10.1130/0091-7613(2002)030<0439:gsii>2.0.co;2
Robin, G. Q. d. (1974). Depth of water-filled crevasses that are closely spaced. *Journal of Glaciology*, *13*, 543–543. https://doi.org/10.3189/S0022143000023285
Ross, N., Corr, H., & Siegert, M. (2020). Large-scale englacial folding and deep-ice stratigraphy within the West Antarctic Ice Sheet. *The Cryosphere*, *14*, 2103–2114. https://doi.org/10.5194/tc-14-2103-2020
Rott, H., Müller, F., Nagler, T., & Floricioiu, D. (2011). The imbalance of glaciers after disintegration of Larsen-B ice shelf, Antarctic Peninsula. *The Cryosphere*, *5*, 125–134. https://doi.org/10.5194/tc-5-125-2011
Rück, M., Rahner, R., Sone, H., & Dresen, G. (2017). Initiation and propagation of mixed mode fractures in granite and sandstone. *Tectonophysics*, *717*, 270–283. https://doi.org/10.1016/j.tecto.2017.08.004
Rutishauser, H. (1971). Observations on a surging glacier in East Greenland. *Journal of Glaciology*, *10*, 227–236. https://doi.org/10.3189/S0022143000013198
Rutter, N. W. (1965). Foliation pattern of Gulkana Glacier, Alaska Range, Alaska. *Journal of Glaciology*, *5*(42), 711–718. https://doi.org/10.1017/S0022143000018700
Scambos, T., Fricker, H. A., Liu, C.-C., Bohlander, J., Fastook, J., Sargent, A., et al. (2009). Ice shelf disintegration by plate bending and hydro-fracture: Satellite observations and model results of the 2008 Wilkins ice shelf break-ups. *Earth and Planetary Science Letters*, *280*(1–4), 51–60. https://doi.org/10.1016/j.epsl.2008.12.027
Scambos, T. A., Bohlander, J. A., Shuman, C. A., & Skvarca, P. (2004). Glacier acceleration and thinning after ice shelf collapse in the Larsen B embayment, Antarctica. *Geophysical Research Letters*, *31*, L18402. https://doi.org/10.1029/2004GL020670
Scambos, T. A., Echelmeyer, K. A., Fahnestock, M. A., & Bindschadler, R. A. (1994). Development of enhanced ice flow at the southern margin of ice stream D, Antarctica. *Annals of Glaciology*, *20*, 313–318. https://doi.org/10.3189/1994AoG20-1-313-318
Scambos, T. A., Hulbe, C., Fahnestock, M., & Bohlander, J. (2000). The link between climate warming and break-up of ice shelves in the Antarctic Peninsula. *Journal of Glaciology*, *46*(154), 516–530. https://doi.org/10.3189/172756500781833043
Schulson, E. M. (2001). Brittle failure of ice. *Engineering Fracture Mechanics*, *68*(17–18), 1839–1887. https://doi.org/10.1016/S0013-7944(01)00037-6
Schumsky, P. A. (1964). *Principles of structural glaciology*. Dover Publications.
Schwarzacher, N., & Untersteiner, N. (1953). *Zum Problem der Bänderung des Gletschereises. Sitzungsberichte der Oesterreich Akadamie der Wissenschften Mathem-Naturio. Klasse Abt. IIa* (Vol. 162(1–4), pp. 111–145). Springer.
Seligman, G. (1955). Comments on crevasse depths. *Journal of Glaciology*, *2*(17), 514. https://doi.org/10.3189/S0022143000032664
Sevestre, H., & Benn, D. I. (2015). Climatic and geometric controls on the global distribution of surge-type glaciers: Implications for a unifying model of surging. *Journal of Glaciology*, *61*(228), 646–662. https://doi.org/10.3189/2015JoG14J136
Shabtaie, S., & Bentley, C. R. (1982). Tabular icebergs: Implications from geophysical studies of ice shelves. *Journal of Glaciology*, *28*(100), 413–430. https://doi.org/10.3189/S0022143000005037
Shabtaie, S., & Bentley, C. R. (1987). West Antarctic ice streams draining into the Ross ice shelf configuration and mass balance. *Journal of Geophysical Research*, *92*, 1311–1336. https://doi.org/10.1029/JB092iB02p01311
Sharp, M. J. (1985). "Crevasse-fill" ridges: A landform type characteristic of surging glaciers? *Geografiska Annaler*, *67*(A), 213–220. https://doi.org/10.1080/04353676.1985.11880147
Sharp, M. J. (1988a). Surging glaciers: Behaviour and mechanisms. *Progress in Physical Geography*, *12*, 349–370. https://doi.org/10.1177/030913338801200302
Sharp, M. J. (1988b). Surging glaciers: Geomorphic effects. *Progress in Physical Geography*, *12*, 533–559. https://doi.org/10.1177/030913338801200403

Sharp, M. J., Lawson, W., & Anderson, R. S. (1988). Tectonic processes in a surge-type glacier. *Journal of Structural Geology*, *10*, 499–515. https://doi.org/10.1016/0191-8141(88)90037-5
Sharp, R. P. (1958). Malaspina glacier, Alaska. *The Geological Society of America Bulletin*, *69*, 617–646. https://doi.org/10.1130/0016-7606(1958)69[617:MGA]2.0.CO;2
Sharp, R. P., Epstein, S., & Vidziunas, I. (1960). Oxygen-isotope ratios in the Blue Glacier, Olympic Mountains, Washington, U.S.A. *Journal of Geophysical Research*, *65*, 4043–4059. https://doi.org/10.1029/JZ065i012p04043
Shaw, J. (1977). Till deposited in arid polar environments. *Canadian Journal of Earth Sciences*, *14*(6), 1239–1245. https://doi.org/10.1139/e77-113
Shoemaker, E. M. (1990). A subglacial boundary-layer regelation mechanism. *Journal of Glaciology*, *36*(124), 263–268. https://doi.org/10.3189/002214390793701309
Shuman, C. A., Berthier, E., & Scambos, T. A. (2011). 2001–2009 elevation and mass losses in the Larsen A and B embayments, Antarctic Peninsula. *Journal of Glaciology*, *57*(204), 737–754. https://doi.org/10.3189/002214311797409811
Siegert, M. J., & Kwok, R. (2000). Ice-sheet radar layering and the development of preferred crystal orientation fabrics between Lake Vostok and Ridge B, central East Antarctica. *Earth and Planetary Science Letters*, *179*(2), 227–235. https://doi.org/10.1016/S0012-821X(00)00121-7
Siegert, M. J., Pokar, M., Dowdeswell, J. A., & Benham, T. (2005). Radio-echo layering in West Antarctica: A spreadsheet dataset. *Earth Surface Processes and Landforms*, *30*, 1583–1591. https://doi.org/10.1002/esp.1238
Siegert, M. J., Welch, B., Morse, D., Vieli, A., Blankenship, D. D., Joughin, I., et al. (2004). Ice flow direction change in interior West Antarctica. *Nature*, *305*, 1948–1951. https://doi.org/10.1126/science.1101072
Small, R. J. (1983). Lateral moraines of Glacier De Tsidjiore Nouve: Form, development, and implications. *Journal of Glaciology*, *29*, 250–259. https://doi.org/10.3189/S0022143000008303
Small, R. J. (1987). Englacial and supraglacial sediment: Transport and deposition. In A. M. Gurnell, & M. J. Clark (Eds.), *Glaciofluvial sediment transfer: An alpine perspective*. Wiley.
Smith, B. E., Lord, N. E., & Bentley, C. R. (2002). Crevasse ages on the northern margin of ice stream C, West Antarctica. *Annals of Glaciology*, *34*, 209–216. https://doi.org/10.3189/172756402781817932
Souchez, R. A. (1967). The formation of shear moraines: An example from south Victoria Land, Antarctica. *Journal of Glaciology*, *6*, 837–843. https://doi.org/10.3189/S0022143000020141
Souchez, R. A. (1971). Ice-cored moraines in south-western Ellesmere Island, NWT, Canada. *Journal of Glaciology*, *10*, 245–254. https://doi.org/10.3189/S0022143000013216
Souness, C., & Hubbard, B. (2012). Mid-latitude glaciation on Mars. *Progress in Physical Geography*, *36*, 238–261. https://doi.org/10.1177/0309133312436570
Souness, C., Hubbard, B., Milliken, R. E., & Quincey, D. (2012). An inventory and population-scale analysis of Martian glacier-like forms. *Icarus*, *217*, 243–255. https://doi.org/10.1016/j.icarus.2011.10.020
Souness, C. J., & Hubbard, B. (2013). An alternative interpretation of late Amazonian ice flow: Protonilus Mensae, Mars. *Icarus*, *225*, 495–505. https://doi.org/10.1016/j.icarus.2013.03.030
Spencer, M. K., Alley, R. B., & Fitzpatrick, J. J. (2006). Developing a bubble number-density paleoclimatic indicator for glacier ice. *Journal of Glaciology*, *52*(178), 358–364. https://doi.org/10.3189/172756506781828638
Staffelbach, T., Stauffer, B., & Oeschger, H. (1988). A detailed analysis of the rapid changes in ice-core parameters during the last ice age. *Annals of Glaciology*, *10*, 167–170. https://doi.org/10.3189/S0260305500004377
Stenborg, T. (1968). Glacier drainage connected with ice structures. *Geografiska Annaler*, *50*(A), 25–53. https://doi.org/10.1080/04353676.1968.11879770
Stenborg, T. (1969). Studies of the internal drainage of glaciers. *Geografiska Annaler*, *51*(A), 13–41. https://doi.org/10.1080/04353676.1969.11879788
Stenborg, T. (1973). Some viewpoints on the internal drainage of glaciers. In Meier, M. F. (Ed.), *Hydrology of glaciers* (Vol. 95, pp. 117–129). IAHS Publication.
St Germain, S., & Moorman, B. (2019). Long-term observations of supraglacial streams on an Arctic glacier. *Journal of Glaciology*, *65*(254), 900–911. https://doi.org/10.1017/jog.2019.60
Stibal, M., Šabacká, M., & Žárský, J. (2012). Biological processes on glacier and ice sheet surfaces. *Nature Geoscience*, *5*, 771–774. https://doi.org/10.1038/ngeo1611
Sun, S., Cornford, S. L., Moore, J. C., Gladstone, R., & Zhao, L. (2017). Ice shelf fracture parameterization in an ice sheet model. *The Cryosphere*, *11*, 2543–2554. https://doi.org/10.5194/tc-11-2543-2017
Swift, D. A., Cook, S. J., Graham, D. J., Midgley, N. G., Fallick, A. E., Storrar, R., et al. (2018). Terminal zone glacial sediment transfer at a temperate overdeepened glacier system. *Quaternary Science Reviews*, *180*, 111–131. https://doi.org/10.1016/j.quascirev.2017.11.027
Swift, D. A., Evans, D. J. A., & Fallick, A. E. (2006). Transverse englacial debris-rich ice bands at Kviarjökull, southeast Iceland. *Quaternary Science Reviews*, *25*, 1708–1718. https://doi.org/10.1016/j.quascirev.2006.01.003
Swift, D. A., & Jones, A. H. (2018). Going against the flow: Testing the hypothesis of pulsed axial glacier flow. *Earth Surface Processes and Landforms*, *43*(13), 2754–2761. https://doi.org/10.1002/esp.4430
Swinzow, G. K. (1962). Investigation of shear zones in the ice sheet margin, Thule area, Greenland. *Journal of Glaciology*, *4*, 215–229. https://doi.org/10.3189/S0022143000027416
Swithinbank, C., Brunt, K., & Sievers, J. (1988). A glaciological map of Filchner-Ronne Ice Shelf, Antarctica. *Annals of Glaciology*, *11*, 150–155. https://doi.org/10.3189/S0260305500006467
Szuman, I., & Kasprzak, L. (2010). Glacier ice structures influence on moraines development (Hørbye glacier, Central Spitsbergen). *Quaestiones Geographicae*, *29*(1), 65–73. https://doi.org/10.2478/v10117-010-0007-4
Telling, J. W., Glennie, C., Fountain, A. G., & Finnegan, D. C. (2017). Analyzing glacier surface motion using LiDAR data. *Remote Sensing*, *9*(3), 283. https://doi.org/10.3390/rs9030283
Tonkin, T. N., Midgley, N. G., Cook, S. J., & Graham, D. J. (2016). Ice-cored moraine degradation mapped and quantified using an unmanned aerial vehicle: A case study from a polythermal glacier in Svalbard. *Geomorphology*, *258*, 1–10. https://doi.org/10.1016/j.geomorph.2015.12.019
Treverrow, A., Budd, W. F., Jacka, T. H., & Warner, R. C. (2012). The tertiary creep of polycrystalline ice: Experimental evidence for stress-dependent levels of strain-rate enhancement. *Journal of Glaciology*, *59*, 301–314. https://doi.org/10.3189/2012JoG11J149
Tweed, F. S., Roberts, M. J., & Russel, A. J. (2005). Hydrological monitoring of supercooled meltwater from Icelandic glaciers. *Quaternary Science Reviews*, *24*(22), 2308–2318. https://doi.org/10.1016/j.quascirev.2004.11.020

Tyndall, J. (1859). On the veined structure of glaciers, with observations on white seams, air bubbles and dirt bands. *Philosophical Transactions of the Royal Society of London*, *149*, 279–307. https://doi.org/10.1098/rstl.1859.0015
Tyndall, J. (1860). *The glaciers of the Alps*. Cambridge University Press.
van der Veen, C. J. (1998a). Fracture mechanics approach to penetration of surface crevasses on glaciers. *Cold Regions Science and Technology*, *27*, 31–47. https://doi.org/10.1016/S0165-232X(97)00022-0
van der Veen, C. J. (1998b). Fracture mechanics approach to penetration of bottom crevasses on glaciers. *Cold Regions Science and Technology*, *27*, 213–223. https://doi.org/10.1016/S0165-232X(98)00006-8
van der Veen, C. J. (1999). Crevasses on glaciers. *Polar Geography*, *23*(3), 213–245. https://doi.org/10.1080/10889379909377677
van der Veen, C. J. (2007). Fracture propagation as means of rapidly transferring surface meltwater to the base of glaciers. *Geophysical Research Letters*, *34*, L01501. https://doi.org/10.1029/2006GL028385
van der Veen, C. J. (2011). Crevasses. In V. P. Singh, P. Singh, & U. K. Haritashya (Eds.), *Encyclopedia of snow and ice* (pp. 165–168). Springer. https://doi.org/10.1007/978-90-481-2642-2_79
Vatne, G. (2001). Geometry of englacial water conduits, Austre Brøggerbreen, Svalbard. *Norwegian Journal of Geography*, *55*, 85–93. https://doi.org/10.1080/713786833
Vaughan, D. G. (1993). Relating the occurrence of crevasses to surface strain rates. *Journal of Glaciology*, *39*(132), 255–266. https://doi.org/10.3189/S0022143000015926
Vaughan, D. G., Corr, H. F. J., Bindschadler, R. A., Dutrieux, P., Gudmundsson, G. H., Jenkins, A., et al. (2012). Subglacial melt channels and fracture in the floating part of Pine Island Glacier, Antarctica. *Journal of Geophysical Research*, *117*, F03012. https://doi.org/10.1029/2012JF002360
Vaughan, D. G., & Doake, C. S. M. (1996). Recent atmospheric warming and retreat of ice shelves on the Antarctic Peninsula. *Nature*, *379*, 328–331. https://doi.org/10.1038/379328a0
Venteris, E. R. (1997). Evidence for bottom crevasse formation on Columbia Glacier, Alaska. In C. J. van der Veen (Ed.), *Calving glaciers: Report of a workshop, Febuary 28–March 2, 1997, Byrd polar research Centre report* (pp. 181–185). The Ohio State University.
Vincent, C., Dumont, M., Six, D., Brun, F., Picard, G., & Arnaud, L. (2018). Why do the dark and light ogives of Forbes bands have similar surface mass balances? *Journal of Glaciology*, *64*(244), 236–246. https://doi.org/10.1017/jog.2018.12
Vornberger, P. L., & Whillans, I. M. (1986). Surface features of ice stream B, Marie Byrd Land, west Antarctica. *Annals of Glaciology*, *8*, 168–170. https://doi.org/10.3189/S0260305500001385
Vornberger, P. L., & Whillans, I. M. (1990). Crevasse deformation and examples from ice stream B, Antarctica. *Journal of Glaciology*, *36*, 3–10. https://doi.org/10.3189/S0022143000005487
Waddington, E. D. (1986). Wave ogives. *Journal of Glaciology*, *32*(112), 325–334. https://doi.org/10.3189/S0022143000011990
Waddington, E. D., Bolzan, J. F., & Alley, R. B. (2001). Potential for stratigraphic folding near ice-sheet centers. *Journal of Glaciology*, *47*(159), 639–648. https://doi.org/10.3189/172756501781831756
Wadham, J. L., & Nuttall, A. (2002). Multiphase formation of superimposed ice during a mass-balance year at a maritime high-Arctic glacier. *Journal of Glaciology*, *48*, 545–551. https://doi.org/10.3189/172756502781831025
Walker, C. C., Bassis, J. N., Fricker, H. A., & Czerwinski, R. J. (2015). Observations of interannual and spatial variability in rift propagation in the Amery ice shelf, Antarctica, 2002–2014. *Journal of Glaciology*, *61*, 243–252. https://doi.org/10.3189/2015JoG14J151
Waller, R. I., Hart, J. K., & Knight, P. G. (2000). The influence of tectonic deformation on facies variability in stratified debris-rich basal ice. *Quaternary Science Reviews*, *19*(8), 775–786. https://doi.org/10.1016/S0277-3791(99)00035-9
Weertman, J. (1961). Mechanism for the formation of inner moraines found near the edge of cold ice caps and ice sheets. *Journal of Glaciology*, *3*, 965–978. https://doi.org/10.3189/S0022143000017378
Weertman, J. (1964). The theory of glacier sliding. *Journal of Glaciology*, *5*(39), 287–303. https://doi.org/10.3189/S0022143000029038
Weertman, J. (1973). Can a water-filled crevasse reach the bottom surface of a glacier? *IASH Publication*, *95*, 139–145.
Weertman, J. (1980). Bottom crevasses. *Journal of Glaciology*, *25*(91), 185–188. https://doi.org/10.3189/S0022143000010418
Weiss, J. (2004). Subcritical crack propagation as a mechanism of crevasse formation and iceberg calving. *Journal of Glaciology*, *50*(168), 109–115. https://doi.org/10.3189/172756504781830240
Westoby, M. J., Brasington, J., Glasser, N. F., Hambrey, M. J., & Reynolds, J. M. (2012). "Structure-from-Motion" photogrammetry: A low-cost, effective tool for geoscience applications. *Geomorphology*, *179*, 300–314. https://doi.org/10.1016/j.geomorph.2012.08.021
Wharton, R. A., McKay, C. P., Simmons, G. M., & Parker, B. C. (1985). Cryoconite holes on glaciers. *BioScience*, *35*, 499–503. https://doi.org/10.2307/1309818
Whillans, I. M., Jackson, M., & Tseng, Y.-H. (1993). Velocity pattern in a transect across ice stream B, Antarctica. *Journal of Glaciology*, *39*, 562–572. https://doi.org/10.3189/S0022143000016452
Whillans, I. M., & Tseng, Y.-H. (1995). Automatic tracking of crevasses on satellite images. *Cold Regions Science and Technology*, *23*(2), 201–214. https://doi.org/10.1016/0165-232X(94)00009-M
Whillans, I. M., & van der Veen, C.J. (1993). Patterns of calculated basal drag on ice streams B and C, Antarctica. *Journal of Glaciology*, *39*, 437–446. https://doi.org/10.3189/S0022143000016324
Williamson, A. G., Willis, I. C., Arnold, N. S., & Banwell, A. F. (2018). Controls on rapid supraglacial lake drainage in west Greenland: An Exploratory Data Analysis approach. *Journal of Glaciology*, *64*(244), 208–226. https://doi.org/10.1017/jog.2018.8
Wilson, C. J. L., Peternell, M., Piazolo, S., & Luzin, V. (2014). Microstructure and fabric development in ice: Lessons learned from in situ experiments and implications for understanding rock evolution. *Journal of Structural Geology*, *61*, 50–77. https://doi.org/10.1016/j.jsg.2013.05.006
Wilson, C. J. L., Russell-Head, D. S., & Sim, H. M. (2003). The application of an automated fabric analyzer system to the textural evolution of folded ice layers in shear zones. *Annals of Glaciology*, *37*, 7–17. https://doi.org/10.3189/172756403781815401
Winter, A., Steinhage, D., Creyts, T. T., Kleiner, T., & Eisen, O. (2019). Age stratigraphy in the east Antarctic ice sheet inferred from radio-echo sounding horizons. *Earth System Science Data*, *11*, 1069–1081. https://doi.org/10.5194/essd-11-1069-2019
Winter, K., Woodward, J., Ross, N., Dunning, S. A., HeinWestoby, A. S.M. J., Culberg, R., et al. (2019). Radar-detected englacial debris in the west Antarctic ice sheet. *Geophysical Research Letters*, *46*(17–18), 10454–10462. https://doi.org/10.1029/2019GL084012
Woodward, J., Murray, T., Clark, R. A., & Stuart, G. W. (2003). Glacier surge mechanisms inferred from ground-penetrating radar: Kongsvegen, Svalbard. *Journal of Glaciology*, *49*(167), 473–480. https://doi.org/10.3189/172756503781830458
Woodward, J., Murray, T., & McCaig, A. (2002). Formation and reorientation of structures in the surge-type glacier Kongsvegen, Svalbard. *Journal of Quaternary Science*, *17*, 201–209. https://doi.org/10.1002/jqs.673
Wright, C. S., & Priestley, R. E. (1922). *British (Terra Nova) Antarctic expedition, glaciology*. Harrison and Sons.

Ximenis, L., Calvet, J., Garcia, D., Casas, J. M., & Sabat, F. (2000). Folding in Johnsons glacier, Livingston Island, Antarctica. In A. J. Maltman, B. Hubbard, & M. J. Hambrey (Eds.), *Deformation of glacial materials* (Vol. 176, pp. 147–157). Geological Society London Special Publications. https://doi.org/10.1144/GSL.SP.2000.176.01.11

Zdanowicz, C. M., Michel, F. A., & Shilts, W. W. (1996). Basal debris entrainment and transport in glaciers of southwestern Bylot Island, Canadian Arctic. *Annals of Glaciology*, *22*, 107–113. https://doi.org/10.3189/1996AoG22-1-107-113